UCLouvain
Faculté des Sciences
Louvain institute of Biomolecular Science and Technology

Autophagic degradation of the iron transporter IRT1 is mediated by its interaction with the stress-induced TSPO protein in *Arabidopsis thaliana*

Thèse présentée par **Haitham Ayeb** en vue de
l'obtention du grade de Docteur en Sciences

Promoteur :	Henri Batoko
Co-promoteur :	Chedly Abdelly
Membres de jury	François Chaumont (Président)
	Xavier Draye
	Najoua Karray Bouraoui
	Enric Zelazny
	Walid Zorrig

Novembre 2022

شُكْرٌ وَتَقْدِيرٌ

ليْس بعد تمام العمل أجمل من الشّكر والإمتنان. إنّ توفيقي للوصول الى هذه المرحلة العلميّة التي مهّدت لي الطّريق لأن أكون بينكم اليوم لأناقش أطروحة الدّكتوراه، هو ناتج عن توفيقي من الله الذي أفاض عليّ من نعمته .هذه الأطروحة تعتبر ثمرة مغامرة دامت سبع سنوات و نصف مثّلت بالنسبة لي تحد وجودي مليء بالعمل الشّاق و المثابرة. هذه الأطروحة زادتني ثقة بالنّفس وعزّزت بداخلي الدأب على التعلّم أكثر و تحقيق الطّموح والأهداف. أتوجّه بالشّكر الجزيل إلى جميع الأشخاص الرائعين الذين ساندوني طوال هاته الرحلة

d

Remerciement

Je souhaite avant tout remercier mon promoteur Prof. Henri Batoko d'avoir accepté de diriger ma thèse, ça m'a été une opportunité d'apprendre et de développer mes compétences. Merci pour votre confiance et votre support pour obtenir les deux bourses, qui m'ont été indispensables pour achever mon doctorat. Merci pour les innombrables discussions scientifiques, les idées et le transfert du savoir-faire. Tout le long de ces années, j'ai appris d'être réaliste, sélectif et surtout d'aller droit au but 😎.

Je tiens à remercier mon co-promoteur Prof. Chedly Abdelly de m'avoir accepté comme doctorant au sein de son laboratoire et pour sa disponibilité administrative.

Je remercie également Dr. Walid Zorrig pour l'initiation du sujet de thèse et pour son support et son aide scientifique au niveau des analyses statistiques des résultats préliminaires.

De plus, je tiens à remercier tous les membres de mon jury pour leur temps, leur lecture critique de ce manuscrit et leurs commentaires utiles.

Je tiens aussi à remercier mes collègues dans l'équipe TSPO et la grande famille FYMO pour les beaux moments quotidiens tout le long de ce doctorat, qui m'ont permis de m'épanouir dans cet environnement scientifique. Merci pour les échanges d'idées et les "pauses-café" qui ont été l'occasion de nombreuses interactions scientifiques et sociales.

Je remercie Marie-Christine, pour sa bienveillance, disponibilité et son aide à la microscopie 😇.

Je remercie aussi ma famille pour son support morale durant cette thèse. Je remercie tout particulièrement Dr. Maroua Kammoun ♥ ma fiancée et la femme de ma vie, qui par son amour, m'a donné la force de persister et de résister dans les moments les plus critiques. Elle a cru en moi et m'a défendu, m'a guidé tout au long du chemin. C'est sa présence à mes côtés pour me supporter, me motiver, me distraire, me choyer et me rassurer a permis l'aboutissement de ce doctorat.

Enfin, je remercie ma plante modèle préférée *Arabidopsis thaliana* 🍃 qui m'a accompagné depuis le premier jour de ce doctorat et sans qui tous ces résultats n'auraient pas été possibles. Je suis désolé pour toutes les personnes que j'ai oublié de remercier.

Haitham Ayeb, Louvain-La-Neuve, 2022

"Achievement is never done by accident. It is always the result of high intention, sincere effort, and skillful execution; It is the wise choice of alternatives and the ability to make obstacles as opportunities. - choice, not chance, determines our destiny."

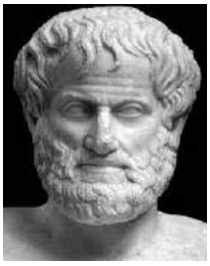

Aristotle
(384–322 BC)

h

Table of content

n

Abstract

Arabidopsis thaliana plant acquires iron from the soil through IRON-REGULATED TRANSPORTER 1 (IRT1). Previous work showed that IRT1 is stabilized and mainly localized at the plasma membrane under iron deficiency. The stabilized pool of this metal transporter protein is potentially detrimental to the cell since the level of iron in the cytosol is regulated and toxic mineral such as cadmium or zinc are also substrate of IRT1. In this work we showed that the constitutive expression of a stress-induced translocator protein TSPO reduces IRT1 levels in the plasma membrane. TSPO expression is transiently induced in the root by iron deficiency and is constitutively expressed in the *irt1*-null mutant. In contrast, overexpression of IRT1 induced TSPO. Pulldown assays and fluorescence microscopy approaches revealed that TSPO established physical interactions with IRT1 in the Arabidopsis root cells and the resulting complex is degraded through autophagy. Interestingly, constitutive expression of TSPO, and treatment resulting in transient TSPO expression such as abscisic acid treatment, salinity, osmotic stress, or pharmacological treatments inducing autophagy in the root cells resulted in IRT1 degradation. TSPO expression triggered IRT1 localization in vesicular structures reminiscent of autophagosomes. These data support a role for TSPO in IRT1 downregulation under multi-stress conditions, and specifically under iron deficiency conditions.

Significance

Some terms widely used in cell biology and biochemistry can have somewhat different meaning depending on the context. It may be worthy specifying the meaning we attribute to some critical concepts commonly used in this thesis.

Stress-related responses (in biology). Stress-related responses are a set of behavioral or physiological responses after diverse noxious stimuli agents. They are defined as changes in biochemical and metabolic processes (Levine, 1985).

Oxidative stress. A biological phenomenon during which the generation of reactive oxygen species could modify macromolecules in a living organism resulting in an imbalance between oxidant and antioxidant levels. It is defined as a state in which the pro-oxidative processes overwhelm cellular antioxidant defense due to redox signaling and adaptation disruption (Ji and Yeo, 2021).

Homeostasis (in biology). The word 'homeostasis' originates from the Greek language meaning "staying the same". It indicates the regulatory mechanism by which certain output variables of a biosystem are kept approximately standards when the input parameters vary (Modell *et al.*, 2015; Golubitsky and Stewart, 2018).

Glycophytes. Plants requiring low levels of sodium for optimal growth and development. Ecosystems containing glycophytes are characterized by standard or low sodium levels (Cheeseman, 2015).

Halophytes. Contrasting with glycophytes, halophytes are considered as “salt loving” or salt tolerant plants. Halophytes can complete their life cycles under 200 to 300 mM NaCl. They are rare plants because the evolution of halophily is complex (0.5% of all angiosperms) due to the relatively small area of the Earth's surface with naturally saline soils (Bessey, 1896; T J Flowers *et al.*, 2003; Cheeseman, 2015).

Transmembrane proteins. Constitute 15-30% of the eukaryotic proteome. These proteins are embedded in biological membranes delimiting the cell or its organelles. They have crucial functions in different cellular processes, such as cell signaling, transport, and cellular organization (Fleishman *et al.*, 2006; Jones, 2007; Pellegrini-Calace *et al.*, 2009).

Post-translational modification. The process that modulates the activity of most eukaryotic proteins. It monitors the target protein's function through specific recognition domains by adding a modifying chemical group or another protein to one or more of its amino acid residues. Post-translational modifications can be separated in time and occur sequentially in more than one site. It includes several forms such as phosphorylation, ubiquitination, acetylation, methylation, and proline hydroxylation (Mann and Jensen, 2003; Li *et al.*, 2017; Deribe *et al.*, 2010; Walsh, 2010).

Endocytosis. In eukaryotic cells, this biological mechanism is used for cargos (mainly lipids and proteins) internalization and delivery from the plasma membrane, most of the time for degradation through the continuous and regulated formation of prolific numbers of membrane

vesicles. These mostly clathrin-coated vesicles, are actin-dependent during their formation. Endosomes are subject to a complex molecular sorting process orchestrating their targeting to specific destinations (Mellman, 2003; Doherty and McMahon, 2009).

ESCRT. The "Endosomal Sorting Complex Required for Transport" is an ancient system. It assembles into multisubunits machinery that serves as a key mediator of delivered cargo destined for degradation to the vacuole or lysosome. This mechanism is related to many biologic processes, mainly to the endosomal sorting for transmembrane proteins for degradation, multivesicular bodies (MBVs) biogenesis, and autophagy (Babst, 2005; Schmidt and Teis, 2012; Henne *et al.*, 2011)**.**

Autophagy. Literally, means 'self-eating'. At the subcellular level, autophagy is an intracellular degradation system that could be activated as an adaptive response to various extracellular and intracellular stimuli. There are different types of autophagy, including microautophagy and macroautophagy. During this process, a double-membrane-bound vesicle, known as an autophagosome, forms in the cytoplasm and engulfs targeted cargoes. These vesicles are targeted to and fused with a lytic compartment to release their content which is then degraded by resident hydrolases. This process contributes in regulating homeostasis in multicellular organisms (Mizushima, 2007; Kelekar, 2006; Rabinowitz and White, 2010).

List of figures

List of abbreviations

IRT1	IRON-REGULATED TRANSPORTER 1
$^{\bullet}$HO	Hydroxyl radicals
°C	Degree celsius
3-MA	3-methyladenine
35S	Cauliflower mosaic virus (CaMV) 35S promoter
5-ALA	5-aminolevulunic acid
ABA	Abscissic acid
ABCG2	ATP-binding cassette transporter
ACA	Automated colorimetric assay
AD	Alzheimer's disease
AHA2	Proton pump AUTOINHIBITED PLASMA MEMBRANE-H^+-ATPase
AIM	Atg8 interacting motif
ALAS	ALA synthetase enzyme
ANOVA	Analysis of Variance
AP	Adaptor Protein
APX	Ascorbate peroxidases
AQPs	Aquaporins
At	*Arabidopsis thaliana*
ATG8	ATG8 UBIQUITIN-LIKE (Ubl) PROTEIN autophagy-related
ATGs	Autophagy-related genes
ATI1	ATG8-INTERACTING PROTEIN1
ATP	Adenosine triphosphate
AtP5A	SINGLE ENDOPLASMIC RETICULUM (ER)-RESIDENT P5-TYPE ATPase
BAK1	BRI1-ASSOCIATED RECEPTOR KINASE 1
BBM	Villus enterocytes cells in the border membrane

BCA	Bicinchoninic Acid
BCRP	Breast Cancer Resistance Protein
BFA	Brefeldin A
bHLH	Basic Helix-Loop-Helix
BiFC	Bimolecular fluorescence complementation
BTH	Benzo(1,2,3)thiadiazole-7-carboxylic acid
BTS1	Brassinosteroid E3 ligase BRUTUS1
BTSL	BRUTUS-LIKE E3 ligase
BV	Biliverdin
C4 path	ALA synthesis by the condensation of succinyl-CoA and glycine
C5 path	ALA synthesis from the skeleton of Glutamate
Ca	Calcium
CATs	Catalases
CCA1	CIRCADIAN CLOCK ASSOCIATED1
CCGs	CLOCK-CONTROLLED GENES
CCVs	Clathrin coated vesicles
Cd	Cadmium
CDF	CATION DIFFUSION FACILITATORS
CelLytic P Cell Lysis Reagent	for plant (Sigma product)
Chl	Chlorophyll
ChlH	H-subunit of Mg-Chelatase H-subunit
CIPK11	CBL-INTERACTING PROTEIN KINASE
CIPK23	Calcineurin-B-like protein (CBL)-interacting protein kinase 23
CLOCK	CIRCADIAN LOCOMOTOR OUTPUT CYCLES KAPUT
cm	Centimeter
CME	Clathrin-Mediated Endocytosis
CO	Carbon monoxide
ConcA	Concanamycin A
Cp	Ceruloplasmin homolog

CP	Core Protease
CPO	Coprogen-III Oxidase
CPP-III	Coproporphyrinogen-III
Cu	Copper
Cytb558	Flavocytochrome b558
DDM	Dodecyl-β-D-maltoside
DMSO	Dimethyl sulfoxide
DUBs	Deubiquitinase enzymes
E	Elution
ECF	Energy-coupling factor
EDTA	Ethylenediaminetetraacetic acid
EE	Early endosome
EHB1	ENHANCED BENDING1
EIL1	ETHYLENE INSENSITIVE3-LIKE1
EIN3	ETHYLENE INSENSITIVE3
EPS	ER-PM contact sites
ER	Endoplasmic reticulum
ERAD	Endoplasmic reticulum-associated protein degradation
Es	*Eutrema salsugineum*
ESCRT	Endosomal sorting complex required for transport
Evs	Extracellular vesicles
FC1	Ferrochelatase 1
Fe	Iron
Fe-S	Iron–sulfur
FE(III)	Ferric iron
Fe^{2+}	Ferrous iron
FeCH	Ferrochelatase enzyme
FER	Ferritin
FeSODs	Iron Superoxide dismutases
FIT	Iron DEFICIENCY INDUCED TRANSCRIPTION FACTOR

FLOT1	FLOTILLIN1
FLU	FLUORESCENT protein
FPN1	FERROPORTIN 1
FPN3	FERROPORTIN 3
frd1	Ferric reductase defective-1 mutant
FRD3	FERRIC REDUCTASE DETECTIVE3
FREE1	FYVE DOMAIN PROTEIN REQUIRED FOR ENDOSOMAL SORTING 1
FRO2	FERRIC REDUCTASE OXIDASE 2
FRO7	FERRIC REDUCTASE OXIDASE 7
FT	Flowt-through
g	Gram
GAPDH	Glyceraldehyde-3-phosphate dehydrogenase
GFP	Green fluorescent protein
GLU	Glutamate
GluS	Glutamyl-synthetase
GluTR	Glutamyl-tRNA-reductase
GluTRBP	PROTON GRADIENT REGULATION7
GSTU	Glutathione transferase
GUN	GENOME UNCOUPLED
gun2	Genome Uncoupled 2
GUN4	Genome Uncoupled 4
h	Hour
HBD	Heme-binding domain
HCP1	Proton coupled folate transporter/heme carrier protein 1
Hcpro	Helper-component proteinase
HDAC	HISTONE DEACETYLTRANSFERASE
HMA3	HEAVY METAL ASSOCIATED3
HMB	Hydroxymethylbilane
HMBS	Hydroxymethylbilane synthase
HO	Heme Oxygenase

HOPS	HOMOTYPIC VACUOLE FUSION AND PROTEIN SORTING
HOZ	Non-canonical dimeric β-barrel HEME OXYGENASE
HY1	NO
HY5	LONGATED HYPOCOTYL 5
ICP-AES	Coupled plasma atomic emission spectroscopy
IDF1	IRT1 DEGRADATION FACTOR1
IL-1β	Interleukin-1β
IMS	Mitochondrial intermembrane space
IN	Input
IREG2	IRON REGULATED GENE2
IRT2	IRON REGULATED TRANSPORTER 2
ISTL1	INCREASED SALT TOLERANCE 1
JA	Jasmonic acid
K	Potassium
KD	Kinase domain
kDa	kilodalton
KIN10	Kinase homolog 10
KO	Knockout
Ko143	Specific inhibitor of ABCG2
L	Liter
LE	Late endosome
LHY	LATE ELONGATED HYPOCOTYL
LIP	Labile-Iron-Pool
LPR1	LOW PHOSPHATE ROOT 1
LPS	Lipopolysaccharides
LST8	LETHAL WITH SEC THIR-TEEN8
LTI6B	LOW TEMPERATURE INDUCED PROTEIN 6B
macOS	Computer operating system (OS) for Apple desktops and laptops
MAM	Mitochondria Associated Membrane
MBVs	Multivesicular bodies

mCherry	Bright red monomeric fluorescent protein derived from DsRed
MDA	Monodehydroascorbate
MDC	Monodansylcadaverine
MDVs	Mitochondria-derived vesicles
MED16	MEDIATOR COMPLEX 16
MFS	Major facilitator superfamily
Mg	Magnesium
mg	Milligram
Mn	Manganese
MOC	Mander's overlap coefficient
mRNA	Messenger Ribonucleic acid
MS	Murashige and Skoog (culture medium)
MTP3	METAL TOLERANCE PROTEIN3
mTq2	Monomeric cyan fluorescent protein mTurquoise
MUB	Membrane-anchored ubiquitin-fold protein
mVenus	monomeric yellow fluorescent protein (variant)
NBR1	NEIGHBOR OF BRCA1
Ncor	NUCLEAR RECEPTOR CO-REPRESSOR
Ni	Nickel
NiCo-PIC1	NICKEL/COBALT TRANSPORTER-PERMEASE IN CHLOROPLASTS
NOX	NADPH oxidase
NRAMP	NATURAL RESISTANCE-ASSOCIATED MACROPHAGE PROTEIN
Nrf2	NUCLEAR FACTOR ERYTHROID 2 RELATED FACTOR 2
Nter	N-terminus
Ø	Diameter
OPT3	OLIGOPEPTIDE TRANSPORTER 3
PBG	Monopyrrole porphobilinogen
PBG	Porphobilinogen
PBGS	Porphobilinogen synthase
PCD	Programmed cell death

Pchlide	Protochlorophyllide
PDR2	PHOSPHATE DEFICIENCY RESPONSE 2
PDR9	PLEIOTROPIC DRUG RESISTANCE 9
PE	Phosphatidylethanolamine
PF	Osmotic water permeability
PhANGs	PHOTOSYNTHESIS-ASSOCIATED NUCLEAR genes
PHR1	HOSPHATE STARVATION RESPONSE 1
PI-3K	Phosphatidylinositol 3-kinases
PIN2	AUXIN EFFLUX CARRIER COMPONENT 2
pLDDT	protein Local Distance Difference Test
PM	Plasma membrane
PPIX	Protoporphyrin-IX
PPOX	Protoporphyrinogen oxidase
PTMs	Posttranslational Modifications
PUB4	Plant U-Box 4
PVDF	Polyvinylidene difluoride
RAF1a	TUMOR NECROSIS FACTOR RECEPTOR-ASSOCIATED FACTORT1a
RbcL	Rubisco large subunit
Rboh	Respiratory burst oxidase homolog
RCBs	Rubisco-containing bodies
RFP	Red fluorescent protein
RIA-J	Root Image Analysis-J
RIPK	PM1-induced protein kinase
ROS	Reactive oxygen species
ROS	Reactive oxygen species
RP	Regulatory Particle
RPS6	PUTATIVE RIBOSOMAL PROTEIN S6
RSA	Root system architecture
SA	Salicylic acid
SAR1	Secretion-associated Ras-related GTPase 1

SARs	Selective autophagy receptors
SDS-PAGE	Sodium dodecyl sulfate–polyacrylamide gel electrophoresis
SE	Sorting endosome
SGS3	SUPPRESSOR OF GENE SILENCING 3
SH3P2	SRC HOMOLOGY-3
shRNA	Short hairpin Ribonucleic acid
SINAT6	SEVEN IN ABSENTIA OF ARABIDOPSIS THALIANA6
siRNA	Small interfering Ribonucleic acid
SLA	Sex-linked anemia
SLC25A38	Solute carrier family-25, member-38 protein
SN	Substantia nigra
SNF1	Sucrose non-fermenting 1
SnRK2	SNF1-related protein kinase 2
SNX1	SORTING NEXIN 1
SOD	Superoxide dismutase
ssRNA	Single-stranded RNA
STEAP	Six-transmembrane epithelial antigen of the prostate protein family
T-DNA	Transfer DNA
TGN	Trans-Golgi-Network
TIC	TIME FOR COFFEE
TOC	TRANSLOCON AT THE OUTER ENVELOPE OF CHLOROPLASTS
TOC1	TIMING OF CAB EXPRESSION1
TOR	Target Of Rapamycin
TPC	Components of endocytic TPLATE complex
TRAF1a	TUMOR NECROSIS FACTOR RECEPTOR ASSOCIATED FACTOR1a
TRP	Non-canonical tetratricopeptide repeat domain
TSET/TPC	TPLATE SET /TPLATE complex
TSPO	Translocator protein
Ub	Ubiquitin
UBL	Ubiquitin-like Protein Conjugation

UbLD	Ubiquitin-like domain
UBQ10	Ubiquitin-10 promoter
UIMs	Ubiquitin-interacting motifs
UPS	Ubiquitin/26S Proteasome System
UROD	Uroporphyrinogen decarboxylases
Urogen-III	Uroporphyrinogen-III
UROS	Uroporphyrinogen synthase
v/v	Volume per volume
VCL1	VACUOLELESS1
VDAC	VOLTAGE-DEPENDENT ANION CHANNEL
VPS	Vascular protein sorting
VPS23A	VACUOLAR PROTEIN SORTING23A
W	Washing
WT	Wild Type
Xcv	Xanthomonas campestris pv. Vesicatoria
YFP	Yellow fluorescent protein
YSL	YELLOW STRIPE LIKE PROTEIN
ZAT12	ZINC FINGER OF *ARABIDOPSIS THALIANA*12
Zn	Zinc
µ	Micro

PART I

General introduction

Problem statement: Iron homeostasis and iron deficiency

Minerals, including micro-elements such as Fe, Zn, Mn, Co, etc., have a significant impact on the growth and health of living organisms (Kravale *et al.*, 2007; Hu and Liu, 2002; Ronen, 2022). Mostly these trace divalent metals come from bioavailable external sources. Living organisms use different uptake mechanisms to acquirer these minerals. These mechanisms involve complex systems of membrane transporters (Pandey, 2015; Landeweert *et al.*, 2001; Mayland and Wilkinson, 1996). However, most of these transporters are specific for the uptake of more than one mineral (Kathpalia and Bhatla, 2018). Iron (Fe) is an essential micro-element for most living organisms. Fe is mainly available in the soil in water-insoluble forms (Lindsay, 2008; Uren, 2008; Colombo *et al.*, 2012). Multicellular eukaryotes such as animals and plants must ensure sufficient iron intake to sustain essential pathways of their metabolism.

Fe uptake and availability is crucial for plants, such as the glycophyte *Arabidopsis thaliana*. Iron is involves in nitrogen and sulfur assimilation, photosynthetic electron transport, NAD(P) synthesis, reactive oxygen species (ROS) scavenging, mitochondrial metabolism, DNA methylation, phytohormones (such as abscisic acid (ABA) and ethylene) biosynthesis, and much more (Gretchen Elizabeth Kroh and Pilon, 2020; Takahashi *et al.*, 2011; Noctor *et al.*, 2011; Jain and Connolly, 2013). Fe deficiency triggers acclimation responses. This

leads to primary visible symptoms such as chlorosis of young leaves dues to the changes in chloroplasts ultrastructure and decrease in expression of chlorophyll (a) and (b) binding proteins and RUBISCO (*Ribulose-1,5-bisphosphate carboxylase/oxygenase*). In addition, iron deficiency causes a reduction in the shoot and root biomass. (Spiller and Terry, 1980; Spiller *et al.*, 1987; Winder and Nishio, 1995; Brown and Jolley, 1989). Iron deficiency also affects mRNA abundance as a consequence of downregulating several photosynthetic processes such as the expression of components of the plastid iron–sulfur (Fe–S) assembly pathway (Gretchen Elizabeth Kroh and Pilon, 2020).

Thesis outline

We first introduce aspects of maintaining cellular iron-related metabolism through the regulation of the iron transporter protein IRT1 for the model plant *Arabidopsis thaliana*. In Chapter I, we briefly describe the autophagy process in *A. thaliana.* We also discuss the interplay between autophagy and posttranslational modifications especially ubiquitination and phosphorylation. We then discuss control of nutrients starvation in *A. thaliana.* We complete this first literature review by discussing the importance of autophagy in controlling nutrient starvation in Arabidopsis. In Chapter II we describe the mechanism of the uptake and translocation of the non-heme iron into the Arabidopsis cell. In addition, we detail the role of the heme molecule as an internal iron source in modulating iron homeostasis in the cell. We recall the heme biosynthesis in the plant cell, as well as its dynamics, including translocation and storage. We then describe the involvement of heme catabolism resulting in iron recycling under ROS detoxification requiring heme overproduction. We discuss heme as a critical cue to modulate the circadian iron system through retrograde signaling, and connected to the iron uptake machinery of *A. thaliana*. We describe the regulation of the iron transporter IRT1 with emphasis in terms of protein structure, translational/post-translational regulation influencing protein trafficking, and subcellular localization. We end this second part of the literature review by highlighting a hypothetic novel concept in the regulation of IRT1 in Arabidopsis. This potential new concept focuses on the critical role of the stress-induced TSPO protein in the modulation of iron homeostasis under stressful

conditions. To experimentally test this hypothesis, the following will be evaluated:

- The potential molecular and physiological impact of TSPO expression in the regulation of IRT1

- Localization of IRT1 and in particular at the PM during iron deficiency and the concurrent regulation of TSPO levels

- The potential role of TSPO protein upon IRT1 degradation under stress conditions in *A. thaliana*.

In the results section, we start (Chapter IV) by studying the effect of iron deficiency upon TSPO expression. We provide evidence suggesting a co-regulatory relationship between TSPO and IRT1 in *A. thaliana*. In Chapter V we show that IRT1 is degraded in *A. thaliana* during oxidative stress via a TSPO-dependent autophagy pathway. Chapter VI is devoted to a general discussion of the results. Then Chapter VI provides a general conclusion of this work. Finally, in Chapter VIII we suggest possible perspectives to our findings.

PART II

Literature review 1

1 Chapter I: How are the LEGO pieces assembled? the interplay between Selective Autophagy and the dual of Ubiquitination/Phosphorylation to control nutrient starvation in *Arabidopsis thaliana*

Abstract

The plant growth and development need an efficient handling with nutrient requirements such as metals including iron, zinc, phosphorus, *et cetera,* in addition to carbon and nitrogen. The plant cell copes with nutrient starvation via multiple responses such as the regulation of transporter proteins to adjust the uptake activity and to regulate nutrients translocation. In addition, under these conditions the plant cell systematically recycles nutrients through the autophagic pathway as a rapid and effective solution to reduce its nutritional needs. Autophagy involves a network of signaling pathways especially at the level of proteins' Posttranslational Modifications (PTMs). PTMs could be classified according to the side chain modification of defined amino acid residue of a given polypeptide. Here, we discuss the importance of reversible PTMs such as ubiquitination, Ubiquitin-like Protein Conjugation (UBL), and phosphorylation during the autophagic process in *Arabidopsis thaliana*. Some cues such as developmental transitions and biotic and abiotic stress, including nutrient starvation, senescence, and dark, activate autophagy as a cellular and organismal response. Here, we summarize the recent advances in the contribution of autophagy in nutrient recycling and remobilization during stress

conditions in *A. thaliana*, with emphasis on PTMs of key components of the molecular machinery involved.

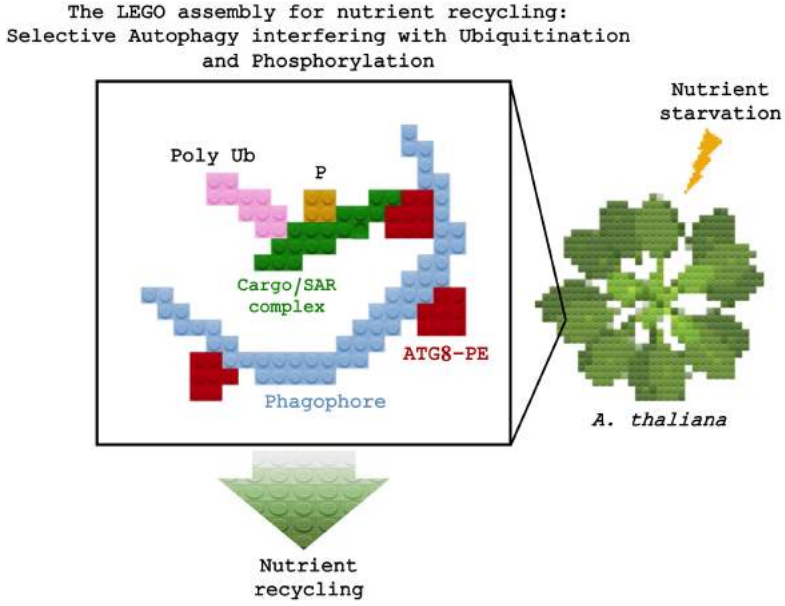

1.1 Introduction

During the lifespan of a plant cell, proteome regulation drives plant growth and development, as well as countering biotic and abiotic stress. In the plant cell, many mechanisms and processes are under the control of stress condition. Autophagy is one of these processes. It is a highly conserved catabolic mechanism in Eukaryotes. Autophagy is upregulated upon nutrient starvation as a mean of recycling the building blocks of unnecessary or superfluous cellular components. Hence, autophagy act as a mechanism of nutrient recycling at the cellular and the whole organism levels (Pottier *et al.*, 2019; Masclaux-Daubresse *et al.*, 2017; Chen, Shinozaki, *et al.*, 2019). Furthermore, autophagy deficient mutants are relatively more sensitive to stressful conditions (Pottier *et al.*, 2019; Chen, Shinozaki, *et al.*, 2019; Magen *et al.*, 2022). machinery. The autophagy pathway can degrade a portion of the cytoplasm including defined organelles (Bassham, 2007; Michaeli *et al.*, 2016; Zeng *et al.*, 2019). During this process, defined cargos are engulfed by a double membrane vesicle, termed autophagosome. The autophagosome's initiation, elongation, and maturation are marshaled by autophagy-related genes (ATGs) (Marshall and Vierstra, 2018; Yoshimoto and Ohsumi, 2018). In the plant cell the mature autophagosome, is targeted and fused with the tonoplast and its content degraded by vacuolar hydrolases. Under normal growth conditions, the autophagic pathway functions at a basal level. Under stressful conditions, autophagy is upregulated as a response to various biotic and abiotic cues (Avin-Wittenberg *et al.*, 2018; Marion *et al.*, 2018). We will discuss the functioning of this resilient pathway in plant metabolism by highlighting the contribution of protein post-translational modifications (PTMs) in the regulation of the autophagic

molecular. PTMs are versatile processes affecting the structure, stability, biological function, activity, and subcellular localization of a target protein. PTMs could be reversible or irreversible modification of the target protein, resulting in structural changes or triggering the recruitment of interactant molecules (Kong *et al.*, 2021) **(Figure 1)**. PTMs could result in protein turnover and protein-protein interaction ((Gough and Sadanandom, 2021; Withers and Dong, 2017; Vu *et al.*, 2018). PTMs have become a major subject in plant protein research, especially reversible PTMs, such as ubiquitination, Ubiquitin like-protein-conjugation (UBL), phosphorylation, and acetylation (Friso and Van Wijk, 2015).

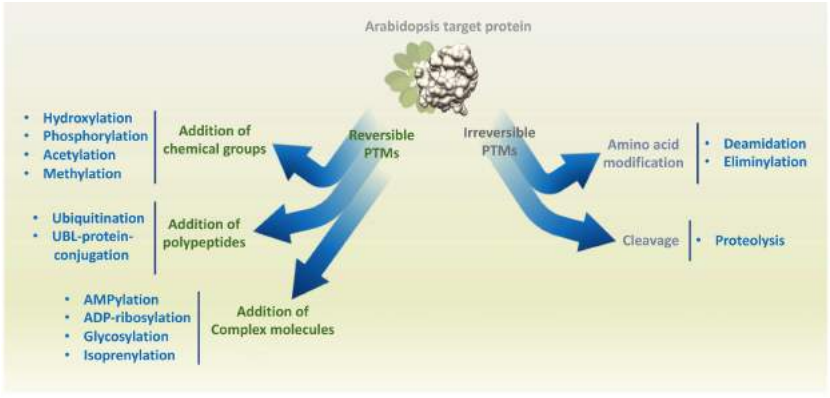

Figure 1. Reversible and irreversible Post-Translational Modifications (PTMs) of a target protein.

1.2 Autophagy mechanism in Arabidopsis : The implication of ubiquitination and phosphorylation

1.2.1 The Ubiquitin-like protein-conjugation complex

The plant ubiquitin-like protein assembly includes a diverse assortment of small proteins. Most of them (75%) are known as UBLs, which are covalent modifiers with analogous E1-like and E2-like activities catalyzing attachment: SUMO (for small ubiquitin-like modifier), ATG8 (for autophagy 8), and ATG12 (for autophagy 12), MUB (for membrane-anchored ubiquitin-fold protein), UFM1 (for ubiquitin-fold modifier1), RUB (for related to ubiquitin), HUB1 (for homology to ubiquitin1), *et cetera* (Vierstra, 2012). The left 15% are Ubiquitin-like domain (UBLD)-containing proteins. UBLD are associated with the ubiquitin system. Despite they have a β-grasp fold and a structural similarity to Ub, they are not able to act as covalent modifiers because of the absence of the ubiquitin coding region in their ORFs (Callis, 2014). UBL-proteins share a similar three-dimensional structure conserving the Ub fold (a globular core with a pocket of four interacting β-strands within whichα-helices are arranged diagonally) (Park *et al.*, 2011). Indeed, Ubiquitin coding regions are highly conserved in plants. It has been shown that ATG8, MUB, and SUMO encode more than 80% of the plant Ub sub-families. Members of ATG8 and MUB Ub-subfamilies were duplicated through whole genome duplications, while SUMO loci were generated through retro position and tandem duplications (Hua *et al.*, 2018).

1.2.1.1 ATG8_PE and ATG12 conjugation systems: Key requirement in autophagosome formation

The central constituents of ATG8_PE and ATG12 conjugation systems: Ubiquitin-like proteins ATG8, ATG12a, ATG12b, and ATG7, in addition to the E2-like enzymes ATG5 and ATG10, are structurally and functionally conserved during evolution in plants (Qi *et al.*, 2021). ATG8 and ATG12 proteins are functionally attached to the lipid phosphatidylethanolamine (PE) and the ATG5 protein during different stages of the autophagy process, including the biogenesis (elongation, engulfment, and then the delivery of the autophagosome to the lytic vacuole) (Chung *et al.*, 2010). ATG8 and ATG12 conjugation systems are crucial for autophagosome expansion and dynamics (**Figure 5**). To be activated, the ATG8 precursor is targeted by the ATP-dependent activating enzyme ATG7 (E1-like enzyme) after being proceeded by ATG4 (This leads to exposing the ATG8 C-terminal glycine). Then, the mature ATG8 is transferred to the conjugating enzyme ATG3 (E2-like enzyme) to be anchored with e to the lipid phosphatidylethanolamine (PE). The linkage between ATG and PE depends on the ATG12 conjugation system (**Figure 2**). ATG12 is proceeded by ATG10 conjugation enzyme and ATG7 to link its C-terminal glycine with a conserved lysine of ATG5. Two complexes ATG12-ATG5 (E3-like enzyme) are associated with a dimeric coiled-coil scaffold protein ATG16 to mediate the lipidation of ATG8. Atg8–PE directly interacts through the noncanonical AIM motif in ATG12. ATG8-PE/ATG12-ATG5 form a complex form through homogeneous oligomers. (Kaufmann *et al.*, 2014; Walczak and Martens, 2013; Fujioka *et al.*,

2008; Marshall and Vierstra, 2018) The complex Atg12–Atg5-Atg16 is flexible and localizes exclusively to the convex face of the phagophore to be able to bind target proteins. This complex could be released before or after autophagosome completion (**Figure 2**). While ATG8 could be found at the convex and concave faces of the autophagosome, most ATG8-PE at the convex face. After finishing the formation of the autophagosome, ATG8-PE on the convex face is delipidated by ATG4, releasing ATG8. While ATG8-PE at the concave face will be consumed in the vacuole (Kaufmann *et al.*, 2014; Marshall and Vierstra, 2018; Barros *et al.*, 2020). ATG8-PE is in conjugation with PI3P, which is bound by a dimer of SRC HOMOLOGY-3 (SH3P2). Dimers of SH3P2 interact with ATG8-PE through its AIM-like motif and stimulate phagophore curvature. The double-membrane phagophore, before closing, is decorated by the PI3P complex, including VPS34, VPS15, VPS38, and ATG6. This complex is crucial for vesicle nucleation (Zhuang *et al.*, 2018). PI3P mediates the anchoring of ATG18, which is needed for the recruitment of ATG9 vesicles from the Golgi–endosomal system (Barros *et al.*, 2020; Geng and Klionsky, 2008; Zhuang and Jiang, 2014; Zhuang *et al.*, 2013; Sun *et al.*, 2022). The recruitment of ATG9 vesicles to the pre-autophagosomal structure promotes phagophore elongation (**Figure 2**). The deleterious mutation in ATG9 affects autophagy flux and triggers to decrease in the level of autophagosome biogenesis and ATG8 cleavage without altering the lipidation process of ATG8, suggesting that alternative membranes might contribute to autophagosome formation (Zhuang *et al.*, 2018). In plants, ATG9 interacts with ATG18 and ATG2 (**Figure 2**). The interaction between ATG9 and ATG18 is transient, while the role of

ATG18-ATG2 in phagophore extension is still unknown (Kotani *et al.*, 2018; Gómez-Sánchez *et al.*, 2018; Wun *et al.*, 2020).

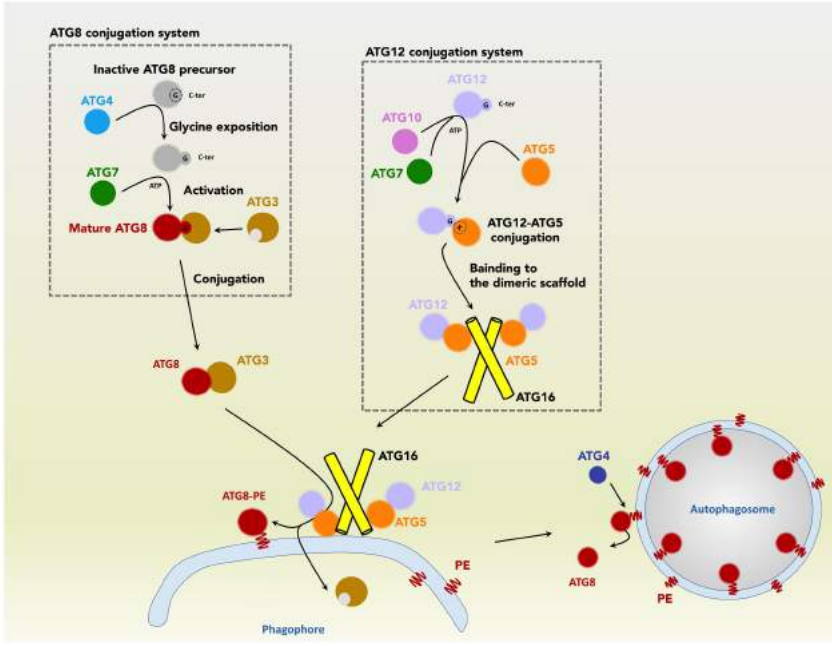

Figure 2. Schematic representation of the ATG conjugation complexes regulation during autophagy.

1.2.2 Autophagy regulation between phosphorylation and dephosphorylation

1.2.2.1 Regulation of the initial core in autophagy machinery: Phosphorylation targets ATG1 complex

Phosphorylation is a quick and reversible regulating mechanism based on the activity of Ser/Thr kinases and phosphatases. It is considered a pivotal signal for autophagy initiation (H., Li *et al.*, 2022). In plants, the ATG1-ULK complex (so-called ATG1/ATG13 complex or simply ATG1 complex) is considered the initial core machinery responsible for autophagy activation leading to initiate the autophagosome formation. The functioning of the ATG1 complex depends on the phosphorylation of its components (**Figure 3**). The ATG11 kinase complex is composed of multiple subunits: principally four ATG1 genes (ATG1a, ATG1b, ATG1c, and ATG1t) and two ATG13 genes (ATG13a and ATG13b), in addition to ATG11 and ATG101 (Li *et al.*, 2014; Wang and Hou, 2022). The Arabidopsis *atg1abct*, *atg11,* and *atg13ab* null mutants are characterized by early senescence. These mutants are hyper-sensitive to nitrogen starvation and only carbon short-term carbon starvation (Suttangkakul *et al.*, 2011; Li *et al.*, 2014). ATG1 proteins are characterized by a conserved kinase domain (KD) at the N-terminal (a kinase active site and a nucleotide (ATP) binding motif), two tandem microtubule-interacting

transport (MIT1 and MIT2) domains at the C-terminal (used to recognize Atg13), and a conserved Atg8 interacting motif (AIM) (mediating the autophagic degradation of the complex Atg1/Atg13/ATG8). The AIM motif exists in ATG1a, b, and c, but not in ATG1t, known for its lack of C-terminal regulatory domain (Wang and Hou, 2022; H., Li *et al.*, 2022). ATG1 does not interact directly with ATG11, which acts with ATG101 as a scaffold. The indirect interaction between ATG1 and ATG11 depends on the bridge ATG13 in interacting with both proteins (Li *et al.*, 2014). ATG13 contains a HORMA regulatory domain at N-terminal and IDR domains at the C-terminal.

1.2.2.2 The dual of TOR /SnRK1 complexes modulates the phosphorylation of ATG1 complex

ATG13a possesses a TOS (TOR signaling) motif, which triggers its binding to RAPTOR (raptor protein in the TOR) to negatively regulate autophagy (Son *et al.*, 2018; Mugume *et al.*, 2020). TOR targets both ATG13 and ATG1b/c (Van Leene *et al.*, 2019). It has been shown that TOR overexpression triggers autophagy inhibition (Pu, Luo and Bassham, 2017; Pu, Soto-Burgos, *et al.*, 2017; Burkart and Brandizzi, 2021; Shi *et al.*, 2018; Liu and Bassham, 2010) (**Figure 3**). During nutrient sufficiency, TOR interacts with its effectors RAPTOR and *LETHAL WITH SEC THIR-TEEN8 (LST8)* to hyper phosphorylates ATG13 and to phosphorylates ATG1b/c (via S182 of ATG1b and S174 in ATG1c) which reduces their activity to interact with ATG13. While, the inactivation of TOR leads to the dephosphorylation of ATG13, which activates autophagy (Alers *et al.*, 2012; Van Leene *et al.*, 2019;

Liao and Bassham, 2020; H., Li *et al.*, 2022). During nutrient starvation, a TOR kinase antagonistic phosphorylation system is established. ATG1 is hyperphosphorylated by KIN10 (subunit of SNRK1), triggering an increase in its activity in autophagy initiation. Overexpression of KIN10 enhances the phosphorylation of ATG1 Proteins. Also, KIN10 interacts with the TOR complex subunit RAPTOR leading to its phosphorylation (Chen *et al.*, 2017). SnRK1 is unable to induce autophagy when TOR is also activated (Soto-Burgos and Bassham, 2017) (**Figure 3**). Furthermore, it has been demonstrated that under long-term carbon starvation, KIN10 hyper phosphorylates ATG6, which promotes the activation of the ATG6-ATG13 complex and phosphorylates the PI3K complex to trigger autophagy (Augustine, 2019).

1.2.2.3 Phosphorylation and autophagy: Further than ATG1 complex regulation

It has been demonstrated that under carbon long-term starvation, autophagy is induced through the phosphorylation of the ATG6 subunit within the PI3K complex by the SNF1 (*sucrose non-fermenting 1*) kinase homolog 10 (KIN10, also known as SnRK1.1 (subunit of SNRK1)). Therefore, this process provokes phagophore nucleation. It is considered an alternative route to activate autophagy, independent of the ATG1/ATG13 complex, under long-term starvation (Huang *et al.*, 2019). Moreover, under nutrient starvation, ATG1a/b/c phosphorylate the *TUMOR NECROSIS FACTOR RECEPTOR-ASSOCIATED FACTOR*T1a (RAF1a) to stabilize it. In addition, this process blocks the ubiquitination of ATG6 and ATG13, physically interacting with

TRAF and SINAT, which triggers its degradation via the proteasome (Qi *et al.*, 2017; Qi *et al.*, 2022).

In Arabidopsis, the ATG18a subunit from the ATG9 complex is targeted to be phosphorylated. The phosphorylation of ATG18a affects autophagosome formation and its subsequent delivery into the vacuole. It has been shown that during infection with the necrotrophic pathogen *Botrytis cinerea*, *BRI1-ASSOCIATED RECEPTOR KINASE 1* (BAK1) kinase interacts with and phosphorylates ATG18a. This leads to a decrease in autophagy levels as a primary response to pathogen infection. BAK1 phosphorylates Thr241, Ser328, Ser361, and Thr387 in ATG18. The degradation or the mutation of BAK1, in addition to the dephosphorylation of Ser344, Ser361, Thr241, Ser328, and Thr387 in ATG18, triggers autophagy during the resistance against *B. cinerea* infection (Zhang *et al.*, n.d.; Sertsuvalkul *et al.*, 2022).

Other complexes in plant autophagy could be potential targets for phosphorylation. Based on results from the mass spectrometric phosphoproteomic database (Willems *et al.*, 2019), Li *et al*., 2022 established a study of phosphorylation sites of all the core ATG proteins in *Arabidopsis thaliana* by using MaxQuant, SEQUEST, and MASCOT algorithms. Most of these predicted phosphorylation sites are- 40 -egulatively confirmed regarding their potential influence on the autophagy process. On the other hand, As was shown in the previous section, Brassinosteroids regulation under stress depends on phosphorylation mediated by the *GSK3-like kinase* (BIN2). This kinase mediates the phosphorylation of the ubiquitin receptor protein DSK2.

Which allows it to interact with the ubiquitinated master regulator in the brassinosteroid *E3 ligase BRUTUS1* (BTS1). This mechanism triggers the interaction between the phosphorylated DSK2 and ATG8, promoting the degradation of the complex via selective autophagy. Phosphorylation of DSK2 yields a negative regulator in the BR pathway under stress.

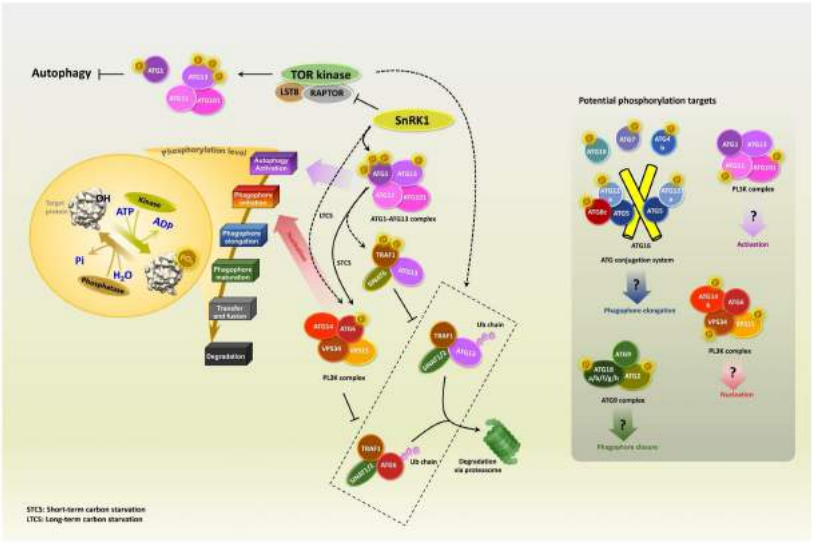

Figure 3. Schematic representation of phosphorylation in the core of ATG proteins during autophagy.

1.2.3 Autophagy and ubiquitination

1.2.3.1 The ubiquitin protein (Ub) in brief

Ubiquitin (Ub) is a hydrophobic small β-grasp fold protein. It is characterized by its high degree of amino acid sequence conservation between animals, fungi, and plants. The about 76 amino acids are structured into 3.5 turns of an amphipathic α-helix and a short 3_{10}-helix packed against a five-strand β-sheet with seven reverse turns containing a core of sixteen to seventeen hydrophobic residues (Callis, 2014; Vijay-kumar *et al.*, 1987) (**Figure 4**). Ubiquitination of a given substrate could result in mono-ubiquitination (addition of a single ubiquitin moeity to the substrate), multi-mono-ubiquitination (mono-ubiquitination of multiple site within the same target), or polyubiquitination (ubiquitin chains of different length can be added to the substrate) (Callis, 2014). Ubiquitin is attached to target proteins via its specific lysine by an enzymatic cascade (Callis, 2014). The ubiquitin attachment by lysine 48 is the most abundant polyubiquitination linkage triggering ATP-dependent protein degradation via the proteasome. In general, ubiquitinated proteins can undergo the reversible path of deubiquitination, resulting in their rescue from degradation and ubiquitin removal. This process is catalyzed by deubiquitinase enzymes (DUBs). All discovered Arabidopsis DUBs contain a conserved cysteine residue in their catalytic domain (Yan *et al.*, 2000; Park *et al.*, 2022)

1.2.3.2 Proteaphagy or ubiquitination-dependent autophagic degradation of the 26S proteasome

In Arabidopsis, ~5% of the proteome (approx.1500 protein-encoded genes) encode for the ubiquitin/26S proteasome system (UPS). About 90% of these genes encode for subunits of the E3 ubiquitin ligases (Moon *et al.*, 2004; Smalle and Vierstra, 2004).

UPS and autophagy are are interconnected, through their respective regulatory mechanisms, and also some substrates. The UPS essentially targets soluble, short-live proteins. In contrast, autophagy can target long-live soluble aggregated proteins. It has been reported that in autophagy defective mutants, the level of proteasome subunits is increased in the cell (Marshall *et al.*, 2015)**.** The level of proteasome-related proteins is higher in *atg5* null mutant as compared to the Arabidopsis WT. When inactivated, the 26S proteasome can be degraded via selective autophagy (Su *et al.*, 2020). This process, coined proteaphagy, first described in Arabidopsis, is also active in yeast and mammalian cells (**Figure 4**). Inactivation can be achieved experimentally using drugs such as bortezomib and MG132, but also some by pathogen effectors such as HopM1 from *Pseudomonas* resulting in proteaphagy. In this process, a specific component of the regulatory complex of the 26S, RPN10 (in Arabidopsis), acts as a selective a autophagy cargo receptor, interacting with lipidated ATG8 within the phagophore (**Figure 4**). RPN10 interacts with the hydrophobic patch on ATG8 known as UIM (ubiquitin interacting

motif) docking site (UDS, UIM docking site), but not the LIR/AIM docking site (LDS) of ATG8. RPN10 contains 3 ubiquitin-interacting motifs at its C-terminus. UIM1 and UIM2 are needed to link ubiquitinated proteasome to ATG8-PE (Marshall and Vierstra, 2019).

The physiological relevance of the 26S proteasome degradation through selective autophagy could be in response to nitrogen starvation (Marshall and Vierstra, 2019). N starvation increases proteaphagy in WT Arabidopsis plants. In contrast, under the same conditions, the proteasome is more active in autophagy-deficient *(atg)* mutants. The autophagy core component ATG6 and ATG13 can be ubiquitinated and degraded by the 26S proteasome

Under nutrient starvation, the RING-type E3 ubiquitin ligase *SEVEN IN ABSENTIA OF ARABIDOPSIS THALIANA 6 (SINAT6)*, directly interacts with ATG13 and induce autophagosome biogenesis. Under this condition, ATG1 phosphorylates and stabilizes the *TUMOR NECROSIS FACTOR RECEPTOR ASSOCIATED FACTOR1a (TRAF1a)*. While during nutrient-rich conditions, TRAF1a and TRAF1b interact with ATG13a and ATG13b in the presence of SINAT1 and SINAT2 to mediate their polyubiquitination and degradation through the 26S proteasome pathway (**Figure 4**). The ubiquitination-triggered degradation of ATG13s under sufficient nutrient condition inhibits autophagy (Qi *et al.*, 2020). Moreover, the same mechanism has been demonstrated for ATG6 destabilization and degradation. TRAF1a and TRAF1b interact with ATG6 and require

SINAT1 and SINAT2 E3 ligases to mediate their ubiquitination and degradation via the 26S proteasome (Lockhart, 2017; Qi *et al.*, 2017; C., Zhang *et al.*, 2019).

1.2.3.3 Examples of ubiquitinated proteins under iron deficiency: a cargo for SARs

SARs (selective autophagy receptors) interact with autophagy cargos. Some ubiquitinated proteins could be considered as cargos for autophagy. SARs selectively bridge cognate ubiquitinated cargos to lipidated ATG8 anchored to the phagophore membrane for their autophagic degradation (Lamark and Johansen, 2021).

For example, drought and nutrient starvation especially iron deficiency promotes the accumulation of brassinosteroids. These polyhydroxylated steroidal plant hormones modulate iron physiological response by mitigating iron deficiency and improving nutritional status. Moreover, brassinosteroids trigger Fe accumulation iron roots, steams, and leaves (Lima *et al.*, 2018; dos Santos *et al.*, 2020; Kapoor *et al.*, 2022). It has been shown that brassinosteroids promote carbon assimilation capacity and chlorophyll contents (Siddiqi and Husen, 2021). Furthermore, under drought and nutrient starvation autophagy regulates brassinosteroids signalling. SINAT2 interacts with BES1 (master regulator of brassinosteroids), mediating its ubiquitination. Ubiquitinated BES1 interacts with the ubiquitin/autophagy receptor DSK2, which is phosphorylated by BIN2 to expose its AIM interaction motif with the autophagy ATG8 protein. Ubiquitination of BES1

triggers its degradation via selective autophagy (Nolan *et al.*, 2017; C., Zhang *et al.*, 2019).

It was demonstrated that under iron deficiency, providing sulfur (S) is beneficial to enhance Fe contents in seeds. Iron storage increases the demand of sulfur which is crucial for iron accumulation. The interaction Fe/S helps in the management of iron under starvation condition. In addition S-containing metabolites are the precursor for the synthesis of ethylene and phytosiderophores needed in iron metabolism (Astolfi *et al.*, 2021). Moreover, S deficiency induces autophagy and increases the level of *NEIGHBOR OF BRCA1(NBR1)* (Y., Zhang and Chen, 2020). Transcriptome analysis showed that the overexpression of NBR1 leads to an alteration in plant response to sulfur deficiency (Tarnowski, Collados Rodriguez, *et al.*, 2020). Furthermore, NBR1 is considered an autophagy receptor for ubiquitinated insoluble proteins in aggregation, so-called aggrephagy (Michaeli *et al.*, 2016; Su *et al.*, 2020). The Arabidopsis ubiquitin receptor NBR1 guides protein aggregates into the autophagosomes (Zhou *et al.*, 2013). NBR1 is also targeted for ubiquitination through the C-terminal UBA domain of the two UBA domains (Y., Zhang and Chen, 2020). NBR1 interacts with ABI5, the regulatory protein of ABA. This interaction requires the UBA domain to mediate ubiquitination and degradation of NBR1 under ABA stress (Y., Zhang and Chen, 2020; Tarnowski, Rodriguez, *et al.*, 2020). Under sulfur starvation, NBR1 modulates the degradation of the *PUTATIVE RIBOSOMAL PROTEIN S6 (RPS6)*, which is known to be linked with autophagy signaling via the TOR-RPS6 kinase-RPS6 pathway. NBR1 recognizes RPS6 and binds it outside the NBR1

ubiquitin-binding domains, then NBR1 binds to ATG8 through its specific short amino acid motifs (LIR). RPS6 degradation via selective autophagy influences ribosome activities and/or biogenesis during sulfur starvation (Tarnowski, Collados Rodriguez, *et al.*, 2020; Sirko and Masclaux-daubresse, 2021).

Furthermore, under iron deficiency plant-specific component of the endosomal sorting complex required for transport (ESCRT) so called *FYVE DOMAIN PROTEIN REQUIRED FOR ENDOSOMAL SORTING1 (FREE1)* is down regulated and transported to the vacuole (Zhang *et al.*, 2021). FREE1 is essential for MVBs biogenesis and plant growth and development. Autophagy *atg5* and *atg7 null mutants* are hypersensitive to iron deficiency and characterized to accumulate more endogenous FREE1 protein than WT (Zhang *et al.*, 2021). It has been shown that ubiquitinated FREE1 is delivered to the vacuole via autophagy under iron deficiency (Zhang *et al.*, 2021). It was demonstrated that iron deficiency promotes the induction of SINA of *Arabidopsis thaliana* 4: SINAT (SINAT-4 E3 ubiquitin ligases). SINAT4-FREE1 is considered as regulatory module for the plant response to iron deficiency stress (Xiao *et al.*, 2020). Ubiquitination mediates the degradation of the key components of ESCRT pathway, such as FREE1 and *VACUOLAR PROTEIN SORTING23A (VPS23A)*, are under the control of SINAT (1 to 4) to modulate ABA related responses and signaling. Under ABA accumulation, ubiquitinated FREE1/VPS23A proteins were co-degraded by the proteasome pathway. While during post-ABA exposure, SINATs form homo- and hetero-oligomers in vivo, mediating the degradation of the

ubiquitinated FREE1/VPS23A via selective autophagy (**Figure 4**). It has not been demonstrated how autophagy targets SINAT oligomers during FREE1/VPS23A degradation (**Figure 4**). Results from Co-IP analysis indicate a potential implication of NBR1 in this process (Xia *et al.*, 2020).

1.2.3.4 Ubiquitination in Xenophagy

Iron plays a complex role in plant-pathogen interactions. Systematically, plant immune response against pathogens and plant response to iron deficiency share some common points such as hormone signaling pathways and secretion of phenolics (Verbon *et al.*, 2017). Iron deficiency promotes plant defense responses. It has been demonstrated that symptom severity, bacterial fitness, and the expression of bacterial pectate lyase encoding genes were reduced in iron-deficient plants. The iron status in the plat mitigates infection by influencing both the pathogen's virulence and the host's defense (Kieu *et al.*, 2012). In addition, plant infection influence iron status in the plant, mostly is involved in ROS accumulation in plant pathogen interaction. This influence the regulation of iron related genes, especially for transport and storage (Verbon *et al.*, 2017). Moreover, Autophagy is apart from the post infection immunity response in the plant. This form of selective autophagy termed as xenophagy, is crucial for pathogen degradation (Gomes and Dikic, 2014). Besides, NBR1 participate as a SAR in xenophagy mediated by ubiquitination to recognize a set of polyubiquitinated bacterial effectors and viral capsids. NBR1 is involved in the immune response against the bacterium *Xanthomonas campestris pv. Vesicatoria* (Xcv). The

bacterial type-III effector (T3E) XopL undergoes self-ubiquitination, mediating the interaction with NBR1 and triggering its degradation via xenophagy. Xpol can interact with the autophagy component SH3P2 via its E3 ligase activity, mediating its degradation via the proteasome. By degrading SH3P2, Xcv is able to suppress autophagy during infection, which decreases the anti-bacterial response (Leong, Raffeiner, *et al.*, 2022; Leong, Langin, *et al.*, 2022). In addition, during plant infection with turnip mosaic virus (TuMV), NBR1 targets the viral RNA silencing suppressor helper-component proteinase (Hcpro) contained in complex PGs in association with virus-induced RNA granules, the stress granule components (UBP1 and eIF4E) and the processing body components (AGO1, DCP1, and VCS, ribosomal P0) to degradation via selective autophagy (Hafrén *et al.*, 2018; Kushwaha *et al.*, 2019). Another example of ubiquitination-mediated xenophagy happens during the suppression of plant RNA silencing (plant antiviral defense by targeting degradation of viral proteins associated with dsRNA-induced RNA silencing from RISC complex and through the dicer enzymes) by the P0 protein from poleroviruses (single-stranded RNA (ssRNA) viruses) suppressor after infection. P0 recruits the host SCF F-box ubiquitin-protein ligase mediating the ubiquitination of the endoplasmic reticulum (ER)-associated AGO1 (a key component of RISC is ARGONAUTE1). This process involves ATG8-interacting proteins 1 and 2 (ATI1 and ATI2) that interact with AGO1 and triggers its degradation via selective autophagy. While autophagy is not the unique pathway for P0-Mediated AGO1 degradation. When autophagy was impaired by using specific autophagy inhibitors such as 3-MA (that block autophagosome formation by the inhibition of type III phosphatidylinositol 3-kinases (PI-3K)) and E64d (inhibit the

degradation of autophagic cargo), P0-Mediated AGO1 degradation is mediated via the 26S proteasome (Y., Zhang and Chen, 2020; Derrien *et al.*, 2012; Michaeli *et al.*, 2019; Clavel *et al.*, 2017). Ubiquitination-mediated xenophagy during RNA silencing Also happens during the infection with the Turnip mosaic virus (TuMV), which causes an increase in the *SUPPRESSOR OF GENE SILENCING 3 (SGS3)* levels. The Potyvirus Silencing Suppressor Protein VPg interacts with SGS3 and triggers its degradation via both the autophagy and ubiquitin-proteasome pathways (Cheng and Wang, 2017).

1.2.3.5 Ubiquitination in Chlorophagy

Chloroplasts are the most system containing iron in plant cells. This is due to the high demand for Fe cofactors during the photosynthetic electron transport. Most of iron in the plant is sequestrated in the chloroplasts predominantly found as heme or Fe–S clusters or stored in ferritins (FER). In plants, the major target process during iron deficiency stress is photosynthesis. During iron starvation, plants young green tissues turn to become chlorotic. At the same time the biosynthesis of chlorophyll is decreased. Young tissues contain developing chloroplasts and need iron remobilization from mature tissues during iron deficiency (Gretchen E. Kroh and Pilon, 2020). In addition, iron deficiency triggers the overgeneration of reactive oxygen species (ROS) by chloroplasts, which results to oxidative stress causing cell damage. This stressful condition trigger rapid mechanisms resulting in dismantling of damaged chloroplasts. Chloroplast could be

degraded via three ways: senescence associated vacuoles (SAV), chloroplast vesiculation (CV) , and autophagy of the whole chloroplast termed chlorophagy (Domínguez and Cejudo, 2021). Most of the time, membrane proteins of the damaged chloroplast are targeted for polyubiquitination. Under light stress, most often but not necessarily, the cytoplasmic-localized E3 ligase PUB4 (Plant U-Box 4) is implicated in triggering selective autophagy (chlorophagy) (Woodson *et al.*, 2015; Kikuchi *et al.*, 2020). Under nutrients starvation, chlorophagy could be provoked through *ATI1 (ATG8-INTERACTING PROTEIN1)-decorated* plastid bodies or by the RCB pathway (autophagy targets a part of stroma via the Rubisco-containing body). It is known that damaged chloroplasts accumulate in Autophagy defective mutants *atg5* and *atg7* (Izumi *et al.*, 2017; Su *et al.*, 2020). It has been suggested that the ubiquitination of complexes in the plastid outer membrane, mainly the *TRANSLOCON AT THE OUTER ENVELOPE OF CHLOROPLASTS (TOC)* by SP1 RING-type ubiquitin E3 ligase could mediate chloroplast degradation in a non-autophagic way during plant development stage (Ling *et al.*, 2012).

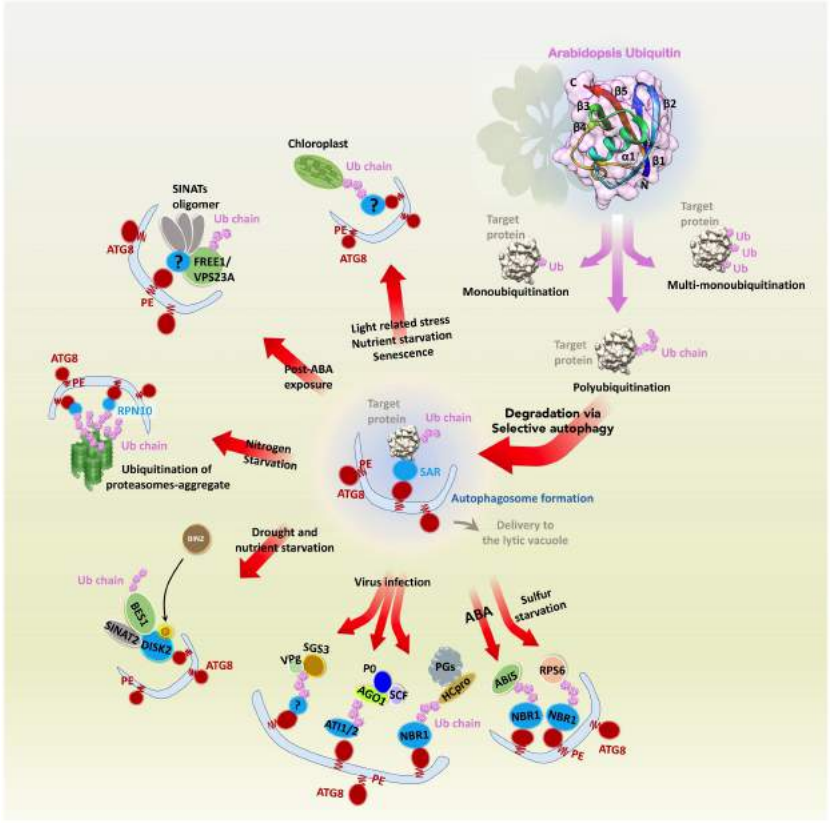

Figure 4. Schematic representation of ubiquitination regulating some protein degradation via autophagy and the proteasome.

1.3 Autophagy and nutrients management in Arabidopsis.

1.3.1.1 Potential link between nutrient starvation, abscisic acid signaling, and autophagy

ABA levels quickly increased due to nutrition starvation. ABA signaling mediates the control of high ROS levels resulting from oxidative conditions caused by nutritional deficiencies (Rubio *et al.*, 2009). It has been shown that ABA induces SnRK1 regulatory subunit expression and controls its activity at the post-translational level (**Figure 5**). The ABA-inactivated PP2C phosphatases (key negative regulators in ABA signaling) dephosphorylate and inactivate both SnRK1 and the related (ABA signaling) SnRK2 kinases (Rodrigues *et al.*, 2013; Hulsmans *et al.*, 2016). Under nutrient starvation, ABA binds to the pyrabactin-like (PYL) protein family and inhibits PP2C proteins from activating SnRK2. Then, SnRK2 phosphorylates the RAPTOR subunit to inhibit TOR activity (Wang *et al.*, 2018; Belda-Palazón *et al.*, 2020). Moreover, ABA could trigger autophagy trough the activation of the *Respiratory burst oxidase homolog* (Rboh) (NADPH oxidase in animals) (Signorelli *et al.*, 2019). It has been shown that *rboh null mutants* are characterized by deficiency in ROS production and reduced autophagic activity under hypoxia (Chen *et al.*, 2015). Besides, hydrogen sulfide is a negative regulator of autophagy through the persulfidation of ATG4. Nitrogen starvation and osmotic trigger the proteolytic activity of ATG4. Under these conditions, ATG4 activity could be inhibited by sulfide. ABA reduces ATG4 persulfidation triggering to activate autophagy in the cell (Laureano-Marín *et al.*,

2020; Sirko *et al.*, 2021). Furthermore, some SARs are associated in ABA signaling pathway. It has been shown in *planta* that NBR1 interacts with three regulatory proteins of ABA (ABI3, ABI4 and ABI5). This suggests the fine-tuning role of NBR1 in the ABA signalling pathway. In addition, ABA levels are enhanced in shoots when NBR1 was overexpressed (Tarnowski, Rodriguez, *et al.*, 2020; Y., Zhang and Chen, 2020). Moreover, in Arabidopsis ABA transiently induces the tryptophan-rich sensory protein-related (TSPO). This results in heme scavenging and targeting to autophagic degradation in the vacuole (Vanhee, Zapotoczny, *et al.*, 2011; Vanhee and Batoko, 2011b).

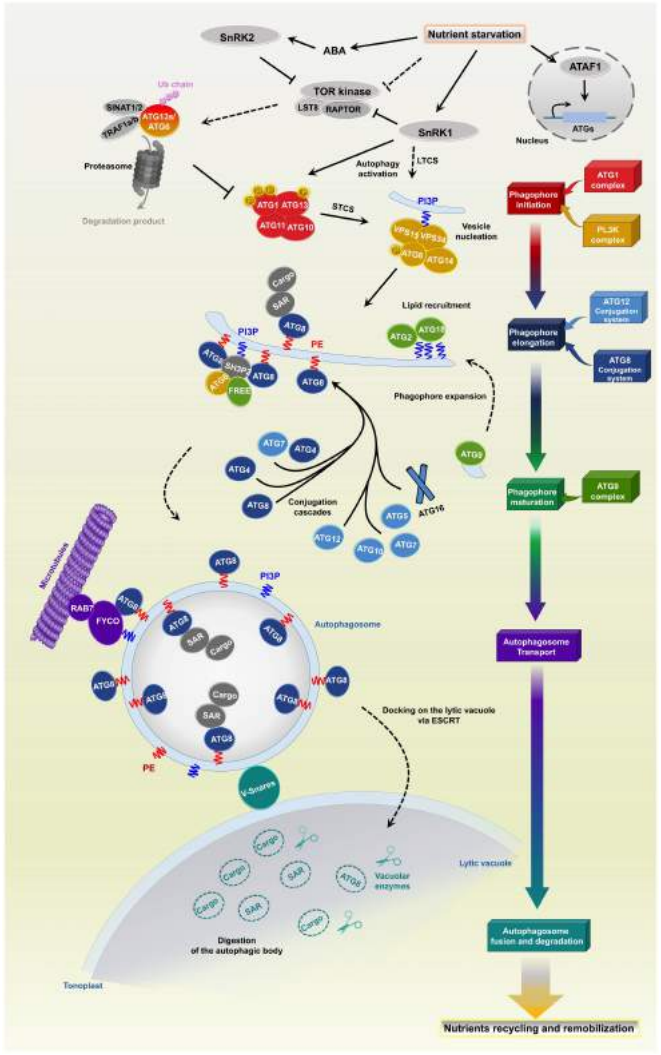

Figure 5. Schematic representation of the ATG-mediated autophagy pathway under nutrient starvation.

1.3.2 Autophagy as a plant nutrient recycling process

1.3.2.1 Autophagy and C/N recycling

In standard growth conditions, autophagy participates at the slightest level in multiple processes to maintain cell homeostasis. While under abiotic stress or senescence, autophagy levels are upgraded to act as a rapid intervention process triggering the degradation of increasing toxic and damaged components. The autophagic degradation occurring in the lytic vacuole results in material recycling. Under nutrient starvation, autophagy leads to creating a quick new source of re-useful nutrients (Masclaux-Daubresse *et al.*, 2017). The plant immediately serves itself from this recycled pool to remobilize nutrients. A good example of nutrient recycling mediated by autophagy is nitrogen. Under N starvation, the autophagic degradation pathway controls N remobilization from source organs (leaves) to sink (seeds). It has been shown that ^{15}N remobilization was decreased (60% less N) *in atg mutants (atg18a RNAi, atg5, and atg9)* under nitrogen deficiency compared to WT. *atg mutants* are characterized by a higher accumulation of N compounds (ammonium, amino acids (AA), and proteins) in their rosette leaves than WT. Under standard conditions, ^{15}N remobilization was also decreased by 40% compared to WT (Havé *et al.*, 2017). ATGs (such as ATG4b and ATG8a) transcript levels were increased under senescence and ethylene treatment mediating petal senescence (Yamada *et al.*, 2009; Shibuya *et al.*, 2013). It has been shown that ^{15}N remobilization from rosette leaves to seeds was increased by 15% in mutants overexpressing ATG8a and ATG8g

compared to the WT (Chen, Soulay, *et al.*, 2019). *Atg mutants* are hypersensitive to N/C starvation (Phillips *et al.*, 2008; Thompson *et al.*, 2005; Ishizaki *et al.*, 2005). Moreover, they suffer from impairment of nitrogen/carbon balance due to overaccumulation of nitrogen compounds. Plants mutants defective in autophagy are known for decreased capacity in nutrient remobilization and the high activity of proteases (carboxypeptidase, aminopeptidase, and endopeptidase) triggering early senescence stage (Guiboileau *et al.*, 2012; Guiboileau *et al.*, 2013). *Atg5 mutant* is known to be defective in autophagy. If grown under short days (SD), this Arabidopsis mutant is smaller than the WT and suffers from alterations in its nutritional metabolisms, such as carbon storage and sugar metabolism. Lower starch, sucrose, and hexose contents, in addition to higher glutamate, aspartate, and threonine contents, were detected in this mutant compared to WT (Guiboileau *et al.*, 2013; Izumi *et al.*, 2013; Masclaux-Daubresse *et al.*, 2014). Carbon resource management is necessary for sugar metabolism and starch production in the dark. Autophagy triggers material degradation leading to carbon recycling and promoting growth in dark/night situations (Masclaux-Daubresse *et al.*, 2017).

1.3.2.2 Autophagy and metal recycling

During senescence, Autophagy plays a key role in the cellular degradation of cytoplasmic components such as organelles. Senescence and dark-promoted senescence in leaves substantially triggers chlorophagy and especially degrades Rubisco-containing bodies (RCBs), which contain 80% of cellular nitrogen (Ishida *et al.*, 2008; Izumi *et al.*, 2010; Ono *et al.*, 2013). A chloroplast is considered an

organelle tank that intensively uses metals. It contains more than ¾ of cellular iron (Nouet *et al.*, 2011). Senescence leads to the quenching and loss of photosystem II- core components resulting in photoinhibition (Guiamét *et al.*, 2002). It has been reported that PSII photoinhibition directly triggers chlorophagy (Nakamura and Izumi, 2018). Iron in chloroplasts is almost stored in ferritins. Dark mediated senescence and photoinhibition promote ferritin genes (*Fer1,2,3,4*) expression (Tarantino *et al.*, 2003). The direct degradation of ferritins via the autophagic pathway called ferrinophagy has been described in animals. While direct involvement of autophagy in the degradation of ferritin has not been demonstrated in plants (Santana-Codina and Mancias, 2018; Wawrzyńska and Sirko, 2020). Based on Fe isotope labeling (^{57}Fe), it has been shown that autophagy is involved in iron recycling and translocation from vegetative tissues to sink organs (seeds). The capacity of iron remobilization is decreased in *atg5 mutant* by 35% compared to WT (Pottier *et al.*, 2019). In addition to impairment in Fe translocation, a decrease in zinc and manganese remobilization was observed in *atg5* and *atg4 mutants* remobilization. While the absorption of the same metals was not affected in *atg9* and *atg8RNAi* characterized by decreased autophagy capacity but not totally inhibited (Pottier *et al.*, 2019). Moreover, autophagic bodies are still detected in these mutants (Guiboileau *et al.*, 2012). Iron recycling via autophagy depends also on zinc status in the cell (**Figure 6**). Zn deficiency triggers an increase in iron by promoting the expression of the core machinery of iron uptake: *IRON-REGULATED TRANSPORTER 1 (IRT1)* and the Ferric Reductase Oxidase2 (FRO2) (Sinclair and Krämer, 2012; Humayan Kabir *et al.*, 2014; Assunção *et al.*, 2013). It has been shown that Fe^{2+} and Zn^{2+} could be transported

by IRT1 (Barberon, Zelazny, Robert, Conéjéro, Curie, Jirí Friml, *et al.*, 2011; Barberon *et al.*, 2014; Sinclair and Krämer, 2012; Vert *et al.*, 2002). Moreover, zinc deficiency promotes the iron distribution from roots to the aerial part by - 59 -egulateng a series of metal transporters (NAS4, YSLs, OPT3, FRD3, *Et cetera.*) (Rogers and Guerinot, 2002; Koen *et al.*, 2013; Waters *et al.*, 2006; Wintz *et al.*, 2003; Conte *et al.*, 2013; Stacey *et al.*, 2008). The increased allocation triggers an upgrade in the level of free Fe able to react with oxygen, generating in the chloroplast harmful free hydroxyl radicals (•OH) by the photosynthetic mediated Fenton reaction triggering chlorosis and cell death (Ravet *et al.*, 2009; J., H., Kim *et al.*, 2014; Richards *et al.*, 2015; W., Zhang and Chen, 2020). Inside the cell, Zn is bound to >5% of protein as well as in many organelles. Zn starvation triggers bulk autophagy to target Zn stores in the cell to be degraded in the lytic vacuole. This degradation process via autophagy promotes Zn recycling to be reused for cell metabolism and to alleviate the Zn deficiency impact (Shinozaki *et al.*, 2020). On the other hand, *atg mutants* are defective in autophagy. under zinc deficiency, *atg5 mutant* suffered from intense chlorosis caused by damaged chloroplast due to intensive production of harmful free hydroxyl radicals (•OH). Resulting in the overproduction of ROS and a higher level of superoxide dismutase ((SOD) antioxidant enzyme) compared to the WT (Shinozaki *et al.*, 2020). Autophagy promotes increasing Zn recycling by vacuolar Zn supplied, which can inhibit increasing Fe uptake and allocation (Shinozaki and Yoshimoto, 2021). Furthermore, the excess of Zn leads to symptoms of Fe-deficient plants (Zargar *et al.*, 2015) (**Figure 6**). The excess of Zn leads to impairment of photosynthesis and intense leaf chlorosis in old leaves (less intense in juvenile leaves) due to the harmful free hydroxyl radicals (•OH)

produced by the photosynthetic mediated Fenton reaction. Zn^{2+} can displace other divalent ions, including primarily Fe^{2+} from most of their binding sites, such as the metal transporter IRT1 (Krämer, 2005). Under this condition, IRT1 and FRO2 expression are increased, as reported in their increase under iron deficiency. While Fe concentration is significantly decreased under Zn excess (Fukao *et al.*, 2011). Damages due to excess Zn were dramatically restored by the addition of Fe (Zargar *et al.*, 2015). Under this condition, high autophagic activity is increased relative to normal Zn conditions. Fe^{3+} is recycled through autophagy, which leads to the distribution of iron to juvenile leaves as a response to the Zn excess. Under the same condition, the *atg5 mutant* is suffering from intense chlorosis even in juvenile leaves caused by a disorder in chloroplasts and a reduction in chlorophyll biosynthesis due to iron starvation (Shinozaki *et al.*, 2021; Shinozaki and Yoshimoto, 2021). Furthermore, iron could be stored in hemic forms, such as hemoproteins or free heme under oxidative stress used in ROS detoxification. A good example of a regulatory protein mediating heme scavenging, and degradation is the multistress regulator TSPO protein (**Figure 6**). Under oxidative stress, the production of heme increases, to be used by catalases and peroxidases in the reactive oxygen species (ROS) detoxification process. Free cytosolic heme is powerful toxic to the cell. In excess, it can cause cell damage by catalyzing the formation of ROS (Singh and Bhatla, 2016; Takemoto *et al.*, 2019). TSPO is transiently induced under ABA and a series of oxidative stress such as high salinity and osmotic stress (Guillaumot, Guillon, Déplanque, *et al.*, 2009). It has been shown that TSPO binds free cytosolic heme and then is targeted by ATG8 to the autophagosome. TSPO triggers the autophagic degradation of heme (Vanhee, Zapotoczny, *et al.*, 2011;

Vanhee, Guillon, *et al.*, 2011; Vanhee and Batoko, 2011a). This process logically results in an increase in the pool of labile iron stored in the lytic vacuole under oxidative stress. Furthermore, excess iron in the plant could be the direct early response to phosphate starvation: *HOSPHATE STARVATION RESPONSE 1* (PHR1) (**Figure 6**). Pi starvation promotes increasing Fe levels (transport, distribution, and accumulation) and coumarin accumulation in Arabidopsis plants, which induces severe metabolic changes (Hirsch *et al.*, 2006; Chutia *et al.*, 2021; Briat *et al.*, 2015). Pi starvation symptoms typically are observed in old rather than young leaves. Mainly leaves become purple with time cause of the accumulation of anthocyanin as a response to photo-oxidative damage. Anthocyanin accumulation precedes chlorophyll breakdown (Feild *et al.*, 2001; Diaz *et al.*, 2006). Under phosphate starvation, the quick N overloading induces impairment in C/N status, which induces chlorophagy. The N oversupply under Pi starvation induces C starvation triggering the formation of Rubisco-containing bodies (RCBs) (Yoshitake *et al.*, 2021). Under this condition, no evidence of ER stress was detected. While Pi starvation induces Autophagy on root tips. Fe excess triggers ROS production, which promotes the formation of callose and pectin polymers at the cell wall (Yoshitake *et al.*, 2021). This isolates the cell and inhibits cell-to-cell communication. Polymer overproduction is correlated with the regulation of the *LOW PHOSPHATE ROOT 1 (LPR1)* ferroxidase. Further, LPR1 is targeted to the ER and interacts with *PHOSPHATE DEFICIENCY RESPONSE 2 (PDR2)* to adjust root meristem activity to external Pi (Ticconi *et al.*, 2009). LPR1 also targets the *SINGLE ENDOPLASMIC RETICULUM (ER)-RESIDENT P5-TYPE ATPase (AtP5A)*. The association between the three proteins leads to control of

LPR1 secretion and to triggers ER-stress mediating autophagy (Naumann et al., 2019). Pi starvation activates *Pi starvation response (PSR),* leading to ER stress-associated autophagy in root tips as a consequence of sensing (Naumann et al., 2019; Yoshitake et al., 2021). In the areal part, under Pi starvation, the expression of PSR genes was higher in *atg2* and *atg5.* Iron accumulation during Pi starvation iron hyper-accumulation leads to ROS production through the Fenton reaction, which triggers ferroptosis (apoptotic cell death) and ER stress associated with autophagy. Autophagy targets membrane lipid and plastid DNA (containing Pi) to the degradation in the lytic vacuole. This mechanism yields in Pi recycling and reuse to alleviate Pi late starvation responses. It has been shown that *atg mutants* (*atg3* and *atg5*) and *OSITOL-REQUIRING ENZYME1* double mutant,ire1a ire1b (defective in ER stress responses) are not able to recycle Pi via ER-phagy under Pi starvation, as HPR1 (Yoshitake *et al.*, 2022).

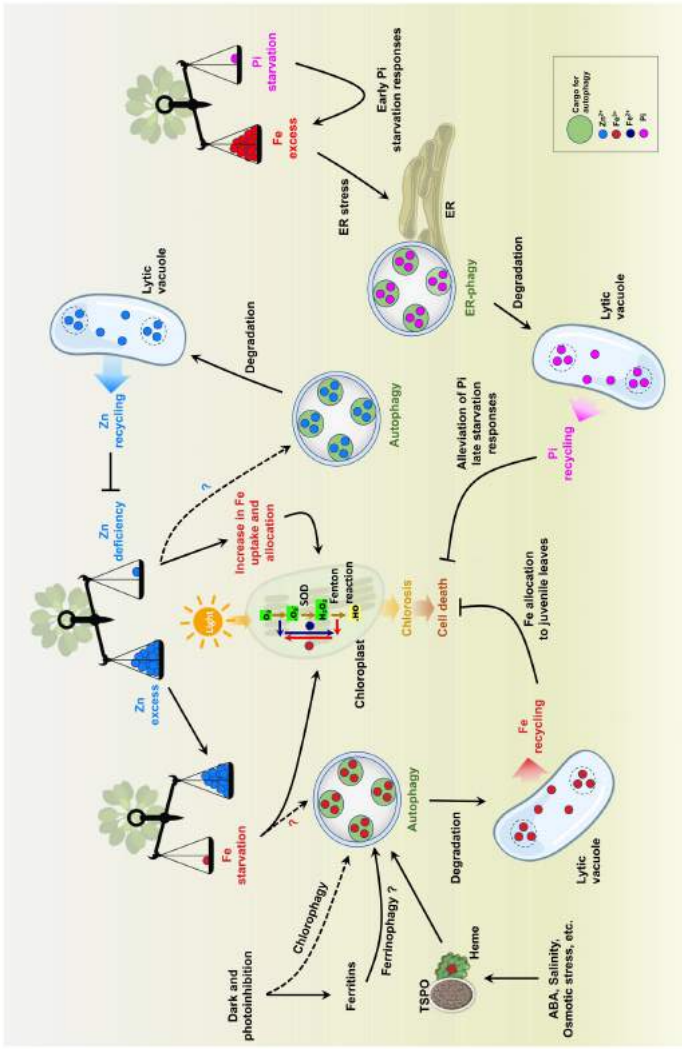

Figure 6. Schematic representation of Zn, Fe, and Pi recycling mechanism via autophagy under starvation and excess.

1.4 Conclusion

Autophagy is an essential process for degrading and recycling cytoplasmic materials in plants. Modulation of the autophagic activity is partly controlled by posttranslational regulations of some component of the dedicated molecular machinery. Understanding how PTMs control the autophagic process would facilitate advances in the comprehension of the coordination between autophagy and different biological pathways during stress. Nutrient limitation is a severe cue for plant growth and devolvement. Nutrient recycling and remobilization mechanisms during stress are rescue tools for the plant to alleviate or escape the damage. Despite the progress of research in autophagy-mediated nutrient recycling and nutrient remobilization under stress and especially under starvation in plants, what is known until today seems to be the tip of the iceberg. The outlook of this topic is to investigate further the regulations of autophagy and the characterization of the involved SARs, cargos, and adaptors under nutrient starvation.

PART III

Literature review 2

2 Chapter II: Acquisition of non-heme iron and translocation mechanisms in plants

Abstract

In a living organism, modulating iron uptake is crucial to maintaining cellular iron-related metabolisms. The regulation of iron transporter proteins is classically subjected to external iron levels. Although, few works demonstrated direct connections between the intracellular iron status and the iron uptake activity. This review detailed the involvement of usable intracellular iron and non-iron metals in regulating the IRT1 iron transporter protein in *Arabidopsis thaliana*. The intracellular iron is available in a non-bound form known as Labile-Iron-Pool (LIP) or bound iron to cofactors, mainly heme. The IRT1 functioning is commonly controlled by the cellular iron availability and the iron signal transduction in addition with other metals. These two parameters are influenced by the reversible conversion between heme-to-LIP, governed by several cellular regulatory pathways under iron-related stress such as oxidative stress. Newly, we display the putative function of the multi-stress regulatory TSPO protein in iron homeostasis regulating IRT1 in *Arabidopsis thaliana* under stress conditions.

2.1 Iron reduction-based strategy and iron translocation in *Arabidopsis thaliana* roots

Iron is generally abundant in soil in complex insoluble form. It is strictly required for photosynthetic organisms. Different approaches to iron uptake were described in *planta*. Gramineous plants (*Poaceae),* including many crops, employ a chelation-based strategy (strategy-II) for their iron uptake. Strategy-II is based on Fe^{3+} chelation by phytosiderophores to transmute iron in a soluble form in the rhizosphere, to be systematically imported into the absorptive root cells (Mori, 1994; Mori, 1998). Non-gramineous plants such as *Arabidopsis thaliana* apply the so-called reduction-based strategy (strategy-I) for iron uptake (Kim and Guerinot, 2007; Marschner and Römheld, 1995) **(Figure 7)**. Strategy-I starts by acidifying the rhizosphere mediated by proton extrusion through the proton pump *AUTOINHIBITED PLASMA MEMBRANE-H^+-ATPase (AHA2)* to facilitate iron solubilization and its entry to the apoplast. AHA2 levels are highly increased under iron deficiency (Santi and Schmidt, 2009) **(Figure 7)**. AHA2 is one of more than eleven proton pump ATPases in *A. thaliana* (DeWitt *et al.*, 1996). Only AHA2 and AHA7 expression depend on iron and phosphorus levels in the cell (X., Zhang *et al.*, 2019). The lack of AHA2 expression in *Arabidopsis* is characterized by a reduction of primary root elongation and low H^+ efflux in the root elongation zone (Yuan *et al.*, 2017; Hoffmann *et al.*, 2019). Arabidopsis root epidermis cells produces and exports secondary metabolite compounds specifically for iron chelation. The ferric iron chelation by coumarin-type compounds (such as fraxetin, esculetin, sideretin, etc.) is crucial for the iron acquisition process during iron deficiency or in alkaline soils (Robe,

Izquierdo, *et al.*, 2021). Coumarins are exported to the rhizosphere via the *PLEIOTROPIC DRUG RESISTANCE 9 protein (ABCG37 transporter, mainly known as PDR9)* (Fourcroy *et al.*, 2014; Fourcroy *et al.*, 2016; Robe, Conejero, *et al.*, 2021) **(Figure 7)**. PDR9 is upregulated under iron deficiency or by a gene mutation related to Fe reduction-based strategy (Fourcroy *et al.*, 2016). The *pdr9 Arabidopsis* null mutant exhibits a chlorotic phenotype in an alkaline growth medium, impairs iron levels, and a dramatic reduction in coumarins export activity in root (Fourcroy *et al.*, 2014). Afterward, the ferric iron is reduced via enzymatic process to the ferrous iron form at the root apoplast by the plasma membrane-localized *FERRIC REDUCTASE OXIDASE 2 (FRO2)*. FRO2 protein contains in its cytoplasmic side specific motifs to interact with NADPH and heme. FRO2 uses an inoxidized NADPH to transfer electrons by flavin and two heme groups to the PM side faced to the rhizosphere, where ferrous iron reduction happens (Schagerlöf *et al.*, 2006). FRO2 is regulated by iron, zinc, and cadmium concentrations (Connolly *et al.*, 2003). FRO2 expression increases under iron deficiency but not by copper (Connolly *et al.*, 2003; Mukherjee *et al.*, 2006; Yuan *et al.*, 2008). The iron deficiency instigates the natural allelic variation of the non-coding sequence at the FRO2 locus, which yields in increased FRO2 transcripts and determines root growth levels (Satbhai *et al.*, 2017). FRO2 is expressed in the epidermis and flowers (Connolly *et al.*, 2003). The Arabidopsis mutant defective in FRO2 gene, so-called *ferric reductase defective-1 mutant (frd1)*, is characterized by reduced capacity in reducing copper and chelated iron causing low iron levels in the cells. This mutant does not translocate iron to the shoots under availability in the chelated form of iron and exhibits a severe chlorotic phenotype (Robinson *et al.*, 1999;

Yi and Guerinot, 1996). Iron should be reduced before being transported into the cytoplasm of the cell's epidermis by the metal transporter *IRON REGULATED TRANSPORTER 1 (IRT1)* **(Figure 7)**. IRT1 expression is transcriptionally derived by iron status (Brumbarova *et al.*, 2015). IRT1 can also transport several divalent non-iron metals such as zinc, manganese, cobalt, cadmium, etc. (Rogers *et al.*, 2000b; Korshunova *et al.*, 1999; He *et al.*, 2017). The deletion of IRT1 in *A. thaliana* leads to iron deficiency and impairs cellular development. *irt1* null plant mutant is characterized by a reduction in rosette biomass and an intense global chlorotic symptom, affecting all the rosette leaves. The photosynthetic process is highly impaired in the knockout (KO) IRT1 mutant: A dramatic decrease in chlorophyll by thylakoids stacking, a perturbation in the Photosystem-II, stopping the development of the palisade parenchyma in leaves, an intense reduction in the stems vascular bundles and a deformation in the root architecture due to the disruption of the pattern through the enlarged endodermal and cortical cells (Henriques *et al.*, 2002; Varotto *et al.*, 2002). The suppression of the IRT1 gene provokes a decrease in the cellular labile iron pool and leads to an increase in transcripts level of several ZIP genes members like IRT2 and ZIP1/2/3 and 4 (Henriques *et al.*, 2002). Right after entering the epidermic cells, iron as essential nutriment is translocated via symplastic and apoplastic routes through the cortex, endodermis, and pericycle before arriving at the vascular tissues xylem and phloem (Jeong *et al.*, 2017; Barberon, 2017). The *Arabidopsis irt1* null mutant is characterized by a low root suberization which increases the permeability for ions in the stele and alleviates bocking activity of the Casparian strip on apoplastic solute transport (Jeong *et al.*, 2017; Quintana *et al.*) **(Figure 7)**. While, iron deficiency induces ethylene

signaling to inhibit suberization (Yoshida *et al.*, 2019). The suberization process is influenced by phytohormones. The abscisic acid (ABA) resulting from salinity, potassium/sulfur deficiency triggers a high suberization which negatively regulates iron translocation, while ethylene has an antagonist effect in promoting the repression of suberization, which positively regulates iron acquisition (Doblas *et al.*, 2017; Barberon, 2017). Two plasma membrane transporter proteins, *FERRIC REDUCTASE DETECTIVE3 (FRD3) and FERRPORTIN 1 (FPN1),* transport citrate-iron chelated and iron from pericycle to xylem vessels (Jeong *et al.*, 2017) **(Figure 7)**. FRD3 is localized in both the root and shoot; it is also highly expressed in *Arabidopsis* seed and flower (Roschzttardtz *et al.*, 2011). The *Arabidopsis frd3* null mutant is characterized by a high accumulation of iron in the root vascular cylinder and shoot part (Scheepers *et al.*, 2020; Green and Rogers, 2004). *frd3 mutant* seeds germinate earlier and give generally dwarf, chlorotic, and completely sterile plants due to pollen abortion (Roschzttardtz *et al.*, 2011; Scheepers *et al.*, 2020). On the other hand, the *FERROPORTIN FPN1* is expressed in the root stele to drive the iron efflux to the xylem, in the root–shoot junctions of seedlings, and in the leaf vein. The *fpn1* mutation triggers a high sensitivity to iron deficiency and abolishes the iron and cobalt accumulation in the shoot (Morrissey *et al.*, 2009; Conte and Walker, 2011). Iron in xylem vessels can be translocated to the phloem via a phloem-specific transporter previously known as *OLIGO PEPTIDE TRANSPORTER 3 (OPT3)* **(Figure 7)**. OPT3 is a plasma membrane iron transporter that facilitates iron recirculation from the xylem to the phloem, which regulates shoot-to-root iron signaling redistribution from aged to early developing tissues (Zhai *et al.*, 2014). The *Arabidopsis opt3* null mutation is

characterized by a high iron and cadmium accumulation in roots and leaves, in addition to an increase in IRT1 expression (Khan *et al.*, 2018; Mendoza-Cózatl *et al.*, 2014).

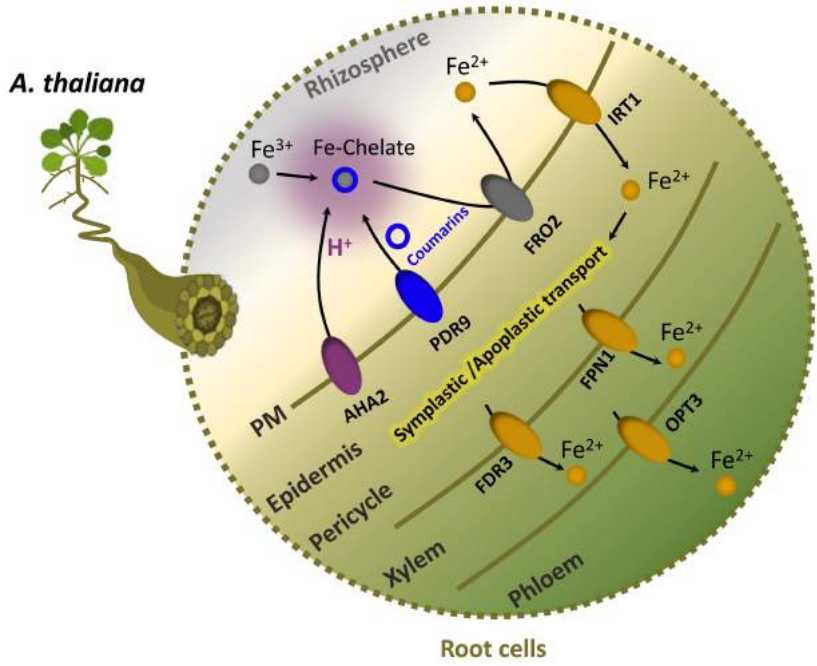

Figure 7. External iron (Fe) uptake and intracellular translocation. The reduction-based iron-uptake strategy in *A. thaliana* epidermis cells and iron translocation to central vessels in the root. The uptake process starts by acidifying the rhizosphere area containing the insoluble iron form. Rhizosphere acidification is mediated by protons extrusion through the AHA2 proton pump. To maintain the

accessible iron pool, the ferric iron is chelated by coumarins-type compounds exported by the ABCG37/PDR9 transporter. Therefore, the ferric chelated iron is easily used by FRO2 iron chelate reductase protein to be reduced to the ferrous accessible form. Afterward, iron is transported into the epidermic cell cytoplasm through the *IRON REGULATED TRANSPORTER 1 (IRT1).* Imported iron undergoes symplastic and apoplastic transport to enrich the apoplast. This transport depends on tissue suberization. It should be transported to the xylem vessels by FDR3 and FPN1 plasma membrane transporters and subsequently to phloem via OPT3 iron transporter protein.

2.2 Heme as internal iron source and signaling molecule modulating iron homeostasis

2.2.1 Heme biosynthesis and catabolism in Arabidopsis cells

2.2.1.1 Iron dynamic in the chloroplast: Import, storage, and translocation

Imported iron into the cytosol is tightly sent for translocation or compartmentalization. Ferrous iron is quickly reduced to the ferric form and chelated by citrate or nicotinamine (NA). Iron serves as a cofactor for three molecular forms: (I) in the porphyrins branch of heme and siroheme biosynthesis (II) in five subtypes of iron-sulfur clusters (III) nonheme cofactors such as ferritin clusters and superoxide dismutase (Hänsch and Mendel, 2009). Most of the cellular iron is in the chloroplast because of is crucial in chlorophyll biosynthesis and electron transport. Fe^{3+}-citrate is the most abundant form to be imported into the chloroplast, which contains an inner (IE) and an outer (OE) envelope and a thylakoid membrane (Schmidt *et al.*, 2020). The ferric iron is reduced to the ferrous form by the *FERRIC REDUCTASE*

OXIDASE 7 (FRO7) for subsequent transport through the IE. The mutation in FRO7 leads to a decrease of function in the chloroplast characterized by a decrease in 75% of Fe(III) chelate reductase, loss of 33% of iron per microgram of chlorophyll, and defect in photosynthetic electron transport. *fro7* null mutants seedlings suffer from strong chlorosis and die before settings seeds in alkaline soil (Jeong *et al.*, 2008). While in standard conditions, this mutation is not lethal because it is possible for the chloroplast to uptake ferrous iron. FRO7 activity is, in general, associated with the *NICKEL/COBALT TRANSPORTER-PERMEASE IN CHLOROPLASTS (NiCo-PIC1 association complex)* crucial for iron transport in the chloroplast IE (Jeong and Connolly, 2009; Schmidt *et al.*, 2020) **(Figure 8)**. Fe^{2+} first is bound to NiCo and then transferred to PIC1 by a proton motif force. Knockout in PIC1 yields an imbalance in the cellular ILP, an increase in ferritin clusters in the cell, a perturbation in chloroplasts development, an unbalancing in Fe-S cluster, and chlorophyll levels, and a differential regulation of iron transport proteins. *pic1* null mutant *Arabidopsis* plants show a chlorotic and dwarfish phenotype compared to the WT (Duy *et al.*, 2007). However, the overexpression of PIC1 triggers a loss of function in the ferritin cluster and iron overloading in the chloroplasts, which creates an oxidated stress. Plant mutants overexpressing PIC1 show a reduction in biomass and leave chlorosis (Duy *et al.*, 2011). FRO7-NiCo-PIC1 protein complex functions in iron transport into the chloroplast via the IE is crucial for iron homeostasis in the cell. Another system for iron homeostasis balancing in chloroplast localized at the IE and composed of an ATP-Binding cassette proteins type ECF/ABC transporter complex, ABCI10 (NAP13), ABCI12 (NAP12), and ABCI11 (NAP14). This novel multisubunit ABC transporter complex

is highly implicated in the iron transport and homeostasis in the chloroplast (Gretchen E. Kroh and Pilon, 2020; Dahuja *et al.*, 2021; Ha *et al.*, 2021) **(Figure 8)**. ABCI10 and ABCI11 fluorescent-tagged are most likely localized at the IE of the chloroplast. Iron transport functions of ABCI11 are still unclear. While the suppression of ABCI11 engenders a severe unbalancing in the chloroplast structures and development, a decrease in PIC1 and FRO7 transcripts, a decrease in Fe concentration in the chloroplast by 18 folds, a severe leaves chlorosis and defects in growth (Shimoni-Shor *et al.*, 2010; Vigani *et al.*, 2019a). The ABCI10 is a single soluble ATP-binding subunit CbiO/EcfA interacting in the IE with ABCI12 energy coupling subunit CbiQ/EcfT. While ABCI12 is anchored in the IE by five predicted α-helical transmembrane domains and represents the membrane-intrinsic subunit of a prokaryotic-type, energy-coupling factor (ECF) ABC-transporter complex. In bacteria, this multisubunit ECF is known for its metal transport activity like nickel and cobalt ions transport. The mutation of ABCI10 in *Arabidopsis* causes a severe alteration in chloroplast biogenesis, especially an increase in Fe levels, an alteration in the expression of iron transporter proteins, leaves chlorosis, and a decrease in biomass (Voith von Voithenberg *et al.*, 2019; Vigani *et al.*, 2019b). According to the iron level inside the chloroplast, the recently imported iron can be considered as (I) needed iron which is used in the heme and siroheme biosynthesis (II) non needed iron which will be sequestrated at ferritin proteins. In *Arabidopsis*, four ferritin genes exist (FER1/FER3/FER4 expressed in the leaf, FER1/FER3 expressed in the meristematic zone, and pericycle root endodermis, while FER2 expressed in the seeds) (Reyt *et al.*, 2015). The four ferritins in *Arabidopsis* are characterized by strong structural conservation,

especially for the hydrophobic subunit E-helix. The *Arabidopsis* ferritin subunits are close to the H-type and L-type animal ferritin subunits. Ferritin proteins complexes make a shell structure that scavenges iron by binding to the organic phosphate (PETIT *et al.*, 2001; Gretchen E. Kroh and Pilon, 2020). During iron excess, the expression of FER genes is increasing, promoting iron scavenging and storage, which prevents oxidative stress, ROS production, accumulation of hydroxyl radicals (•HO), and hydrogen peroxide via Fenton reaction (Reyt *et al.*, 2015; Gretchen E. Kroh and Pilon, 2020). The triple mutation form fer1/fer2/fer3 triggers to increase in the activity of catalases and peroxidases, which promotes toxic ROS accumulation in the cell. During iron excess, the *Arabidopsis fer1/fer2/fer3* null mutant alters the root system architecture (RSA) mediated by H_2O_2/O_2^- (Reyt *et al.*, 2015; Gretchen E. Kroh and Pilon, 2020). The non-need iron in the chloroplast from the released form from ferritin or recent imported form is exported to be transported to other organelles in the cell. The iron export from the chloroplast is mediated by two *YELLOW STRIPE LIKE PROTEINS (YSL4* and *YSL6).* The double mutation in ysl4/ysl6 causes iron trapping in the chloroplasts, ferritin over accumulation, and inhibition of the vacuolar iron export by NRAMP3/4 **(Figure 8)**. However, the constitutive expression of YSL4/6 leads to a decrease in iron level in the chloroplast, limiting the plant's capacity to adapt to iron deficiency (Divol *et al.*, 2013). The iron exit from the chloroplast is also mediated by the *FERROPORTIN 3 (FPN3)* expressed in shoots. Iron deficiency promotes the accumulation of FDPN3 in roots. The *fpn3* null mutant *Arabidopsis* shows a decrease in iron levels in the shoot, especially in chloroplast and mitochondria, and an impaired growth

under the iron deficiency compared to the WT (Kim *et al.*, 2021) **(Figure 8)**.

2.2.1.2 Heme biosynthesis machinery in Arabidopsis chloroplasts

The plant cell needs iron for multiple biological processes. Mostly iron plays the cofactor role for many proteins and organic signaling molecules such as heme, siroheme, and Fe-S clusters. These molecules are required for ROS-scavenging, electron transport, and catalysis (Balk and Schaedler, 2014). In plants, the synthesis of heme, siroheme, and chlorophyll occurs in plastids via the tetrapyrroles biosynthesis pathway. Unlike mammals using the C4 path (ALA synthesis by the condensation of succinyl-CoA and glycine), plants use the C5 pathway (ALA synthesis from the skeleton of Glutamate) (Oborník, 2021) **(Figure 8)**. The tetrapyrroles biosynthesis process is based on multiple enzymatic reactions in the biogenesis of organic molecules. It begins with the ligation of Glutamate (Glu) to Glutamyl-tRNA by the glutamyl-synthetase (GluS), then to Glutamate-1-demialdehyde by a reductase enzyme glutamyl-tRNA-reductase (GluTR) (Tanaka *et al.*, 2011). This reaction product gives afterward by a transmission reaction ensured by Glu 1-semialdehyde aminotransferase, the universal precursor of all tetrapyrroles in the plant: The Aminolevulinic acid (ALA). GluTR acts as an enzyme regulator able to bind to several proteins like the *PROTON GRADIENT REGULATION7 (GluTRBP).* GluBP binding stimulates GluTR catalytic efficiency and instigates its hydride-transferring state (Zhao *et al.*, 2014). GluTRBP contributes to the ALA metabolism by encouraging the heme biosynthetic pathway. The GluTRBP knockout *Arabidopsis* mutant decreases the heme

content (Czarnecki *et al.*, 2011). The heme accumulation via ALA overfeeding leads to the CLP-protease-dependent degradation of Arabidopsis GluTR (isoform1). The post-translational regulation of GluTR by heme content helps create a balance in chlorophyll and heme availability (Richter *et al.*, 2019).

ALA is the rate-limiting step in tetrapyrrole biosynthesis in the plant. Heme levels control ALA biosynthesis. Heme can bind to the N-terminus of GluTR, which is considered a heme-binding domain (HBD), and inhibit its activity. At the same time, the truncated form of GluTR missing its N-terminus part (lacking 29 amino acid residues) is resistant to the inhibitory effect of heme in vitro (Richter *et al.*, 2019; Czarnecki *et al.*, 2011; Apitz *et al.*, 2016). Another negative regulator of ALA biosynthesis is driven by the membrane-bound FLUORESCENT protein (FLU).

FLU can bind the C-terminal part of GluTR by its non-canonical tetratricopeptide repeat domain (TRP) and limits its functions. The regulation of ALA biosynthesis by FLU and heme prevents overaccumulation of protochlorophyllide (Pchlide) in the dark (Czarnecki *et al.*, 2011; Zhang *et al.*, 2015; Hou *et al.*, 2021). ALA undergoes a series of enzymatic reactions to form the protoporphyrin-IX, giving eight intermediate tetrapyrroles: Porphobilinogen (PBGB) by ALA dehydratase condenses two ALA molecules **(Figure 8)**. Four linear molecules of PBGB are polymerized to give the Hydroxymethylbilane by PBG deaminase. Hydroxymethylbilane is isomerized and provides the ring with molecule Uroporphyrinogen-III (UrogenIII) by Urogene-III decarboxylase. At this level in tetrapyrroles biosynthesis, Urogen-III continues the enzymatic reactions, giving two

branches. In the first branch, this molecule is methylated and gives the Sirohydrochlorin, which undergoes an iron insertion by Fe-Chelatase, giving the Siroheme (Papenbrock and Grimm, 2001; Tanaka and Tanaka, 2007; Nagahatenna *et al.*, 2015). Siroheme is a cofactor for nitrite and sulfite reductase involved in nitrogen and sulfur assimilation (Tanaka *et al.*, 2011). In the second branch, the Urogen-III undergoes a decarboxylation to give coprogen-III, which is oxidized by the Coprogen-III Oxidase (CPO), resulting in the protoporphyrinogen-IX, which is further oxidized by the Protogen-IX Oxidase (PPO) and engenders Protoporphyrin-IX (PP-IX), the precursor of heme and chlorophyll **(Figure 8)**. The tetrapyrroles biosynthesis continues further and is devised in two distinct branches: (I) the Fe branch, ferrous iron is inserted into the PPIX organic macrocycle by Fe-chelatase to form heme. (II) the Mg branch, Mg^{2+} transported by MRS2-11 into the chloroplast, is inserted in the PPIX by Mg-chelatase containing three subunits CHLD, CHIH, and CHLI. The Mg-PPIX undergoes four enzymatic reactions to finally give the chlorophyll (a). The Mg-Proto-IX monomethyl ester (Mg-Proto ME) results from an addition of a methyl group of S-adenosyl L-methionine. Then, Mg-Proto ME cyclase leads to protochlorophyllide (DV-Pchlide) by forming a fifth isocyclic ring. Pchlide reductase continues further to synthesize the Chlorophyllide (a), which can be oxidized to give chlorophyllide (b) the precursor of the Chlorophyll (b) or to be esterified and catalyzed by Chlorophyll synthase (Chl-synthase) to provide the Chlorophyll with (a) (Yuan *et al.*, 2016; Tanaka and Tanaka, 2007; Tanaka *et al.*, 2011) **(Figure 8)**. Recently synthesized heme in the chloroplast is quickly bound to heme protein or exported to the cytoplasm. A transit hemoprotein SOUL4 is imported into the chloroplast and targets the

plastoglobules (PGs) to be phosphorylated by Casein kinase II α subunit and bind heme. SOUL4 maybe contributes to the heme buffering inside the chloroplast (Shanmugabalaji *et al.*, 2020) **(Figure 8)**. The heme exit mechanism from the chloroplast is still unknown. Many studies suggest a possible role of chaperones such as tau glutathione transferase (GSTU) in the export of heme outside the chloroplast. GSTU is known to bind heme by a hydrophobic binding pocket in addition to its capacity to interact with ABC transporters (Sylvestre-Gonon *et al.*, 2020). Moreover, in mammalian cells, several ABC transporters mediate heme transport (Taketani *et al.*, 2003).

2.2.1.3 Heme overproduction modulates ROS detoxification and activates heme-catabolism machinery promoting iron nutritional recycling

Oxidative stress conditions promote the expression of FeChs in the chloroplast, enhancing the flux of heme production and accumulation through the tetrapyrroles biosynthesis (J.,-G., Kim *et al.*, 2014). The chloroplastic Heme in excess follows two paths: Inside the chloroplast, the accompanying increase in the heme level promotes the expression of the canonical *α-helical HEME OXYGENASE1 (HO1),* which leads to a catalyzing cleavage resulting in biliverdin (BV) with the release of Fe and carbon monoxide (CO) (Li *et al.*, 2013) **(Figure 8)**. Accumulated heme can be mainly bound by SOUL5 and phosphorylated SOUL4 proteins (Lee *et al.*, 2012; Shanmugabalaji *et al.*, 2020). HO1 interacts with the complex SOUL5-heme to mediate heme catabolism and Fe releasing. The overexpression of HO1 decreases the heme level in the cell, promotes the expression of FC1,

IRT1, and FRO2, and leads to the increase in LIP in the cell by heme catabolism. HO1 expression generates more NO (Li *et al.*, 2013). NO acts as a signaling molecule that regulates positively the iron uptake process (Meiser *et al.*, 2011; Koen *et al.*, 2012). Another heme oxygenase in the chloroplast, a non-canonical dimeric *β-barrel HEME OXYGENASE (HOZ),* can bind heme and trigger its degradation differently from HO1 (Wang *et al.*, 2020). Under oxidative stress, accumulated heme in the chloroplast can be retranslocated to the cytosol and cofactor in the enzymatic ROS scavenging and detoxification process. Free cytosolic heme is targeted by heme-containing enzymes such as Ascorbate peroxidases (APX) and Catalases (CATs) **(Figure 8)**. APX mainly occurs in the cytosol, mitochondria, peroxisomes, and chloroplast. They are known for high affinity to H_2O_2 (Anjum *et al.*, 2016). APX bind to heme and use ascorbate as an electron donor to reduce H_2O_2 to H_2O in cyclic reactions known as "peroxidase-ping pong." APX first reacts with H_2O_2 to produce a two-electron-oxidized compound (compound I) through the heme oxidation to oxyferryl species (Fe^{4+}=O) and free radical R•. Then, the compound I undergoes two successive one-electron reactions to be reduced back to resting ferric APX and producing two molecules of monodehydroascorbate radical (MDA) in addition to the H_2O molecule (Miyake and Asada, 1996). NO is mainly derived from the posttranslational modification of APX in plants (Saxena and Shekhawat, 2013; Clark *et al.*, 2007). APX is also induced under salinity and ABA treatment (Begara-Morales *et al.*, 2014; Lu *et al.*, 2014). Likewise, CATs are localized mainly in plant peroxisomes and mitochondrial matrix (Anjum *et al.*, 2016). The catalytic capacity of CAT depends on the level of H_2O_2. Under low levels, CAT works like

peroxidase to oxidize most hydrogen donors. While under high H_2O_2 levels, CAT works in catalytic mode. H_2O_2 oxidizes the heme iron of CAT to form an intermediate form (an oxygen-rich iron peroxide + generated porphyrin cation radical) in addition to an H_2O molecule. Then, the intermediate iron peroxide is reduced by a hydrogen donor such as ethanol, ascorbic acid, phenols, formaldehyde, etc. to return to the resting state or by using catalytically another H_2O_2 as redundant to return to the resting state in addition to an $H_2O + O_2$ molecules (Mhamdi *et al.*, 2010; Anjum *et al.*, 2016). In *Arabidopsis*, CAT genes are expressed under ABA treatment. CAT2 is mainly induced by salinity, cold, and drought stress. While CAT3 is mainly induced during senescence and salinity (Du *et al.*, 2008; Xing *et al.*, 2008; Xing *et al.*, 2007). Under oxidative stress, levels heme increase in the cytosol (Espinas *et al.*, 2012; Voigt *et al.*, 2010). A part of heme stays free and unbound by APX and CATs. It could be highly cytotoxic by reacting with oxygen to produce ROS (Kumar and Bandyopadhyay, 2005).

In *Arabidopsis*, under oxidative stress, the free heme could be bound by the translocator protein (TSPO) known as *OUTER MEMBRANE TRYPTOPHAN-RICH SENSORY PROTEIN.* Oxidative stress-related TSPO localizes at the outer membrane of ER, Golgi, and TGN and can bind heme invitro and in vivo (Vanhee, Zapotoczny, *et al.*, 2011) **(Figure 8)**. ABA triggers increase free toxic heme levels in the cell and induce transiently TSPO (Vanhee, Zapotoczny, *et al.*, 2011; Guillaumot, Guillon, Déplanque, *et al.*, 2009). The constitutive expression of TSPO seems to be toxic and leads to increased ROS levels and peroxidases activity. The heme-binding pocket within the TSPO protein requires the TSPO histidine at position 91 (H91) at the beginning of TM2. The substitutional mutation H91A (histidine

replacement by alanine) strongly decreases TSPO capacity in binding heme. The *Arabidopsi*s mutant overexpressing TSPO(H91A) exhibits higher heme levels under ABA treatment compared to the mutant overexpressing the wild TSPO protein (Vanhee, Zapotoczny, *et al.*, 2011). The TSPO-heme complex interacts with *ATG8 UBIQUITIN-LIKE (Ubl) PROTEIN autophagy-related (ATG8)* through TSPO AIM conserved motif (121-LYLY-125). Which promotes the engulfment of the cargo TSPO-heme into the autophagosome and the delivery to the lytic vacuole (Vanhee, Zapotoczny, *et al.*, 2011) **(Figure 8)**. The mutation in the AIM motif in TSPO yields to abolish the degradation of the heme bound by TSPO via the selective autophagy pathway (Vanhee, Zapotoczny, *et al.*, 2011). Selective autophagy is a precise form of autophagy triggered through well-defined physiological conditions (mostly stress-related conditions). It degrades a specific cargo that can be a macromolecule, a protein, or even a cellular organelle (Veljanovski *et al.*, 2014). Autophagy could include multiple forms of degradation ways depending on the degraded target (cargo). Cargo could be protein (proteophagy), aggregates (aggregophagy), pathogens (xenophagy), chloroplast (chlorophagy), ER (reticulophagy), mitochondria (mitophagy), etc. Autophagosome biogenesis and its delivery process are under the control of ATG kinases proteins forming several complexes: The protein kinase complex (ATG1 complex), the lipid kinase complex (ATG6 complex), the ubiquitin-like conjugation complex (ATG5-12-16 complex) and the cyclable vesicle complex (ATG9 complex) (Noda and Inagaki, 2015; Rubinsztein *et al.*, 2011; Liu and Bassham, 2012). Autophagosome formation includes several steps: Initiation, elongation, closure, and maturation (Tsuboyama *et al.*, 2016; Fujioka *et al.*, 2008; Koyama-

Honda *et al.*, 2017; Kuma *et al.*, 2017). The initiation step begins with the ATG8 proteins through the lipidation (via the interaction of ATG8/ATG12-PE (phosphatidylethanolamine)) and incorporated into the membrane of the developing autophagosome, which serves as a docking site for the engulfment of the cargo-receptor into the autophagosome (Chung *et al.*, 2010; Hanada *et al.*, 2009; Noda *et al.*, 2010; Shpilka *et al.*, 2011). TSPO is considered an autophagy receptor for its capacity to bind the cytosolic free heme and triggers its engulfment into the autophagosome via specific interaction with ATG8 (Bu *et al.*, 2020; Tang and Bassham, 2021). The overexpression of the fluorescent-tagged TSPO in *Arabidopsis* cells under treatment with Concanamycin A (ConcA), a specific inhibitor of vacuolar V-type H^+-ATPase, shows under confocal microscopy, the accumulation of autophagic bodies containing TSPO (Hachez *et al.*, 2014). The overexpression of TSPO localized at ER, Golgi, and TGN membranes, affects the quantity of PI(4,5)P2 at the Golgi membrane (Jurkiewicz *et al.*, 2020). PI(4,5)P2 is required for the initiation and trafficking of autophagosome membrane precursors as well as for the fusion of the autophagosome with lytic compartments such as the lytic vacuole. PI(4,5)P2 is bound by Barkor/ATG14 via its BATS domain to be delivered to the autophagosome during the initiation phase (Tan *et al.*, 2016). Autophagosome is characterized by a double membrane vesicle sequestering the cytosolic compounds such as the autophagy receptor and the cargo. The outer membrane of the mature autophagosome fuses with the tonoplast, which leads to the release of the cytosolic compounds into the lytic milieu inside the vacuole (Krüger and Schumacher, 2018). The *Arabidopsis* null mutant *vcl1* cells *(lacking the VACUOLELESS1 (VCL1))* show an inability of vacuole biogenesis,

a failure to form a central vacuole, and accumulation of structures morphologically similar to autophagosomes (Rojo *et al.*, 2001). In *Arabidopsis*, the machinery controlling the fusion of the autophagosome with the vacuole is based on the involvement of SNAREs (VTI family, mainly VTI12), Rab GTPase (RABG1, G2, and G3a-f), and *HOMOTYPIC VACUOLE FUSION AND PROTEIN SORTING (HOPS)* (Yoshimoto and Ohsumi, 2018; Zeng *et al.*, 2019). The heme bound by TSPO and delivered to the vacuole via autophagy undergoes the enzymatic degradation into a lytic milieu. Heme's massive degradation yield increases the iron pool inside the vacuole. Vacuolar iron is mainly exported from the vacuole for the nutritional reutilization during iron requirement events such as germination, iron deficiency, photosynthesis, etc. Iron efflux from vacuole is based on iron exporter proteins *NATURAL RESISTANCE-ASSOCIATED MACROPHAGE PROTEIN 3 and 4 (NRAMP3/4)* (Kurt and Filiz, 2020; Ravet *et al.*, 2009) **(Figure 8**. NRAMP3 is involved in starch metabolism, pathogen defense, and nutrients mobilization during senescence. While NRAMP4 is involved in acclimatization and seeds dormancy. NRAMP3/4 are induced under iron deficiency and target the tonoplast via the complex AP4 sorting process, including their N-terminal dileucine-based motif (Müdsam *et al.*, 2018). The *Arabidopsis* double mutant nramp3/4 cannot retrieve stored iron in the vacuolar globoids, and it is characterized by high expression of IRT1 and FRO2 (Bastow *et al.*, 2018).

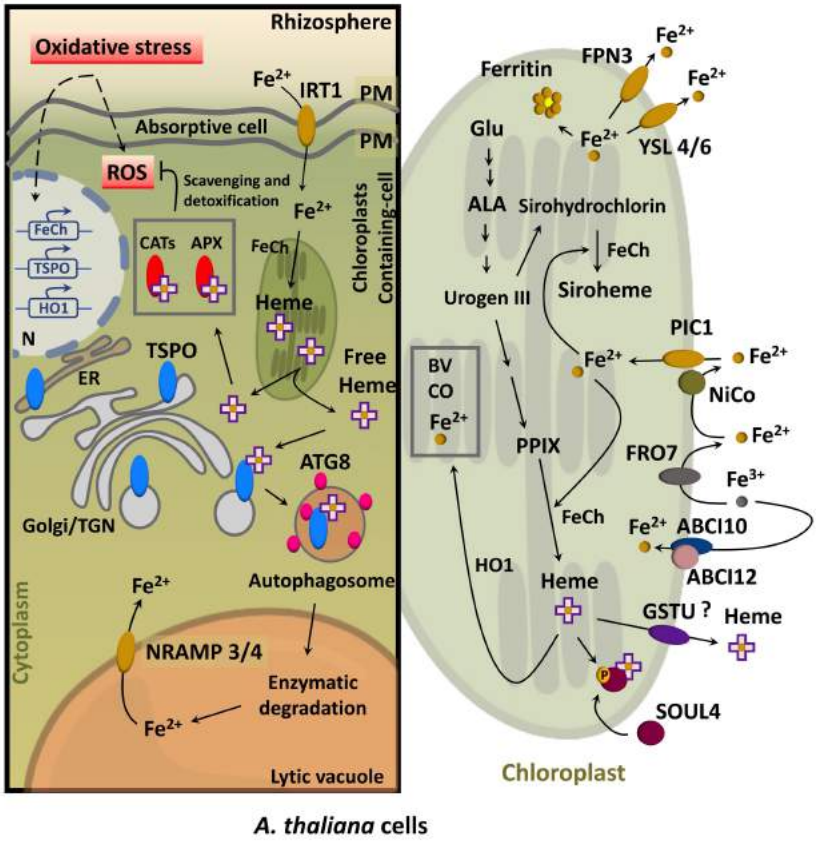

Figure 8. Heme biosynthesis and dynamics. Heme biosynthesis in Arabidopsis-cell chloroplast and cellular translocation. Classically, ferric iron comes from the iron uptake via IRT1, and intracellular translocation is reduced through the chloroplast's inner membrane by FRO7 reductase, giving ferrous iron irons. Resulted iron is transferred and transported into the chloroplast by NiCo-PIC1 association complex. The ferric iron can also be parallelly reduced and transported into the chloroplast through the multisubunit ATP-Binding proteins type ECF/ABC transporter complex. which contains ABCI10 (NAP13), ABCI12 (NAP12). Recently, imported iron has been a central component in heme molecules

biosynthesized in the chloroplast. Accordingly, to produce heme, *A. thaliana* uses the C5 pathway in tetrapyrroles biosynthesis (ALA synthesis from the skeleton of Glutamate). ALA undergoes multiple subsequent enzymatic reactions to give Urogen III molecule. This continues in two routes: (I) Urogen III can be converted to Sirohydrochlorin, then to Siroheme (II), or give the PPIX precursor molecule of heme and chlorophyll subsequently. The ferrous iron is inserted through enzymatic chelation derived from Fe-chelatase (FeCh) to form heme and Siroheme molecules. Indeed, the recently synthesized heme depends on its concentration in the chloroplast. It can be sequestered via interacting with the phosphorylated form of SOUL4 hemoprotein. Otherwise, chloroplast gets rid of accumulated heme in two ways: (I) Catalytic reaction by the heme oxygenase enzyme, mainly HO1 leading to heme cleavage. This gives biliverdin (BV) with the release of Fe2+ and carbon monoxide (CO). Ferrous iron inside the chloroplast can be later sequestered by ferritin proteins or exported to the cytoplasm by FPN3 and YSL4/6 iron transporters. (II) the heme in excess is mainly translocated from the chloroplast by putative mechanisms. Such as the possible involvement of chaperones glutathione transferase (GSTU) in heme export from the chloroplast. Furthermore, oxidative stress promotes ROS production, the induction of FeCh leading to heme accumulation, and HO1 induction leading to heme catalysis. Under stress conditions, free heme levels increase in the cytosol. Which serves in ROS scavenging and detoxification hemoproteins such as catalases (CATs) and peroxidases (APX). Free toxic heme in the cytosol, is scavenged by the multitrees induced TSPO protein. TSPO is localized at the inner membrane of ER, Golgi stacks, and TGN. Moreover, TSPO binding heme recruits the autophagy-related protein ATG8. Which interacts with TSPO, initiates the autophagosome formation, and promotes the engulfment of the cargo TSPO-heme into the autophagosome. which triggers the complex delivery to the lytic vacuole. The enzymatically degraded heme releases and increases the level of Fe2+ in the vacuole, leading, therefore, to the export of iron to the cytoplasm via NRAMP3/4 iron transporters.

2.2.1.4 Heme accumulation and Plastid-to-nucleus retrograde signaling

In addition to chlorophyll, heme is one of the major tetrapyrroles synthesized in the chloroplast. Heme levels can auto regulates its biosynthesis mechanism (Richter *et al.*, 2019; Czarnecki *et al.*, 2011; Apitz *et al.*, 2016). Heme acts as a retrograde signaling molecule. The heme pool's export, accumulation, and subchloroplastic location modulate the plastid communication signals, which regulate the expression of hundreds of nuclear genes during development and in response to stress. Signals emanating from organelle, so-called

retrograde signals, modulate genes expression in the nucleus. *The GENOME UNCOUPLED genes (GUN)* are critical for the chloroplast retrograde signaling and during tetrapyrroles Biosynthesis (Nott *et al.*, 2006). GUN4 (Mg-chelatase) and GUN5 (H-subunit of Mg-Chelatase) modulate the formation of Mg-PPIX. The mutation in GUN4 and GUN5 genes engenders a deficiency in Mg chelation of PPIX and impairs the chlorophyll biosynthesis pathway. Moreover, gun2 (heme oxygenase1) and *gun3* (Phyto-chromo globin synthase) null mutant are characterized by a deficiency in heme catabolism to Phyto-chromo globin leading to its accumulation (Terry and Kendrick, 1999; Woodson *et al.*, 2011). The heme accumulation leads to feedback regulation of chlorophyll biosynthesis. Heme binds to GUN1, which activates the ferrochelatase 1 (FC1), regulating tetrapyrroles biosynthesis flow and generating positive signals promoting the expression of photosynthetic genes in the nucleus (Shimizu *et al.*, 2019; Masuda *et al.*, 2020) **(Figure 13)**. Oxidative stress yields FC1 activation, which mediates heme accumulation in the chloroplasts. FC1 is transcriptionally activated under cadmium exposure. The *Arabidopsis fc1* null mutant is sensitive to Cd provision. This mutation triggers to downregulation of 522 genes, including metal transporters. While overexpression of FC1 leads to more Cd tolerance, biomass and chlorophyll content improvement, and a decrease in H_2O_2/O^{2-} contents (Song *et al.*, 2017). Under salinity, FC1 leads to more tolerance, reduces Na^+ levels in the cell, and accumulates K^+ ions to prevent the cell membrane from lysis. The suppression of FC1 under salinity engenders downregulating 380 gene-specific to salt-induced oxidative stress response, monovalent cation-proton (Na^+/H^+) exchange, and Na+ detoxification (Zhao *et al.*, 2017; Fan *et al.*, 2019). FC1 is also strongly

induced by wounding and ozone exposure (Nagai *et al.*, 2007). The activation of FC1 targets principally increases the expression of GUN4, CA1, HEMA1, LHCB2.1, Mg-chelatase, and H-subunit (ChlH) nuclear-encoded chloroplast photosynthetic genes (Page *et al.*, 2020). The overexpression of FC1 leads to the heme accumulation and the increase in the expression of Fe-chelatase-dependent heme synthesis and the *PHOTOSYNTHESIS-ASSOCIATED NUCLEAR genes (PhANGs)* (Woodson *et al.*, 2011) **(Figure 13)**. The mutation gun4 triggers the alteration in rhythmic mRNA levels of circadian genes such as *CIRCADIAN CLOCK ASSOCIATED1 (CCA1), the LATE ELONGATED HYPOCOTYL (LHY),* and *TIMING OF CAB EXPRESSION1 (TOC1)*. GUN4 can interact with SRP43 and SRP54 to coordinate the LHCB protein assembly, promoting photosynthesis and sucrose production (Li *et al.*, 2021). Indeed, the metabolism resulting from photosynthesis, such as sucrose accumulation, modulates the circadian rhythmicity (Dalchau *et al.*, 2011; Haydon *et al.*, 2017; Feugier and Satake, 2013). The retrograde pathway from plastid to nucleus regulates a sensing mechanism governing the circadian iron responses via phytochrome (Salomé *et al.*, 2013) **(Figure 13)**. To modulate the iron uptake activity according to the external iron status, The *Arabidopsis* plant changes its circadian periods. The period becomes longer when Fe is limiting and progressively shorter under external iron availability. The circadian clock regulates IRT1 expression. While plants with impaired chloroplast are characterized by longer circadian period (Chen *et al.*, 2013) **(Figure 13)**. The mutation in the central clock genes, CCA1 and LHY, causes the reduction of iron uptake capacity, especially the reduction in activity and expression of IRT1/FRO2 and the reduction in photosynthetic efficiency. While CCA1

overexpression leads to an opposite effect (Xu *et al.*, 2018). In addition, the *irt1* null mutant, which lacks a major iron uptake capacity, is characterized by an altered circadian period (Hong *et al.*, 2013). Fer1 gene expression coding for ferritin is also under control by the circadian clock nuclear regulator gene *TIME FOR COFFEE (TIC).* TIC negatively regulates the expression of several iron uptake-related genes like IRT1 and FRO2 during iron deficiency (Duc *et al.*, 2009). The MEDIATOR COMPLEX 16 (MED16) subunit is a positive regulator of the expression of circadian clock genes, such as CCA1and LHY (Knight *et al.*, 2008). MED16 promotes the expression of IRT1 and FRO2 by interacting with their specific transcription factors. The suppression of MED16 triggers a strong decrease in IRT1/FRO2 expression leading to low iron concentration in the cell and to leaves chlorosis (Y., Zhang *et al.*, 2014).

2.3 The regulation of the first barrier iron transporter driving the systematic iron metabolism: What is important to know?

2.3.1 IRT1 protein: tridimensional modeling and structural properties

In *Arabidopsis thaliana*, the *AT4G19690* gene located on the chromosome 4 is encoding for the *ARABIDOPSIS IRON-REGULATED TRANSPORTER 1 (IRT1).* IRT1 protein sequence is composed of 347 amino acid residues. This protein has a molecular weight around 36.7 kDa. IRT1 was discovered in 1996 by the group of Ms. Guerinot (Eide et al., 1996) and belongs to the family of the ZIP metal transporters

which are mainly responsible for metal uptake in the plant. The ZIP family takes its name from ZRT and IRT-related metal transporter Proteins (Eng *et al.*, 1998; Guerinot, 2000). Several ZIP members have been identified and characterized in *A. thaliana*. ZIP proteins are predicted to be localized at the plasma membrane. They are known for their topological similarity in the constitution of eight to nine transmembrane domains (309-476 amino acids and similar molecular weight 33-42.72 kDa) (Guerinot, 2000). Most ZIP family members are predicted to have very short cytoplasmic C-terminus and a large cytosolic loop including a stretch of histidines which is characterized by its metal-binding affinity issential for the transport cations such as Fe^{2+} as well as Mn^{2+}, Co^{2+}, Zn^{2+}, and Cd^{2+} (Guerinot, 2000; Dubeaux *et al.*, 2018; Grossoehme *et al.*, 2006).

As ZIP a protein, The IRT1 tridimensional model showing the atomic structure of the protein (Q38856) was obtained from the 3D structure Alphafold database (alphafold.ebi.ac.uk) (Varadi *et al.*, 2022) **(Figure 9 A and B**). The PDB file underwent sidechain energy minimization on FoldIt Standalone (Kleffner *et al.*, 2017), using RosettaCM algorithms (Das and Baker, 2008), to resolve sidechain atomic clashes on the model. PDB file was then visualized by UCSF Chimera (Pettersen *et al.*, 2004). PDB file was used to run PDB2PQR tool, which prepared the structure by reconstructing missing atoms, adding hydrogens, assigning atomic charges and radii from specified force fields developed specifically for Poisson-Boltzmann calculations (APBS calculations). PDB2PQR computations were done in combination with Dock Prep tool. Then water solvent was omitted from the APBS calculation. Rosetta computations leads to avoid clashes between

residues (hydrogen bonds and disulfides) after reactions between solvent-hydrophobic residues.

IRT1 protein contains nine hydrophilic domains shown as helix in the **Figure 9 .C**, and tubes in the **Figure 9. D**. The functional analysis of IRT1 by the InterPro server (https://www.ebi.ac.uk/interpro) (Blum *et al.*, 2021), shows eight transmembrane domains (53-73), (85-106), (126-143), (193-213), (225-245), (275-280), (286-306), (327-346) and a transmembrane signal polypeptide (1-30). IRT1 is known for its metal coordination loop (144-192) containing a histidine rich motif HGHGHGH which is crucial in many cations sensing such as Zn^{2+}, Mn^{2+}, Cd^{2+}, Co^{2+} (Rogers *et al.*, 2000a; Dubeaux *et al.*, 2018; Grossoehme *et al.*, 2006) **(Figure 9 .C and K) (Figure 10)**. The confidence metric measurement of the 3D model showed high pLDDT values for most of the residues, while the cytoplasmic region of the protein was characterized by low pLDDTs indicating a potential high flexibility of this region compared to the protein backbone or an intrinsic disorder (Blum *et al.*, 2021). pLDDT (protein Local Distance Difference Test) is a score for the automated assessment of PDB structure prediction servers without manual intervention. This score evaluates local distance differences of all atoms in a PDB model, including validation of stereochemical plausibility (Mariani *et al.*, 2013).

The cavity analysis in the 3D model of IRT1 by MOLE2.5 (https://mole.upol.cz/) (Luk´ *et al.*, 2018) showed the localization of interconnected cavities (25639 $Å^3$) 68.41% of the total volume of IRT1 atomic structure (37476 $Å^3$) **(Figure 9 .G)**. Cavities are important features of biomolecular structures. They are involved in the trafficking

of molecules through the transporter protein (Luk´ *et al.*, 2018). Moreover, the structural analysis of electrostatic surface of IRT1 showed that most of regions surrounding cavities, are composed by negative charged residues (colored in red). While the histidine rich motif at the metal coordination loop was composed by positive charged residues (colored in blue) **(Figure 9 .H)**. Potentially, this repartition of charged residues leads the selective transport of divalent cations by the protein. It has been shown that in ZIP proteins The scaffold domain is generally electrostatically neutral or hydrophobic, while the transport domain is typically considerably polar (Wiuf *et al.*, 2022). It was known that electrostatic complementation between surfaces plays an important role in to facilitate the metal transfer (Huffman and Vincent O'halloran, 2001). The negative electrostatic surface of a cytoplasmic domain of a transporter protein increases the local concentrations of metal ions inside the intracellular funnel, favoring the direction of metal flux. The ability for a protein to transport metals depends on its electrostatic state. The electrostatic stabilization of an ion by a water-filled cavity in a protein can be understood through a calculation based on the Born theory of solvation. This is given by the relation: " $\Delta G\,(Q) = \frac{1}{2}\,AQ^2 + BQ + C$ " where Q is the ion charge, A is the reaction field created by the ion in the protein dielectric environment ,B is the static field created by the protein charges, and C is the effect of the ion dielectric on the protein charges (Tan *et al.*, 2009).

The mutational substitution of some amino acids in IRT1 protein, leads to an alteration in the selective transport of iron, zinc, manganese (Kerkeb *et al.*, 2008; Potocki *et al.*, 2013; Barberon, Zelazny, Robert, Conéjéro, Curie, Jirí Friml, *et al.*, 2011). **Figure 10** highlights the

essential amino acid residues for the transport of Fe^{2+} (colored in red)(Quintana *et al.*; Felipe *et al.*, 2022), Zn^{2+} transport (colored in purple) (Rogers *et al.*, 2000a; Potocki *et al.*, 2013; Blindauer, 2015; Felipe *et al.*, 2022) and Histidines in the metal coordination loop necessary for metal sensing (colored in black) (Grossoehme *et al.*, 2006; Dubeaux *et al.*, 2018; Cointry and Vert, 2019). The 3D model of IRT1 shows also cytosolic sites of phosphorylation (colored in pink) (Dubeaux *et al.*, 2018; Cointry and Vert, 2019) and ubiquitination (colored in blue) (Barberon *et al.*, 2014; Barberon, Zelazny, Robert, Conéjéro, Curie, Jiří Friml, *et al.*, 2011; Dubeaux *et al.*, 2018; Cointry and Vert, 2019) that are important post-translational modifications affecting the fate of IRT1, as detailed hereafter.

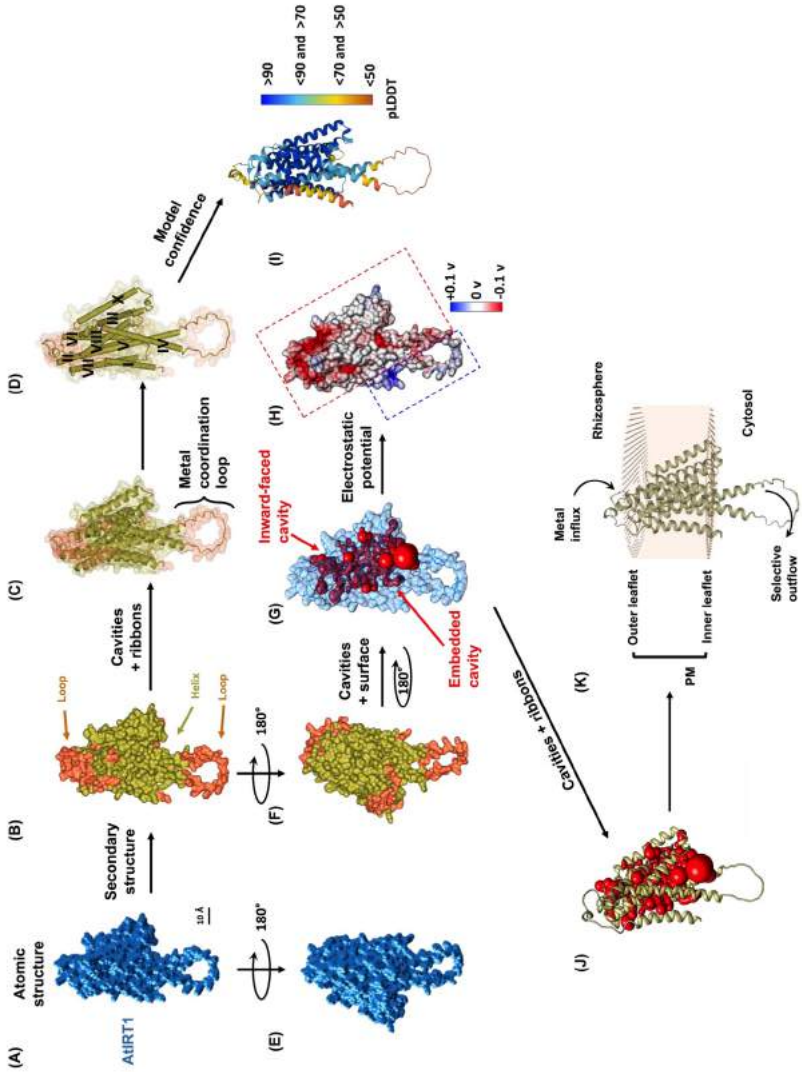

Figure 9. Structural analysis of the 3D model of IRT1.

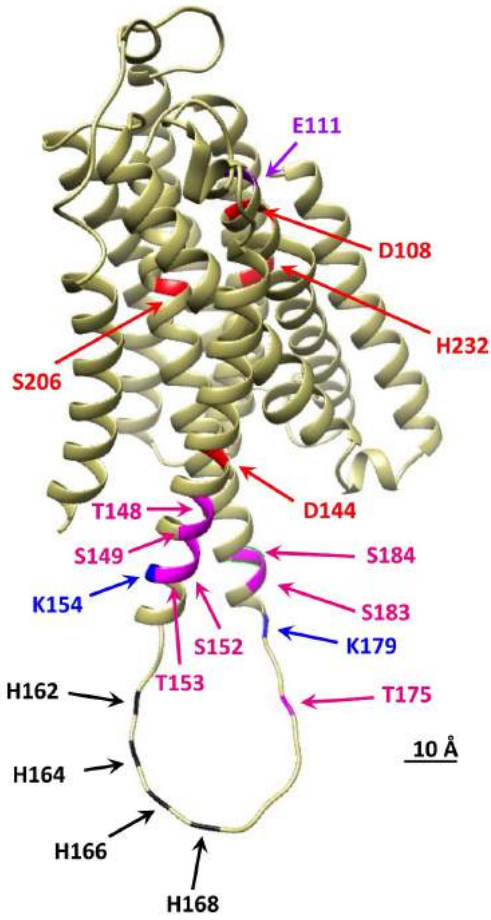

Figure 10. Essential residues for metal transport, metal sensing, phosphorylation, and ubiquitination in IRT1

2.3.2 The dual transcriptional/post-translational regulations orchestrate IRT1 uptake activity under different physiological conditions

2.3.2.1 Transcriptional-regulatory-system strictly oversights IRT1 expression

In *A. thaliana*, the iron uptake through IRT1 is crucial for many cellular metabolisms. Uncontrolled iron importation can directly affect iron homeostasis in the cell. The continuous iron uptake triggers ferric toxicity, while the iron deficiency leads to chlorosis. To avoid these risks, a functional transcriptional regulatory system, including specific transcription factors (TFs), controls *IRT1* expression under multiple physiologic conditions. *FER-LIKE IRON DEFICIENCY-INDUCED transcription factor* (FIT) is induced by iron deficiency. It heterodimerizes with four *basic Helix-Loop-Helix* TFs from the family of $bHLH_{Ib}$ (bHLH038, bHLH039, bHLH100, and bHLH101) to activate IRT1 expression under iron deficiency (N., Wang et al., 2013; Yuan et al., 2008; Brumbarova et al., 2015) **(Figure 11)**. Overexpression of FIT with either AtbHLH38 or AtbHLH39 in plants converted the expression of the iron uptake genes *FRO2* and *IRT1* from induced by iron deficiency to constitutive (Yuan et al., 2008). While the suppression of these TFs genes causes a dramatic decrease in IRT1 and FRO2 expression. Transcriptomic studies show that the triple mutation *bhlh39, bhlh100, and bhlh101* impairs the regulation of 198 genes, 15% of these genes are related to iron homeostasis, (Maurer et al., 2014; N., Wang et al., 2013; Sivitz et al., 2012).

FIT acts as a master regulator of iron homeostasis. Its capacity of dimerization with $bHLHI_{bs}$ is driving the control of multiple genes expression related to iron transport and metal non-iron transport. The combination of FIT/$bHLH_{Ib}$ positively regulates COPT2, FRO4, and FRO5 during Cu transport (Cai et al., 2021). Likewise, the FIT/bHLH38/bHLH39 combination regulates the expression of the *HEAVY METAL ASSOCIATED3* (HMA3), the *METAL TOLERANCE PROTEIN3* (MTP3), the *IRON REGULATED TRANSPORTER2* (IRT2) and the *IRON REGULATED GENE2* (IREG2) implicated in metal detoxification in Arabidopsis cells during Zn, Ni and Cu excess (Wu et al., 2012; Wang et al., 2007). FIT negative turnover is crucial during iron availability to prevent the cell from iron toxic hyperaccumulation. Two *BRUTUS-LIKE E3* ligases (BTSL1 et BTSL2) mediate FIT recycling. The double mutation *btsl1-2* triggers FIT stabilization, resulting in IRT1 overexpression (Rodríguez-Celma et al., 2019). In addition, the *ZINC FINGER OF ARABIDOPSIS THALIANA12* (ZAT12) can interact with FIT, allowing its degradation under high levels of H_2O_2 in the cell **(Figure 11)**. ZAT12 acts as indirect repressor of *IRT1* induction (Le et al., 2016). During iron deficiency, FIT is highly phosphorylated through its serine at position 272 by the *CBL-INTERACTING PROTEIN KINASE* (CIPK11). FIT phosphorylation by CIPK11 promotes homodimerization and heterodimerization with bHLH39 regulating *IRT1* expression **(Figure 11)**. The iron deficiency instigates the accumulation of Ca^{2+} in the cytosol, which activates CBL1/9 mediating CIPK11 (Gratz et al., 2019; Wu and Ling, 2019; Gu et al., 2021). FIT stabilization depends on phytohormone signaling. The *ETHYLENE INSENSITIVE3* (EIN3) and *ETHYLENE INSENSITIVE3-LIKE1* (EIL1) act as stabilizer interactors

of FIT. The Arabidopsis *ein3 eil1 double mutant* is susceptible to iron deficiency (J. Meiser et al., 2011; García et al., 2010; Lingam et al., 2011).

FIT stabilization also depends on Gibberellin signaling DELLA repressors which interact with FIT in the root epidermal cells and prevent the DNA binding and transactivation of IRT1 during iron availability (Wild et al., 2016). While the inhibition of Gibberellin biosynthesis downregulates IRT1 in the cell (Matsuoka et al., 2014). Moreover, the Jasmonic acid (JA) negatively controls *IRT1* gene expression by inducing TFs bHLH $_{(Iva)}$: bHLH18, bHLH19, bHLH20, and bHLH25. $bHLH_{Iva}$ are antagonists to $bHLH_{Ib}$ and can form heterodimers with FIT, leading to its degradation (Cui et al., 2018). *FIT* and *bHLH$_{Ib}$* are transcriptionally controlled **(Figure 11)**. A member of $bHLH_{IVc}$, the bHLH121, activates *FIT* expression through interacting with *FIT* promoter. The deletion of this $bHLH_{IVc}$ transcription factor highly impairs the iron uptake machinery in the plant and causes a severe chlorosis (Lei et al., 2020). Four $bHLH_{IVc}$: bHLH34, bHLH104, bHLH105/ILR3 and bHLH11, can form a heterodimer to promote $bHLH_{Ib}$ induction. Another TF: POPEYE (PYE, bHLH47) from the $bHLH_{IVb}$ family acts with bHLH11 as negative regulators of *IRT1* expression (Tanabe et al., 2019; Long et al., 2010). During iron deficiency, BTS E3 ligase negatively regulates PYE via the 26S proteasome pathway (Selote et al., 2015). Under iron sufficiency, increased levels of Fe are sensed through the HHE domains altering BTS conformation and stability to trigger its proteolysis (Selote *et al.*, 2014). PYE downregulates iron uptake and promotes iron allocation in the plant **(Figure 11)**. It can bind directly to *NICOTIANAMINE SYNTHASE 4* (*NAS4)*, *FRO3*, and *ZINC INDUCED FACILITATOR 1*

(ZIF1) promoters, which upgrades the iron distribution in plant organs (Van Dingenen, 2021; Selote et al., 2015).

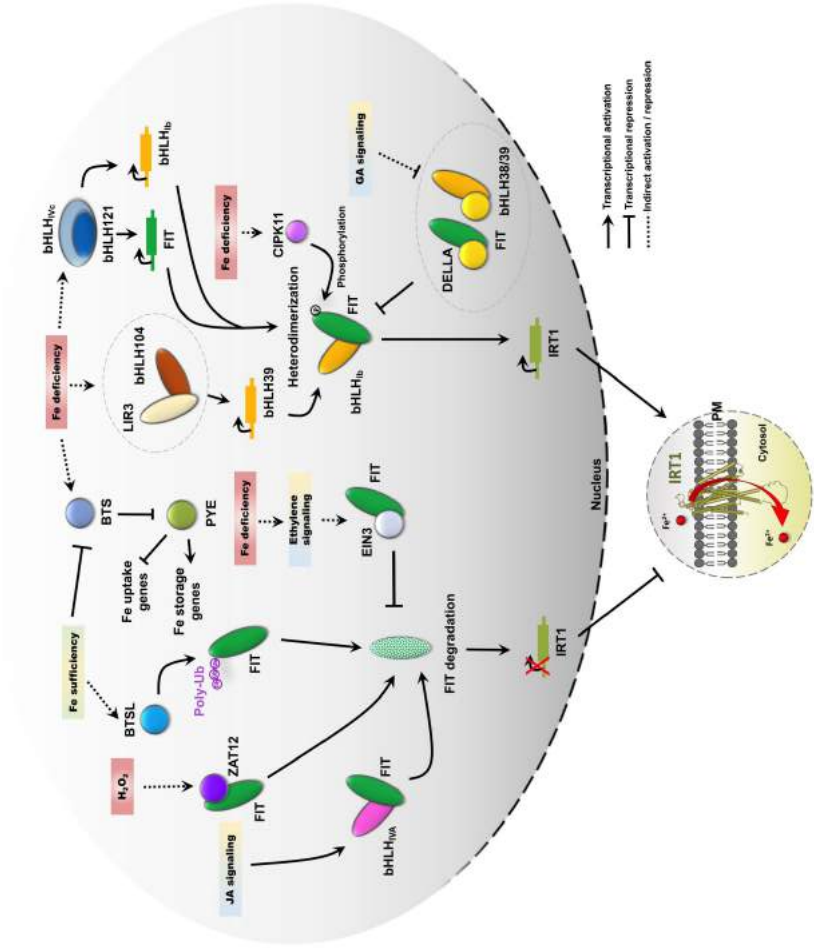

Figure 11. Model of transcriptional regulation of IRT1 depending on Fe status and phytohormones signaling

2.3.2.2 What about IRT1 polarity? IRT1 endocytosis and degradation are controlled by IRT1 non-iron metal substrates in a ubiquitin-dependent manner

2.3.2.2.1 IRT1 polarity, turnover and degradation depends on the level of its non-iron metal suberates

In addition to the transcriptional network system, which strictly controls *IRT1* expression, a post-translational regulome drives IRT1 recycling and degradation during different nutritional conditions. IRT1 is a plasma membrane protein, known for its capacity of multi-metal transport, with iron as primary metal substrate. IRT1 can transport a range of non-Fe metals such as Zn, Mn, Co and Cd (Quintana *et al.*; Felipe *et al.*, 2022; Rogers *et al.*, 2000a; Potocki *et al.*, 2013; Blindauer, 2015; Grossoehme *et al.*, 2006; Dubeaux *et al.*, 2018; Cointry and Vert, 2019; Barberon *et al.*, 2014; Barberon, Zelazny, Robert, Conéjéro, Curie, Jiří Friml, *et al.*, 2011). Under starvation of IRT1 secondary metal substrates, this transporter protein is polarly localized at PM (Barberon *et al.*, 2014; Dubeaux *et al.*, 2015). IRT1 is also targeted to be ubiquitinated through its cytosol-exposed lysine residues K154 and K179. The mutant IRT1(K154R, K179R) is known for its impaired ubiquitination, this mutant protein accumulates at the PM (Barberon *et al.*, 2014). The availability of non-iron metals triggers IRT1 monoubiquitination by IDF E3, then its internalization and endosomal sorting. This result in decreasing the IRT1 pool at PM by a turnover

between Endosomes and PM to prevent metal accumulation and to ensure a possible iron uptake during iron requirement conditions (Barberon *et al.*, 2014). Recycling of IRT1 requires the presence of *SORTING NEXIN 1* (SNX1) and probably deubiquitination (Blum *et al.*, 2014; Brumbarova *et al.*, 2015) **(Figure 12.B)**. The deletion of *SNX1* gene provokes a decrease in IRT1 levels and promotes its degradation (Ivanov *et al.*, 2014). In addition, the *snx1 null mutant* is sensitive to iron deficiency. The SNX1 mutation increases FIT and bHLHIb transcripts in roots (Ivanov et al., 2014). Interestingly, in excess of non-Fe metals under iron deficiency, the IRT1 regulation is strictly requested to reduce the metal accumulation associated with the request for iron uptake (Barberon, Zelazny, Robert, Conéjéro, Curie, Jirí Friml, *et al.*, 2011; Barberon *et al.*, 2014; Vert *et al.*, 2002). Sensing of non-Fe metals through IRT1, requires the binding of these metals to histidine residues at the multi-histidine IRT1 loop (H-stretch) situated at the permeation exit domain (Dubeaux *et al.*, 2018). Mechanistically, this process likely results from multi-histidine-loop folding of metal-loaded IRT1 which directly recruits *CBL-INTERACTING PROTEIN KINASE (CIPK) CIPK23* leading to IRT1 phosphorylation at some serine/threonine residues. In addition, this creates a docking site for *IRT1 DEGRADATION FACTOR1 (IDF1)* E3 ligase, which targets IRT1 (Shin *et al.*, 2013; Dubeaux *et al.*, 2018; Cointry and Vert, 2019). Phosphorylation by CIPK23 is essential to increase the IDF1/IRT1 interaction resulting in K63 polyubiquitination of IRT1 (Dubeaux *et al.*, 2018; W., Li *et al.*, 2022) **(Figure 12.C)**. Moreover, the Arabidopsis plant *mutant idf1* shows a higher level of IRT1 and a resistant phenotype under iron deficiency compared to the WT (Chen et al., 2013). Furthermore, the ubiquitination defective form of IRT1, is

stabilized at PM and cannot undergo the internalization (Barberon, Zelazny, Robert, Conéjéro, Curie, Jirí Friml, *et al.*, 2011). IRT1 is also localized at PM when there is no excess of its secondary metal substrates. IRT1 ubiquitination leads to its internalization, targeting to MVBs and then transport to the lytic vacuole(Barberon, Zelazny, Robert, Conéjéro, Curie, Jirí Friml, *et al.*, 2011; Dubeaux *et al.*, 2018). Besides, K63 polyUb is a Ub linkage mediating the internalization and endosomal sorting of proteins (Johnson and Vert, 2016).

2.3.2.2.2 Endocytosis mechanism of a membrane protein transporter via CME

As many of membrane transporters, the ubiquitinated IRT1 is a considered as cargo for Clathrin-Mediated Endocytosis (CME) mechanism during essential for its internalization (Barberon, Zelazny, Robert, Conéjéro, Curie, Jìří Friml, *et al.*, 2011; Zelazny and Vert, 2015; Chen *et al.*, 2011; Baisa *et al.*, 2013). In this pathway several specific proteins move on the MP and bind at the same time to specific sequences on the cargo as well as Clathrin. A well-known example is the *Adaptor Protein 1 and 2* (AP1 and AP2), which belong to the heterotetramic subunit family called adaptin (Fan *et al.*, 2013; Chen *et al.*, 2011). APIs complexed with the cargo leads to the formation of a vesicle covered with Clathrin (Clathrin coated vesicles: CCVs) which will be delivered to the endosome (Mosesso *et al.*, 2019; Reynolds *et al.*, 2018). These AP proteins share the same origin with other vesicular complex multiproteins such as COPI (Coat complex I) and TSET/TPC (TPLATE SET /TPLATE complex). Generally, COPI-related vesicles are responsible for intra-Golgi retrograde as well as Golgi-RE (Svitáková, 2018; Boruc and Van Damme, 2015; Yperman *et al.*, 2021).

TPLATE complex is considered an alternative adapter system of APIs. TCP is virtually the most essential system of endocytosis in the plant that recruits both AP2, Clathrin, and several other dynamic proteins (Gadeyne *et al.*, 2014). Other systems also exist in the endocytosis of transmembrane proteins, such as the Clathrin-independent pathway, observed during salinity and dependent on ADP-Ribosylation Factor-guanidine / (ARF-GEF) *VACUOLARPROTEIN SORTING6* (Lam *et al.*, 2007; Brumm *et al.*, 2020; Jaillais and Gaude, 2007). It has been shown that API2 is functional exclusively at PM. In the CME, API2 it is essential for the initiation, assembly, and maturation of CCVs (McMahon and Boucrot, 2011). Another issential protein *FLOTILLIN1 (FLOT1)* is involved in the formation of the endocytic vesicle (Li *et al.*, 2012; Cao *et al.*, 2020). After detachment from the PM, the endocytic vesicle is transported to an affinity of the TGN most often known as TGN/EE. In the plant cell, TGN/EE lacks phosphatidylinositol 3-phosphate (PI3P) which instead accumulates in MVBs, LEs and at the vacuolar membrane (Noack and Jaillais, 2017; H., N., Lee *et al.*, 2020). The next step is mediated through a protein complex of called ENDOSOMAL SORTING COMPLEX REQUIRED FOR TRANSPORT (ESCRT). ESCT complexes are necessary for the transport and exit of endocytosed cargoes to be internalized into MVBs and then to reach the lytic vacuole for degradation (Paciorek *et al.*, 2005; Uemura *et al.*, 2004; Saint-Jore-Dupas *et al.*, 2004).

2.3.2.2.3 The transport and fusion mechanism of endocytosed membrane protein transporter with MVBs

It has been demonstrated that the K63 polyubiquitination chain promotes the interaction with Ub-binding receptors from the ENDOSOMAL SORTING COMPLEX REQUIRED FOR TRANSPORT (ESCRT) complex which triggers the endosomal sorting of many membrane proteins such as Brassinosteroid-Insensitive-1 (BRI1) (plasma membrane-localized receptor kinase for brassinosteroids) and *AUXIN EFFLUX CARRIER COMPONENT 2* (PIN2) (required for cellular efflux of auxin) (Leitner *et al.*, 2012; Martins *et al.*, 2015). Moreover, *TOM-like proteins (TOL)* are known for their ability to recognize the K63 polyubiquinated proteins triggering their endosomal sorting to the lytic vacuole, such as PIN2 (Gao *et al.*, 2017). Some TOLs, such as TOL6 are mainly observed near to the PM, which indicates that the sorting of Ub-cargos could be happened just after internalization (Romero-Barrios and Vert, 2018). Also, The *SH3 domain-containing protein 2* (AtSH3P2) is known to be localized at the PM, in clathrin-coated vesicles and in endosomes. This protein is known by its highest affinity for vesicles containing PtdIns(3,4,5)P3 through its capacity to bind phosphatidylinositol-phosphate (Zhuang *et al.*, 2013). It targets the K63 polyUb proteins for delivery and mediating ESCRT pathway (Romero-Barrios and Vert, 2018). ESCRT is a well conserved and classic mechanism for membrane protein sorting for further degradation in plants. This multi sub-unit complex system mediates endocytosis through the sorting and delivery of polyubiquitinated cargoes in LEs/MVBs to the lytic

vacuole. Plants lack canonical ESCRT-0 subunits as compared to animals. While three ESCRT-I subunits are known in plants: VPS23, VPS28 and VPS37. Accordingly, VPS23 is localized in endosomes and directly binds Ub. It also interacts with an ESCRT-1 homolog *(VPS23p/TSG101 homolog)*. ECL is able to bind Ub and also localize in endosomes (Spitzer *et al.*, 2006; Dubeaux and Vert, 2017). Also, VPS23 interacts with VPS37 and VPS38 (Spitzer *et al.*, 2006). *vps28* and *vps37* knockout plants are characterized by an impaired endosomal sorting, especially during the immune response (Spallek *et al.*, 2013). Sub-units of the ESCRT-I complex are known by their high ability to bind polyubiquitinated proteins. FREE1 (FYVE1) is an example of atypical member of ESCRT-I complex. This protein can bind phosphatidylinositol-3-phosphate (to be recruited to the LE) as well as Ub (Barberon *et al.*, 2014; Gao *et al.*, 2014). FREE1 interacts with VPS23 (ELC/AtVPS23A and AtVPS23B) via a PTAP-like tetrapeptide motif (Gao *et al.*, 2014; Barberon *et al.*, 2014). The knockout plant of this gene is unable to develop, it fails in MVB biogenesis , as well as in endosomal sorting (Gao *et al.*, 2014; Kolb *et al.*, 2015; Zhao *et al.*, 2015). It has been shown that FREE1 binds to IRT1 (Barberon *et al.*, 2014) **(Figure 12.C)**. Interestingly, FREE1 is degraded during iron starvation through the interplay between SINAT1 and RING E3 ligases (Xia *et al.*, 2020). FYVE1 was shown to control the subcellular localization of IRT1. This endosome-recruited protein interacts with IRT1 in the endocytic pathway. It is essential for IRT1 polarity, via its recycling to the PM (Barberon *et al.*, 2014; Dubeaux *et al.*, 2015). Thus, the overexpression of FYVE1 results in IRT1 accumulation at the PM in an apolar manner, in condition where IRT1 is normally mainly present in early endosomes (Barberon *et al.*, 2014). ESCRT-like

complexes are crucial for the delivery of endocytoses proteins to the lytic vacuole. ESCRT-II complex is composed of three subunits: VPS22, VPS25 and VPS36. VPS22 is known to be involved endosomal sorting through its capacity in binding Ub and regulating MVBs biogenesis (Wang *et al.*, 2017). Then, ESCRT-III complex is made up of several sub-units: CHMP proteins (*CHARGED MULTI VESICULAR BODY PROTEINS*), *INCREASED SALT TOLERANCE 1 (ISTL1)* protein, SNF7, VPS20, VPS24, VPS2 and VPS60 proteins. The suppression of any protein from the ESCRT-III complex triggers failure in MVB biogenesis (Cai *et al.*, 2014; Spitzer *et al.*, 2006). In addition, *vps.2.1* and *chmp1a-chmp1b* mutations are lethal (Cai *et al.*, 2014; Katsiarimpa *et al.*, 2013). Two sub-units of the ESCRT-III complex (VPS2.1 and VPS24.1) bind to the complex containing the polyubiquitinated cargo, mediating its delivery to the LE/MVB by ALIX protein. This complex interfere with AMSH3 involved in cargo deubiquitination (Dubeaux and Vert, 2017) **(Figure 12.C)**.

2.3.2.2.4 Other regulatory interactants of IRT1 at the plasma membrane

Recently, IRT1 was shown to interact with two membrane proteins essential for iron uptake: the proton pump AHA2 and the reductase FRO2 (Martín-Barranco et al., 2020). It has been shown that the three proteins form a tripartite complex through direct interaction. It was proposed that this complex may create a local environment of low pH and high Fe^{2+} concentration in the rhizosphere to optimize iron uptake by IRT1 under iron starvation. FRO2 and AHA2 are ubiquitinated in a constitutive manner and, contrary to IRT1, they are not massively endocytosed in response to non-Fe metals excess, due to the

dissociation of the IRT1-AHA2-FRO2 complex following IRT1 phosphorylation (Martín-Barranco et al., 2020). Furthermore, it has been shown that IRT1 interacts with the C2 domain-containing peripheral membrane protein ENHANCED BENDING1 (EHB1). EHB1, complexed with two calcium ions, binds to the rich histidine cytosolic loop of IRT1. EHB1 is recruited to the PM and binds phosphoinositides such as PtdIns4P. EHB1 triggers the inhibition of IRT1 transport activity through a mechanism that remains unknown. The mutation of *EHB1* reinforces IRT1 stabilization at the PM leading to an increase in the cellular iron levels (Khan et al., 2019) **(Figure 12.B)**.

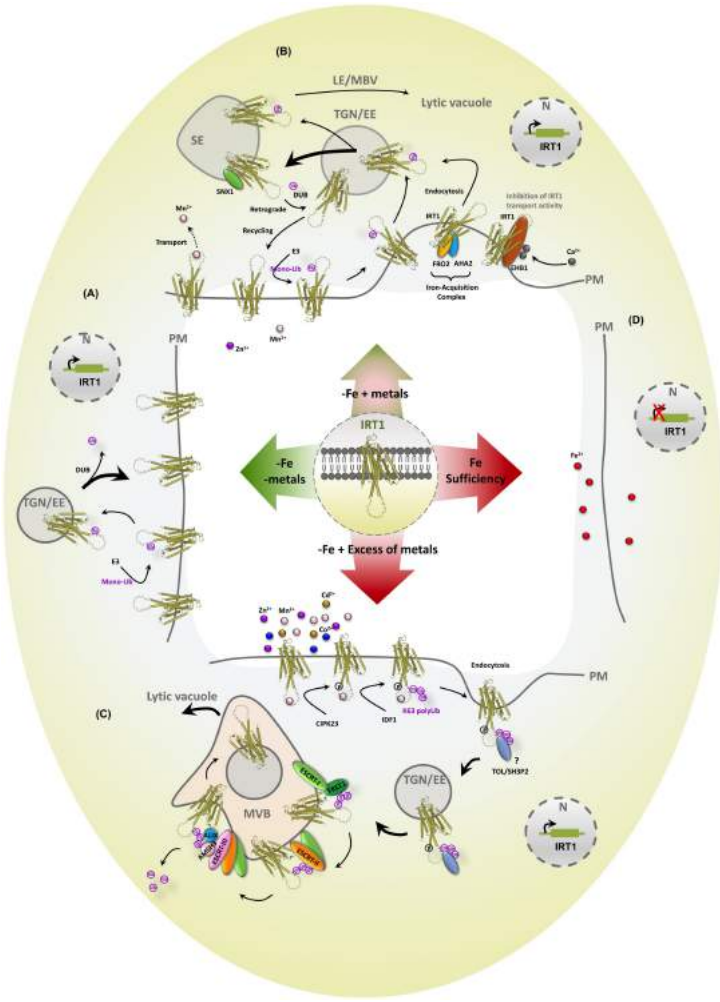

Figure 12. Model of post-translational regulation of IRT1 depending on non-Fe metal substrates and ubiquitin mediating endocytosis and degradation

2.4 Out-of-sight involvement of the multi-stress regulator TSPO in the modulation of iron uptake under stress: New tracks in the regulation of IRT1 in Arabidopsis

2.4.1 Relationship between the toxic side of IRT1 and LIP modulation during stress

The IRT1 is expressed in many organs in *A. thaliana,* such as the flowering parts and many root-related structures, including cells in roots, primary roots, root tip, lateral roots, maturation zone, radicle, root phloem companion cells, etc. (Vatansever *et al.*, 2015). During the plant development stages, IRT1 is expressed in germinated seeds seedlings and young rosette stages (Vatansever *et al.*, 2015). The expression of AtIRT1 in yeast *Saccharomyces cerevisiae* leads to an increase in iron uptake. While the addition of cadmium (Cd) in the culture medium blocks its capacity for iron transport. Moreover, the overexpression of IRT1 in *S. cerevisiae* in the presence of Cd in the culture medium causes a Cd hyper uptake and toxicity to the yeast organism (Rogers *et al.*, 2000b). In *A. thaliana*, the constitutive expression of IRT1 triggers an increase in the labile iron pool level in the cells (up to 10x more than in the Wild Type (WT) plants). IRT1 overexpression drives an increase in Mn, Co, and Zn levels in the plant (Barberon, Zelazny, Robert, Conéjéro, Curie, Jirí Friml, *et al.*, 2011). The IRT1 overexpressor *Arabidopsis* plant mutant suffers from dramatic metal accumulation, provoking oxidative stress. This plant mutant is characterized by the decrease in the root biomass and aerial organs development (Barberon, Zelazny, Robert, Conéjéro, Curie, Jirí Friml, *et al.*, 2011). The plant

cell needs iron in small quantities. The IRT1 overexpression evokes a toxic iron hyper uptake and iron stocking (Eide *et al.*, 1996; Robinson *et al.*, 1999; BRIAT and LOBREAUX, 1997; Wei and Theil, 2000). IRT1 functional localization at PM triggers the uptake of potentially toxic metals such as manganese, zinc, cobalt, and cadmium. IRT1 stability at the PM could be very toxic to the cell and yield metal overload and oxidative stress (Barberon, Zelazny, Robert, Conéjéro, Curie, Jirí Friml, *et al.*, 2011).

IRT1 transcripts and protein levels are rapidly degraded by increasing LIP after iron deficiency, whereas the mutation btsl1/2 causes its stabilization under the same conditions (Rodríguez-Celma *et al.*, 2019) **(Figure 4B)**. In addition, the mutation of IDF1 triggers also stabilizing IRT1 during increasing LIP after iron deficiency (Shin *et al.*, 2013). The expression of IRT1 under stress is influenced by stress phytohormones, such as ABA, triggering to decrease in levels of IRT1 in roots, which limits the toxic metal loading (Fan *et al.*, 2014; Pan *et al.*, 2020; Gu *et al.*, 2021; P., Zhang *et al.*, 2019). Osmotic stress and salinity trigger cellular ABA accumulation and influence the expression of iron uptake-related genes. IRT1 expression is downregulated under salinity and mannitol treatment (Séguéla *et al.*, 2008). Also, salinity, osmotic stress, and ABA treatment trigger to decrease in FIT levels in the cell (Kanwar *et al.*, 2021). During oxidative stress, the heme production branch in tetrapyrroles biosynthesis is highly activated (Zhao *et al.*, 2017; Fan *et al.*, 2019) **(Figure 4B)**, which promotes heme accumulation in the chloroplast and enhances the levels of free heme in the cytosol. The signal transduction of abiotic stimuli such as salinity and osmotic stress and hormonal responses such as ABA yields increased HO activity, especially HY1 (HO1) (Xie *et al.*, 2016; Wang

et al., 2016). HO1 plays a central role in heme catabolism in the chloroplast by producing carbon monoxide involved in ABA-induced stomatal closure (Xie *et al.*, 2016) and increasing LIP in the cell (Li *et al.*, 2013). Salinity, osmotic stress, and ABA treatment lead to a transitory increase of TSPO levels in the cell (Guillaumot, Guillon, Déplanque, *et al.*, 2009). TSPO is known to act as a heme scavenger leading to its degradation via selective autophagy. Downregulation of TSPO triggers an increase in the free heme levels in the cell under oxidative stress (Vanhee, Zapotoczny, *et al.*, 2011). Heme degradation yields to iron releasing and increasing LIP (Li *et al.*, 2013) **(Figure 4B)**. Although, endogenous IRT1 is usually localized at TGN/EE in the steady-state (Barberon, Zelazny, Robert, Conéjéro, Curie, Jirí Friml, *et al.*, 2011; Ivanov and Vert, 2021; Ivanov *et al.*, 2014). Indeed, TSPO is a transmembrane protein localized at the outer membrane of ER, Golgi stacks, and TGN (Guillaumot, Guillon, Déplanque, *et al.*, 2009; Vanhee, Guillon, *et al.*, 2011; Jurkiewicz *et al.*, 2020). The *Arabidopsis* TSPO interacts physically with the membrane protein aquaporin PIP2;7 at the endoplasmic reticulum and Golgi membranes. The complex containing both proteins is degraded via autophagy (Hachez *et al.*, 2014). Under stress conditions, TSPO reduces water loss by depleting PIP2;7 in the plasma membrane (Jurkiewicz *et al.*, 2020). During evolution, TSPO homologs share a highly conserved sequence, especially on transmembrane domains from plants to humans in the mitochondrial membrane (Y., Lee *et al.*, 2020). The Arabidopsis is characterized by a conserved polybasic, plant-specific N-terminal extension necessary to bind signaling Lipids, especially PI(4,5)P2 mediating TSPO-PIP2;7 Interactions Vivo (Jurkiewicz *et al.*, 2020). On the other hand, the direct relation between IRT1 and TSPO seems

enigmatic. Yet, there is no proof of potential physical interaction, whereas the two proteins are localized at TGN/EE.

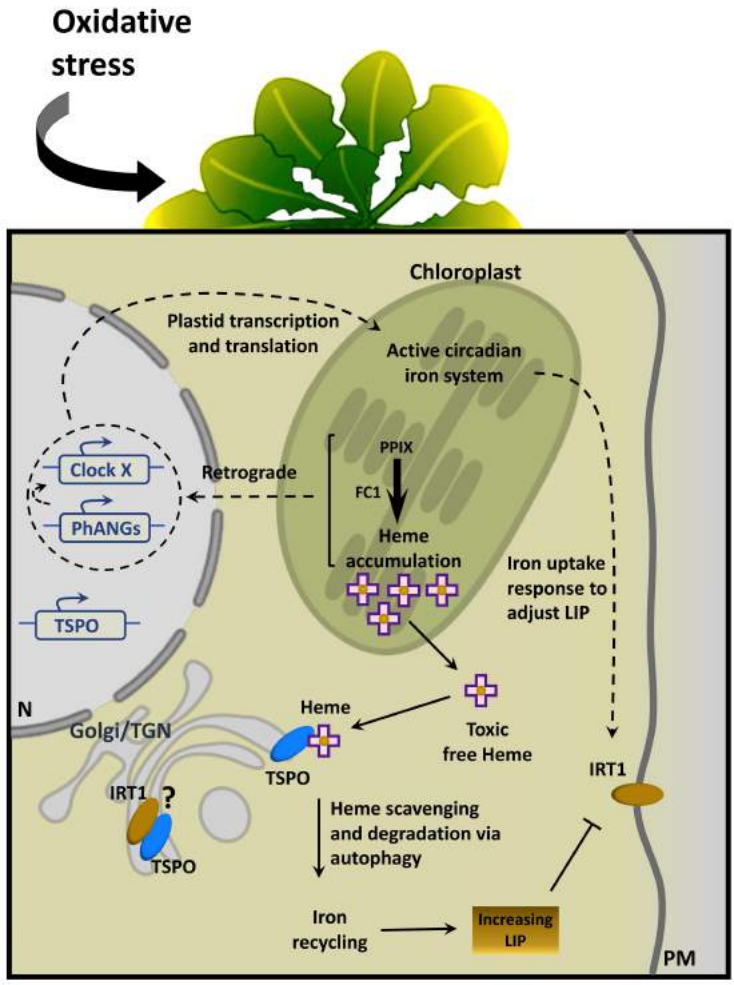

Figure 13. The implication of the heme modulation under stress on the regulation of Arabidopsis IRT1 iron transporter.

3 Chapter III: Recapitulation of the Literature review 2: Concluding Remarks and future perspectives

This part introduces a newfangled concept about the modulation of iron uptake in the plant model *Arabidopsis thaliana*. The regulation of iron transporter protein IRT1 in Arabidopsis has always been a challenging area to study. Here, we demonstrate the impact of the cellular iron availability in regulating IRT1 in steady conditions and especially under iron-related stress. Iron availability depends on altering levels between heme-iron and non-heme iron, mainly LIP **(Figure 14)**. This fluctuation is strictly governed by regulatory pathways such as heme catabolism, circadian clock, etc. An increased understanding of this regulation leads us to provoke the putative involvement of the multi-stress regulatory protein TSPO in modulating the iron uptake process driven IRT1 **(Figure 14)**. Moving forward, we consider the direct regulatory effect of TSPO on iron transporters as an outstanding subject in the future to mitigate oxidative stress in plants. The Arabidopsis TSPO as a multi-stress transiently induced protein serves to scavenge free toxic heme and triggers its degradation via the autophagic pathway **(Figure 15)**. This degradation process may allow the cell to rapidly recycle iron under stress conditions. Understanding the probable crosstalk between this potential heme-degradation mechanism and iron uptake process, depending on the IRT1 regulation, could be considered a promising research area for iron homeostasis.

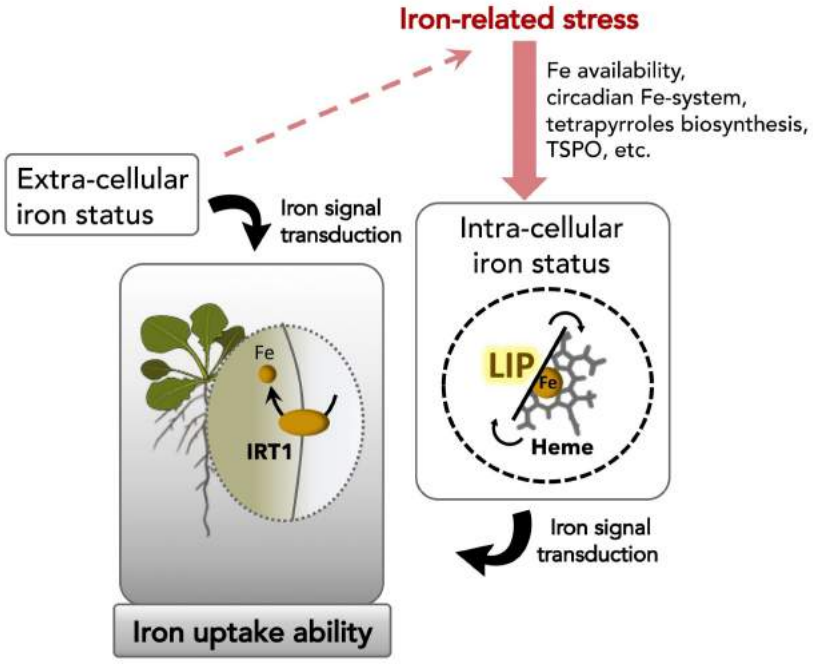

Figure 14. A simplified schematic diagram about the modulation of iron uptake in the plant model *Arabidopsis thaliana*.

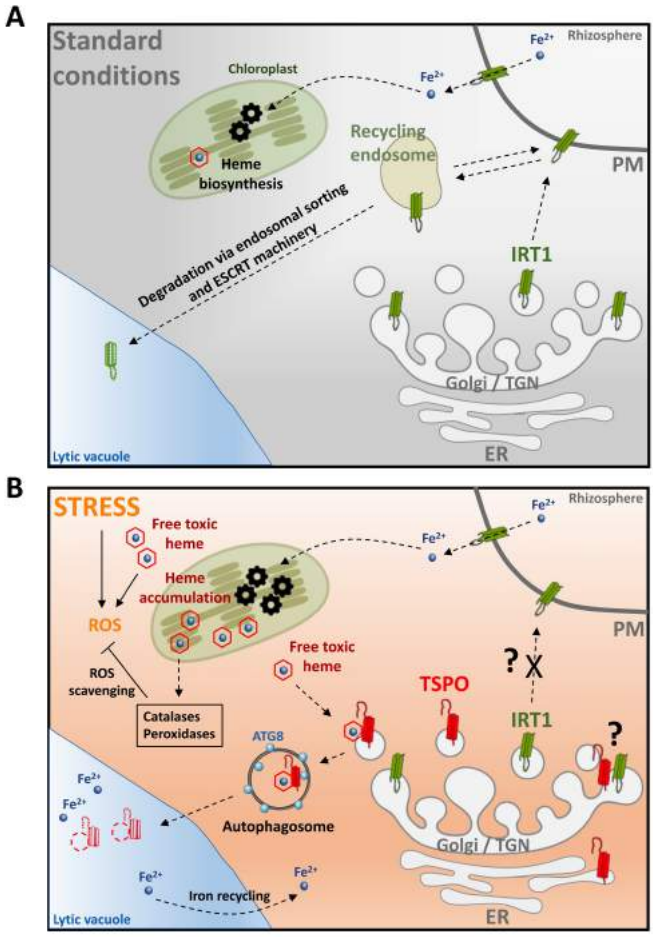

Figure 15. Hypothetical model **(A)** Subcellular trafficking and degradation of IRT1 during standard conditions **(B)** The impact of TSPO in binding free heme, triggering its degradation via autophagy pathway under oxidative stress conditions, which promotes cellular iron recycling.

PART IV

Objectives

In this thesis, our research focuses primarily on the regulation of the iron transporter protein IRT1 in *Arabidopsis thaliana.* It has for reflection origin three main bases: **First and foremost**, The IRT1 degradation mechanism depends on the iron and metal levels in the growth medium and on the plant's requirement for iron. Under stress such as iron deficiency, root cells strictly regulate IRT1 levels at the PM to avoid excessive metal uptake. **Secondly**, it is ascertained that the Arabidopsis multi-stress-induced protein TSPO plays a potential role in iron recycling through its indispensable implication on heme degradation via the selective autophagy pathway. **Thirdly**, it has been shown in previous work that under oxidative stress, TSPO plays a significant role in mitigating the targeting of a transmembrane protein (The water channel transporter aquaporin PIP2;7) to the PM. TSPO physically interacts with PIP2,7 in the ER and Golgi membranes and triggers its degradation via the autophagic pathway.

In this context, this thesis seeks to answer a series of biological questions: • Is there any proof indicating that iron deficiency triggers TSPO expression? • Is there evidence for co-regulation between TSPO and IRT1? • Is there any direct involvement of TSPO in the IRT1 degradation mechanism?

To achieve these purposes, this work is divided into three sub-targets: (1) To study the potential impact of TSPO induction in IRT1 regulation. **(2)** To investigate the potential effect of IRT1 overexpression in the regulation of TSPO. **(3)** To check the potential role of TSPO protein, known as an autophagy receptor, on the mechanism of IRT1 degradation under multi-stress conditions in *A. thaliana.*

PART V

Results & discussion

4 Chapter IV: Co-regulation between the stress induced transmembrane hemoprotein TSPO and the plasma membrane iron transporter IRT1 in *A. thaliana*: Molecular and physiological evidence

Abstract

The *Arabidopsis thaliana* translocator protein (AtTSPO) is transiently induced under several abiotic stress conditions, including osmotic stress, salinity, and abscisic acid treatment. The level of AtTSPO in the cell is tightly regulated, and AtTSPO is actively degraded through a selective autophagy pathway. The endoplasmic reticulum and mainly Golgi-localized AtTSPO degradation requires heme binding, with the histidine residue at position 91 (H91) acting as a heme axial coordinator. The potential link between heme scavenging through AtTSPO degradation resulting in iron recycling from the vacuole and its possible effect on iron homeostasis, including the iron uptake mechanism, remains unclear. In this study, we show that constitutive expression of AtTSPO resulted in transgenic *Arabidopsis* lines with substantially reduced levels of *IRON-REGULATED TRANSPORTER 1* (IRT1) and a significant increase in iron levels in *Arabidopsis* dry seeds.

Furthermore, we found that AtTSPO expression is transiently induced by iron deficiency and is constitutively induced in the *irt1* null mutant. In addition, overexpression of IRT1 induces AtTSPO

expression. These findings suggest that heme scavenging by the autophagic degradation of AtTSPO contributes to iron recycling. In particular, the levels of IRT1 in the cell may be regulated by the relative levels of AtTSPO.

4.1 Introduction

The management of the labile iron pool in the cell (LIP) under iron-limiting conditions is directly related to the iron uptake capacity and distribution mechanisms. Iron (Fe^{2+} and Fe^{3+}) is crucial in many plants' metabolic processes. In *A. thaliana*, the reduction-based Fe-uptake strategy is established to facilitate iron uptake from the soil into the root cells. This strategy involves many proteins: such as the plasma membrane H^{+}-ATPase proton extrusion pump required for the apoplast acidification leading to iron solubilization (Santi and Schmidt, 2009). Then Fe^{3+} is chelated by phenolic compounds. These compounds are exported by the pleotropic ABC transporter ABCG37/PDR9 (Fourcroy *et al.*, 2016). During iron acquisition, the chelated Fe(III) is reduced to Fe(II) by a *PLASMA MEMBRANE-BOUND FERRIC CHELATE REDUCTASE* (FRO2). Fe^{2+} is then transported into the cell root by the *IRON-REGULATED TRANSPORTER 1* (IRT1), a transmembrane metal transporter protein required to uptake also non-iron divalent metal ions such as $Mn^{2+,}$ Zn^{2+}, CO^{2+}, and Cd^{2+} (Vert *et al.*, 2002; Han *et al.*, 2014; Brumbarova *et al.*, 2015). It was suggested that IRT1 acts as a transporter and a receptor (transceptor)(Dubeaux *et al.*, 2018; Cointry and Vert, 2019). IRT1 may sense non-iron metals excess during iron deficiency deficiency in the rhizosphere, resulting in its downregulation and degradation by a substrate-dependent regulatory mechanisms (Dubeaux et al., 2018). Furthermore, the intracellular iron

status seems to be a controlling factor for IRT1 expression, while metal status controls IRT1 polarity. IRT1 trafficking is known to be between the plasma membrane, endosomes, trans-Golgi network (TGN), MVBs, and lytic vacuole (Dubeaux *et al.*, 2018; Barberon, Zelazny, Robert, Conéjéro, Curie, Jirí Friml, *et al.*, 2011; Barberon *et al.*, 2014; Ivanov *et al.*, 2014). Under metal excess in iron deficient medium, IRT1 senses the relative abundance of its secondary metal substances. Under this condition, IRT1 at the plasma membrane is mainly phosphorylated by CBL-interacting protein kinase 23 (CPK23). Phosphorylated IRT1 is then polyubiquitylated, leading its clathrin-dependent endocytosis (Dubeaux *et al.*, 2018; Barberon, Zelazny, Robert, Conéjéro, Curie, Jirí Friml, *et al.*, 2011; Shin *et al.*, 2013) and triggering IRT1 degradation via ESCRT complex. Under iron deficiency, several components of the endocytic machinery are involved in this process, such as the sorting nexin 1 (SNX1), promoting either the endosomal sorting of IRT1 (recycling process) to the plasma membrane (Khan *et al.*, 2019; Ivanov *et al.*, 2014; Ivanov and Vert, 2021). Under iron limitation, several processes, such as photosynthesis and cellular respiration, are severely affected, causing chlorosis correlated with decreased cellular heme levels in young leaves and photo-oxidative damage caused by reactive oxygen species (ROS) (Yu and Xie, 2017; Hirayama *et al.*, 2018). Plant acclimation to abiotic stress, such as salinity, osmotic stress, drought, nutrients deficiency, etc., requires a complex gene regulatory network in response to such unfavorable conditions (Yasuda *et al.*, 2008; Davletova *et al.*, 2005). Phytohormones play a crucial role in controlling downstream stress responses by regulating multiple stress-responsive genes. Abscisic acid (ABA) is one of the essential phytohormones in stress signaling, which plays a critical role in plant

development and vegetative growth (Tuteja, 2007). For example, water-related stress is sensed in the root and aerial parts of *Arabidopsis thaliana*, inducing the accumulation of ABA, mainly in the leaf to trigger the stomatal closure to reduce water lost by evapotranspiration (Shatil-Cohen *et al.*, 2011; de Zelicourt *et al.*, 2016; Hachez *et al.*, 2014). Overall, ABA is produced under dehydration conditions and plays a vital role in enhancing vegetative tissues' tolerance against drought stress (Uno *et al.*, 2000; Finkelstein *et al.*, 2002; Xiong and Zhu, 2003; Fujita *et al.*, 2005). The drought-induced ABA in the xylem reduces the osmotic water permeability (Pf) by downregulating the activity of Aquaporins (AQPs) (Shatil-Cohen *et al.*, 2011). Transcriptionally, ABA treatment also induces the multi-stress tryptophan-rich sensory protein/translocator (TSPO) (peaking around ~3-6 h post-induction) (Guillaumot, Guillon, De Planque, *et al.*, 2009; Hachez *et al.*, 2014). The *Arabidopsis* TSPO was shown to be a heme scavenger contributing in free heme degradation via a selective autophagy mechanism (Vanhee et al., 2011). Boosting tetrapyrrole biosynthesis increases the degradation of AtTSPO, while ABA-induced AtTSPO may be partly involved in reducing potentially toxic free heme in the cytosol. The return to the steady-state of free heme in the cell is concomitant with the downregulation of AtTSPO (Vanhee, Guillon, *et al.*, 2011). It has been shown that TSPO can bind free heme in vivo and in vitro through its axial histidine residue at position 91 (H91). Accordingly, the upregulation of AtTSPO triggers a decrease in the relative levels of unbound heme in the cell (Vanhee, Guillon, *et al.*, 2011), suggesting possible recycling of iron from the lytic vacuole as a consequence of heme degradation through AtTSPO-heme complex autophagic degradation (Vanhee, Guillon, *et al.*, 2011).

In this report, we provide evidence suggesting that the expression of AtTSPO affects the relative levels of IRT1 in the cell and vice versa. We propose that there may be a fine co-regulation between IRT1 and AtTSPO to coordinate iron uptake and intracellular recycling, in particular during stressful conditions.

4.2 Results

4.2.1 Iron deficiency transiently induces AtTSPO

Under iron deficiency, many essential metabolic pathways directly related to LIP management and signaling are severely imbalanced in plant cells. In particular, previous studies reported that iron deficiency was accompanied by increased active ABA in the plant within 6 h (Lobreaux *et al.*, 1993; Connolly *et al.*, 2002). In parallel, heme levels in the plant decreases under iron deficiency (Hirayama *et al.*, 2018; Santos *et al.*, 2019). Since ABA induces AtTSPO, we wondered whether AtTSPO is regulated by iron deficiency as a response of ABA upregulation in *Arabidopsis* cells (Lei *et al.*, 2014; Hirayama *et al.*, 2018). We grew *A. thaliana* seedlings in vitro in ½ Murashige and Skoog (MS) agar (control medium). We used three genetic backgrounds: wild-type (WT) Col-0 line, a transgenic line constitutively expressing AtTSPO (OE TSPO), and an AtTSPO knockout line (KO TSPO) (Guillaumot, Guillon, De Planque, *et al.*, 2009; Vanhee, Zapotoczny, *et al.*, 2011). **Figure 16A** shows that AtTSPO was not detectable by western blotting in 7-days-old WT seedlings under standard growth as compared OE TSPO line which constitutively expresses the protein. We transferred the seedlings on ½

MS broth with or without 150 µM ferrozine (iron chelator; 3-(2-Pyridyl)-5,6-diphenyl-1,2,4-triazine-p,p-disulfonic acid monosodium salt hydrate). Interestingly, as shown in **Figure 16B**, right panel), after 24 h of incubation under iron deficiency, interestingly AtTSPO expression was detected in WT seedlings, a band of the same relative molecular size as in OE TSPO seedlings, with, as expected, no signal in KO TSPO seedlings. Transcriptionally, stress and ABA-induced AtTSPO is stronger in the aerial part as compared to the roots (Rasheed *et al.*, 2018). Therefore, we probed AtTSPO expression comparatively in the aerial part and the root separately. **Figure 16C** shows that most if not all the weak AtTSPO signal detected by western blot after iron deficiency of WT seedlings is contributed by the root extract, as no signal could be detected in the shoot extract.

Next, we co-assessed the expression kinetics of both AtTSPO and IRT1 under iron deficiency condition as above, in a time course experiment. **Figure 16D** shows that increase in endogenous IRT1 expression was noticeable as from 7h after transfer to an iron-deficient medium, and IRT1 levels increased up to 32 h after the transfer. In contrast, AtTSPO was clearly detected between 24–32 h, reminiscent of the peak observed after ABA induction (Guillaumot, Guillon, De Planque, *et al.*, 2009). These results suggest that AtTSPO expression is also relatively early response to iron deficiency.

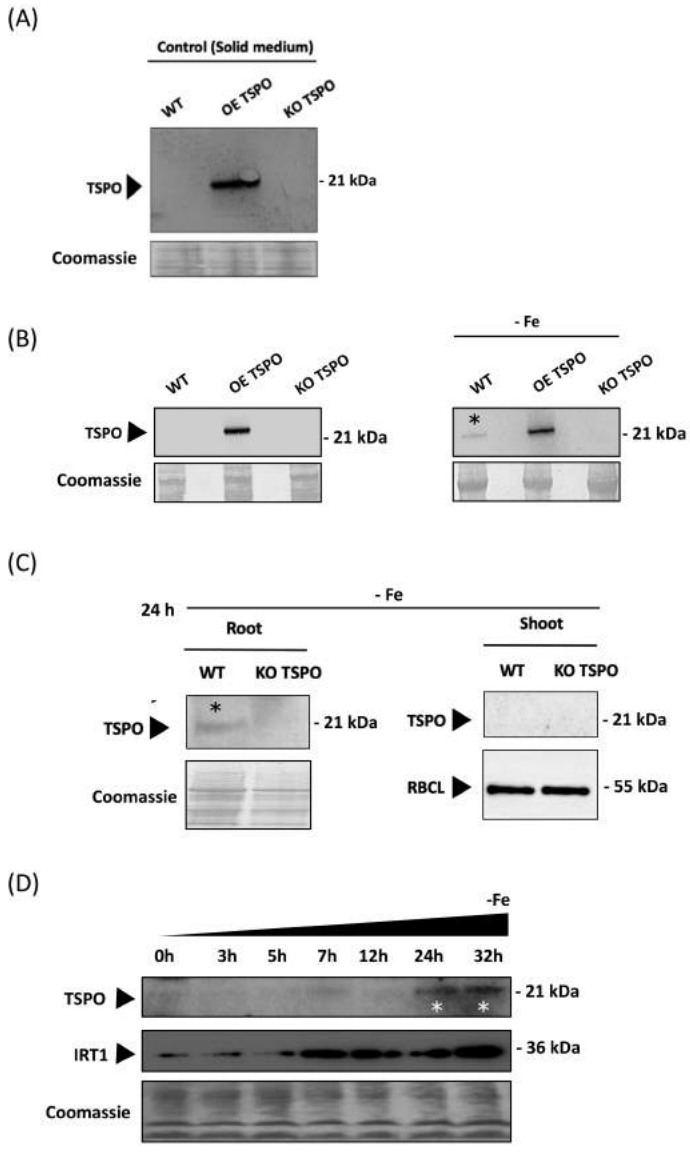
(A)
Control (Solid medium)
WT
OE TSPO
KO TSPO
TSPO
- 21 kDa
Coomassie
(B)
- Fe
WT
OE TSPO
KO TSPO
TSPO
- 21 kDa
Coomassie
*
(C)
24 h
- Fe
Root
Shoot
WT
KO TSPO
TSPO
- 21 kDa
Coomassie
RBCL
- 55 kDa
(D)
-Fe
0h
3h
5h
7h
12h
24h
32h
TSPO
- 21 kDa
IRT1
- 36 kDa
Coomassie

Figure 16. Iron deficiency induces AtTSPO in the *A. thaliana* root tissues. **(A)** and **(B)**: *Arabidopsis* wild-type seedlings (WT), transgenic seedlings overexpressing AtTSPO (OE TSPO), and seedlings knockout for AtTSPO (KO TSPO) were gown for seven days in ½ MS solid medium in (A) and were transferred to a free iron ½ strength MS liquid medium in (B); the expression of AtTSPO (≈21 kDa) was monitored by immunoblotting of total protein extract from seedlings. AtTSPO was not detected in WT and KO TSPO (A and right panel in B). expression was detected in WT seedlings after incubation in iron-free medium for 24 h. Coomassie blue-stained replica gel was used for relative loading comparison. **(C)** After incubating WT and knockout seedlings in an Iron-free medium for 24 hours, AtTSPO expression was probed by western blotting. Total proteins extractswere prepared from sampled roots and shoots . AtTSPO expression was detectable only in the root sample after iron deficiency treatment. We used Rubisco large subunit (RBCL) and replica gels stained with Coomassie blue as a loading control. **(D)** Time course induction of AtTSPO and IRT1 (≈36 kDa) in root. WT seedlings were incubated in iron-free ½ strength MS liquid medium for 0, 2, 5, 7, 12, 24, and 32 hours. Total protein extracts were subjected to protein gel blotting and probed using anti-AtTSPO and anti-IRT1. Coomassie blue-stained replica gel is shown as loading control. AtTSPO expression was after 24 and 32 hours of incubation, while the increase of detectable IRT1 was evidence as from 7 h of treatment.

Stress-dependent expression of ATSPO in vegetative tissues is transient (Kreps *et al.*, 2002; Winter *et al.*, 2007; Guillaumot, Guillon, De Planque, *et al.*, 2009; Vanhee and Batoko, 2011a; Hachez *et al.*, 2014). After ABA treatment, AtTSPO expression is concomitant to a transient increase in unbound heme levels in the cell (Vanhee, Zapotoczny, *et al.*, 2011). To further investigate the induction of AtTSPO in the root by iron deficiency, (WT, KO AtTSPO), overexpressing mutant OE AtTSPO) and a relatively stable point mutant OE AtTSPO(H91A (Vanhee, Zapotoczny, *et al.*, 2011) seedlings were first grown on a standard solid medium and then transferred and incubated in liquid medium with or without extended iron deficiency (7 days). Total protein extracts from roots were analyzed using western blotting. **Figure 17A** shows that AtTSPO was not detected in the extract of WT plants incubated for 7 days in an iron deficiency medium. In contrast, a relatively weak signal of AtTSPO expression could be detected after 24h of iron deficiency **(Figure 16B)**. We quantified this expression and normalized it using actin levels as an

internal control **(Figure 17B)**. The ratio AtTSPO/actin as histogram in **Figure 17B** suggest that extended iron deficiency resulted in substantial reduction in AtTSPO express in seedlings as compared to untreated sample. However, this was not the case with the mutant sample overexpressing the AtTSPO (H91A) variant, which has lower affinity for heme and is relatively stable **(Figure 17B)**. Indeed, AtTSPO(H91A) was not affected by iron deficiency, and the relative quantity of TSPO(H91A) was not significantly decreased as compared to control sample **(Figure 17B)**.

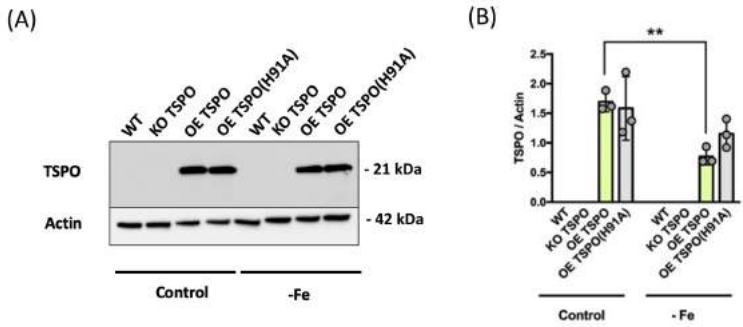

Figure 17. Iron deficiency can modulate AtTSPO expression and stability. **(A)** Seven-day old Arabidopsis wild-type (WT) seedlings or Transgenic seedlings were transferred from control ½ strength MS solid medium to liquid medium with or without ferrozine and incubated for 7 days. The levels of AtTSPO (≈21 kDa) were monitored by immunoblotting of total protein extract from seedlings. Anti-actin (≈42 kDa) was used as loading control. **(B)** Relative quantification of AtTSPO levels: the ratio of AtTSPO over actin signal for each treated or control was plotted as histograms. Statistical significance was assessed by a one-way ANOVA followed by Tukey's test (** $p < 0.01$).

Under iron deficiency, root growth and development and particularly the length of the primary and the number of lateral roots decrease (Satbhai *et al.*, 2017; Gruber *et al.*, 2013). We found that the root length of AtTSPO knockout and overexpressing seedlings was altered after iron deficiency treatment, as compared to WT seedlings **(Figure S1C)**.

During 7 DAS (Days After Stratification), KO AtTSPO seedlings significantly exhibit lower roots elongation under iron limitations as compared to the WT (± 49 % shorter primary root on the 7th day). Otherwise, the constitutive expression of AtTSPO seems to significantly raise the root length under iron deficiency (by ± 39.2 % on the 7th day) compared to the WT. At the same time, compared to the WT seedlings, Fe deprivation seems not to influence the length of the primary roots in the seedlings overexpressing the relatively stable form of AtTSPO(H91A) **(Figure S1D to H)**.

It is known that Iron deficiency induces a severe alteration in multiple physiological parameters such as the plant biomass and chlorophyll alteration (Nenova, 2008; López-Millán *et al.*, 2013; Hantzis *et al.*, 2018; Li *et al.*, 2019). Iron is required for the photosynthetic metabolism, such as the electron transfer reaction, the biosynthesis of chlorophyll, the iron-sulfur cluster proteins, and superoxides dismutases (FeSODs), etc. (Marsh *et al.*, 1963; Hu *et al.*, 2017; Gallie and Chen, 2019). During iron deficiency, chlorophyll content was three timeless in WT seedlings compared to standard conditions. Besides, under the same conditions, KO AtTSPO seedlings significantly exhibit

a decrease in chlorophyll content and lower biomass compared to WT **(Figure S1 I and J)**.

4.2.2 Constitutive expression of AtTSPO decreases the level of IRT1 in *A. thaliana* root

Iron uptake machinery involves IRT1, FRO2, and coumarin biosynthetic genes, which are downregulated by osmotic and salinity stress (Kanwar *et al.*, 2021). It was shown previously in response to salinity or osmotic stress, the stressed-induced AtTSPO is involved in the downregulation of the plasma membrane aquaporin PIP2;7 (Hachez *et al.*, 2014; Jurkiewicz *et al.*, 2020). AtTSPO expression was shown to trigger the degradation of aquaporin en route to the plasma membrane and decreases its abundance in the plasma membrane to protect the cell from water deficit (Hachez *et al.*, 2014). Accordingly, we investigated any possible regulatory effect of the expression of AtTSPO on IRT1 levels. After 24 h of incubation in control and iron-deficient liquid medium, protein extracts from treated and control samples were analyzed by western blotting to assess the expression of AtTSPO and IRT1. As shown in **Figure 18** (left panel), under standard conditions, IRT1 was readily detected in the Arabidopsis WT and transgenic KO TSPO seedlings. Interestingly, no IRT1 expression was detected in seedlings overexpressing wild type AtTSPO, in contrast to seedlings expressing the relatively stable variant AtTSPO(H91A). **(Figure 18)**. It was known that iron deficiency triggers IRT1 induction and accumulation in Arabidopsis plants (Vert *et al.*, 2002; Barberon, Zelazny, Robert, Conéjéro, Curie, Jirí Friml, *et al.*, 2011). Figure 18 shows that iron deprivation for 24h boosts IRT1 accumulation in root

extracts respectively in WT, KO AtTSPO, and mutants overexpressing the WT ATTSPO and the relatively stable version AtTSPO(H91A). The gel immuno-botting clearly shows that, in contrast with the WT, iron deficiency triggers less IRT1 accumulation in the presence of the constitutively expressed AtTSPO. At the same time, his effect is slighted when a relatively stable version of AtTSPO was overexpressed (**Figure 18)**.

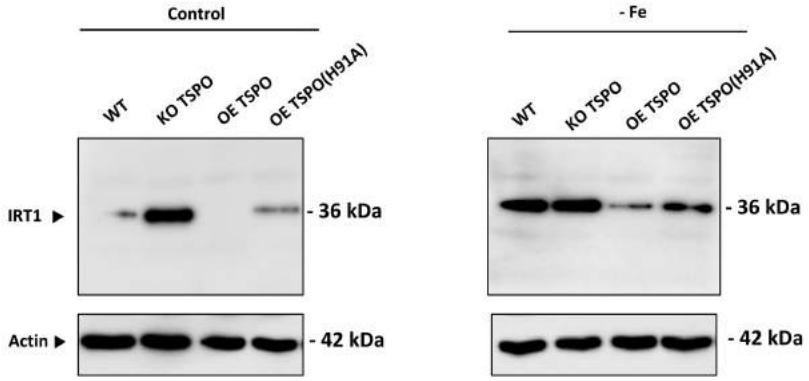

Figure 18. AtTSPO modulates IRT1 accumulation under iron deficiency. *Arabidopsis* 7 days old wild-type seedlings (WT), KO AtTSPO, OE AtTSPO and OE of the relatively stable version AtTSPO(H91A) were transferred from control ½ Ms solid medium to control and a free iron ½ Ms liquid for 24 h. IRT1 (≈36 kDa) levels were monitored by immunoblotting of total protein extract from seedlings. Anti Actin (≈42 kDa) antibody was used for loading comparisons in a replica Western blot.

4.2.3 Constitutive expression of IRT1 induces AtTSPO

It was shown that constitutive expression of IRT1 leads to metal over-accumulation and oxidative stress in the plant ((Barberon, Zelazny, Robert, Conéjéro, Curie, Jirí Friml, *et al.*, 2011; Barberon *et al.*, 2014).

To alleviate the over-accumulation of potential toxic metals, the plant cell accumulates ABA (Pan *et al.*, 2020; Hu *et al.*, 2020). Therefore, we checked the expression levels of endogenous AtTSPO when IRT1 was constitutively expressed. We used functional tagged IRT1 (mCherry fluorescent protein) to generate homozygous transgenic plant overexpressing IRT1-mCherry in different genetic backgrounds: WT, KO AtTSPO, OE AtTSPO, and OE AtTSPO(H91A). Homozygous transgenic seedlings were grown simultaneously in a standard ½ strength MS medium followed by total protein extracts preparation. We then compare the relative expression of AtTSPO in these samples using western blotting. Interestingly, **Figure 19A** shows that co-expression of IRT1-mCherry resulted in stable expression of AtTSPO in the WT background. The normalized quantification (ratio of TSPO/actin) in **Figure 19B** shows a significant decrease of about 30% in AtTSPO relative level in the double mutant OE AtTSPO IRT1-mCherry as compared to the single mutant OE AtTSPO. Comparatively, expression of IRT1-mCherry in the stable point mutant AtTSPO(H91A) resulted in a decrease of approximately 50% of detected AtTSPO under the same growth conditions.

Next, we subjected seedlings overexpressing IRT1-mCherry to iron deficiency in liquid medium as above. As shown in **Figure 19C**, the level of IRT1-mcherry and the endogenous IRT1 protein increased in the WT compared to the OE TSPO background. However, the levels of IRT1-mCherry transgene expression was higher in the KO TSPO. Besides, free mCherry (detected at 21 kDa) is coming from the IRT1-mCherry transgene degradation product, indicating an accumulation of the fluorescent tag protein in the vacuole. The free mCherry levels were lower under iron deficiency, indicating the stabilization of IRT1 at the

PM. It is known that most of IRT1 could be targeted to be recycled and resent from the endosomes to the PM (Barberon, Zelazny, Robert, Conéjéro, Curie, Jìří Friml, *et al.*, 2011; Dubeaux *et al.*, 2018). Interestingly, as shown in **Figure 19C,** no free mCherry was detected in the KO AtTSPO background in control and iron deficiency conditions compared to the WT background. This indicates that the absence of AtTSPO influences the IRT-mCherry degradation process. **Figure 19C** clearly shows that iron deficiency enhances AtTSPO levels in plants constitutively expressing IRT1-mCherry.

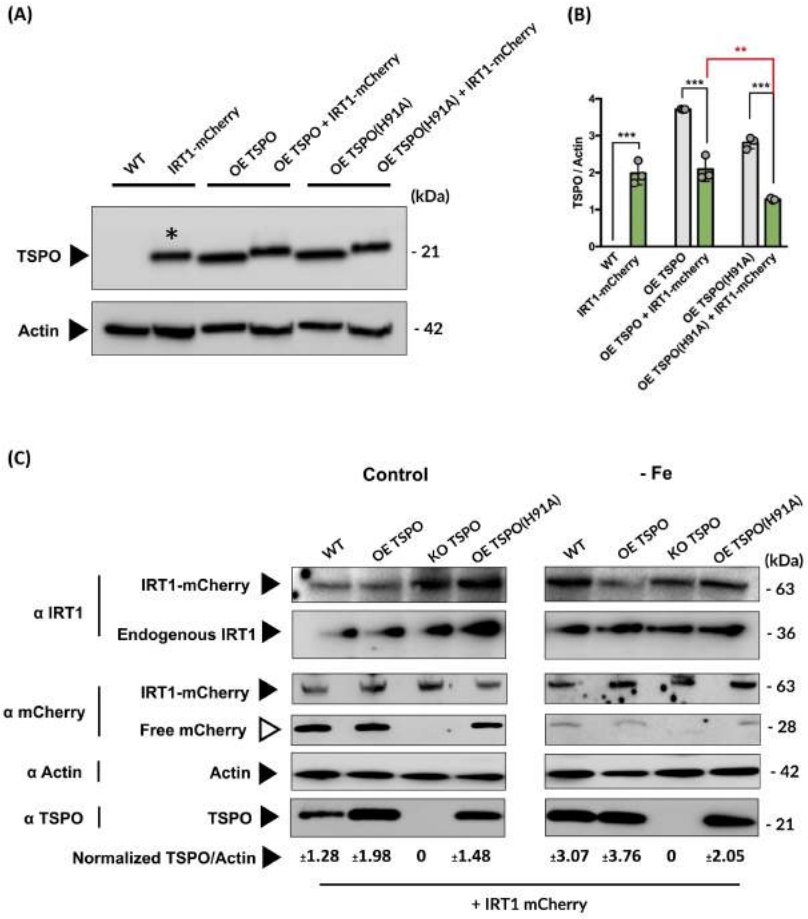

Figure 19. IRT1 overexpression triggers TSPO accumulation in *A. thaliana*. **(A)** Arabidopsis 7 days old wild-type seedlings (WT) and transgenic seedlings were grown in ½ Ms medium. AtTSPO (≈21 kDa) was monitored by immunoblotting of total protein extract from roots. Anti Actin antibody was used for loading comparisons (≈42 kDa). **(B)** The normalized ratio (AtTSPO/Actin) in each treated sample was compared with those in control. Statistical significance was assessed by one-way ANOVA followed by Tukey's tests (** $p < 0.01$, *** $p < 0.001$). **(C)** *Arabidopsis* 7 days old transgenic seedlings overexpressing IRT1-mCherry in the wild-type background (WT), OE AtTSPO, KO AtTSPO, and OE AtTSPO(H91A) backgrounds were transferred from control ½ Ms solid medium to control and a free iron ½ Ms liquid for 24 hours. The levels of IRT1 (≈36 kDa), AtTSPO (≈21 kDa), IRT1-mcherry (63

kDa), and mCherry monomer (28 kDa) were monitored by immunoblotting of total protein extract from roots. Anti Actin antibody was used in replica gel for loading comparisons (≈42 kDa). The ratio (AtTSPO/Actin) in control and each treated sample was measured and normalized.

Furthermore, IRT1 transgene overexpression, in addition to the endogenous protein in the absence of AtTSPO, significantly influenced the root morphology, especially in primary root lengths and in alteration of roots elongation rate under iron deficiency during 7 DAS, as shown in **Figure S2C to G.** Under iron limitation, homozygous transgenic seedlings overexpressing IRT1-mCherry in KO AtTSPO background have significantly ($p < 0.001$) longer roots compared to homozygous transgenic seedlings overexpressing IRT1-mCherry in WT and OE AtTSPO backgrounds, in contrast when transgenic plants only express endogenous IRT1 (previously shown in **Figure S1C to G)**. **Figure S2C to G** shows under iron deficiency, transgenic plants exhibiting the same phenotype of root length when IRT1-mCherry is constitutively co-expressed with the relatively stable version AtTSO(H91A) or expressed in KO AtTSPO background.

Moreover, in the rosette stage (20 d), the constitutive expression IRT1-mCherry, in addition to the endogenous IRT1, triggered a significant decrease in rosette diameter compared to plants expressing only the endogenous protein **(Figure S3A-B)**. **Figure S3C** shows a different flowering time point. KO AtTSPO was early flowering on day 28 after seed sowing. OE AtTSPO and OE AtTSPO(H91A) were flowering later than the WT (day 33 and day 35). In addition to that, in WT and TSPO genetic backgrounds (KO AtTSPO, OE AtTSPO, and OE AtTSPO(H91A)), this phenotype was altered by overexpressing IRT1-mCherry. The homozygous transgenic plants expressed

constitutively IRT1-mCherry were characterized by late-flowering (afterward for 34 days). Besides, KO AtTSPO transgenic plants undergo accelerated senescence compared to the WT and the mutants overexpressing AtTSPO and the relatively stable version AtTSPO(H91A). On day 40, as shown in **Figure S3D and E,** the shoot brunching number was significantly less in OE AtTSPO compared to the WT. At the same developmental stage, the constitutive expression of IRT1-mCherry triggers a decrease in shoot branching in the WT background.

4.2.4 AtTSPO modulates iron storage in Arabidopsis seeds

Seeds are sink organs for metal metabolism, especially iron, which is translocated from source organs (leaves) to sink organs (seeds). Under stress conditions such as zinc excess, iron is transported to seeds via autophagy, promoting intracellular iron recycling (Shinozaki *et al.*, 2021). Heme degradation through autophagy, which can be mediated by the degradation of AtTSPO, increases iron levels in the vacuole. Therefore, we wondered whether knockouted AtTSPO or ectopically overexpressed in addition to endogenous AtTSPO, could affect iron levels in dry seeds.

We analyzed metal content in dry seeds by Inductively Coupled Plasma Atomic Emission Spectroscopy (ICP-AES). **Figure 20A** shows Fe, Zn, Mn, Mg, K, Ca, and Cu content fold change by comparing WT to KO AtTSPO, OE AtTSPO, and AtTSPO(H91A) seeds. Interestingly, iron content increased in OE AtTSPO as compared to WT ($p < 0.001$), but also in AtTSPO(H91A) seeds ($p < 0.05$). The AtTSPO constitutive

expression triggered a significant increase in divalent metal levels such as zinc and manganese. In addition to magnesium and potassium contents in dry seeds. As shown in Figures **20E** to **F**, the constitutive expression of AtTSPO triggers its accumulation in dry seeds.

Furthermore, Knockouting AtTSPO has no significant effect on iron levels in dry seeds. Interestingly, overexpression of IRT1-mCherry in KO AtTSPO background significantly boosted the iron contents in dry seeds compared to IRT1-mCherry overexpressed in WT background, as shown in Figures **20 B to C**. Besides, the constitutive expression of IRT1-mCherry in OE AtTSPO background leads to a decrease in iron contents, to similar levels compared to OE AtTSPO. The coexpression of AtTSPO and IRT1-mCherry leads to a decrease in iron and zinc as divalent metals but not manganese levels in dry seeds. **Figures 20E to F** clearly show a significant reduction of AtTSPO quantities accumulated in seeds by overexpressing IRT1-mCherry. This may influence the iron recycling process coming from heme scavenging by AtTSPO.

These results suggest that overexpression of AtTSPO may promote upgrading the iron content in the seeds. On the other hand, overexpression of AtTSPO may protect the seeds from iron hyperaccumulation risks due to the overexpression of IRT1. It was shown that due to increased iron levels in *Arabidopsis* seeds, germination capacity decreases (Curie *et al.,* 2000).

The metal(loid) homeostasis influences seed metabolisms and performance. Metals translocation from the source organs to the sink organs subsequently influences seed germination under stressful

conditions (Eroglu *et al.*, 2017; Kranner and Colville, 2011). Indeed, as shown in **Figure. S2 A-B**, we observed a significant alteration in germination activity, in control conditions and not under iron deficiency, of KO AtTSPO and OE AtTSPO(H91A) when IRT1-mCherry is coexpressed compared to WT background. This suggests that the significant decrease or increase in seed-iron content may affect germination activity. Besides, iron deficiency influences the germination activity of seeds coexpressing OE AtTSPO and IRT1-mCherry compared to these overexpressing IRT1-mCherry in WT background, as shown in **Figure S2 A-B**.

Furthermore, we visualized Fe levels (Fe^{3+}) in roots (from seven-days old seedlings of WT, KO AtTSPO and OE AtTSPO grown on control and iron deficient media) using a sensitized, Fe-specific histochemical procedure (Perls staining) (Roschzttardtz *et al.*, 2009; Müller *et al.*, 2015). Under control medium (iron sufficiency), images revealed a same pattern of Fe accumulation along the root axis of WT and TSPO mutants. While patterns were changed dramatically under iron deficiency. OE AtTSPO roots showed increased Fe staining compared to WT. While no Fe staining was detected in KO AtTSPO roots (**Figure S1 K)**. These observations suggest that the presence and absence of AtTSPO influences Fe^{3+} accumulation in Arabidopsis roots under Fe deficiency.

(A)

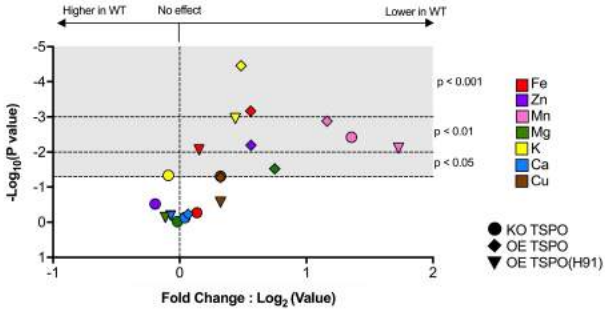
Higher in WT
No effect
Lower in WT
-Log10(P value)
Fold Change : Log2 (Value)
p < 0.001
p < 0.01
p < 0.05
Fe
Zn
Mn
Mg
K
Ca
Cu
KO TSPO
OE TSPO
OE TSPO(H91)

(B)

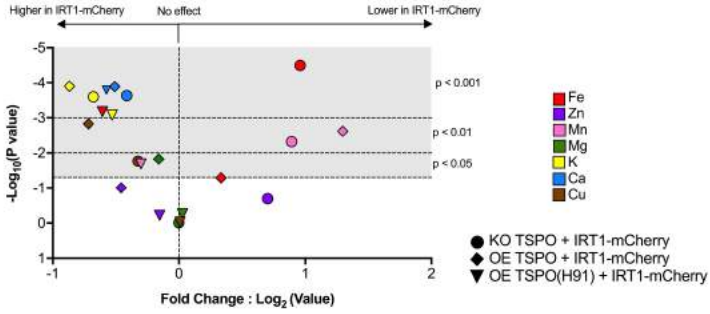
Higher in IRT1-mCherry
No effect
Lower in IRT1-mCherry
-Log10(P value)
Fold Change : Log2 (Value)
p < 0.001
p < 0.01
p < 0.05
Fe
Zn
Mn
Mg
K
Ca
Cu
KO TSPO + IRT1-mCherry
OE TSPO + IRT1-mCherry
OE TSPO(H91) + IRT1-mCherry

(C)

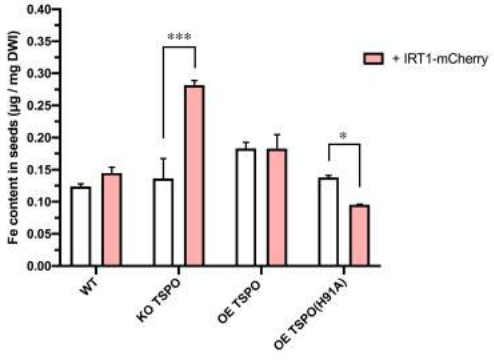
Fe content in seeds (µg / mg DWI)
+ IRT1-mCherry
***
*
WT
KO TSPO
OE TSPO
OE TSPO(H91A)

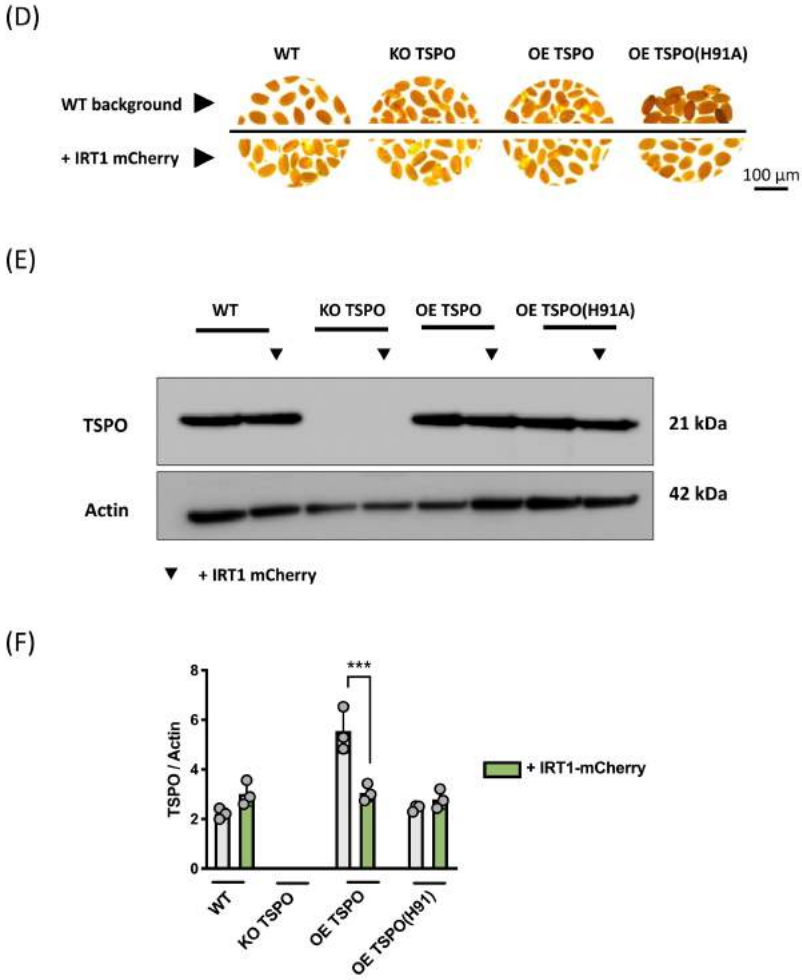

Figure 20. AtTSPO upgrades iron storage and prevents iron hyperaccumulation in dry seeds. **(A)** and **(B)** Volcano plots showing dry seeds' metal contents. The y-axis shows the significance (P-value), and the x-axis shows the Fold-change compared with the WT background in (A) and the IRT1-mCherry background in (B). The grey area presents the significance thresholds of P-values < 0.05, < 0.01 and < 0.001 respectively. **(A)** Minerals rates in KO AtTSPO, OE AtTSPO and AtTSPO(H91A) **(B)** Minerals

rates in KO AtTSPO + IRT1-mCherry, OE AtTSPO + IRT1-mCherry and AtTSPO(H91A) + IRT1-mCherry. **(C)** Histogram showing Fe content in dry seeds, indicating the effect of the constitutive expression of IRT1-mCherry in WT and AtTSPO mutants' backgrounds. Statistical significance was assessed by one-way ANOVA followed by Tukey's tests (* $p < 0.05$, *** $p < 0.001$). **(D)** Mature dry WT and homozygous transgenic seeds **(E)** Gel immunoblotting showing TSPO levels in mature dry WT and homozygous transgenic seeds. AtTSPO (≈21 kDa) was monitored by immunoblotting of total protein extract. Anti Actin antibody was used for loading comparisons (≈42 kDa). **(F)** The normalized ratio (AtTSPO/Actin) from (E): Statistical significance was assessed by one-way ANOVA followed by Tukey's tests (** $p < 0.01$, *** $p < 0.001$).

4.2.5 *irt1* null mutation triggers AtTSPO induction

The iron homeostasis in *Arabidopsis* can be altered by knocking outing central player genes in the iron uptake machinery such as the main iron transporter IRT1 or the Pleiotropic Drug Resistance 9 (PDR9) exporter scopoletin and phenolics derivatives essentials for iron chelation, which is necessary for its uptake into the root cell by IRT1. Therefore, *irt1* null mutant is characterized by full rosette chlorosis, drastic reduction in growth and fertility **(Figure 21C)**, and deficiency in iron transport (Vert *et al.*, 2002; Henriques *et al.*, 2002; Barberon, Zelazny, Robert, Conéjéro, Curie, Jirí Friml, *et al.*, 2011; Shanmugam *et al.*, 2011). Also, the *pdr9* null mutation is characterized by downregulation in the transcripts abundance of many iron-uptake related proteins such as IRT1 and AtFRO2 (Fourcroy *et al.*, 2014). We investigated the AtTSPO regulation when IRT1 was downregulated or knockout. Interestingly, **Figure 21A** shows a week induction of AtTSPO in both irt1 and *pdr9* null mutants. This signal was weaker than seedlings expressing constitutively IRT1-mCherry in WT background (lines 1 and 3). In this experiment, we used the WT, KO TSPO, and double mutant KO TSPO + IRT1-mCherry (Lines 1 and 2)

as negative controls. **Figure 21B** shows that nondetected IRT1 in irt1 mutants is weakly detected in *pdr9*. Those results suggest that the IRT1 knock-down or knock-out positively regulates AtTSPO expression.

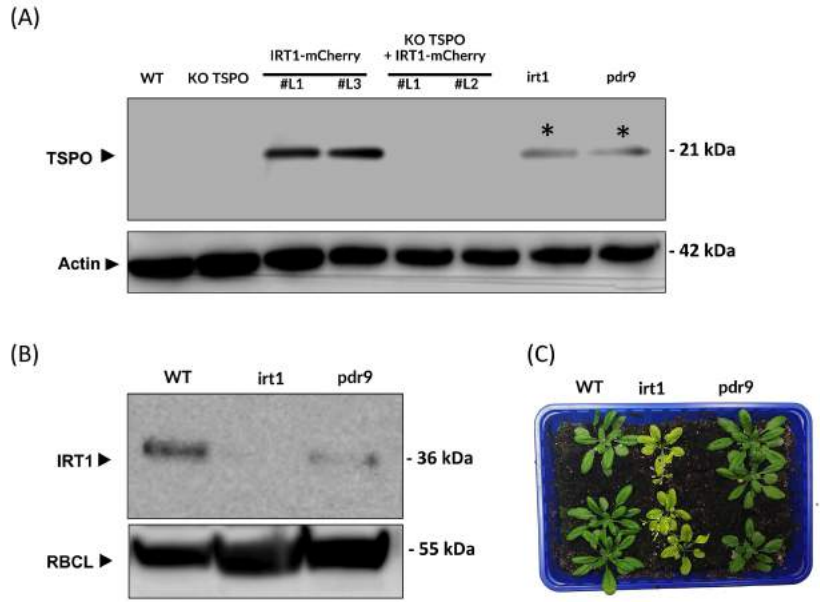

Figure 21. AtTSPO expressed in *irt1* and *pdr9* null mutants. The level of IRT1 (36 kDa) and AtTSPO (21 kDa) were monitored by immunoblotting of total protein extract from 7 days old seedlings. For loading comparisons. For loading control, the Anti-Actin antibody was used in **(A),** and the anti-RBCL antibody was used in **(B)**. Two homozygous lines of IRT1-mCherry (#L1 and #L3) are used as a positive control. In addition, two homozygous lines of KO ATSPO + IRT1-mCherry (#L1 and #L2), WT, and KO TSPO are used as a negative control. (C) Plant of WT as compared to *irt1*, and *pdr9* mutants at 25 days old.

4.3 Discussion

4.3.1 Iron depletion in the growth medium induces a transient expression of the Arabidopsis AtTSPO

The multi-stress regulator AtTSPO protein is known to be transiently induced under oxidative stress conditions such as salinity, osmotic stress, and ABA treatment (Guillaumot, Guillon, De Planque, *et al.*, 2009). Moreover, AtTSPO is a heme scavenger that modulates free toxic heme levels in the cell via an autophagy-dependent degradation mechanism(Vanhee, Zapotoczny, *et al.*, 2011). It was shown that the root cell starts to accumulate ABA under iron deficiency within six hours. This accumulation leads to upregulating genes related to iron remobilization of the available iron in the vacuole to increase the level of useful cytoplasmic iron (Song *et al.*, 2019). Iron deficiency transcriptionally upregulates the iron uptake machinery, especially in active levels of the metal-iron transporter IRT1(Brumbarova *et al.*, 2015; Sivitz *et al.*, 2011; Yuan *et al.*, 2008). Due to the IRT1 capacity of transporting divalent metals into the root cell (Connolly *et al.*, 2002; Dubeaux *et al.*, 2018; Grossoehme *et al.*, 2006). The iron limitation promotes a hyperaccumulation of metals in the root, which causes tissue damage and has a detrimental effect on plant growth by increasing oxidative stress. The hyperaccumulation of metals triggers increase levels of stress markers, such as the iron-binding protein ferritin and ascorbate peroxidase in leaves (Fourcroy *et al.*, 2004; Ravet *et al.*, 2009; Barberon, Zelazny, Robert, Conéjéro, Curie, Jirí Friml, *et al.*, 2011; Connolly *et al.*, 2002). Thus, complex post-transcriptional

regulatory mechanisms allow the plant to delicately control the level above functional IRT1 levels in the plasma membrane. We showed that iron deficiency triggers a weak induce of AtTSPO in root cells **(Figure 16)**, which may promote free toxic heme scavenging and degradation. This hypothesis could be understood by the decrease of heme level in the cell under iron deficiency (Hirayama *et al.*, 2018) and by taking into account AtTSPO capacity in scavenging free heme triggering its degradation in the vacuole (Vanhee, Zapotoczny, *et al.*, 2011). The heme degradation allows the plant cell rapidly to recycle iron to be reused in cell metabolisms. This iron pool is highly requested to be sent to the sink organs, especially seeds (Ravet *et al.,* 2009; Briat *et al.,* 2010). We demonstrate that the constitutive expression of AtTSPO leads to increase iron levels in the dry seeds. While the constitutive expression of IRT1 boosts iron levels in the absence of AtTSPO. Therefore, AtTSPO upgrades iron storage in the seeds and mitigates the toxic effect of IRT1 overexpression **(Figure 20)**.

Furthermore, in the seedling stage, we showed that AtTSPO was induced within 24 h under iron deficiency. It was detected mainly in roots **(Figure 16)**. Besides, levels of AtTSPO constitutively expressed were lower under iron deficiency **(Figure 17)**. Suggesting that AtTSPO was consumed during iron limitation.

Moreover, the iron machinery uptake could be altered by knock outing the PDR9 gene responsible for phenolics export needed in the iron uptake strategy I (Fourcroy *et al.,* 2004; Barberon *et al.,* 2011; Shanmugam *et al.,* 2011). Iron uptake capacity is severely reduced by knock outing IRT1 (Vert *et al.,* 2002; Henriques *et al.,* 2002; Barberon et *al.,* 2011; Shanmugam *et al.,* 2011). Resulting in a disorder in

photosynthetic parameters, morphology, and life cycle. We showed that these null mutants (*irt1* and *pdr9*), known to be suffering from iron limitation, were constitutively expressing AtTSPO in control conditions, contrary to the WT seedlings **(Figure 21)**.

4.3.2 The multi-stress induced AtTSPO protein and the iron transporter IRT1 are co-regulated under iron deficiency

Often, IRT1 is known to be localized in the external cell layers at the root epidermis of *A. thaliana*, including the lateral branching zone to import iron from the rhizosphere. Then, iron is remobilized to the shoot via xylem and be translocated to sink organs after nicotinamide chelation or loading into phloem (Durrett *et al.*, 2007; Pottier *et al.*, 2014; Robinson *et al.*, 1999; Vert *et al.*, 2002; Santi and Schmidt, 2009; Fourcroy *et al.*, 2014; Lefèvre *et al.*, 2018; Morrissey and Guerinot, 2009; Schuler *et al.*, 2012). It was shown that IRT1 expression is highly upregulated in flowers and siliques in *nas4 mutant* (Klatte *et al.*, 2009). IRT1 is also detected in flowers before pollination (Vert *et al.,* 2002). Under Iron deficiency, IRT1 starts to accumulate exponentially in the root cells within the first 12 to 24 h (Connolly *et al.,* 2002a; Sivitz *et al.,* 2011). We showed that under iron depletion, AtTSPO was detected within the first 24 hours **(Figure 16D)**.

It has been shown that the high influx of divalent metals triggers oxidative stress in *Arabidopsis* (Weber *et al.*, 2006; Shanmugam *et al.*, 2011; Besson-Bard and Wendehenne, 2009). In addition, under iron limitation, IRT1 accumulation triggers toxic metal overload in root cells (Barberon *et al.,* 2014, 2011). Moreover, the IRT1 overexpression

leads to toxic metal accumulation triggering oxidative stress (Barberon *et al.,* 2011). On the other hand, AtTSPO is a multi stress-related membrane protein transiently induced in vegetative tissues by ABA, osmotic stress, salinity, high light conditions, magnesium deficiency, and water-related stress (Kreps *et al.*, 2002; Zimmermann *et al.*, 2004; Winter *et al.*, 2007; Guillaumot, Guillon, De Planque, *et al.*, 2009; Hermans *et al.*, 2010; Hachez *et al.*, 2014; Jurkiewicz *et al.*, 2020). We demonstrate that the constitutive expression of IRT1 leads to a stable expression of AtTSPO in standard conditions **(Figure 19 A and B)** and increase under iron deficiency **(Figure 19 C)**. Conversely, the knockout of IRT1 is problematic to the plant. *irt1* null mutant is characterized by a substantial decrease in iron uptake capacity and photosynthetic parameters (Vert *et al.,* 2002; Henriques *et al.,* 2002; Barberon *et al.,* 2011; Shanmugam *et al.,* 2011). We demonstrate by gel protein analysis that AtTSPO was expressed in *irt1* null mutant **(Figure 21)**. Indicating that the IRT1 knockout promoted AtTSPO accumulation.

AtTSPO is transiently expressed under stress conditions (Guillaumot *et al.,* 2009). The level of constitutively expressed AtTSPO decreases under ABA treatment occurred concurrently with a reduction in the free heme level (Vanhee *et al.,* 2011). Moreover, it is known that heme levels also decrease under iron deficiency (Hirayama *et al.,* 2018), mediating IRT1 increased levels in the cell. Furthermore, we demonstrate that iron deficiency decreases the quantity of AtTSPO constitutively expressed **(Figure 17)**. At the same time, we also showed that AtTSPO overexpression leads to a decrease in IRT1 levels. Although, IRT1expresison was boosted in the root cells in the absence of AtTSPO **(Figure 18)**. These data reported the evidence of co-regulation between IRT1 and AtTSPO.

4.4 Methods

4.4.1 Wild type and Transgenic plant lines

We used *Arabidopsis thaliana* (ecotype Columbia-0) WT and transgenic plants expressing full-length AtTSPO (OE AtTSPO), point-mutated AtTSPOH91A (OE AtTSPO(H91A)) , all under the control of the p35S promoter (Guillaumot *et al.,* 2009; Vanhee *et al.,* 2011). An Arabidopsis homozygous T-DNA insertional line (KO) in TSPO (KO AtTSPO) (Guillaumot *et al.,* 2009) was also used. *Pdr9* null-mutant transgenic homozygous seeds are a gift from Marc Boutry (SALK T-DNA #055721). *Irt1* null-mutant transgenic homozygous seeds are a gift from Gregory Vert (Vert *et al.,* 2002).

4.4.2 Plant transformation and growth

pJNC1 IRT1 vector is a gift from Rumen Ivanov. This vector was used to constructively express IRT1-mCherry in the plants. Transgenic *A. thaliana* plants overexpressing IRT1-mCherry were generated by the standard floral dip method (Clough and Bent, 1998). WT Col-0, KO AtTSPO, OE AtTSPO, and OE AtTSPO(H91A) plants were grown until flowering. *A. tumefaciens* GV3101 bacteria containing the pJNC1 IRT1 vector grown in a liquid medium containing selective antibiotics (bacteria grown until the mid-log phase). After 3x spin down and resuspension in 5% sucrose solution containing 0.03 % Silwet L-77 (Lehle Seeds, Round Rock, USA, #VIS-01). Plant shoots containing flower buds were dipped in bacterial solution for 5 seconds with slow manual agitation. After that, the plant pots were covered with dusky plastic foil to maintain high humidity. One day later, plants were

transferred into the phytotron and grown under a regular watering regime (twice a week) until seed maturation.

Seeds sterilization was done as described in (Lindsey *et al.*, 2017) and growth conditions as described previously (Guillaumot *et al.,* 2009; Vanhee *et al.,* 2011; Jurkiewicz *et al.,* 2020).

Growing seedlings were screened for homozygous transformants using 20 µg/ml hygromycin B for IRT1-mcherry in WT and KO AtTSPO background. The plants co-overexpressing IRT1-mCherry and AtTSPO / AtTSPO(H91A) were genotyped by PCR amplification of two sequence fragments (35Spro-IRT1-mCherry and IRT1-mCherry).

4.4.3 Plant Material and Treatments

After surface sterilization and stratification for 2-3 days at 4°C in the dark, seeds were transferred into a growth chamber (16h/8h light/dark regime, 22–25°C, 90 µmol photons. s-1.m-2). For standard medium, seeds germinated and grown upright on ½ MS (Murashige and Skoog, MP Biomedicals, Eschewege, Germany, #0926230) agar plates supplemented with 50 µM ferric iron in the form of EDTA iron(III) sodium salt (Sigma-Aldrich, Germany, #EDFS) during 7 days. For iron deficiency, no iron was added, and 150 µM of FerroZine iron chelator (PDT disulfonate monosodium salt hydrate, (Sigma-Aldrich, Germany, #63451-29-6) was added to the medium. After 7d, plants grown in a standard medium were transferred to a liquid medium (same standard medium or without iron) for 24h or 7 d. Seedlings were grown in the same culture chamber in transparent Multiwell plant culture plates (VWR-Avantor, Belgium, #734-2323).

4.4.4 Protein Extraction and Analyses

After being mixed with CelLytic P (Cell Lysis Reagent) buffer (Sigma-Aldrich, Germany, #C2360) containing a cocktail of proteases inhibitors (Sigma-Aldrich, Germany, #200-664-3), Plant tissues were homogenizer by a Tissue Homogenizer (Bertin, USA, #13190079) using glass beads 2 mm Ø (VWR, Belgium, #1.04014.0500) and then gently spoon down of supernatant collect. Extracted proteins were quantified by BCA (Bicinchoninic Acid) Protein Assay as described in (Smith et al., 1985; Walker, 2009), mixed with 5× Laemmli buffer, and incubated for 30 min at 37°C prior to SDS-PAGE (iD PAGE Gel, 4-20 %, Eurogentec, Belgium, #ID-PA4201-010) and transfer into mini PVDF membranes 0.2 µm (Trans-Blot Turbo transfer packs, Biorad, USA, #1704156) using the Trans-Blot Turbo Transfer System. Membranes were saturated for 1 h at 25°C in blocking buffer (5% non-fat milk in TBS-Tween-20 supplemented with 0.5% Tween-20 in 1× TBS) and incubated at 4°C overnight with primary antibodies diluted in blocking buffer. After washing three times in washing buffer (0.5% milk in TBS Tween-20 supplemented with 0.1% Tween-80 in 1× TBS), membranes were incubated with secondary Horseradish peroxidase (HRP)-conjugated antibodies for 1 h at room temperature. After washing three times in washing buffer, membranes were incubated for 3-5 min with ECL (Roche, Germany, #11500694001) or with ECL kit SuperBright (Agrisera, Sweden, AS16 ECL-SN). Emitted light was detected using a digital imaging device (Amersham Imager 600, GE Healthcare Life Sciences). Some western blots were revealed by the Alkaline phosphatase Staining technique (Atanasov et al., 2008) using an alkaline phosphatase-coupled secondary antibody (Anti-Rabbit IgG, Sigma-Aldrich, Germany, #A3687). Polyclonal anti-AtTSPO

antibodies were designed by the host laboratory and previously used in (Guillaumot et al., 2009, Vanhee, 2011, Hachez, 2014, Jurkiewicz, 2020). Polyclonal anti-IRT1 was purchased from Agrisera (#AS11 1780). Also, Antibodies against *Arabidopsis* RbcL were purchased from Agrisera (#AS03037). Anti-mCherry was from ROCKLAND antibodies and assays (#600-401-P16). The mouse monoclonal anti-actin (β-actin) was purchased from Proteintech (#60008-1-Ig). For western blotting, anti-AtTSPO and anti-RbcL were diluted at 1:10,000, Anti-IRT1 and Anti-mCherry were diluted at 1:5,000. HRP-conjugated anti-rabbit, anti-mouse, and the alkaline phosphatase-coupled secondary anti-rabbit antibodies were diluted at 1:10,000.

4.4.5 Statistical Analysis of the Data

The number of replicates and statistical methods for each experiment is stated within figure legends. GraphPad Prism version 8 for macOS (GraphPad Software; San Diego, California, USA; www.graphpad.com) was used to analyze statistical significance. For western blot signal quantification, we used the Image-Lab Software package for macOS version 6.1 (SOFT-LIT-170-9690-ILSMAC-V-6-1). For band signal intensities quantifications, we ensured that exposure conditions provided by the digital imager were below the saturation threshold.

4.4.6 Mineral analysis

Arabidopsis dry seeds were weighted before digestion. Digestion was carried out in Pyrex tubes. Samples have undergone acidic mineralization with HNO3 (Fisher TraceMetal grade). They were then brought to dryness before taking up 10 ml of 10% aqua regia. Then

samples were analyzed on an ICP-AES (Inductively Coupled Plasma - Atomic Emission Spectroscopy, Thermo ICAP 600 series, MOCA - Mineral & Organic Chemical Analysis center in UCLouvain).

4.4.7 Chlorophyll analysis

Approximately 20 mg of green seedling tissues were extracted in 80% (v/v) DMSO (dimethyl sulfoxide). To avoid the acidification of chlorophylls, 2 % v/v of Mg2(OH)2CO3 was added. Pigment extraction required approximately 2 h at 65°C in the dark. Tissue remains were removed by centrifugation. Absorbances measurements and calculations were made according to (Wittmann, 2016).

4.4.8 Root length and rosette diameter measurement

Images of grown plants on plates were taken by a NIKON Coolpix P950 camera. Each generated image was analyzed using a custom-made Fiji-ImageJ2 plugin, Root Image Analysis-J (or RIA-J). Then we extracted the root lengths or the rosette diameter measurements.

4.5 Supplemental figures

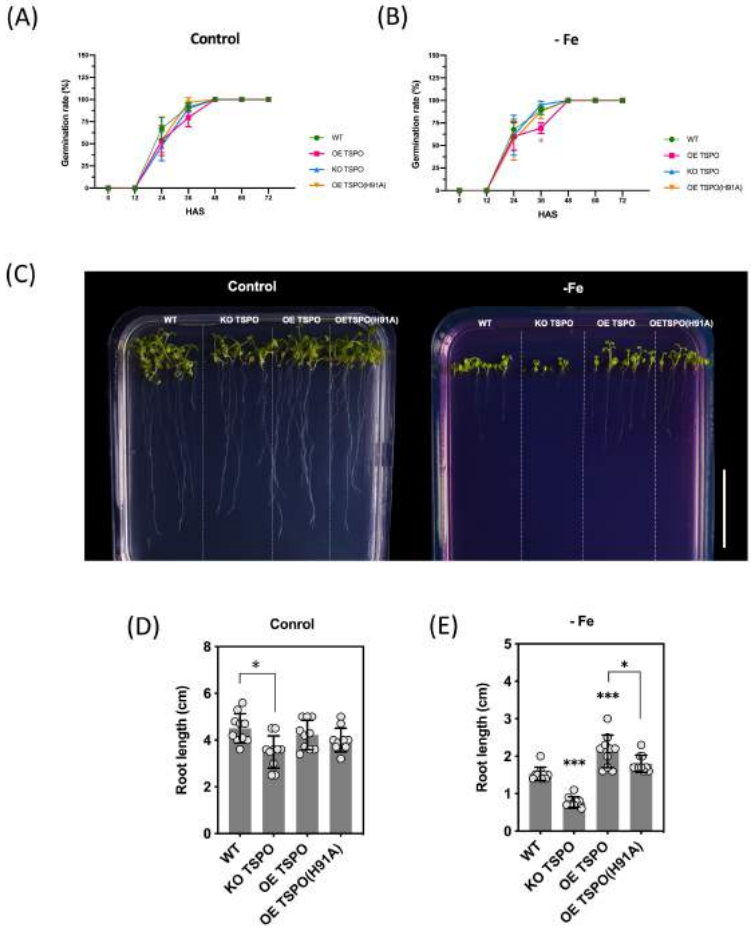

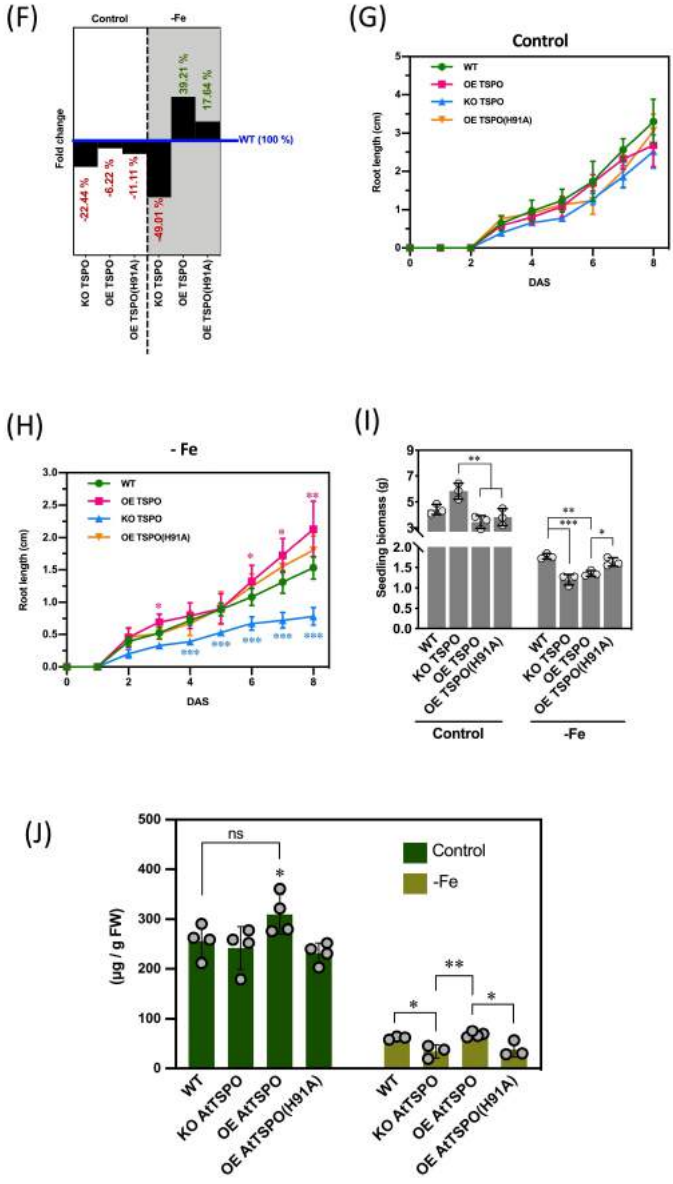
(F)
Control
-Fe
Fold change
WT (100 %)
-22.44 %
-6.22 %
-11.11 %
-49.01 %
39.21 %
17.64 %
KO TSPO
OE TSPO
OE TSPO(H91A)
KO TSPO
OE TSPO
OE TSPO(H91A)
(G)
Control
WT
OE TSPO
KO TSPO
OE TSPO(H91A)
Root length (cm)
DAS
(H)
- Fe
WT
OE TSPO
KO TSPO
OE TSPO(H91A)
Root length (cm)
DAS
(I)
Seedling biomass (g)
WT
KO TSPO
OE TSPO
OE TSPO(H91A)
Control
-Fe
(J)
(µg / g FW)
ns
Control
-Fe
WT
KO AtTSPO
OE AtTSPO
OE AtTSPO(H91A)

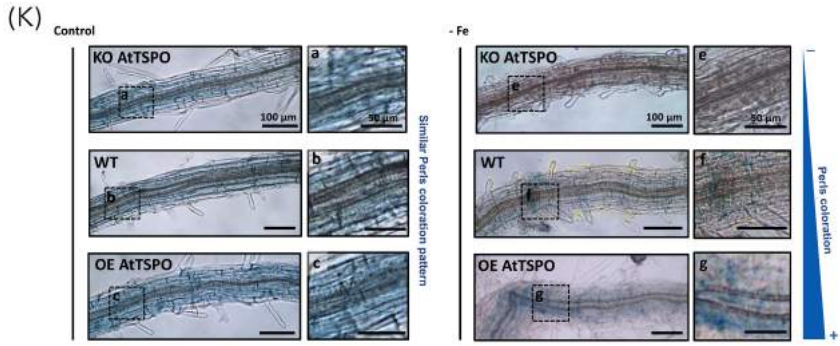

Figure S1. AtTSPO modulates Arabidopsis development under iron starvation as well in standard conditions. **(A)** and **(B)** Germination profiles: Germination of WT, KO AtTSPO, OE AtTSPO, and OE AtTSPO(H91A). Seeds were stratified at 4°C for 24 h under dark before growing them in the plant culture room. Statistical significance was assessed by one-way ANOVA followed by Tukey's tests (* $p < 0.05$). **(C)** seven-day-old seedlings of WT, KO AtTSPO, OE AtTSPO, and OE AtTSPO(H91A) were grown on a standard medium and iron-free medium. **(D)** and (**E)** Root length quantification of plant grown in (C). Error bars represent SD (n=10). Statistical significance was assessed by one-way ANOVA followed by Tukey's tests (* $p < 0.05$ and *** $p < 0.001$). **(F)** Fold change values of (D) and (E) compared to WT**. (G)** and **(H)** Time curse of root elongation during one week after stratification from (A) and (B). **(I)** Seedling biomass measurement from **(C).** Statistical significance was assessed by one-way ANOVA followed by Tukey's tests (* $p < 0.05$, ** $p < 0.01$ and *** $p < 0.001$). **(J)** Total chlorophyll measurement in seedlings from **(C).** Statistical significance was assessed by one-way ANOVA followed by Tukey's tests (* $p < 0.05$ and *** $p < 0.001$). (K) The presence and absence of AtTSPO influences Fe^{3+} accumulation in roots under Fe deficiency. Fe accumulation patterns as indicated by Perls staining in the roots of seven-day-old WT, KO AtTSPO and OE AtTSPO seedlings grown on control and iron deficient media.

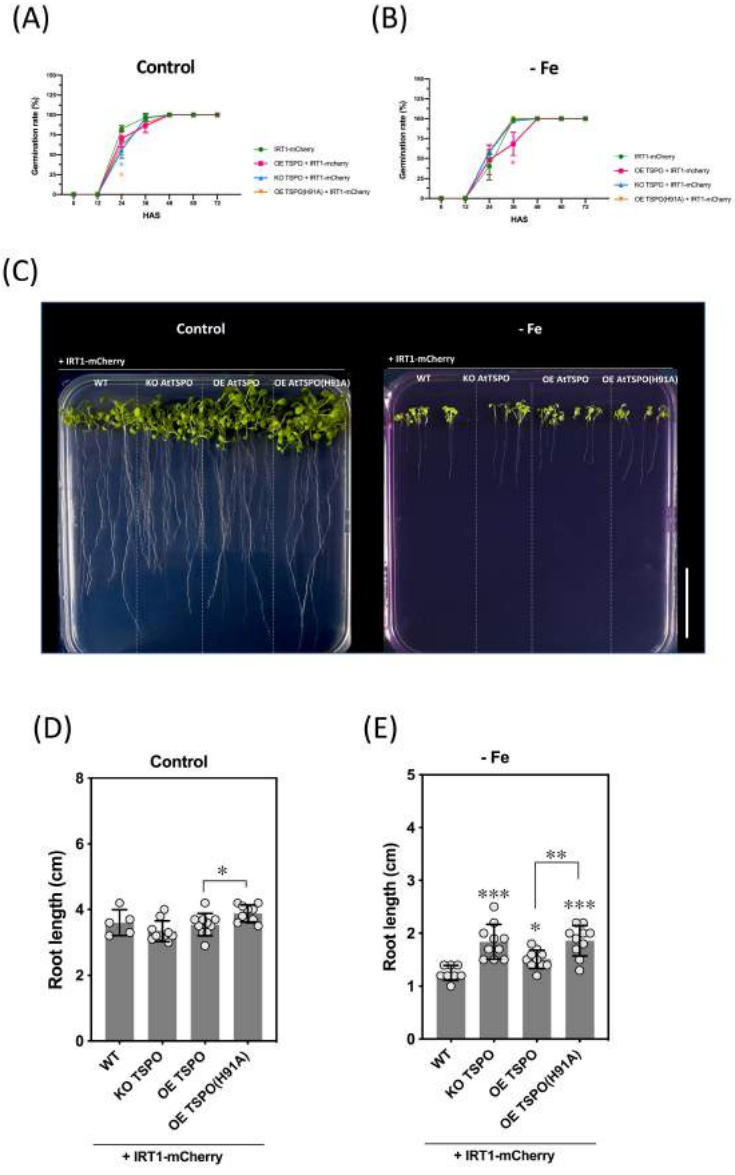
(A)
Control
Germination rate (%)
HAS
IRT1-mCherry
OE TSPO + IRT1-mcherry
KO TSPO + IRT1-mCherry
OE TSPO(H91A) + IRT1-mCherry
(B)
- Fe
Germination rate (%)
HAS
IRT1-mCherry
OE TSPO + IRT1-mcherry
KO TSPO + IRT1-mCherry
OE TSPO(H91A) + IRT1-mCherry
(C)
Control
+ IRT1-mCherry
WT
KO AtTSPO
OE AtTSPO
OE AtTSPO(H91A)
- Fe
+ IRT1-mCherry
WT
KO AtTSPO
OE AtTSPO
OE AtTSPO(H91A)
(D)
Control
Root length (cm)
WT
KO TSPO
OE TSPO
OE TSPO(H91A)
+ IRT1-mCherry
(E)
- Fe
Root length (cm)
WT
KO TSPO
OE TSPO
OE TSPO(H91A)
+ IRT1-mCherry

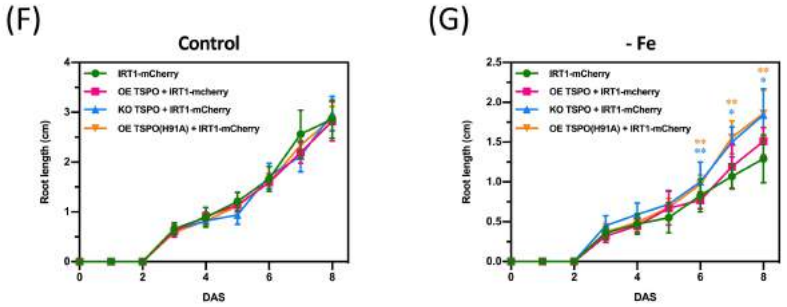

Figure S2. IRT1 regulation modulates Arabidopsis development under iron starvation as well in standard conditions. **(A)** and **(B)** Germination profiles: Germination of WT, KO AtTSPO, OE AtTSPO, and OE AtTSPO(H91A) constitutively expressing IRT1-mCherry. Seeds were stratified at 4°C for 24 h under dark before growing them in the plant culture room. Statistical significance was assessed by one-way ANOVA followed by Tukey's tests (* $p < 0.05$). **(C)** seven-day-old seedlings of WT, KO AtTSPO, OE AtTSPO, and OE AtTSPO(H91A) constitutively expressing IRT1-mCherry, were grown on standard medium and iron-deficient medium. **(D)** and **(E)** Root length quantification of plant grown in **(C)** error bars represent SD (n=10), Statistical significance was assessed by one-way ANOVA followed by Tukey's tests (* $p < 0.05$, ** $p < 0.01$ and *** $p < 0.001$). **(F)** and **(G)** Time curse of root elongation during 1 week after stratification from (A) and (B). Statistical significance was assessed by one-way ANOVA followed by Tukey's tests (* $p < 0.05$ and ** $p < 0.01$).

(A)

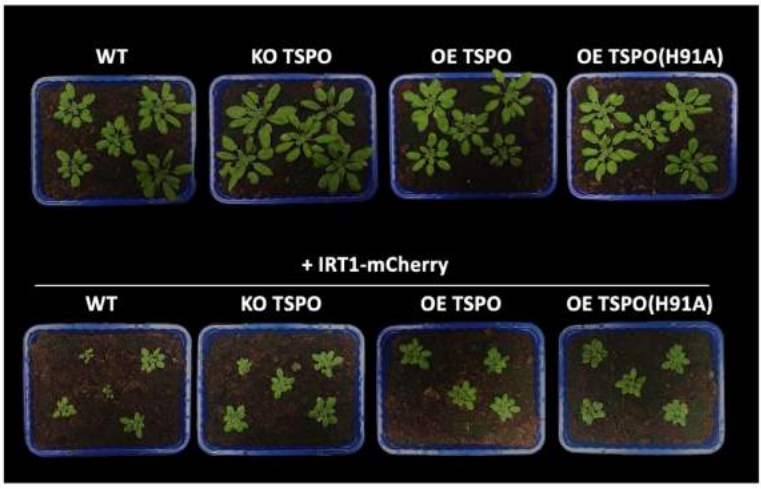
WT
KO TSPO
OE TSPO
OE TSPO(H91A)
+ IRT1-mCherry
WT
KO TSPO
OE TSPO
OE TSPO(H91A)

(B)

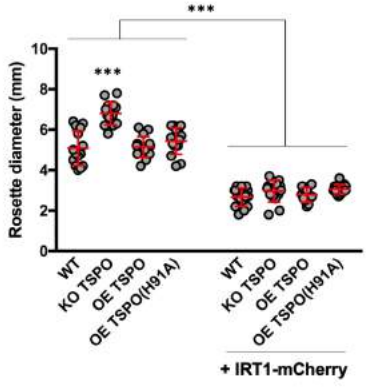
***
***
Rosette diameter (mm)
10
8
6
4
2
0
WT
KO TSPO
OE TSPO
OE TSPO(H91A)
WT
KO TSPO
OE TSPO
OE TSPO(H91A)
+ IRT1-mCherry

(C)

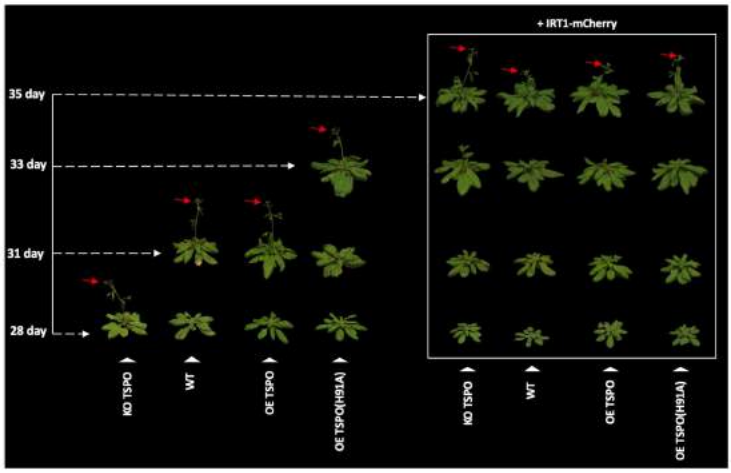
+ IRT1-mCherry
35 day
33 day
31 day
28 day
KO TSPO
WT
OE TSPO
OE TSPO(H91A)
KO TSPO
WT
OE TSPO
OE TSPO(H91A)

(D)

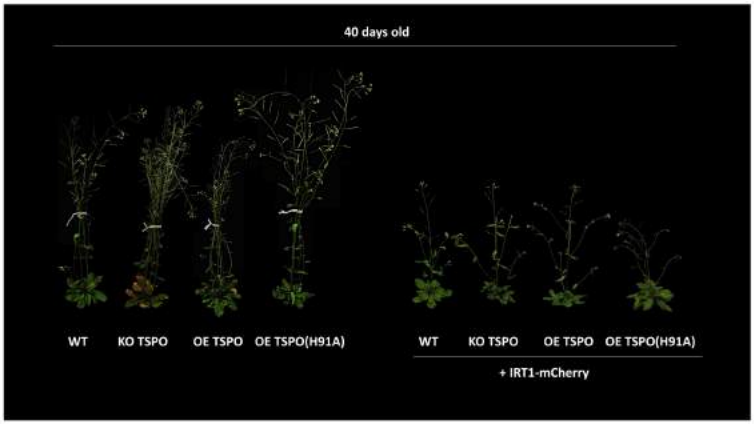
40 days old
WT
KO TSPO
OE TSPO
OE TSPO(H91A)
WT
KO TSPO
OE TSPO
OE TSPO(H91A)
+ IRT1-mCherry

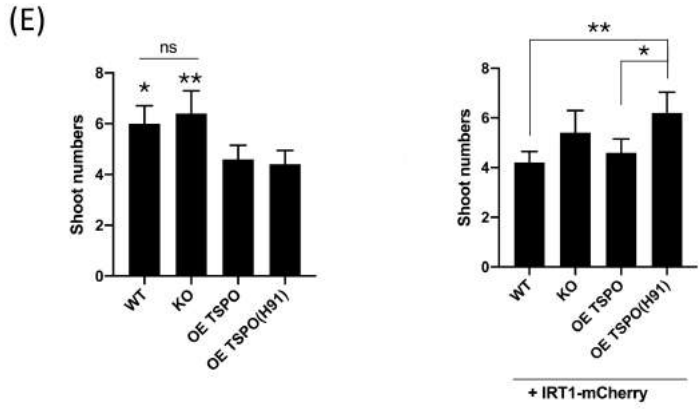

Figure S3. IRT1-AtTSPO Co-regulation modulates Arabidopsis development, flowering, and senescence. **(A)** Plant rosette profiles of WT, KO AtTSPO, OE AtTSPO, OE AtTSPO(H91A), and the same genetic backgrounds constitutively expressing IRT1-mCherry. **(B)** Plant rosettes diameter measurement from (A). Error bars represent SD (n=10). Statistical significance was assessed by one-way ANOVA followed by Tukey's tests (*** $p < 0.001$). **(C)** Flowering profile and time curse of WT, KO AtTSPO, OE AtTSPO, OE AtTSPO(H91A), and same genetic backgrounds constitutively expressing IRT1-mCherry. **(D)** Plant rosette and shoot profiles of WT, KO AtTSPO, OE AtTSPO, OE AtTSPO(H91A), and same plants constitutively expressing IRT1-mCherry at 40 days. **(E)** Shoot branching numbers at 40 days. Error bars represent SD (n=10). Statistical significance was assessed by one-way ANOVA followed by Tukey's tests (* $p < 0.05$ and ** $p < 0.01$).

5 Chapter V: The Arabidopsis iron transporter IRT1 can be degraded through the autophagy pathway in an AtTSPO-dependent manner

Abstract

The *Arabidopsis* translocator protein (TSPO) is transiently induced under oxidative stress conditions. This work reports findings on the molecular function of this transmembrane protein in a novel pathway in the downregulation of Arabidopsis *IRON-RELATED TRANSPORTER 1* (AtIRT1) under multi-stress conditions. Pulldown assays and fluorescence microscopy approaches revealed that AtTSPO established physical interactions with IRT1 in the *Arabidopsis* root cells. Interestingly, the constitutive expression of AtTSPO in the root cells expressing fluorescent-tagged IRT1 resulted in the formation of body degradation structures in the cytoplasm. It markedly decreased IRT1 levels in the plasma membrane. Abscisic acid treatment, salinity, osmotic stress, or chemical treatment inducing autophagy leads to IRT1 degradation in root cells in the presence of AtTSPO. Knocking out AtTSPO abolished the considerable degradation of IRT1 under the same conditions. AtTSPO stabilization by mutation of the histidine residue at position 91 markedly decreases its capacity to establish physical interactions with IRT1 in vivo. This physical interaction was abolished by its Brassicaceae conserved cysteine mutation at position 94. Pulldown assay and fluorescence microscopy revealed that the complex of the two proteins was degraded through autophagy. These

data support the physiological and molecular role of AtTSPO in the downregulation of the related iron transporter under multi-stress conditions, especially under iron deficiency conditions, which confers cell protection against hyperaccumulation of toxic divalent metals.

5.1 Introduction

The stress-induced translocator TSPO-related protein has been identified and described in plants (Corsi *et al.*, 2004; Fan *et al.*, 2012; Lindemann *et al.*, 2004; Guillaumot, Guillon, De Planque, *et al.*, 2009; Batoko *et al.*, 2015). The molecular functions of TSPO depends to the evolution between species. Plant TSPOs possess a polybasic charged N-terminal extension absent in bacteria and animals (Balsemão-Pires *et al.,* 2011; Batoko *et al.,* 2015; Jurkiewicz *et al.,* 2020). The Arabidopsis N-terminal extension is necessary for the phospholipid PI(4.5)P2 interaction in vitro and depletes the level of AtPIP2;7 aquaporins in the plasma membrane (Jurkiewicz *et al.,* 2020). It has been demonstrated that AtTSPO establishes physical interactions with AtPIP2;7 at the endoplasmic reticulum and Golgi membranes (Hachez *et al.,* 2014; Jurkiewicz *et al.,* 2020). Likewise, AtTSPO-AtPIP2;7 complex proteins are degraded via the autophagic pathway (Hachez *et al.,* 2014). The downregulation of AtTSPO expression reduces water loss during water stress by depleting the PIP2; 7 levels on the cell surface (Hachez *et al.,* 2014). In addition, AtTSPO levels are increased by abscisic acid (ABA) treatment, salinity, and osmotic stress (Guillaumot *et al.,* 2009; Vanhee *et al.,* 2011). AtTSPO transiently modulates redox homeostasis by scavenging free toxic heme molecules under stress (Batoko *et al.,* 2015; Vanhee *et al.,* 2011).

Cellular redox imbalance leads to oxidative stress and disorder of metal levels in plants (Sharma *et al.*, 2016). Iron is an essential metal nutrient and a cofactor for several enzymes involved in oxidation-reduction reactions, such as photosynthesis and respiration (Barberon *et al.,* 2014; Curie *et al.,* 2001). Plants risks accumulating an extremely toxic iron level under hypoxia (Drew, 1997). While, cellular iron is mainly found in heme, hemoproteins (catalases and cytochromes), and non-heme proteins (ferredoxins and ferritins) (Smith and Morgan, 1984). Over and above that, plants strictly modulate and balance the cellular iron homeostasis. The primary visible symptom of iron deficiency is the development of intercostal chlorosis in young leaves due to changes occurring in the chloroplast ultrastructure, leading to a remarkable decrease in the expression of small and large subunits of Rubisco, chlorophyll level, and chlorophyll a/b binding proteins (Winder and Nishio, 1995). Iron deficiency increases cell respiration and the upregulation of enzymes related to anaerobic respiration in roots. However, iron deficiency causes starch degradation and phloem-loading in shoots (Thimm *et al.*, 2001). Thereby, iron uptake machinery is the earliest portal for iron transport into plant cells. In *Arabidopsis thaliana*, the strategy I so-called reduction-based strategy is established for iron uptake from the apoplast into the cytosol of root cells (Marschner *et al.*, 1986; Vert *et al.*, 2002; Schmidt, 2003). Using strategy I, the ferric iron (Fe^{3+}) is systematically subjected to be solubilized and chelated in acidified medium and reduced to the ferrous form (Fe^{2+}) by the *FERRIC REDUCTION OXIDASE* (FRO2). After that, Fe^{2+} is transported into the cell by the *IRON-REGULATED TRANSPORTER* IRT1. Accordingly, both IRT1 and FRO2 levels are upregulated under iron deficiency (Eide *et al.,* 1996; Connolly *et al.,*

2002; Vert *et al.,* 2002; Wang *et al.,* 2013; Santi and Schmidt, 2009). It has been known that IRT1 ensures the transport of several divalent minerals, such as zinc, manganese, and cobalt, in addition to toxic heavy metals, such as cadmium (Barberon *et al.,* 2011). Plants strictly use systemic signaling mechanisms to manage IRT1 abundance in the plasma membrane. IRT1 senses excess levels of non-iron metal elements out of the cytoplasm during iron deficiency, leading to IRT1 degradation (Dubeaux *et al.,* 2018; Cointry and Vert, 2019). The downregulation of IRT1 is driven by polyubiquitination mediating endocytosis and triggering its degradation via ESCRT pathway to the lytic vacuole during metal excess. Indeed, several mechanisms exist in turnover proteins, especially transmembrane transporter proteins, which depend on post-translational modification, including endocytosis, autophagy, and endoplasmic reticulum-associated protein degradation (ERAD) (Stein *et al.*, 2014). This study demonstrated that AtTSPO established physical interactions with the iron transporter IRT1 in *Arabidopsis* root cells and mitigates its distribution at the plasma membrane under stress conditions, such as iron deficiency, ABA treatment, salinity, and osmotic stress. Thus, the uptake of toxic metals is limited under abiotic stress conditions.

5.2 Results

5.2.1 AtTSPO interacts physically with the Arabidopsis plasma membrane iron transporter IRT1 in vivo and in vitro

The *Arabidopsis* TSPO protein is known to be a potential interactant that forms a partner-heterocomplex with diverse bait-membrane proteins (Hachez *et al.*, 2014; Vanhee, Zapotoczny, *et al.*, 2011). Based on this capacity, AtTSPO is considered a regulator is limiting several protein levels in the cell (Hachez *et al.*, 2014; Vanhee, Zapotoczny, *et al.*, 2011). AtTSPO establishes physical interactions with the plasma membrane aquaporin PIP2;7 and downregulates its abundance in plant cells (Hachez *et al.*, 2014; Jurkiewicz *et al.*, 2020). By decreasing the levels of active PIP2.7 in the plasma membrane, AtTSPO substantially contributes to the limitation of water transport activity under osmotic stress and salinity conditions (Hachez *et al.,* 2014; Jurkiewicz *et al.,* 2020). Likewise, IRT1 is a membrane protein that ensures iron uptake into the cell via the plasma membrane. Under iron deficiency conditions, the multi-metal transporter IRT1 is considerably induced, and its high abundance leads to the occurrence of metal toxicity in plant cells (Barberon *et al.,* 2011). We concluded that the AtTSPO overexpression downregulated IRT1 levels in the root cell, AtTSPO was induced by iron deficiency, and the constitutive expression of IRT1 induced AtTSPO **(Figures 7 and 11)**, which helped ascertain whether AtTSPO established interactions with IRT1 to downregulate its abundance in the cell. Therefore, we examined the possibility of copurifying both proteins. We used two different plant materials to

confirm this hypothesis: dry seeds and 7-day-old seedlings from the homozygous transgenic mutant overexpressing IRT1 tagged with mCherrey at the C-terminus. Based on our previously reported results, AtTSPO was markedly induced and was detected in this mutant. We concluded that if IRT1-mCherry established interactions with the endogenous AtTSPO, affinity purification of mCherry could help pull down AtTSPO. We used RFP-Trap beads (Chromotek) to purify IRT1-mCherry from total protein extracts. For negative control, we used Nano-trap blocked beads derived from the same magnetic-agarose matrix **(Figure 22)**. Gel blotting results of proteins derived from different fractions of the pull-down assay (dry seeds in the upper panel and seedlings in the middle panel). Using antibodies against mCherry and IRT1, we detected IRT1-mCherry in the elution fraction in both cases. The gel protein blots showing co-eluted AtTSPO signals derived from dry seed and seedling extract fractions using RFP-trap beads have been presented in each blot down panel. This was not the case when using the control trap beads.

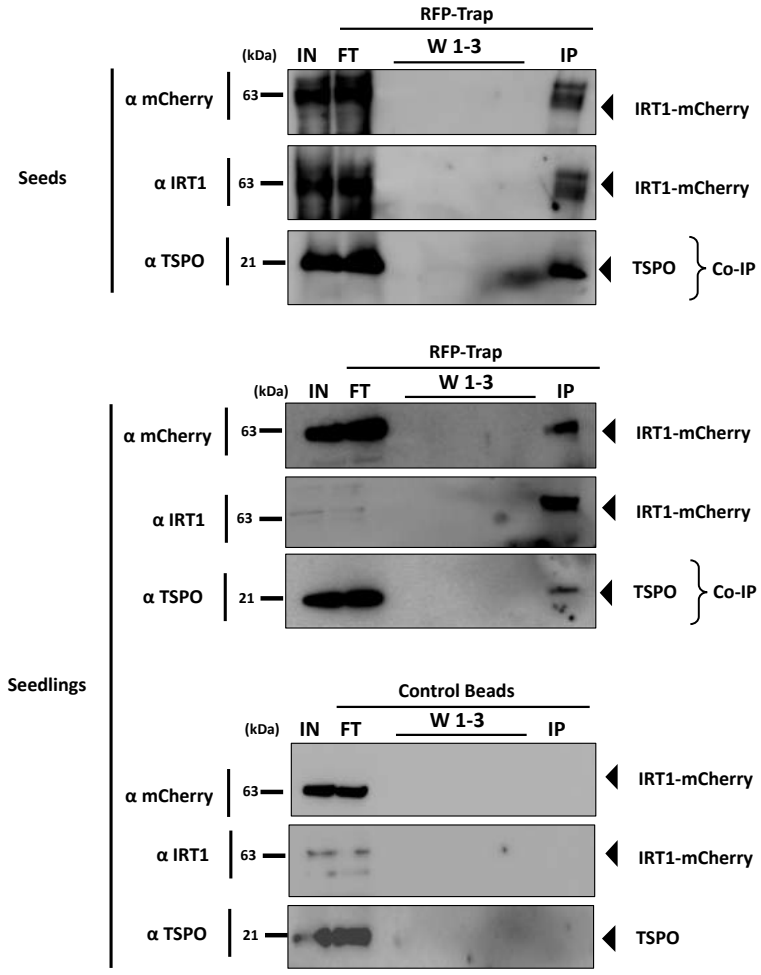

Figure 22. Copurification of AtTSPO and IRT1 from *A. thaliana* Extracts**.** Total protein was extracted from *Arabidopsis transgenic* dry seeds and seven-day-old seedlings constitutively expressing IRT1-

mCherry. Samples were purified using RFP-Trap, then analyzed by immunoblotting. The input (IN), the Flow-through (FT), Three successive washes (W 1-3), and eluted fraction (E). Denaturated magnetic-agarose beads were used as a negative control.

Next, we investigated whether this interaction was active in an artificial system. IRT1-mCherry (under the control of the cauliflower mosaic virus p35S promoter) was transiently expressed in transgenic tobacco (*Nicotiana tabacum*) constitutively expressing *Arabidopsis* YFP-AtTSPO (under control of the p35S promoter) (Guillaumot *et al.,* 2009). Transient expression was achieved using *Agrobacterium tumefaciens*-mediated transfection, according to the previously described method (Batoko *et al.*, 2000). Total protein extraction from infiltrated leaves was performed, and affinity-purified fusion proteins using RFP-trap and GFP-trap magnetic-agarose beads, separately and in parallel with blocked beads used as a negative control from the same magnetic-agarose matrix, were obtained. In the first case, using RFP-trap beads, YFP-AtTSPO was copurified with IRT1-mCherry **(Figure 23, upper panel)**. In reverse, IRT1-mCherry was copurified using GFP-trap beads with YFP-AtTSPO **(Figure 23, middle panel).** No protein signals were detected in the elution fraction using the control beads **(Figure 23, down panel)**.

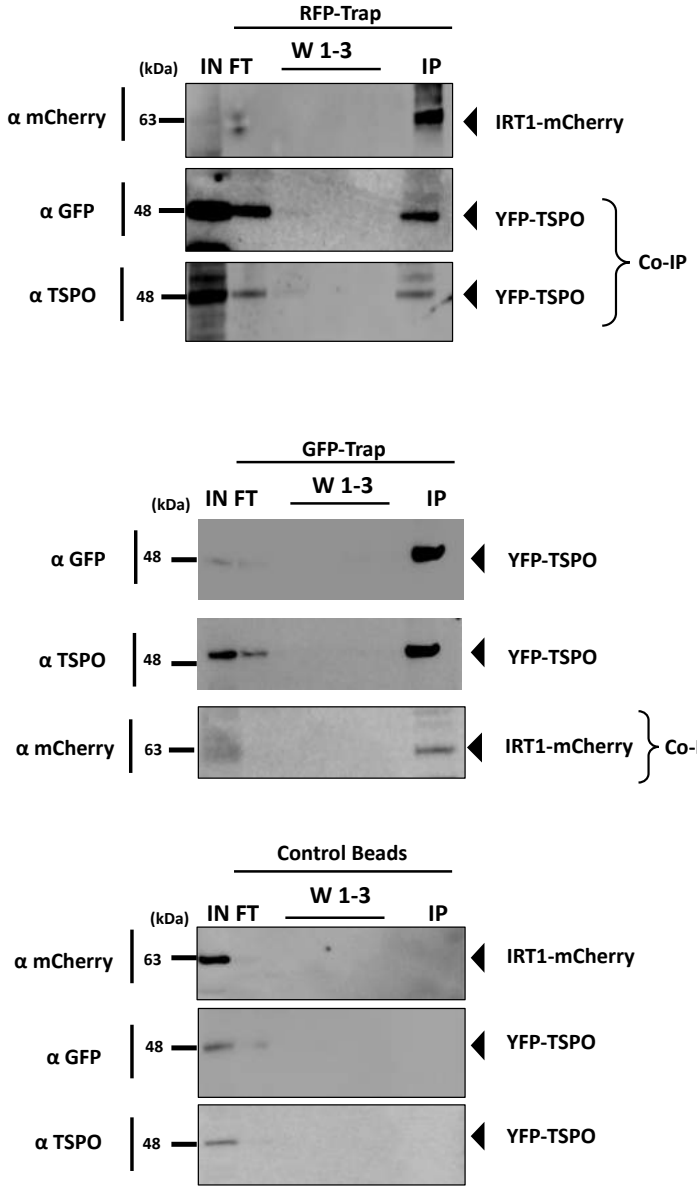
RFP-Trap
W 1-3
(kDa)
IN FT
IP
α mCherry
63
IRT1-mCherry
α GFP
48
YFP-TSPO
Co-IP
α TSPO
48
YFP-TSPO
GFP-Trap
W 1-3
(kDa)
IN FT
IP
α GFP
48
YFP-TSPO
α TSPO
48
YFP-TSPO
α mCherry
63
IRT1-mCherry
Co-IP
Control Beads
W 1-3
(kDa)
IN FT
IP
α mCherry
63
IRT1-mCherry
α GFP
48
YFP-TSPO
α TSPO
48
YFP-TSPO

Figure 23. Copurification of AtTSPO and At IRT1 from transgenic *N. tabaccum* Extracts**.** Total proteins were extracted from *N. tabaccum* leaves. IRT1-mCherry was transiently expressed in transgenic *N. tabaccum leaves* over-expressing *Arabidopsis* TSPO tagged with the Fluorescent YFP protein at the N-terminal side. Samples were purified separately using RFP-Trap and GFP-Trap, then analyzed by immunoblotting. The input (IN), the Flow-through (FT), Washes (W 1-3), and eluted fraction (E). Denaturated magnetic-agarose beads were used as a negative control.

Furthermore, we used the bimolecular fluorescence complementation technique (BiFC) (Gookin and Assmann, 2014). To analyze protein-protein interactions in vivo, we used a monomeric Venus (mVenus) split at residue 210 in a streamlined double ORF expression system. The BiFC signal was established by complementing the previous fragment of mVenus with the second fragment (mVenus210) (Gookin and Assmann, 2014). The system contained an integrated XT protein (Golgi-marker) tagged with mTurquoise2 and was used to identify transformed cells. We prepared genetic constructs encoding chimeric fusion proteins. AtTSPO was fused with the N-terminal (VenusN), and interactor candidates were fused with Venus-$_{C}$. The chimeric constructs driven by the Ubiquitin-10 promoter (UBQ10) were transiently expressed in tobacco leaf epidermal cells (*Nicotiana benthamiana*). The BiFC signal driven by Venus reconstitution was evaluated through confocal microscopy imaging. For establishing a positive control, we used a combination of Venus$_{C}$-AtTSPO and Venus$_{N}$-AtPIP2;7 (Jurkiewicz *et al.,* 2020). It has been shown that AtTSPO and AtPIP2.7 established physical interactions at the endoplasmic reticulum (ER) and Golgi membranes in plants (Hachez *et al.,* 2014; Jurkiewicz *et al.,* 2020). **Figure 24(d-f)** illustrates this finding. White arrowheads have been used to show the colocalization of BiFC and XT-mtq2 signals in the Golgi stacks, and red arrowheads have been used to show the subcellular distribution of the BiFC signal in the ER. Panel **(a)** shows

the absence of BiFC signal when $Venus_N$-PiP2;7 was combined with $Venus_C$ alone. We used another combination to establish the negative control **(Figure. 15j-l)**, containing $Venus_C$-AtTSPO and $Venus_N$-AtLTI6B (low temperature-induced protein 6), known as a plasma membrane marker (Krebs *et al.*, 2012; Kim *et al.*, 2021).

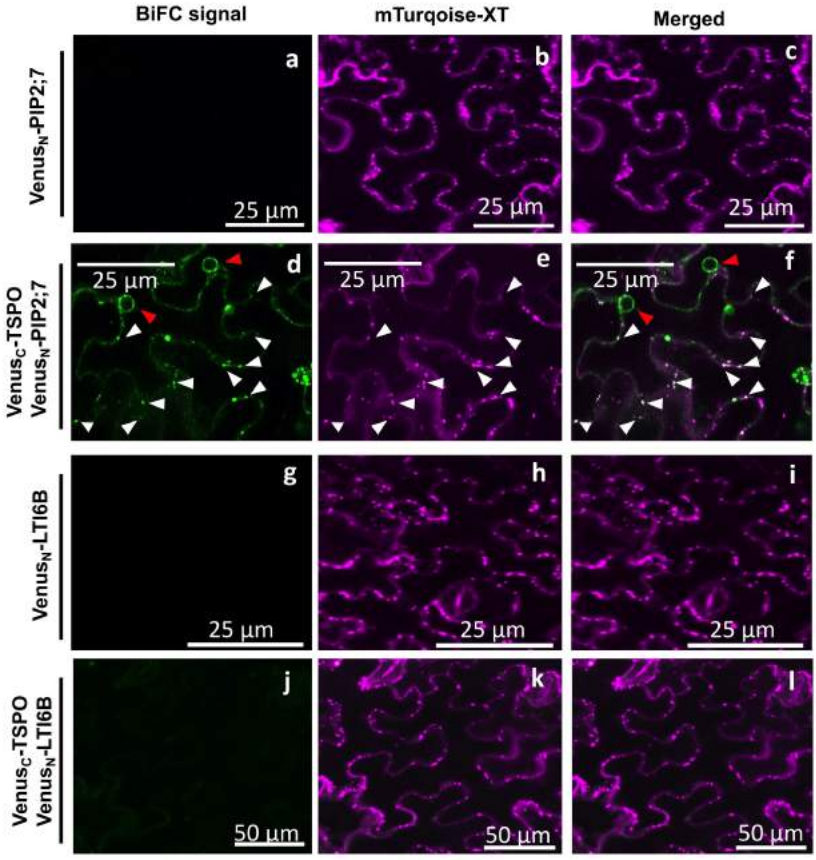

Figure 24. BiFC Demonstrate the selective interaction between AtTSPO and membrane proteins. **(a-i)** Confocal images of tobacco epidermal cells transiently expressing $Venus_N$-PIP2;7 **(a-c)**, $Venus_C$-TSPO + $Venus_N$-PIP2;7 **(d-f),** $Venus_N$-LTI6B **(g-i),** and $Venus_C$-TSPO + $Venus_N$-LTI6B **(j-i**). BiFC signal in left panels was shown in green. Middle panels show XT-mtq2 signal (Golgi marker in magenta). Right panels show merged signals.

We investigated the interaction established between AtTSPO and IRT1 using the same BiFC assay system. For the first time, the empty plasmid was infiltrated and considered mock infiltration; after that, $Venus_C$-AtTSPO with $Venus_N$ and $Venus_N$-IRT1 with $Venus_C$ were used in parallel. These combinations served as controls, demonstrating the absence of independent reconstitution of the full-length mVenus **(Figure 25 (a-i))**. The panels **(m)**, **(r)**, and **(v)** show the resulting BiFC signals after the co-expression of $Venus_C$-AtTSPO and $Venus_N$-IRT1. White arrows have been used to show the colocalization between BiFC and XT-mTq2 signals. In contrast, red arrows have demonstrated that the BiFC signal was not colocalized with the Golgi marker, suggesting that the interaction occurred in a compartment different from the Golgi. Based on the results of the pulldown assay, the BiFC data demonstrate that AtTSPO and IRT1 establish interactions in the plant cell.

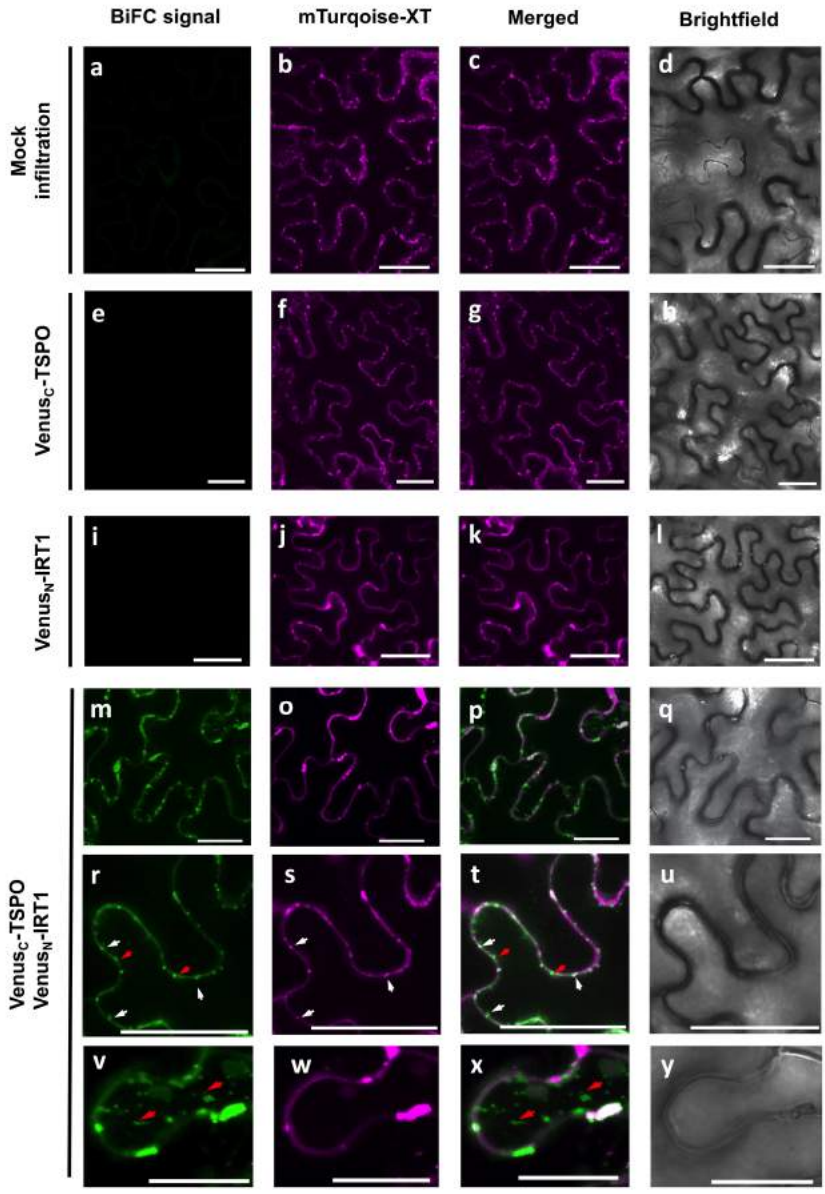
BiFC signal
mTurqoise-XT
Merged
Brightfield
Mock infiltration
VenusC-TSPO
VenusN-IRT1
VenusC-TSPO
VenusN-IRT1
a
b
c
d
e
f
g
h
i
j
k
l
m
o
p
q
r
s
t
u
v
w
x
y

Figure. 25. BiFC Demonstrate the AtTSPO-IRT1 interaction in *planta*. **(a-y)** Representative confocal images of tobacco epidermal cells transiently expressing: $Venus_C$-TSPO **(e-h),** $Venus_N$-IRT1 **(i-l)**, $Venus_C$-TSPO + $Venus_N$-IRT1 **(m-y)**, and empty vector infiltration **(a-d).** BiFC signal in the outer left panels was shown in green. Middle-left panels show XT-mtq2 signal (magenta). Middle-Right panels show merged signals. The outer-right panels show transmitted light images.

5.2.2 The mutation of TSPO histidine at position 91 decreases but does not abolish the capacity of interaction with IRT1

To confer protection to plants against tissue dehydration and osmotic stress, *Arabidopsis* cells must downregulate the level of AtPIP2;7 aquaporin expression through AtTSPO induction in specific tissues (Hachez *et al.,* 2014). The intracellular interaction established between AtTSPO and AtPIP2;7 leads to degradation of the aquaporin protein via selective autophagy. This downregulation helps the plant reduce water loss through stomatal opening associated with evapotranspiration (Hachez *et al., 2014*; Jurkiewicz *et al.,* 2020). It has been shown that downregulation of AtTSPO required heme-binding through its distal histidine at position 91 (Vanhee *et al.,* 2011). The AtTSPO(H91A) is relatively more stable than the wild-type protein in the cell (Vanhee *et al.,* 2011; Hachez *et al.,* 2014). Despite this, this stabilized form of AtTSPO could interact physically with AtPIP2;7. But this interaction is not conducive to the degradation of the aquaporin. The stabilized form of TSPO harboring the H91A point mutation has a sparsely effect on the reducing process of AtPIP2;7 levels in the cell (Hachez *et al.,* 2014). In addition, to establish the physical interactions with AtPIP2;7 in vivo, AtTSPO relies on its first 41 residues at the N-terminus (Jurkiewicz *et al.,* 2020). Deleting the specific N-terminus did not affect AtTSPO targeting and degradation in the lytic vacuole but abolished the

protein's binding capacity for PI(4,5)P2 and dramatically reduced the interaction with PIP2;7 in vivo (Jurkiewicz *et al.,* 2020). Based on that, we aimed to decipher whether the H91A point mutation affects the physical interaction between AtTSPO and IRT1 and if AtTSPO relies on its N-terminus to establish this physical interaction. We conducted biomolecular fluorescence complementation (BiFC) experiments using $Venus_C$-AtTSPO(H91A) co-expressed with $Venus_N$-AtLTI6B **(negative control in Figure 26A (a-c))**, and $Venus_N$-IRT1 **(Figure 31A (d-f)]**. Panel **(f)** shows a BiFC signal partially colocalizing with XT-mTq2 (white arrows). Red arrows have been used to show BFiC signals in different compartments than Golgi. It has been shown previously that downregulation of AtTSPO is dependent on heme binding in vivo via selective autophagy (Vanhee *et al.,* 2011). The substitution of the histidine residue at position 91 to alanine critically decreases the capacity of AtTSPO to bind free heme through its iron axial coordination (Vanhee *et al.,* 2011). Unpublished results reported by a previous study (Vanhee *et al.,* 2011) indicate that the cysteine residue at position 94 probably plays an important role in the heme-binding process. We also prepared a genetic construct for the BiFC assay, encoding the TSPO protein (EsTSPO) derived from *Eutrema salsugineum*, a plant halophyte exhibiting stress tolerance (relatively close to *A. thaliana*). AtTSPO and EsTSPO had an overall identity of 87%. **Figure 26B** shows that the distal histidine residue is also conserved in the *Eutrema* TSPO. However, the cysteine residue in AtTSPO is naturally replaced by arginine. $Venus_C$-EsTSPO and $Venus_N$-IRT1 were co-expressed using the BiFC assay **(Figure 26A (g-i))**. Interestingly, **(g)** and **(h)** show that no BiFC signal was detected. The quantified BiFC signals are shown in **Figure 31C** and present a

highly significant ($p<0.001$) decrease between AtTSPO(h91A) and AtTSPO. While the signal level in EsTSPO was extremely low. These results highlight the feckless capacity of *E. salsugineum* TSPO to bind IRT1.

Furthermore, we conducted three biomolecular fluorescence complementation (BiFC) experiments using $Venus_C$-AtTSPO(ΔNter) co-expressed with $Venus_N$-AtPIP2;7 **(negative control 1 in Figure S4(d-f))**, $Venus_N$-AtLTI6B **(negative control 2 in Figure S4(a-c))**, and $Venus_N$-IRT1 **(in Figure S4(g-i))**. Interestingly, **Figure S4(g-i)** illustrates a BiFC signal (white arrows). These results indicate that the N-terminus of AtTSPO is not involved in the establishment of physical interactions with IRT1.

(A)

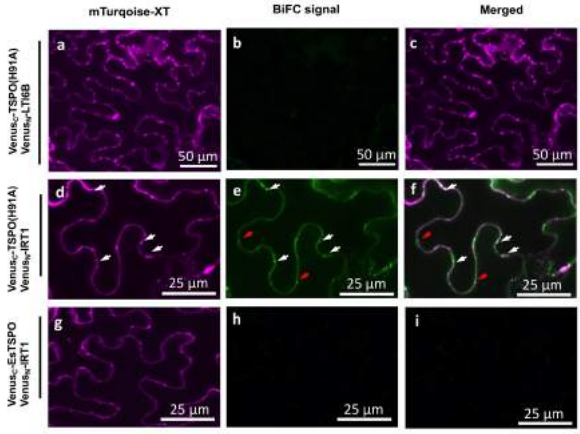
mTurqoise-XT
BiFC signal
Merged
Venus$_C$-TSPO(H91A)
Venus$_N$-LTI6B
Venus$_C$-TSPO(H91A)
Venus$_N$-IRT1
Venus$_C$-EsTSPO
Venus$_N$-IRT1
a
b
c
d
e
f
g
h
i
50 µm
25 µm

(B)

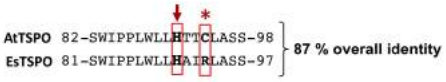
AtTSPO 82-SWIPPLWLLHTTCLASS-98
EsTSPO 81-SWIPPLWLLHAIRLASS-97
87 % overall identity

(C)

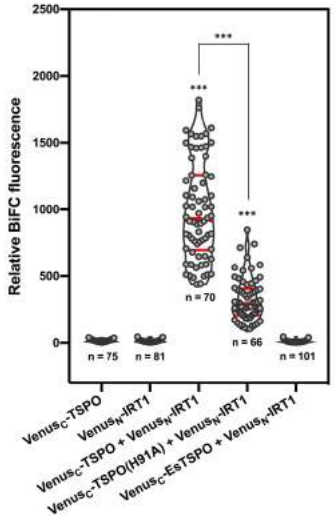
Relative BiFC fluorescence
2500
2000
1500
1000
500
0
***
***
***
n = 75
n = 81
n = 70
n = 66
n = 101
Venus$_C$-TSPO
Venus$_N$-IRT1
Venus$_C$-TSPO + Venus$_N$-IRT1
Venus$_C$-TSPO(H91A) + Venus$_N$-IRT1
Venus$_C$-EsTSPO + Venus$_N$-IRT1

Figure 26. The Distal histidine (H91) substitution does not abolish AtTSPO interaction with IRT1. **(A): (a-i)** Representative confocal images of tobacco epidermal cells transiently expressing $Venus_c$-TSPO(H91A) **(a-c),** $Venus_C$-AtTSPO(H91A) + $Venus_N$-IRT1 **(d-f)**, and $Venus_C$-EsTSPO + $Venus_N$-IRT1 **(g-i).** BiFC signal in the middle panels was shown in green. Left panels show XT-mtq2 signal (magenta). Right panels show merged signals. White arrows show colocalized BiFC with the Golgi marker, and the red arrows show non-colocalized BiFC with XT-mTq2. **(B):** Protein alignment slice between AtTSPO and EsTSPO shows histidine conservation. **(C):** BiFC signal quantification. Violin plot shows the individual measurements, and middle red horizontal lines define the means for each dataset. The asterisks indicate a very high significant difference (Tukey, $p < 0.001$).

5.2.3 The TSPO cysteine at position 94 is crucial for the physical interaction with IRT1

The tryptophan-rich sensory protein/translocator protein (TSPO) is a conserved protein involved in plant evolution. It is implicated in response to multi-stress conditions (Guillaumot *et al.,* 2009; Veenman *et al.,* 2016). Sequence comparison revealed an important divergence (less than 70% identity) conferring a conserved fold preserving structural Tspo/MBR domain (Guillaumot *et al.,* 2009). Our phylogenetic analysis of (putative) AtTSPO homologs across the pentapetales (*Pentapetaleae*) clade showed a distal histidine as a highly conserved amino acid. Surprisingly, in *Brassicacea* TSPO homologs, the three following residues were mismatched, while the distal histidine was well conserved. The third residue was 50% cysteine in glycophytes and 50% arginine in halophytes **(Figure 27)**. Based on these results and the results shown in **Figure 26**, we aimed to examine whether cysteine residue at position 94 in AtTSPO was necessary to establish physical interaction with IRT1. For this purpose, we prepared genetic constructs encoding chimeric TSPO by swapping a homologous residue fragment (Ω) between AtTSPO and EsTSPO (TSPO from *Eutrema salsugineum* halophyte). **Figure 28A** shows the Ω fragment in AtTSPO and EsTSPO

after subjection to swapping, and an *Arabidopsis* TSPO mutation at the cysteine residue at position 94 replaced by an arginine (AtTSPO(C94R)). We analyzed in silico these mutations using the PROVEAN server (http://provean.jcvi.org) (Choi et al., 2012; Sun et al., 2020) using the default cutoff score of −2.5. The PROVEAN output shows a deleterious effect in many molecular functions by substituting histidine 91 with an alanine (PROVEAN score = -3.2) in AtTSPO. Interestingly, for the three H91 following amino acids, only the substitution of cysteine 94 with arginine is also deleterious (PROVEAN score = -2.778) **Figure 28B**. Contrariwise, in EsTSPO, the substitution of the arginine 93 with a cysteine upgrades its molecular capacity (PROVEAN score = 2.778) (**Figure 28B**). Interestingly as predicted, the BiFC signal between IRT1 and AtTSPO was abolished by swapping the EsΩ fragment from EsTSPO (**Figure 28B**). Next, the three constructs were considered and used separately in the BiFC assay as $Venus_C$- partner for $Venus_N$-IRT1. A salient effect was observed by swapping the AtΩ fragment from EsTSPO to AtTSPO. Interestingly, A strong BiFC signal was detected **(e-g)** and did not exhibit colocalization with the XT-mTq2 Golgi marker as shown in **(k)** and in mVenus and mTurquoise relative fluorescence intensity profiles **(l).** The substitution of the cysteine residue at position 94 in AtTSPO by arginine abolished the interaction with IRT1 **(m-q)**. These results strongly suggest that the cysteine residue at position 94 in *Arabidopsis* TSPO is necessary to establish physical interactions with IRT1 *in vivo*.

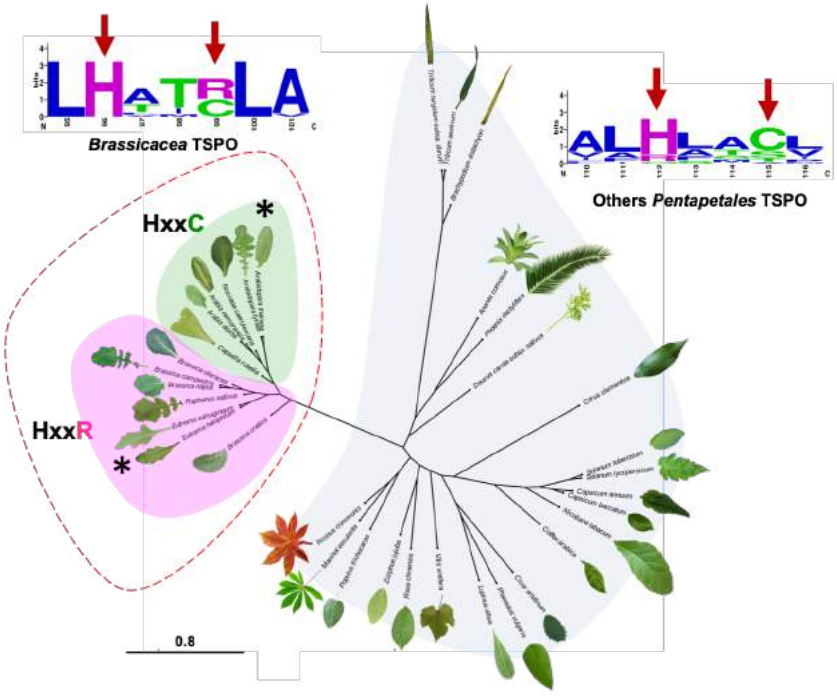

Figure 27. Phylogenetic tree of TSPO homologous proteins in *Penthapetalae.* Multiple alignments and the phylogenetic tree were generated with CLC Main Workbanch7. The scale bar in the sequence motifs indicates expected substitutions per site. The green area shows the glycophytes TSPO homologous conserving distal cysteine. The pink area shows the halophytes TSPO homologous conserving distal arginine.

(A)

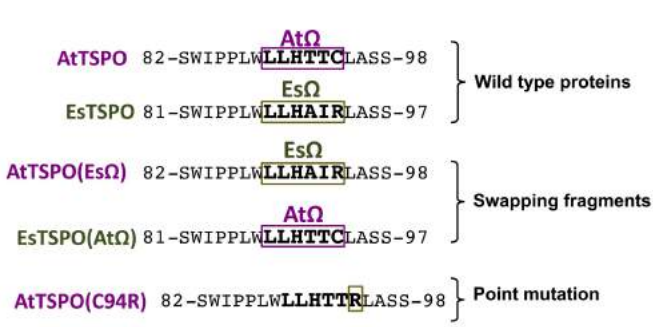
AtΩ
AtTSPO 82-SWIPPLWLLHTTCLASS-98
EsΩ
EsTSPO 81-SWIPPLWLLHAIRLASS-97
Wild type proteins
EsΩ
AtTSPO(EsΩ) 82-SWIPPLWLLHAIRLASS-98
AtΩ
EsTSPO(AtΩ) 81-SWIPPLWLLHTTCLASS-97
Swapping fragments
AtTSPO(C94R) 82-SWIPPLWLLHTTRLASS-98
Point mutation

(B)

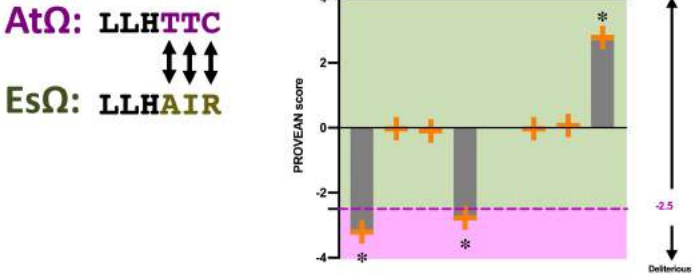
AtΩ: LLHTTC
EsΩ: LLHAIR
A. thaliana
E. salsugineum
EsΩ
AtΩ
Mutation
H91A
T29A
T93I
C94R
A91T
I92T
R93C
PROVEAN score
4
2
0
-2
-4
Neutral
-2.5
Deliterious

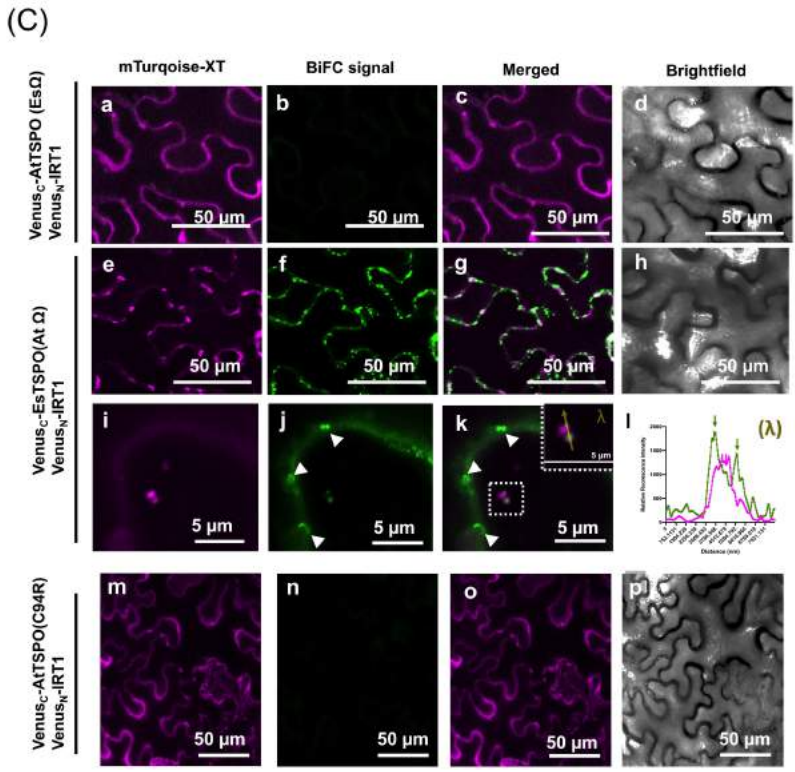

Figure 28. The substitution of TSPO distal cysteine abolishes its physical interaction with IRT1**. (A):** Protein alignment slice showing the Ω swapping regions between AtTSPO and EsTSPO. The last slice sequence shows the cysteine substitution at position 94 by an arginine. **(B):** PROVEAN point mutation effect prediction**. (C): (a-p)** Representative confocal images of tobacco epidermal cells transiently expressing Venus$_c$-AtTSPO(EsΩ) + Venus$_N$-IRT1 **(a-d)**, Venus$_c$-ESTSPO(AtΩ) + Venus$_N$-IRT1 **(e-k)**, and Venus$_c$-AtTSPO(C94R) + Venus$_N$-IRT1 **(m-p).** BiFC signal in the Middle-left panels was shown in green. Outer-left panels show XT-mtq2 signal (magenta). Middle-Right panels show merged signals. The outer-right panels **(d,h and p)** show transmitted light images. Relative fluorescence profile was shown in **(l).**

5.2.4 The subcellular localization of tagged IRT1 is altered in the presence of AtTSPO in *A. thaliana* root cells

We checked whether the expression of IRT1-mCherry in different genetic backgrounds, respectively, in WT, KO AtTSPO, OE ATTSPO, and OE AtTSPO(H91A). *Arabidopsis 7-day-old* seedlings were grown on standard ½ MS the transferred to a liquid medium under shaking (same medium). Roots from five different transgenetic lines from each mutant were analyzed by Airyscan super-resolution imaging microscopy. **Figure 29A** shows the subcellular localization of constitutively expressed IRT1-mCherry in the root cell. In the WT background, the mCherry fluorescence signal was observed in the cell-periphery in addition to some mobile punctate structures.

Interestingly, the number of these puncta bodies was very highly significantly increased when we coexpressed AtTSPO **(Figure 29B)**. Compared to the WT background, the fold change increased to 580,50 % **(Figure 29C)**. Moreover, this aspect was less observed when we coexpressed the relatively stable form of AtTSPO (AtTSPO(H91A). The number of punctate structures was very highly significantly increased compared to the WT background (205.01 %) **(Figure 29B and C)**. In Knockout AtTSPO overexpressing IRT1-mCherry, the mCherry fluorescence was observed very often in the cell periphery and rarely in punctate structures **(Figure 29A, B, and C)**. when AtTSPO was expressed, the distribution of IRT1-mCherry was more in the puncta bodies comparing to the cell periphery **(Figure 29E)**.

Moreover, the mCherry relative fluorescence intensity was higher in puncta structures compared to the cell periphery when AtTSPO was expressed. Although, by knock outing AtTSPO, mCherry relative intensity was more elevated, and IRT1-mCherry was stabilized at the cell periphery **(Figure 29E)**. The puncta number decreased by 83 % compared to the WT background **(Figure 29C)**. Furthermore, we checked the expression of another tagged plasma membrane protein, LTI6B-mRFP, in the same genetic backgrounds. Airyscan super-resolution imaging shows no change in the subcellular localization of LTI6B-mRFP by coexpressing or knocking outing AtTSPO **(Figure 29D)**. The mRFP signal was consistently observed in the cell periphery without any other intermediate form. These data suggest that AtTSPO explicitly regulates the differential level of IRT1 in the root cell.

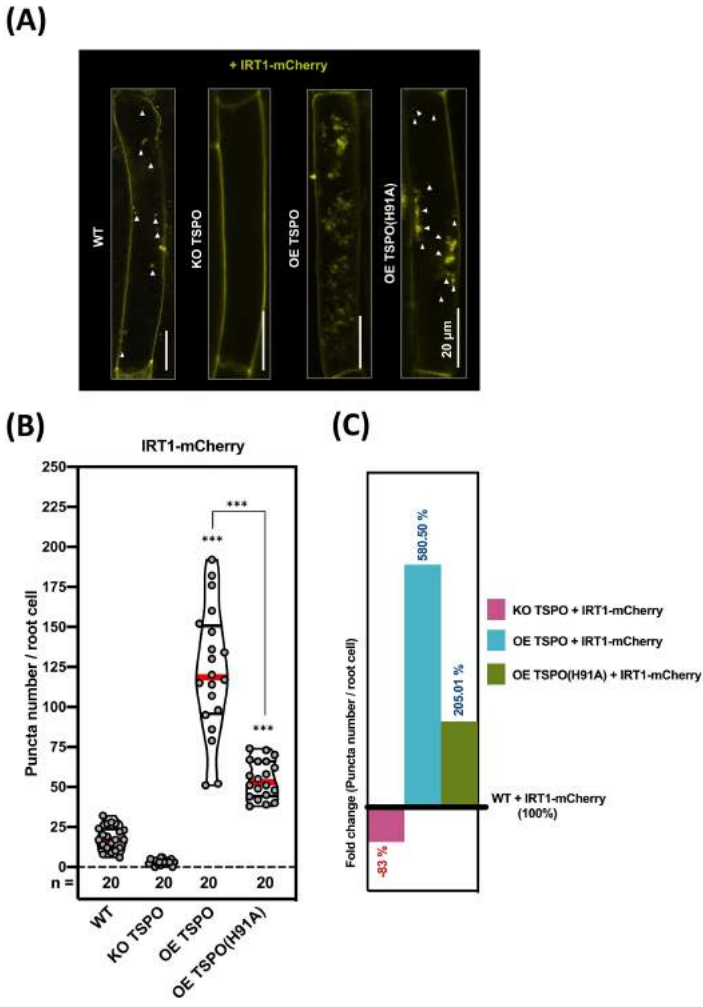
(A)
+ IRT1-mCherry
WT
KO TSPO
OE TSPO
OE TSPO(H91A)
20 µm
(B)
IRT1-mCherry
Puncta number / root cell
250
225
200
175
150
125
100
75
50
25
0
***
***
***
n =
20
20
20
20
WT
KO TSPO
OE TSPO
OE TSPO(H91A)
(C)
Fold change (Puncta number / root cell)
580.50 %
205.01 %
-83 %
WT + IRT1-mCherry
(100%)
KO TSPO + IRT1-mCherry
OE TSPO + IRT1-mCherry
OE TSPO(H91A) + IRT1-mCherry

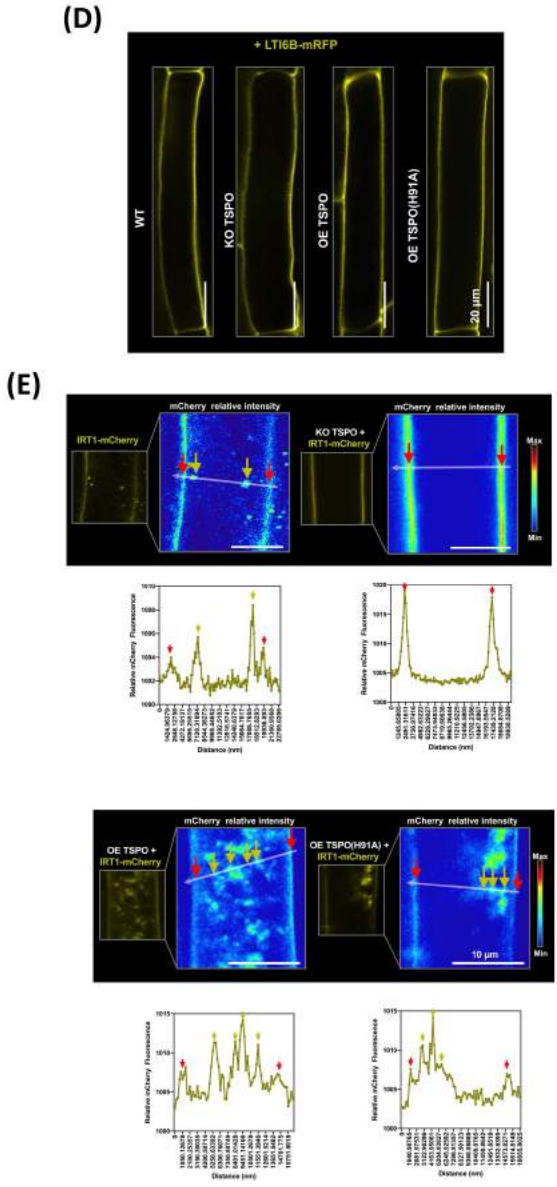
(D)
+ LTI6B-mRFP
WT
KO TSPO
OE TSPO
OE TSPO(H91A)
20 µm
(E)
IRT1-mCherry
mCherry relative intensity
KO TSPO +
IRT1-mCherry
Max
Min
Relative mCherry Fluorescence
Distance (nm)
OE TSPO +
IRT1-mCherry
OE TSPO(H91A) +
IRT1-mCherry
10 µm

Figure 29. AtTSPO regulates the subcellular localization and level of constitutively expressed IRT1-mCherry in *A.thaliana* roots. **(A)** Presentative Airyscan super-resolution images of *Arabidopsis* root cells overexpressing IRT1-mCherry in WT, KO TSPO, OE TSPO, and OE TSPO(H91A) backgrounds. Arrowheads show intracellular puncta. **(B)** The intercellular puncta number per root cell. The Violin plot shows the individual root cell measurements, and the middle red horizontal lines define the means for each dataset. The asterisks indicate a significant difference (Tukey, *** $p < 0.001$). **(C)** The percent of fold change compared to IRT1-mCherry (WT background = 100%). **(D)** Presentative Airyscan super-resolution images of *Arabidopsis* root cells overexpressing ILTI6B-mRFP in WT, KO TSPO, OE TSPO, and OE TSPO(H91A) backgrounds. **(E) The cell** section shows the distribution of IRT1-mCherry in different backgrounds. Red arrows indicate the cell periphery localization, and yellow arrows indicate intracellular puncta. The IRT1-mCherry relative fluorescence profile shows the relative fluorescence intensity.

5.2.5 ABA, salinity, and osmotic stress enhance the degradation of IRT1 in *A. thaliana* root cells

AtTSPO could be transiently induced in vegetative tissues through ABA treatment, osmotic stress, and salinity (Guillaumot *et al.,* 2009; Vanhee *et al.,* 2011). It was shown that ABA-dependent induction of AtTSPO triggers steady degradation of PIP2;7 through the autophagy pathway (Hachez *et al.,* 2014). After ABA incubation, it has been shown that *Arabidopsis* plant cell constitutively expressing YFP-PIP2;7 accumulates YFP fluorescence in punctate structures known as autophagosomes (Hachez *et al.,* 2014). In parallel, under conditions of ABA treatment, salinity, and osmotic stress, IRT1 mRNA accumulation was decreased via inhibition of the expression of FIT and bHLH093 (Séguéla *et al.*, 2008; Gu *et al.*, 2021; Fan *et al.*, 2014). We wonder whether these dependent AtTSPO-induction-conditions promote the accumulation of the constitutively expressed IRT1-mCherry in cytoplasmic puncta structures.

Accordingly, we incubated transgenic seedlings overexpressing IRT1-mCherry in both WT and KO AtTSPO backgrounds with and without 50 µM of ABA for 24 h under shaking in two different media: a Control liquid medium (½ MS + 10 µM iron) and a liquid iron-deficient medium (½ MS + 150 µM Ferrozine iron chelator). The presentative Airyscan super-resolution images showed a very highly significant increase ($p<0.001$) in the number of cytoplasmic mCherry bodies puncta under ABA treatment in WT background and a highly significant increase ($p<0.01$) in Knockout AtTSPO background **(Figure 30A and B)**. In standard conditions, the knock outing of AtTSPO triggered a decrease of 86.61 % in the number of mCherry puncta bodies compared to the IRT1-mCherry expressed in the WT background **(Figure 30C)**. Moreover, the limitation of iron promotes hyper induction of IRT1 (Vert et al., 2002a; Barberon et al., 2011).Under iron deficiency with standard metal level, IRT1 is more stabile at the plasma membrane which decreases its remobilization to the endosomes (Barberon *et al.,* 2014; Dubeaux et al., 2018). Iron deficiency reduces the puncta structures in the root cell cytoplasm by 67.14 % in the WT background and 34.24 % in the KO TSPO background **(Figure 30A and D)**.

Interestingly, in plants expressing IRT1-mCherry in WT background and transferred to the iron-deficient medium containing 50 µM of ABA, the mCherry fluorescence was highly observed in mobile puncta structures **(Figure 30A)**. The number of cytoplasmic puncta was very highly significantly increased by 694.49 % more than the control condition and 369.17 % more than ABA treatment alone **(Figure 30D)**. Under the same treatment, no significant difference in puncta number was observed in KO AtTSPO background compared to ABA treatment

alone **(Figure 30A, B, and D)**. The mCherry fluorescence profile in the cell section showed higher fluorescence intensity in puncta structures than in plasma membrane under ABA incubation. It was clear that Abscisic acid treatment triggered to increase in the distribution of IRT1-mCherry in cytoplasmic punctate bodies, even under iron deficiency **(Figure 30E)**.

Furthermore, high salinity induces ABA accumulation triggered by an osmosensing and osmotic adjustment mechanisms in the root cells (Jia *et al.*, 2002; LaRosa *et al.*, 1987; Grillo *et al.*, 1995). In addition, under salt stress, AtTSPO protein is transiently induced, and its expression is boosted with the increase of osmolarity in the medium (Guillaumot et al., 2009a). To examine the effect of salinity on the IRT1 regulation and cellular localization, we realized the same previous experiment using 200 mM of NaCl instead of ABA treatment. Presentative Airyscan super-resolution images show a very highly significant increase ($p < 0.001$) in the mCherry punctate structures under salt treatment by 273.71 % and salt treatment in addition to iron deficiency by 492.41 % compared to standard conditions in WT background **(Figure 30F, G, and H)**.

On the other hand, in the KO AtTSPO background, the salt treatment increased puncta by 572,72 %. Contrariwise, the salt stress did not affect the puncta number under iron deficiency **(Figure 30F, G, and H)**. The mCherry fluorescence profile analysis showed that NaCl treatment triggers the formation of cytoplasmic puncta containing higher mCherry fluorescence compared to the cell periphery in the WT background. This aspect was observed even under iron deficiency in addition to salt treatment **(Figure 30I).**

However, TSPO is transiently highly expressed by osmotic stress (Kreps *et al.,* 2002; Seki *et al.,* 2002; Zimmermann *et al.,* 2004; Winter *et al.,* 2007; Guillaumot *et al.,* 2009a; Hermans *et al.,* 2010). Likewise, the osmotic stress is repressed by overexpression of the *Arabidopsis* Target Of Rapamycin (AtTOR), which interacts with RAPTOR1 (regulatory protein of AtTOR) to regulate the activity of S6 Kinase in response to osmotic (Mahfouz *et al.*, 2006; Pu, Soto-Burgos, *et al.*, 2017). In addition, the negative regulation of AtTOR by the SnRK1 protein kinase complex acts as a positive regulator of autophagy under nutrient deficiency, osmotic stress, and salinity (Soto-Burgos and Bassham, 2017; Liu *et al.,* 2017). The inhibition of AtTOR by RAP and AZD chemical compounds triggers upregulating ABA biosynthesis-related genes, increasing ABA levels in the cell and activating the autophagy pathway (Li *et al.,* 2021; Pu *et al.,* 2017a). To investigate IRT1 regulation and cellular distribution under osmotic stress and AtTOR inhibition, we incubated *Arabidopsis* transgenic seedlings expressing constitutively IRT1-mCherry in WT and KO AtTSPO backgrounds for 24 h in a standard medium containing respectively 400 mM of sorbitol and 0.5 µM of t AZD8055 TOR-inhibitor. Presentative Airyscan super-resolution imaging analysis shows a very highly significant increase ($p<0.001$) of the punctate cytoplasmic structures under Sorbitol (up to 659.41 %) and TOR inhibitor (up to 518.83 %) in WT background compared with the standard condition. At the same time, there was no significant change in terms of puncta number in the KO AtTSPO background under the same conditions **(Figure 30J, K, and L)**. Under osmotic stress or treatment with AZD8055, in the presence of AtTSPO, IRT1-mCherry was primarily localized in the cytoplasmic punctate bodies, where the mCherry fluorescence was

higher than the PM. Contrariwise, the AtTSPO knock outing triggered to stabilize IRT1-mCherry at the plasma membrane, even under these treatments **(Figure 30L)**.

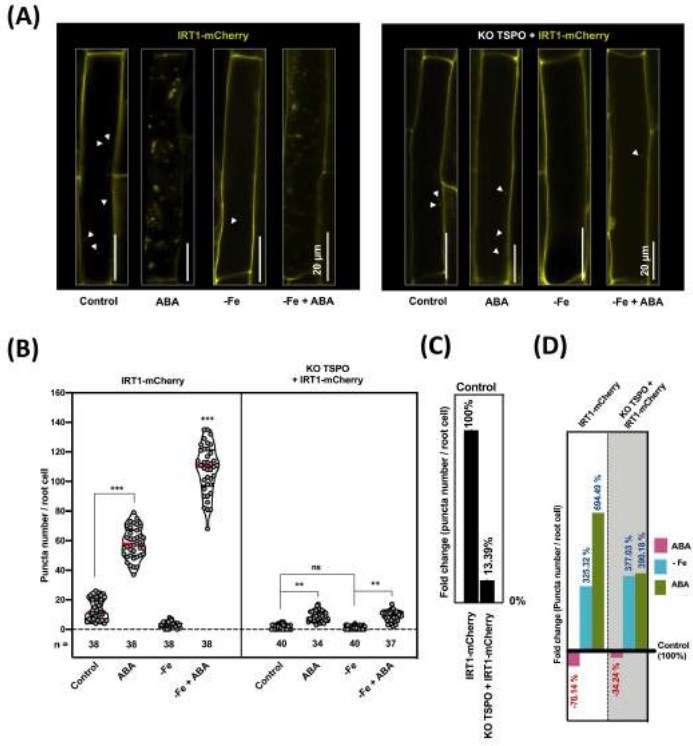

(E)

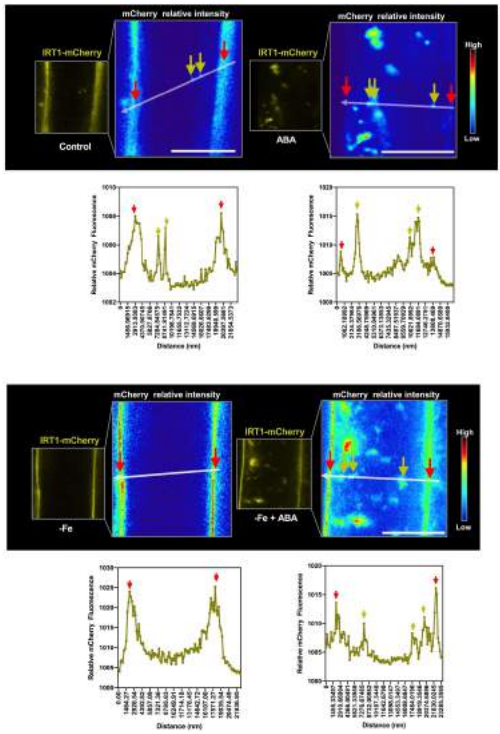
mCherry relative intensity
IRT1-mCherry
Control
ABA
High
Low
Relative mCherry Fluorescence
Distance (nm)
-Fe
-Fe + ABA

(F)

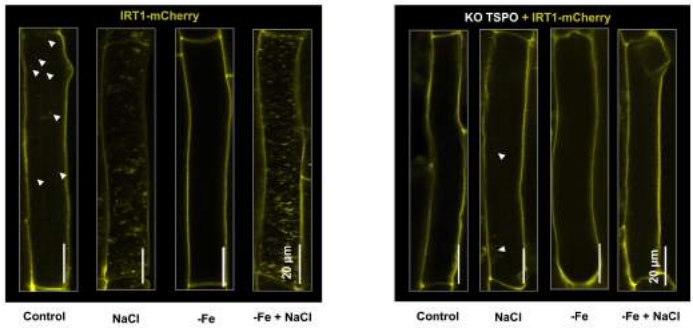
IRT1-mCherry
KO TSPO + IRT1-mCherry
20 µm
Control
NaCl
-Fe
-Fe + NaCl

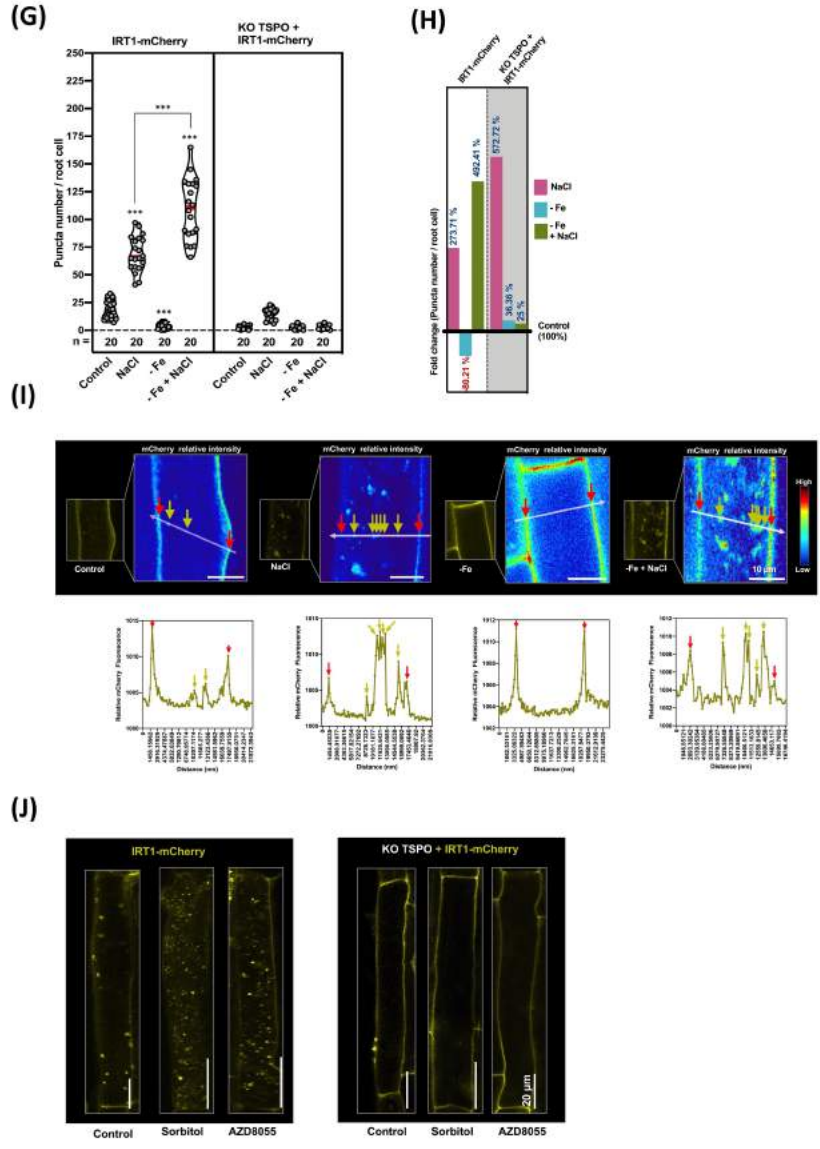
(G)
IRT1-mCherry
KO TSPO + IRT1-mCherry
Puncta number / root cell
n =
Control
NaCl
- Fe
- Fe + NaCl
(H)
IRT1-mCherry
KO TSPO + IRT1-mCherry
Fold change (Puncta number / root cell)
273.71 %
-68.21 %
492.41 %
572.72 %
38.38 %
25 %
Control (100%)
NaCl
- Fe
- Fe + NaCl
(I)
mCherry relative intensity
Control
NaCl
-Fe
-Fe + NaCl
High
Low
10 µm
(J)
IRT1-mCherry
KO TSPO + IRT1-mCherry
Control
Sorbitol
AZD8055
20 µm

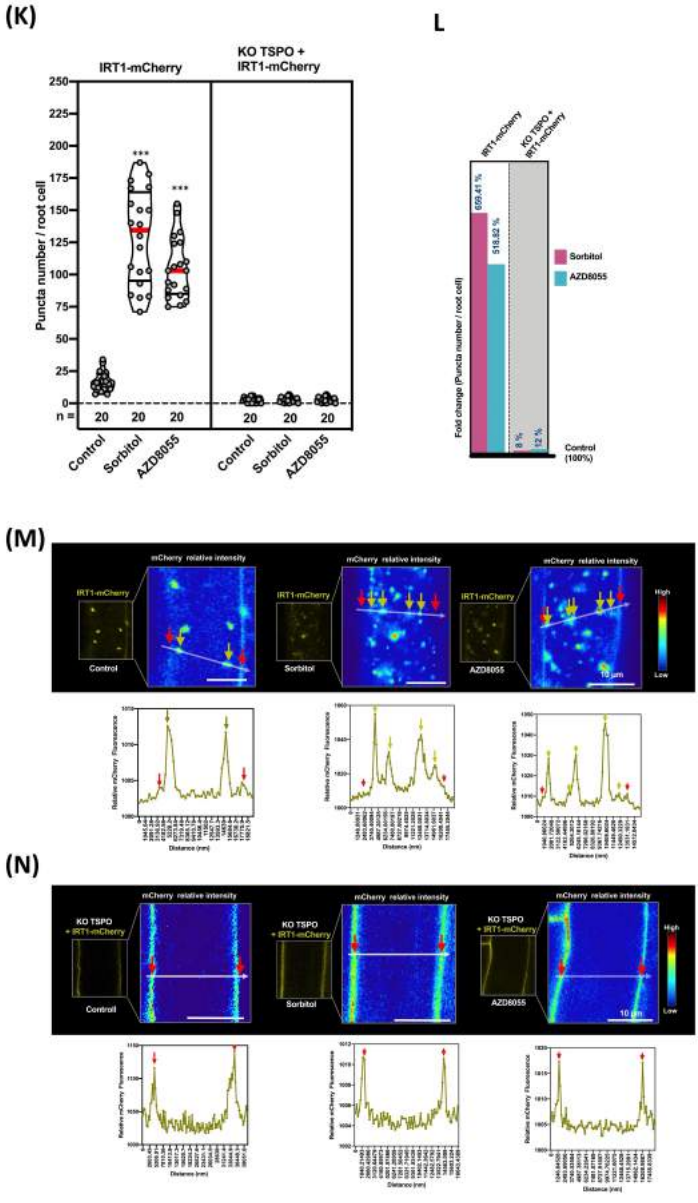
(K)
IRT1-mCherry
KO TSPO + IRT1-mCherry
Puncta number / root cell
250
225
200
175
150
125
100
75
50
25
0
***
***
n =
20 20 20 20 20 20
Control
Sorbitol
AZD8055
Control
Sorbitol
AZD8055
L
IRT1-mCherry
KO TSPO + IRT1-mCherry
659.41 %
518.82 %
8 %
12 %
Sorbitol
AZD8055
Control (100%)
Fold change (Puncta number / root cell)
(M)
mCherry relative intensity
IRT1-mCherry
Control
Sorbitol
AZD8055
High
Low
10 µm
Relative mCherry Fluorescence
Distance (nm)
(N)
KO TSPO + IRT1-mCherry
Controll
Sorbitol
AZD8055

Figure 30. ABA, salinity, and osmotic stress enhance the degradation of IRT1 in *A.thaliana* root cells. **(A to E)** ABA treatment triggers to IRT1-mCherry degradation**. (A)** Presentative Airyscan super-resolution images of *Arabidopsis* root cells overexpressing IRT1-mCherry in the control condition, incubation for 24 h in ABA (50 µM), incubation for 24 h under iron deficiency (150 µM Ferrozine) and double treatment (ABA + iron deficiency). **(B)** The intercellular puncta number per root cell. Violin plot shows the individual measurements, and middle red horizontal lines define the means for each dataset. The asterisks indicate a significant difference (Tukey, *** $p < 0.001$). **(C and D)** The percent of fold change compared to the control condition (=100%). **(E)** The cell section shows the distribution of IRT1-mCherry in different conditions. Red arrows indicate the plasma membrane localization, and yellow arrows indicate intracellular puncta. The IRT1-mCherry relative fluorescence profile shows the relative fluorescence intensity. **(F to I)** Salinity leads to IRT1-mCherry degradation. **(F)** Presentative Airyscan super-resolution images of *Arabidopsis* root cells overexpressing IRT1-mCherry in the control condition, incubation for 24 h in NaCl (200 mM), incubation for 24 h under iron deficiency (150 µM Ferrozine), and double treatment (NaCl + iron deficiency). **(G)** The intercellular puncta number per root cell. Violin plot shows the individual measurements, and middle red horizontal lines define the means for each dataset. The asterisks indicate a significant difference (Tukey, *** $p < 0.001$). **(H)** The percent of fold change compared to the control condition (=100%). **(I)** The cell section shows the distribution of IRT1-mCherry in different conditions. Red arrows indicate the plasma membrane localization, and yellow arrows indicate intracellular puncta. The IRT1-mCherry relative fluorescence profile shows the relative fluorescence intensity. **(J to N)** Osmotic stress and TOR inhibitor promote IRT1-mCherry degradation. **(J)** Presentative Airyscan super-resolution images of *Arabidopsis* root cells overexpressing IRT1-mCherry in the control condition, incubation for 24 h in Sorbitol (400 mM), incubation for 24 h in AZD8055 (0.5 µM). All media contained the same level of DMSO. **(K)** The intercellular puncta number per root cell. Violin plot shows the individual measurements, and middle red horizontal lines define the means for each dataset. The asterisks indicate a significant difference (Tukey, *** $p < 0.001$). **(L)** The percent of fold change compared to the control condition (=100%). **(M and N)** The cell section shows the distribution of IRT1-mCherry in different conditions. Red arrows indicate the plasma membrane localization, and yellow arrows indicate intracellular puncta. The IRT1-mCherry relative fluorescence profile shows the relative fluorescence intensity.

5.2.6 AtTSPO induction triggers the degradation of IRT1 via the autophagic pathway

It is known that IRT1 is mainly localizing in the plasma membrane and endosomes. Under iron deficiency with metal excess, IRT1 is depleted from the PM and highly accumulates in internal vesicles (Barberon *et al.,* 2014). IRT1 polyubiquitinated by the ENDOSOMAL

SORTING COMPLEX FOR TRANSPORT (ESCRT-1) and targeted for the degradation in the vacuole (Zelazny and Vert, 2015; Dubeaux *et al.,* 2018). We investigate whether in what compartment was localized the IRT1-mCherry punctate structure found exclusively in the presence of AtTSPO. For that, we used a fluorescent acidotropic dye monodensylcadaverine (MDC) to stain a probable acidic small vesicle such as autophagosomes in *Arabidopsis* root cells (Contento *et al.,* 2005; Merkulova *et al.,* 2014; Patel and Dinesh-Kumar, 2008; Wang *et al.,* 2019; Liu *et al.,* 2017; Olenieva *et al.,* 2017; Floyd *et al.,* 2015). In vivo, the MDC fluorescence preferentially accumulates in autophagic vesicles and fewer in late endosomes (Biederbick et al., 1995; Murugan and Amaravadi, 2016). Our objective was to determine whether IRT1-mCherry colocalizes with the MDC-stained structures. And if the expected colocalization is altered by the presence or the absence of AtTSPO? Roots of homozygous transgenic seedlings constitutively expressing IRT1-mCherry in both WT and KO AtTSPO backgrounds are stained with 30 μM MDC and then assessed by confocal microscopy imaging. In the WT background, mCherry fluorescence of punctate structures was mostly colocalized with MDC (**yellow arrowheads in Figure 31a, b and c**). MDC fluorescent-stained structures are partially colocalized with mcherry punctate bodies (**red arrowheads in Figure 31 Insets d to f**). The fluorescence profile analysis shows that the mCherry fluorescent puncta colocalized with a part of MDC labeled structures **(Figure 31g and h)**. Interestingly, in the absence of AtTSPO, the mCherry puncta number was very highly significantly decreased ($p<0.001$) compared to the WT background **(Figure 31o)**. In addition, a very low colocalization between IRT1-mCherry and MDC was observed **(Figure 31i, j, and k)**. **Figure 31 Insets l to n** show no

colocalization between mcherry fluorescence punctate bodies (red arrowheads) and MDC labeled structures (white arrowheads). Then, we measured Manders overlapping colocalization between mCherry and MDC fluorescence. Moreover, **Figure 31p** shows a very high significant difference in terms of mCherry-MDC colocalization between WT background (up to 65 %) and KO AtTSPO background (up to 20 %). These data suggest that the expression of AtTSPO enhances the cellular localization of IRT1 in small acidic punctate structures, probably autophagosomes.

Accordingly, we scrutinize from which cell compartment these acidic vesicles in which AtTSPO and IRT1 do physically interact came from. It is known that AtTSPO is transiently localizing in the ER and the Golgi stacks (Guillaumot et al., 2009a; Hachez et al., 2014).

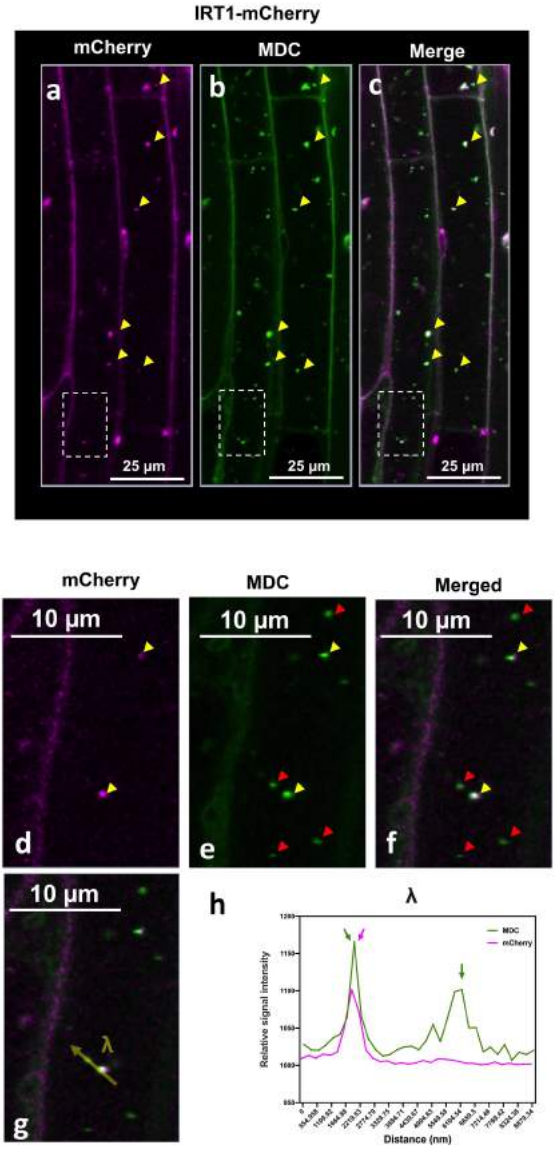
IRT1-mCherry
mCherry
MDC
Merge
a
b
c
25 µm
25 µm
25 µm
mCherry
MDC
Merged
10 µm
10 µm
10 µm
d
e
f
10 µm
λ
g
h
λ
MDC
mCherry
Relative signal intensity
Distance (nm)

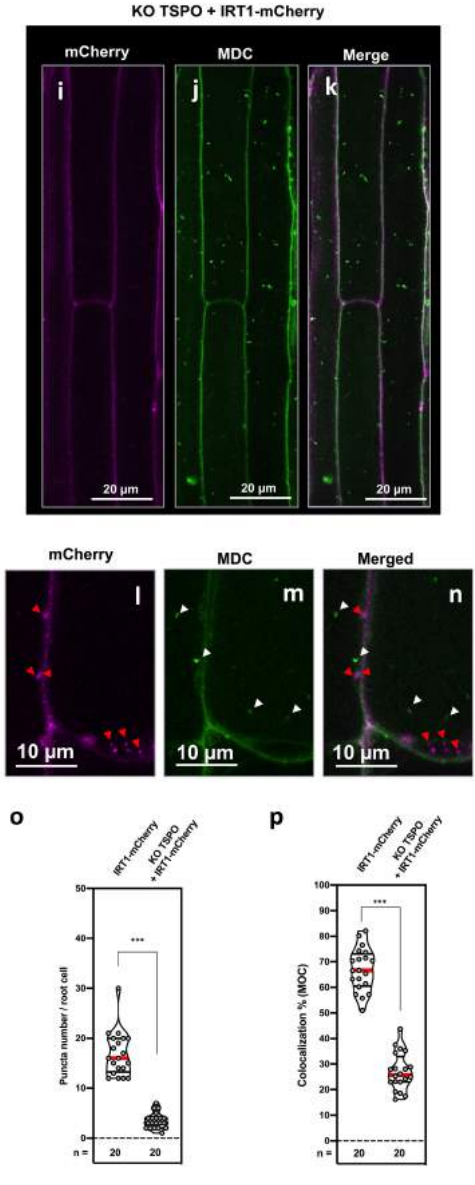
KO TSPO + IRT1-mCherry
mCherry
MDC
Merge
i
j
k
20 µm
20 µm
20 µm
mCherry
MDC
Merged
l
m
n
10 µm
10 µm
10 µm
o
p
IRT1-mCherry
KO TSPO + IRT1-mCherry
Puncta number / root cell
Colocalization % (MOC)
***
n =
20
20

Figure 31. TSPO promotes IRT1-mCherry localization in acidic bodies**.** Panels **(a to g)** show Representative confocal MDC-staining images of *Arabidopsis* root cells expressing constitutively IRT1-mCherry in a WT background**.** Yellow arrowheads show the colocalized IRT1-mCherry with MDC-stained vesicles. Red arrowheads indicate no colocalization. Relative fluorescence profile from **(g)** was shown in **(h)** Panels **(i to n)** show Representative confocal MDC-staining images of *Arabidopsis* root cells expressing constitutively IRT1-mCherry in KO TSPO background **(i-n)**. White arrowheads show IRT1-mCherry, and red arrowheads indicate MDC-stained vesicles. **(o)** The intercellular puncta number per root cell. **(p)** Percent of colocalization (Menders overlapping coefficient). Violin plots in **(o)** and **(p)** show the individual measurements, and middle red horizontal lines define the means for each dataset. The asterisks indicate a significant difference (Tukey, *** $p < 0.001$).

In addition, under stress conditions and ABA treatment, AtTSPO could be localized in the autophagosome compartment complexing with the ubiquitin-like autophagy-related 8 protein (ATG8) through the heme-binding (Vanhee *et al.,* 2011) or the physical interaction with the membrane protein AtPIP2;7 (Hachez *et al.,* 2014; Jurkiewicz *et al.,* 2020). **Figure 32 (A-C)** shows the colocalization state between YFP tagged AtTSPO and, respectively: XT Golgi marker tagged with mTq2, LTI6B plasma membrane marker tagged with mRFP, and PI3P-specific biosensor tagged with mCherry as a marker for endosomes in tobacco epidermis cells (transient expression). Confocal images show that most YFP-AtTSPO was detected in the Golgi (MOC = 0.914, **Figure 32A**). In effect, there was no colocalization between YFP-AtTSPO and LTI6B-mRFP (MOC = 0.274, **Figure 32B**). Also, YFP-AtTSPO was observed in punctate structures far from being located at the PM **(Figure 32B inset and fluorescence profiles analysis)**. Moreover, no YFP-AtTSPO was observed in the endosomes (MOC = 0.096, **Figure 32C**). Red arrowheads show endosomes as mobile vesicles (magenta) not colocalizing with YFP fluorescent structures (**Figure 32C inset and fluorescence profiles analysis)**. Whereas IRT1-mCherry was widely colocalizing with the endosome marker (PI3P-specific biosensor

tagged with YFP) **(Figure 32D)**. Most of the mCherry puncta colocalized with the YFP fluorescent structures (MOC = 0.88) **(Figure 32D inset and fluorescence profiles analysis)**. Therefore, to investigate the localization of the complex AtTSPO-IRT1, we took advantage of the BiFC system already used in (**Figure 25).** Remembering that the physical interaction between AtTSPO and IRT1 did not happen in the Golgi **(Figure 25)**, we wonder whether we could detect BiFC in the endosomes or PM. **Figure 32E** shows no colocalization between BIFC and LI6B-mRFP (MOC = 0.26). Red arrow heads show that the mRFP fluorescence does not overlap with the YFP fluorescence mentioned by the white arrow heads **(Figure 32.E insets and fluorescence profiles analysis)**. In addition, no BiFC was colocalizing with the endosome marker (MOC = 0.176) **(Figure 32F)**. The confocal images insets shows clearly that the interaction between AtTSPO and IRT1 was not happening in the endosomes. The red arrowheads (magenta) showed a different compartment mentioned by the white arrowheads (Green) **(Figure 32F insets and fluorescence profiles analysis)**.

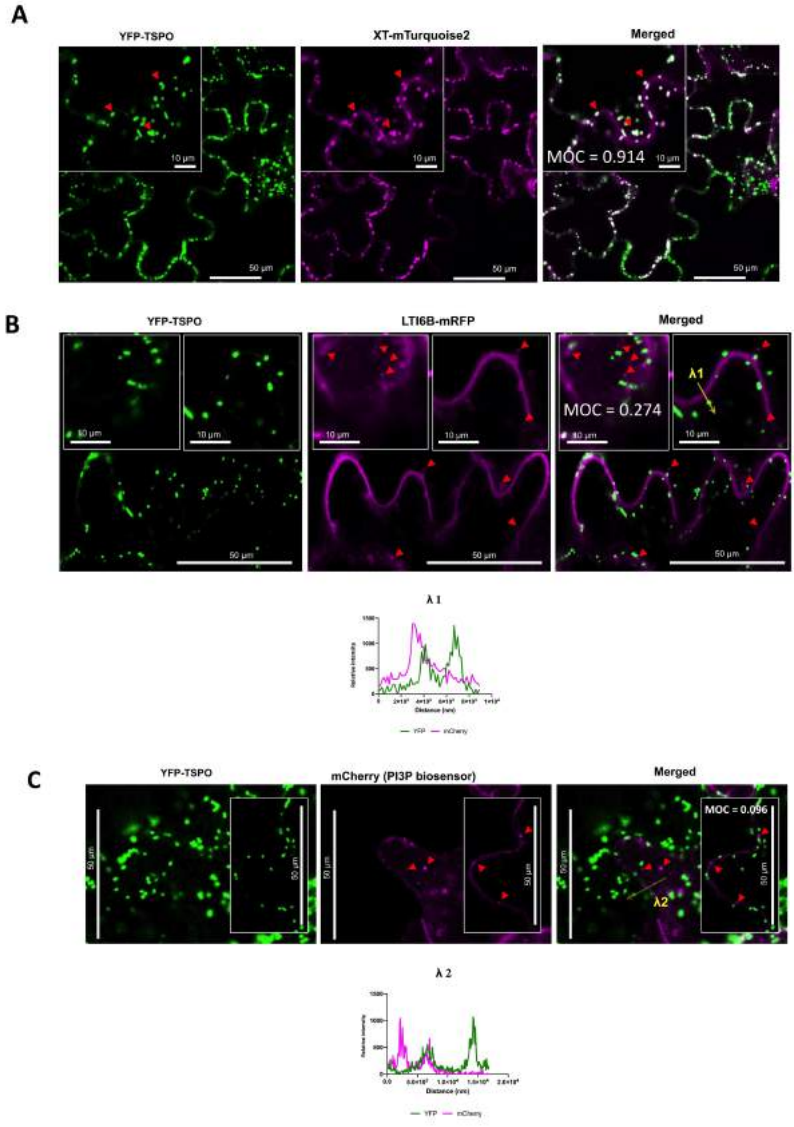
A
YFP-TSPO
XT-mTurquoise2
Merged
MOC = 0.914
B
YFP-TSPO
LTI6B-mRFP
Merged
MOC = 0.274
λ1
λ 1
C
YFP-TSPO
mCherry (PI3P biosensor)
Merged
MOC = 0.096
λ2
λ 2

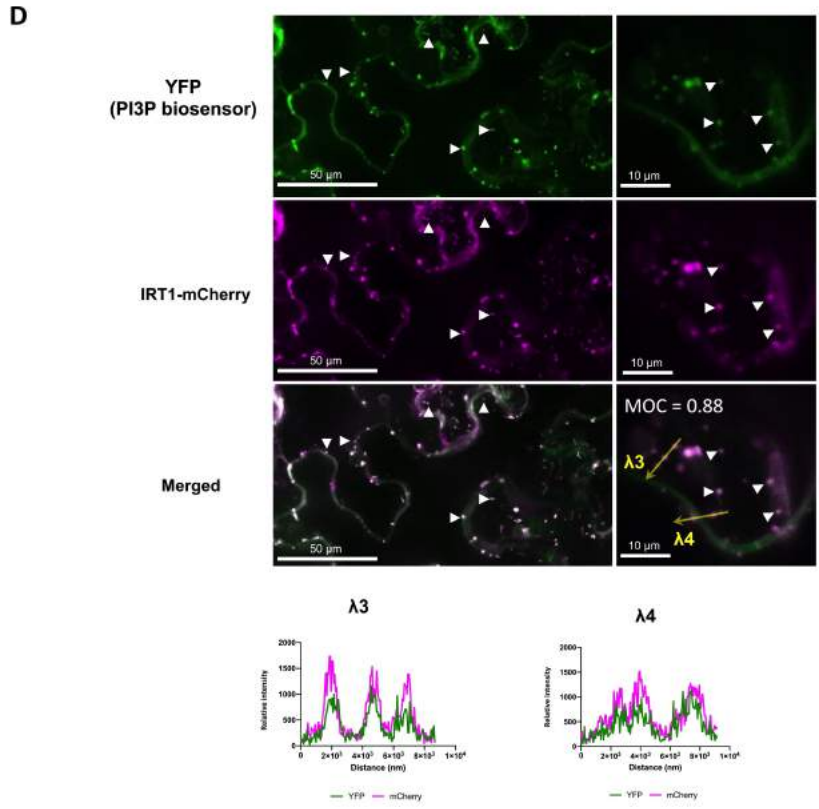
D
YFP
(PI3P biosensor)
IRT1-mCherry
Merged
50 µm
10 µm
MOC = 0.88
λ3
λ4
λ3
λ4
Relative Intensity
Distance (nm)
YFP
mCherry

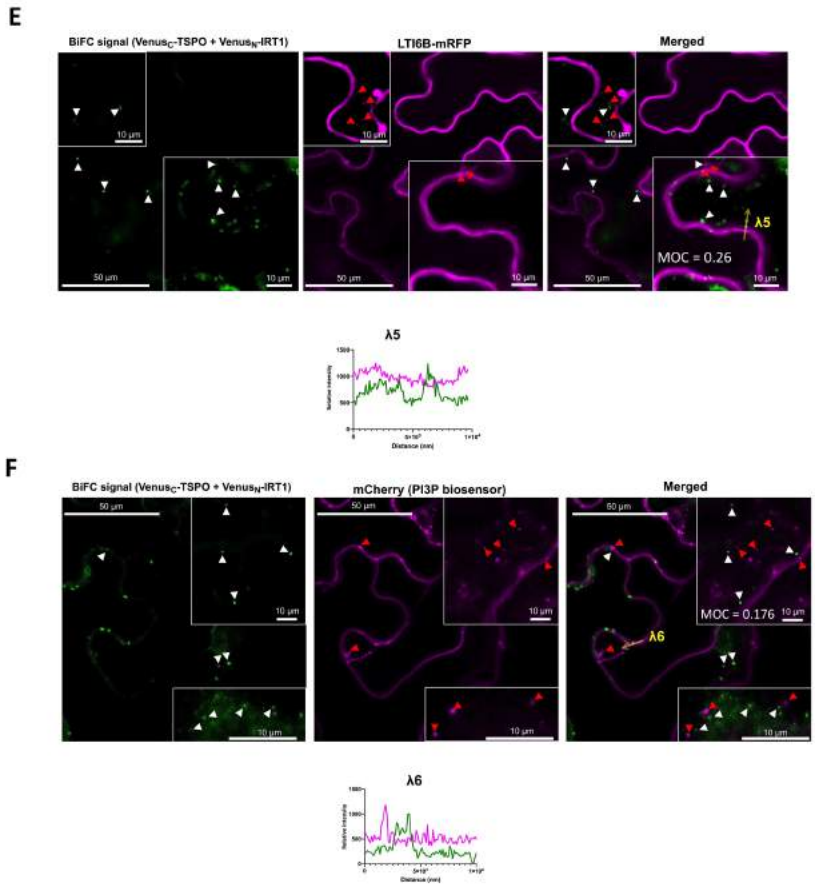

Figure 32. Transient protein expression demonstrates the AtTSPO-IRT1 interaction in *planta***.** Representative confocal images of tobacco epidermal cells expressing YFP-TSPO transiently coexpressed with: The Golgi maker **(A)**, the plasma membrane marker (LTI6B-mRFP) **(B)**, and endosomes marker tagged to mCherry (PI3P biosensor) **(C)**. MOC is the Menders overlapping coefficient (colocalization value). **(D)** Representative confocal images of tobacco epidermal cells transiently coexpressing IRT1-mCherry and PI3P biosensor. **(E and F)** Representative confocal images of tobacco epidermal cells transiently coexpressing Venus$_C$-TSPO + Venus$_N$-IRT1 with: LITI6B-mRFP **(E)** and PI3P biosensor tagged to mCherry **(F)** White arrowheads were BIFC signals. BiFC signal in the

left panels was shown in green. Middle panels show XT-mtq2 signal (magenta). Right panels show merged signals.

Figures 22 and 23 indicate that AtTSPO interacts with IRT1 in acidic vesicles different from Golgi stack, endosomes, and PM. These moving punctate structures were labeled by MDC, and they were reminiscent of autophagosomes.

ABA signaling depends on endomembrane trafficking, including the complex relationship between autophagy and endosomal trafficking, to regulate the degradation in the vacuole (Yu and Xie, 2017; Barth and Köhler, 2014). Under stress conditions, ABA response is induced through the activation of SNF1-related protein kinase 2 (SnRK2)(Shinozawa *et al.*, 2019). These also inactivate TOR and parallelly induce Autophagy (Sirko *et al.,* 2021; Wang *et al.,* 2018; Fujii and Zhu, 2009; Soon *et al.,* 2012). Accordingly, we investigated the effect of autophagy through ABA treatment inducing AtTSPO, which triggers IRT1 downregulation. *Arabidopsis* transgenic homozygous seedlings constitutively expressing IRT1-mCherry were exposed during 24 h to 5 mM of autophagy inhibitor 3-methyladenine (3-MA) and 50 µM ABA with and without 3-MA **(Figure 33.A to D)**. The presentative Airyscan super-resolution images show a very highly significant decrease of punctate structures ($p < 0.001$) in the presence of 3-MA (97,76 %), even under ABA treatment (70.76 %). The Fluorescence profile analysis shows that in the presence of the autophagy inhibitor, most of the mCherry fluorescence was detected in the cell periphery **(Figure 33D)**.

Next, we verified if IRT1 is degraded via autophagy. Furthermore, we treated *Arabidopsis* seedlings overexpressing IRT1-mCherry with 1

µM of Concanamycin A (ConcA) vacuole-hydrolases inhibitor, 100 µM of benzo(1,2,3)thiadiazole-7-carboxylic acid (BTH) autophagy inducer or both for 24 h **(Figure 33E to H)**. Compared to the standard condition, interestingly, a very highly significant ($p < 0.001$) proliferation of the punctate bodies (371.85 %) possibly in the vacuole was observed by using ConcA. Also, the application of BTH increased very highly significantly ($p < 0.001$) the number of puncta bodies (470.21 %) compared to the standard conditions. When we combined BTH with ConcA, the detected number of punctate vesicles was highly significantly ($p < 0.01$) increased compared to BTH treatment (659.56 % more than the control condition). The fluorescence profile analysis shows high mCherry distribution in punctate forms upon BTH and ConcA treatment compared to the control condition **(Figure 33H).**

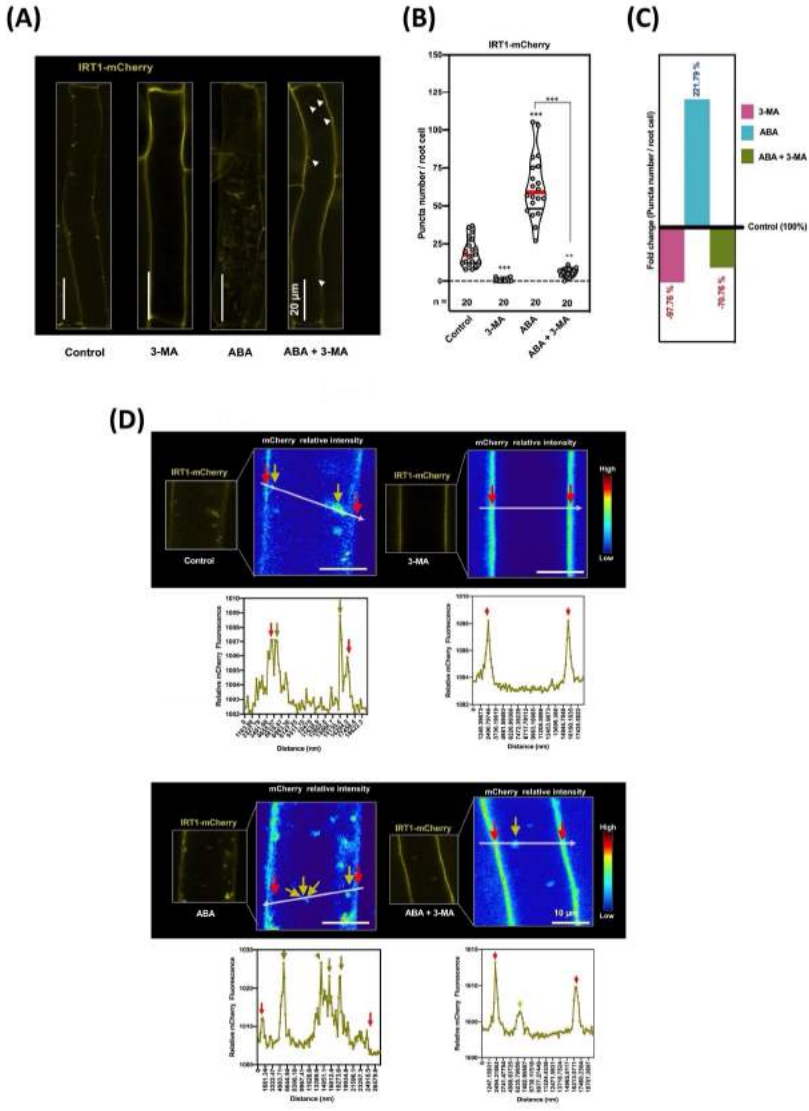
(A)
IRT1-mCherry
20 μm
Control
3-MA
ABA
ABA + 3-MA
(B)
IRT1-mCherry
Puncta number / root cell
n =
20
Control
3-MA
ABA
ABA + 3-MA
(C)
Fold change (Puncta number / root cell)
3-MA
ABA
ABA + 3-MA
Control (100%)
221.79 %
-87.76 %
-76.76 %
(D)
mCherry relative intensity
IRT1-mCherry
Control
3-MA
High
Low
Relative mCherry Fluorescence
Distance (nm)
ABA
ABA + 3-MA
10 μm

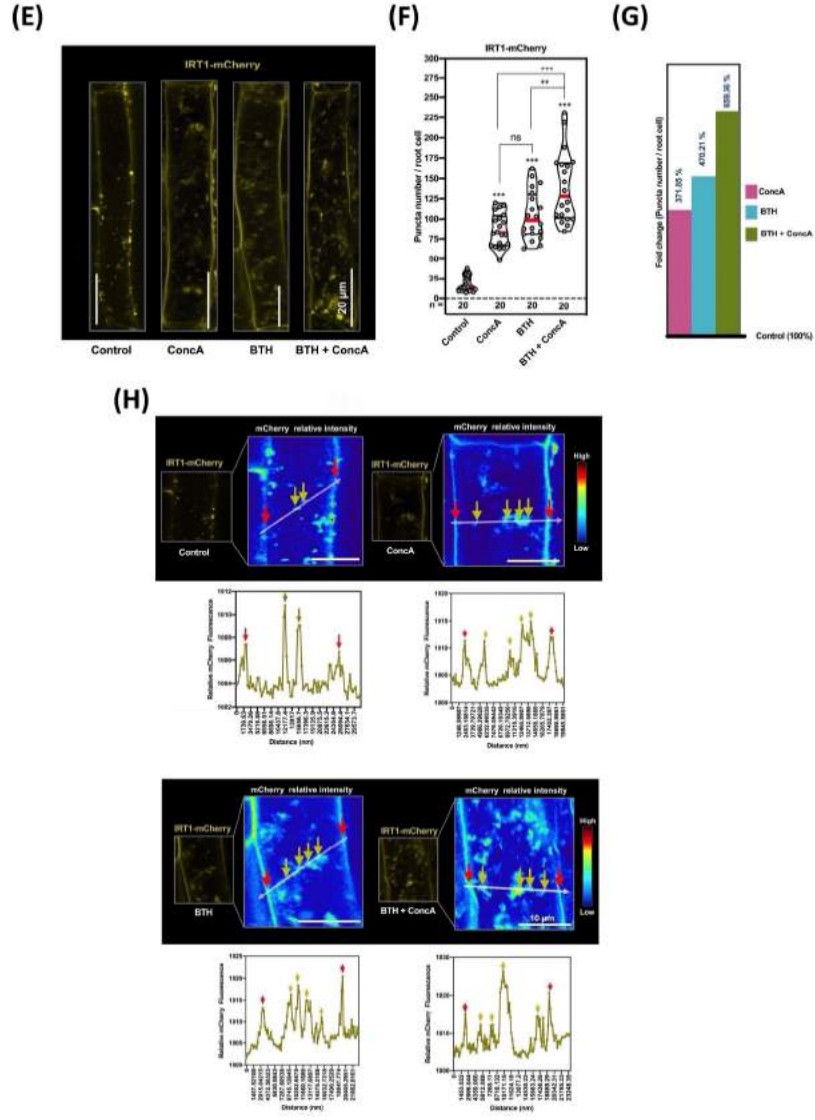
(E)
IRT1-mCherry
Control
ConcA
BTH
BTH + ConcA
20 µm
(F)
IRT1-mCherry
Puncta number / root cell
ns
Control
ConcA
BTH
BTH + ConcA
(G)
Fold change (Puncta number / root cell)
371.85 %
470.21 %
ConcA
BTH
BTH + ConcA
Control (100%)
(H)
mCherry relative intensity
IRT1-mCherry
Control
ConcA
High
Low
Relative mCherry Fluorescence
Distance (nm)
BTH
BTH + ConcA
10 µm

Figure 33. Autophagy induction triggers IRT1-mCherry degradation. **(A to D)** Autophagy inhibition reduces the formation of punctate bodies containing IRT1-mCherry. **(A)** Presentative Airyscan super-resolution images of *Arabidopsis* root cells overexpressing IRT1-mCherry in the control condition, incubation for 24 h in ABA (50 µM), incubation for 24 h with 3-MA (5 mM), and double treatment (ABA + 3-MA). All media contained the same level of DMSO. **(B)** The intercellular puncta number per root cell. The Violin plots show the individual measurements, and middle red horizontal lines define the means for each dataset. The asterisks indicate a significant difference (Tukey, *** $p < 0.001$). **(C)** The percent of fold change compared to the control condition (=100%). **(D)** The cell section shows the distribution of IRT1-mCherry in different conditions. Red arrows indicate the plasma membrane localization, and yellow arrows indicate intracellular puncta. The IRT1-mCherry relative fluorescence profile shows the relative fluorescence intensity. **(E to H)** Autophagy promotes the accumulation of IRT1-mCherry degradation bodies. **(E)** Presentative Airyscan super-resolution images of *Arabidopsis* root cells overexpressing IRT1-mCherry in the control condition, incubation for 24 h in ConcA (1 µM), incubation for 24 h BTH (100 µM), and double treatment (BTH + ConcA). All media contained the same level of DMSO. **(F)** The intercellular puncta number per root cell. Violin plots show the individual measurements, and middle red horizontal lines define the means for each dataset. The asterisks indicate a significant difference (Tukey, *** $p < 0.001$). **(G)** The percent of fold change compared to the control condition (=100%). **(H)** The cell section shows the distribution of IRT1-mCherry in different conditions. Red arrows indicate the plasma membrane localization, and yellow arrows indicate intracellular puncta. The IRT1-mCherry relative fluorescence profile shows the relative fluorescence intensity.

Furthermore, it has been shown that autophagy bodies are highly accumulated during carbon/nitrogen starvation and during senescence to encourage nutrient remobilization (Doelling *et al.,* 2002; Suttangkakul *et al.,* 2011) and preserve cells by removing damaged chloroplasts (Wang and Blumwald, 2014). Leaf senescence leads to programmed cell death (PCD) that triggers to accumulation of reactive oxygen species (Overmyer *et al.*, 2003). An early accelerated senescent phenotype characterizes some autophagy null mutants as *atg5, atg2, atg7, atg11*, and the double mutant *atg13a-b* (Li *et al.,* 2014; Yoshimoto *et al.,* 2009; Suttangkakul *et al.,* 2011). Moreover, TSPO transcripts are detected in desiccation resistant plant structures and to some extent in senescing leaves, whereas AtTSPO is transiently induced by ABA treatment, osmotic and high salinity (Kreps *et al.,* 2002; Seki *et al.,* 2002; Zimmermann *et al.,* 2004; Winter *et al.,* 2007;

Guillaumot *et al.,* 2009; Hermans *et al.,* 2010). YFP-AtTSPO, constitutively expressed in tobacco, is sensitive to leaf senescence (Vanhee *et al.,* 2011). Its presence in the cell is highly downregulated via selective autophagy (Vanhee and Batoko, 2011). Considering that Arabidopsis plants expressing constitutively AtTSPO and the relatively stable mutant protein (AtTSPO(H91A)) were flowering later than the WT **(Figure S3C)**. We observed that overexpressing of AtTSPO alleviated the senescence in these transgenic lines compared to the WT **(Figure S5.A)**. Visible phenotypical alteration in rosette leaves color was recognized by using an automated colorimetric assay (ACA). OE AtTSPO and OE AtTSPO(H91) rosette leaves were characterized by a very highly significant ($p<0.001$) level of greenish colors compared to the WT. At the same time, greyish colors related to dry tissues are very highly significantly ($p<0.001$) detected in KO AtTSPO compared to WT **(Figure S5B)**. Western blotting analysis shows that the constitutively expressed WT AtTSPO and the relatively stable mutant AtTSPO(H91A) were downregulated in senescent leaves of *A. thaliana* **(Figure S5E)**. Besides, the constitutive expression of IRT1-mCherry triggered to delay in the flowering **(Figure S3C)** and alleviated the senescence compared to the plants not overexpressing IRT1-mCherry **(Figure S5C and D).** The gel blotting analysis shows a down-regulation and an increase in the post-translational modification PTM of IRT1-mCherry, triggered by senescence. The PTM was less detected in KO AtTSPO background senescent leaves. Then we investigate more the role of Autophagy senescence related to the downregulation of IRT1 through AtTSPO interaction. We artificially induce senescence by exposing *Arabidopsis* plants to constant darkness (dark) for five days. It has been shown that autophagy is highly induced under

prolonged darkness in *Arabidopsis* cells (Chung *et al.,* 2010; Chen *et al.,* 2015; Barros *et al.,* 2021). Under dark treatment, we observed more senescence aspects in rosette leaves constitutively expressing WT AtTSPO and AtTSPO(H91) **(Figure S6 A and B)**. The wild-type plants and knockout AtTSPO plants were very highly significantly ($p<0.001$) greener compared to OE AtTSPO and OE AtTSPO(H91A) **(Figure S6 C)**. Interestingly, the protein gel blotting analysis shows a drastic decrease in AtTSPO level in OE AtTSPO under darkness compared to the control. Under the same conditions, the level of relative stable mutant AtTSPO(H91A) seems to be stable compared to the control condition. We reasoned that the downregulation of AtTSPO requires heme binding to be degraded via selective autophagy (Vanhee, 2011). Also, AtTSPO needs its histidine at position 91 for heme binding. The substitution of this histidine with an alanine stabilizes the protein in the cell (Vanhee *et al.,* 2011). On the other hand, when IRT1-mCherry was constitutively expressed, we observed under dark treatment that there was more senescence in rosette leaves in WT and OE ATSPO backgrounds than in the knockout AtTSPO and the relatively stable mutant H91A backgrounds **(Figure S6E and F)**. The Yellowish color in WT and OE TSPO backgrounds in the presence of IRT1-mCherry is very highly significantly detected ($p<0.001$) compared with other genetic backgrounds **(Figure S6G)**. Protein gel analysis shows a striking decrease in AtTSPO levels in WT and OE AtTSPO backgrounds under dark treatment. While the relatively stable mutant form AtTSPO(H91A) was not decreased under the same conditions. Interestingly, IRT1-mCherry was drastically decreased under darkness in WT and OE AtTSPO backgrounds. The mCherry signal was not detected in these backgrounds. In addition, in the relatively stable

mutant AtTSPO(H91A) background, the IRT1-mCherry level was detectible and lower under dark treatment than in the standard condition. Although, the mcherry signal was not affected by the dark treatment in the KO AtTSPO backgrounds **(Figure S6H)**. These results indicate the effect of dark inducing autophagy in the degradation of IRT1 through the downregulation process of AtTSPO.

5.2.7 AtTSPO-IRT1 The hetero-complex colocalizes and physically interacts with the autophagy-related protein AtATG8

During the autophagy process and especially the encapsulation of the autophagic vesicles known as autophagosomes, many conserved genes family known as ATG proteins are known as the core machinery of autophagy and required in the formation of the autophagosome membrane (Bestebroer *et al.,* 2013; Wesselborg and Stork, 2015; Mauthe and Reggiori, 2016; Mizushima *et al.,* 2011; Noda and Inagaki, 2015). Essential autophagy-related proteins, ATG8, are required to regulate autophagosome size, curvature, and expansion rate. ATG8 interacts with PE in a ubiquitin-like reaction conjugated to phosphatidylethanolamine and attached to both faces of the double-membrane autophagosome to be involved in autophagosome closure. Then, the mature autophagosome decorated with ATG8 is transported to the vacuole to be degraded (Kirisako *et al.,* 2000; Nakatogawa *et al.,* 2007; Xie *et al.,* 2008). ATG8 binds to specific ATG8-interacting-cargos or receptors containing AIM or LIR motifs (Noda *et al.,* 2010; Birgisdottir *et al.,* 2013). The fluorescent-tagged ATG8 protein was primarily used in the *Arabidopsis* cell as a marker to detect by size and

dynamic movement of the ATG8-containing autophagosome (Slavikova *et al.,* 2008; Chung *et al.,* 2010; Merkulova *et al.;* Wang et *al.,* 2016). It was known that the controlled turnover of AtTSPO occurs through its interaction with ATG8 by a selective engulfment of the complex AtTSPO-heme or AtTSPO-AtPIP2;7 in the autophagosomes (Vanhee *et al.,* 2011; Hachez *et al.,* 2014; Jurkiewicz *et al.,* 2020). We reasoned that when coexpressed and even in the absence of stress or starvation, the mCherry tagged AtATG8 could occasionally result in colocalization with the BiFC fluorescence encoding for chimeric fusions between AtTSPO and IRT1. To test this idea, we transiently coexpressed mCherry-AtATG8E with $Venus_C$-TSPO + $Venus_N$-IRT1. The representative confocal images **(Figure 34A)** show the detection of mobiles autophagosomes (magenta) colocalized with the BiFC signal (green). The inset images and the fluorescence profiles analysis **(λ)** show a high level of colocalization (MOC=0.92). We extracted total protein from transiently transformed tissues to confirm this interesting observation. Then we used RFP-Trap to pull down mCherry-ATG8E. The protein gel analysis **(Figure 34D)** shows that in addition to mCherry-ATG8E affinity-purified in the elution fraction, we were able to copurify $Venus_C$-TSPO and $Venus_N$-IRT1. These results suggest that mCherry-AtATG8E engulfed the complex AtTSPO-IRT1 in the autophagosome. Strengthening the idea that IRT1 needs AtTSPO to be degraded through autophagy, we performed a second biomolecular fluorescence complementation assay. We prepared genetic constructs encoding chimeric fusion between $Venus_C$-ATG8E and $Venus_N$-IRT1 coexpressed with mCherry-TSPO and without. Interestingly, no BiFC signal was detected in the transiently transformed tobacco epidermis cells expressing $Venus_C$-ATG8E and $Venus_N$-IRT1 **(Figure 34B)**.

While **(Figure 34C)** shows clearly a detected BiFC signal (green) colocalizing with mCherry-TSPO signal (magenta). These results suggest that AtTSPO is crucial and plays an essential key role in the engulfing process of IRT1 in the autophagosome.

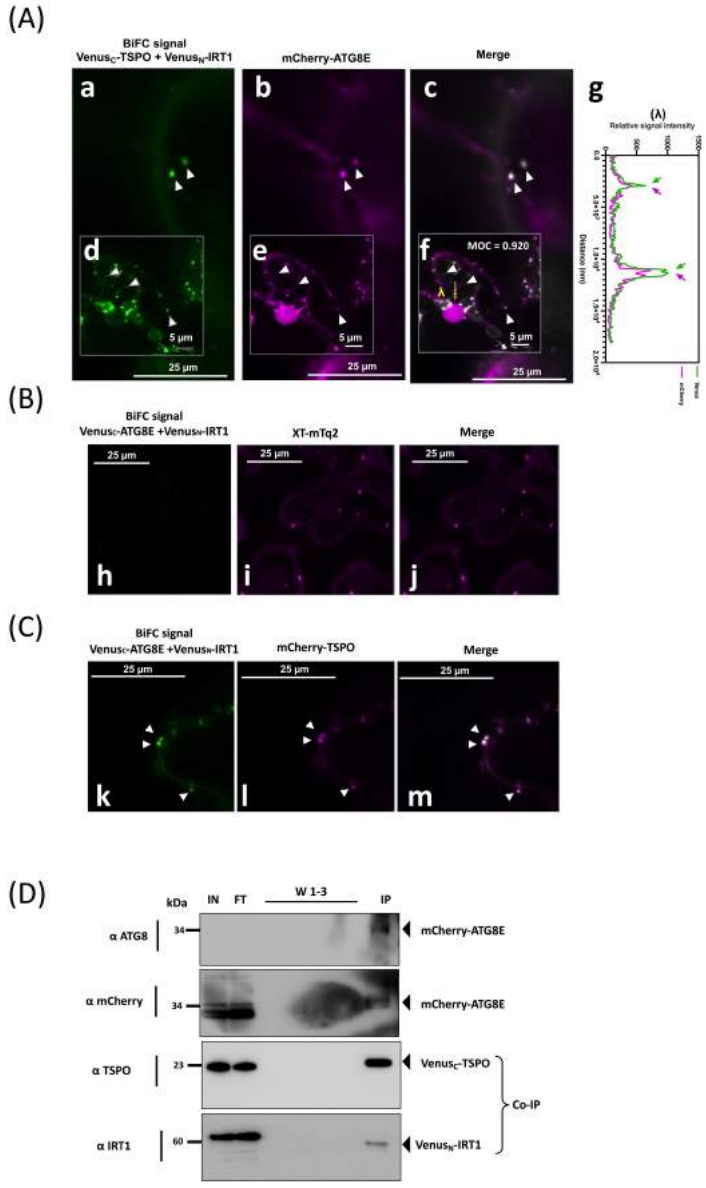
(A)
BiFC signal
VenusC-TSPO + VenusN-IRT1
mCherry-ATG8E
Merge
a
b
c
d
e
f
g
MOC = 0.920
5 µm
25 µm
(B)
BiFC signal
VenusC-ATG8E +VenusN-IRT1
XT-mTq2
Merge
h
i
j
(C)
BiFC signal
VenusC-ATG8E +VenusN-IRT1
mCherry-TSPO
Merge
k
l
m
(D)
kDa
IN
FT
W 1-3
IP
α ATG8
α mCherry
α TSPO
α IRT1
34
23
60
mCherry-ATG8E
VenusC-TSPO
VenusN-IRT1
Co-IP

Figure 34. AtTSPO and IRT1 colocalize and interact in autophagosome. **(A)** Representative confocal images of tobacco epidermal cells transiently coexpressing $Venus_C$-TSPO + $Venus_N$-IRT1 and mCherry-ATG8E. White arrowheads were BIFC signal colocalizing with ATG8E. BiFC signal in the left panels was shown in green. Middle panels show mCherry-ATG8E signal in magenta. Right panels show merged signals. Relative fluorescence profiles of BiFC and mCherry are shown in (**g**). **(B)** Representative confocal images of tobacco epidermal cells transiently coexpressing $Venus_C$-ATG8E + $Venus_N$-IRT1. **(C)** Representative confocal images of tobacco epidermal cells transiently coexpressing $Venus_C$-ATG8E + $Venus_N$-IRT1 and mCherry-TSPO. (**B)** Copurification of AtTSPO and At IRT1 from *N. benthamiana* Extracts. Total proteins were extracted from **(A).** Samples were purified using RFP-Trap, then analyzed by immunoblotting. The input (IN), the Flow-through (FT), Washes (W 1-3), and eluted fraction (E).

5.3 Discussion

5.3.1 AtTSPO acts as a functional interactant partner for IRT1

The *Arabidopsis* TSPO is often transiently localized in the ER, the Golgi stacks, and the Trans-Golgi Network (TGN) (Guillaumot *et al.,* 2009; Hachez *et al.,* 2014; Jurkiewicz *et al.,* 2020). Also, AtTSPO could interact physically with some membrane proteins en route to the PM, such as the *Arabidopsis* aquaporin PIP2;7. This interaction happens most likely in the ER and the Golgi membrane (Hachez *et al.,* 2014; Jurkiewicz *et al.,* 2020). On the other hand, in standard conditions, IRT1 is localized in the PM to transport mainly iron and metals into the root cell. To ensure an optimal iron uptake non-needed AtIRT is shuttling between PM and the recycling endosomes or degraded via the ESCRT pathway in the lytic vacuole via endosomal sorting (Dubeaux *et al.,* 2018; Barberon *et al.,* 2011, 2014). The reduction of IRT1 level via protein-protein interaction within the *Arabidopsis* cell was already described. Under high metal levels, the

IRT1 degradation mechanism begins its phosphorylation by the CIPK23 kinase, mediating its polyubiquitination. This mechanism is required for IRT1 endocytosis (Barberon *et al.,* 2011; Ivanov *et al.,* 2014; Shin *et al.,* 2013; Dubeaux *et al.,* 2018). Polyubiquitinated IRT1 is endocytosed to early endosome. Then it is mostly sent via ESCRT complex to be targeted for degradation in the vacuole. The interaction between FYVE1/FREE1 and IRT1 is crucial for this process (Gao *et al.,* 2014, 2017; Barberon *et al.,* 2014; Ivanov and Vert, 2021). It has been known that FREE1 interacts with VPS23 via its PTAP-like tetrapeptide motif to be incorporated into the ESCRT-I complex (Gao *et al.,* 2014). Furthermore, we demonstrate that AtTSPO did not reach the PM and the endosomes **(Figure 32B and C).** Interestingly, we found that AtTSPO and IRT1 interact in vitro and in vivo **(Figures 13, 14, and 16)**. Contrary to AtTSPO-AtPIP2;7, the interaction between AtTSPO and IRT1 was not detected in the Golgi membrane, nor the PM and endosomes **(Figure 25 and 32 (E and F))**. The interaction is physiologically relevant as it leads under stress conditions to decrease the quantity of functional IRT1. The presence of AtTSPO triggers a striking reduction in IRT1 level at the plasma membrane and leads to the accumulation of punctate structures in the cytoplasm **(Figure 29)**. Interestingly we found that in the absence of AtTSPO, most IRT1-mCherry was localized in the PM, and a very low number of punctate structures was observed in the root cell **(Figure 29)**. We revealed in previous work that the substitution of the histidine at position 91 to alanine in AtTSPO is required to bind heme in vivo (Vanhee *et al.,* 2011). The downregulation of AtTSPO evolves the H91 (in the heme-binding process) and the active autophagy pathway (Vanhee *et al.,* 2011). We showed that the point mutation in the histidine at position

91 highly decreased the AtTSPO capacity to interact physically with IRT1 **(Figure 26)**. The coexpression of AtTSPO(H91) and IRT1-mCherry triggered a lower accumulation of the punctate structures than when the wild-type AtTSPO was expressed **(Figure 29)**. The phylogenic analysis of TSPO homologous proteins in *Penthapetalae* showed a conserved histidine (at position 91 in *A. thaliana*) in *Brassicaceae.* Furthermore, we found that the conserved cysteine (at position 94 in *A. thaliana*) in TSPO glycophytes was naturally substituted by arginine in TSPO halophytes. Compared to *A. thaliana* TSPO, the TSPO halophyte *E. salsugenum* could not interact physically with IRT1 despite its conserved distal histidine **(Figure 26)**. Moreover, the point mutation in the AtTSPO cysteine at position 94 by an arginine abolished its capacity to interact with IRT1. Furthermore, swapping a protein fragment containing C94 from AtTSPO to EsTSPO allows it to acquire the ability to interact physically with IRT1 **(Figure 28).**

5.3.2 AtTSPO plays a crucial role in degrading IRT1 under stress conditions through selective autophagy

Abiotic stress induces major catabolic changes in the plant cell, directing resources from the growth process to stress response pathways. Autophagy is a recycling process involved in nutrient homeostasis, stress tolerance, and senescence. The word ‘autophagy’ was a token from the Greek language meaning self-eating. It was

invented by Christian De Duve (De Duve and Wattiaux, 1966). It consists of the intercellular degradation of the cytoplasmic component in the vacuole for better cell maintenance. Under stress, potential crosstalk between autophagy and phytohormones is established. Besides, ABA acts as a cell endogenous systematic signaling messenger under abiotic stress (Zhang and Tardieu, 1996; Signorelli *et al.,* 2019; Yu and Xie, 2017). The accumulation of ABA triggers the activation of respiratory burst oxidase homolog (Rboh), the negative regulation of ERF1 and ERF6 induction, and the inhibition of the activity of plant TOR complex through SNRK2, which induce Autophagy under stress (Signorelli *et al.,* 2019). ABA is accumulated during high salinity and osmotic stress-inducing upregulation of some ATG genes, such as ATG8 and ATG18, in the plant cell (Liu *et al.,* 2009; Slavikova *et al.,* 2008). It has been shown that AtTSPO is transiently expressed under ABA, high salinity, and osmotic stress (Guillaumot *et al.,* 2009). We showed that IRT1 was degraded under these stress conditions in addition when TOR complex was inhibited, exclusively when AtTSPO was present **(Figures 21)**. In the absence of AtTSPO, when the fluorescent-tagged IRT1-mCherry was expressed, the level of the punctate cytoplasmic structures was drastically decreased. Indicating the essential role of AtTSPO under ABA, salinity, and osmotic stress in the IRT1 degradation process. Furthermore, autophagosome formation could be highly stimulated using BTH, considered analogous to the phytohormone Salicylic acid (SA), and activate the SA signaling. This chemical was known as an inducible component required for the early senescence in atg plant mutants and as an influencing agent of immune response inducing a hundred proteins (Yang *et al.,* 2018; Wang *et al.,* 2011; Yoshimoto, 2010).

IRT1-mCherry was highly degraded using BTH **(Figure 33E to H)**. Interestingly, these structures accumulated in the vacuole when we inhibited the vacuolar hydrolases using ConcA **(Figure 33E to H)**. ConcA-BTH cotreatment is highly triggered by the accumulation of intravacuolar punctate structures in the root cell constitutively expressing IRT1-mCherry **(Figure 33E to H)**. Furthermore, we observed that in the presence of AtTSPO, IRT1-mCherry mostly colocalized in vesicular structures labeled with the fluorescent dye MDC **(Figure 31)**. It was known that MDC is a fluorescent drug especially used in vivo for the labeling of small acidic vesicles (Murugan and Amaravadi, 2016; Biederbick *et al.,* 1995), and most of the time to stain autophagosomes in animals (Munafó and Colombo, 2001) and *Arabidopsis* (Patel and Dinesh-Kumar, 2008; Wang *et al.,* 2019; Liu *et al.,* 2017; Olenieva *et al.,* 2017; Floyd *et al.,* 2015). We showed that the absence of AtTSPO highly decreases the colocalization between IRT1-mCherry and MDC **(Figure 31).** Contrariwise, we showed by using an autophagy inhibitor 3-MA that even under ABA treatment, the degradation of IRT1 was highly rescinded **(Figure 33A to D)**. Moreover, autophagy is an essential vesicular mechanism to ensure the remobilization and recycling of nutrients during plant aging leading to senescence. Although atg mutants defective in autophagy are characterized by an early senescence phenotype (Avila-Ospina *et al.,* 2014). Leaf Senescence and Starvation-Induced Chlorosis are accelerated by disrupting the expression of the Arabidopsis autophagy-related genes (Hanaoka *et al.,* 2002; Yoshimoto, 2010; Suttangkakul *et al.,* 2011; Li *et al.,* 2014). The shift from light to obscurity activates Autophagy and induces ATGs expression, which increases plant resistance to dark (Chao Yang, 2020). Indeed, dark treatment

accelerates senescence in the leaves, while atg mutants leaves are hypersensitive to dark treatment (Doelling *et al.,* 2007; Minina *et al.,* 2018; Slavikova *et al.,* 2008). In the absence of AtTSPO, we found that the aged rosette leaves exhibited a high senescent phenotype compared to the WT. In opposite, when AtTSPO was constitutively expressed, old plants looked greener than WT. Interestingly, AtTSPO and IRT1-mCherry were degraded in senescent leaves compared to young green leaves **(Figure S6)**. Likewise, AtTSPO was highly downregulated under dark, and dark treatment has no striking effect on the stable point mutation AtTSPO(H91A). Moreover, it has been shown that IRT1 is very sensitive to dark under stress conditions (Dubeaux *et al.,* 2018). In addition to that, we observed that in a dark situation, IRT1-mCherry was mostly degraded when TSPO was present **(Figure S6)**. Besides, under this condition, the substitution of the histidine at position 91 by an alanine alleviated the degradation of IRT1-mCherry. It was known that AtTSPO interacts physically with AtATG8 (Vanhee *et al.,* 2011; Hachez *et al.,* 2014). We demonstrated that the complex AtTSPO-AtIRT interacted in vivo and in vitro with AtATG8 through AtTSPO **(Figure 34)**. While AtTSPO is considered a selective receptor (Batoko et al., 2015; Bu *et al.,* 2020; Avin-Wittenberg, 2018; Michaeli *et al.,* 2016), it could intercept IRT1 en route to the PM through the Golgi / TGN. The complex AtTSPO-IRT1 could interact via the AtTSPO part to the initiated phagophore-bound AtATG8 or to AtATG8 to initiate the phagophore initiation machinery. Then the engulfed AtTSPO-IRT1 complex in the autophagosome is targeted to degradation in the lytic vacuole. In this work, we demonstrated that, in parallel with the classical IRT1 degradation pathway by endosomal sorting to ESCRT machinery, under stress conditions, AtTSPO could play a key role in

the IRT1 degradation process via the selective autophagy pathway **(Figure 35).**

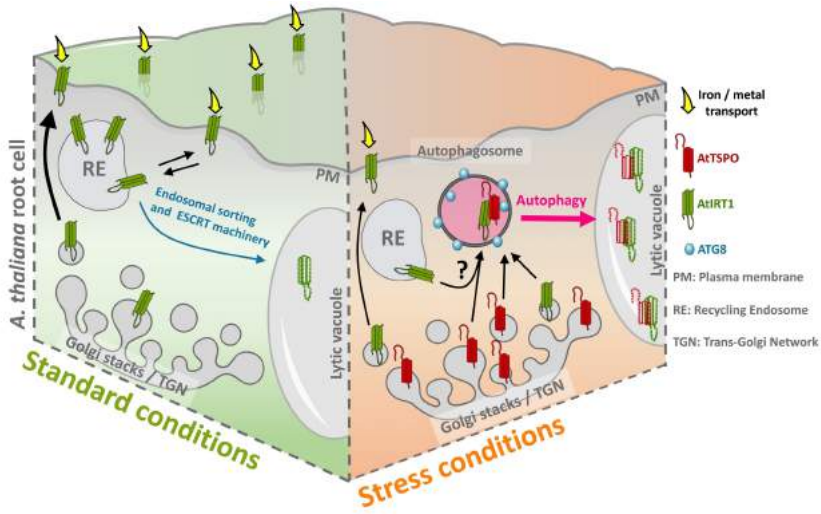

Figure 35. Hypothetical model of IRT1 downregulation by AtTSPO-related autophagy during stress conditions.

5.4 Material and methods

5.4.1 Plant transformation, growth, and treatment

A. thaliana (ecotype Columbia-0) WT and transgenic plants constitutively expressing AtTSPO (OE AtTSPO), stable point-mutated AtTSPOH91A (OE AtTSPO(H91A)) (Guillaumot *et al.,* 2009; Vanhee *et al.,* 2011) and the *Arabidopsis* T-DNA insertional line in TSPO (KO AtTSPO) (Guillaumot *et al.,* 2009) were used to be transformed by floral dipping (Clough and Bent, 1998). To constitutively express IRT1-mCherry and LTI6B-mRFP separately. pJNC1 IRT1 and pB7RWG2 LTI6B vectors are a gift from Rumen Ivanov (Ivanov et al., 2014). Seeds sterilization was described (Lindsey *et al.,* 2017), and growth conditions were described previously (Guillaumot et al., 2009a; Vanhee et al., 2011a; Jurkiewicz et al., 2020). After seeds stratification, 2-3 days at 4°C in the dark, 7 days old seedlings grown on ½ MS (Murashige and Skoog, MP Biomedicals, Eschewege, Germany, #0926230) agar plates supplemented with 50 µM ferric iron in the form of EDTA iron (III) sodium salt (Sigma-Aldrich, Germany, #EDFS), were transferred to ½ MS liquid medium with or without chemical treatments under shaking in the growth chamber (16 h/8 h light/dark, 22-25°C, 90 µmol photons.s-1 .m-2) in transparent Multiwell plant culture plates (VWR-Avantor, Belgium, #734-2323) for microscopy analyses. All treatments were performed for 24h in transparent Multiwell plant culture plates. We added 150 µM of FerroZine iron chelator (PDT disulfonate monosodium salt hydrate, (Sigma-Aldrich, Germany, #63451-29-6) to create iron deficiency stress. To induce

autophagy, we used 100 µM of 1,2,3-Benzothiadiazole-7-carboxylic acid (BTH) (Sigma-Aldrich, Germany, #35272-27-6) with or without 1 µM of Concanamycin A (ConcA) (Sigma-Aldrich, Germany, #80890-47-7). We used 5 mM of 3-Methyladenine (3-MA) (Sigma-Aldrich, Germany, #5142-23-4) to inhibit autophagy. For senescence analysis, 7 days old seedlings were transferred to the soil in square plastic planters with drainage holes and kept growing in the phytotron (average temperature 20°C, approx. 65% humidity, 16 h photoperiod, ~120 µmol.m-2.s-1) and watered twice per week. To induce dark stress, *Arabidopsis* plants grown in a square planter were transferred to a black/transparent box (52L) for 5 days in the previous phytotron to keep the same temperature and humidity.

5.4.2 Monodansylcadaverine (MDC) staining

Arabidopsis seedlings were stained with 0.05 mM MDC (Merk, Germany, #10121-91-2) in PBS for 10 minutes at room temperature under gentle shaking. After staining, the seedlings were washed with PBS three times x 5 min to remove excess stain.

5.4.3 Protein Extraction and Analyses

Plant tissues (*Arabidopsis seedlings/seeds* and Tobacco leaf disks) were grounded using Precellys lysing kit 15 ml with ceramic beads (Bertin Instruments, France, #P000947-LYSK0-A) in Precellys Evolution - Tissue Homogenizer (Bertin Instruments, France, #EQ02520-300-RD000.0). Tissues grinding was done in lysis buffer (75 mM Tris, pH 7.5, 300 mM NaCl, 1% Protease inhibitor cocktail, 1 mM PMSF, 10% glycerol and 2% DDM). Cell debris was removed by centrifugation (15.000 g, 10 min). For Co-immunoprecipitation assays,

5 ml of supernatant was mixed with 4 ml of lysis buffer and incubated with anti-GFP/RFP beads (10 µL, GFP/RFP-trap; Chromotek) for 2h at RT under mild rotation. Beads were collected by Poly-Prep Chromatography columns 10 ml (Bio-Rad, USA, #7311550). They were washed 3 times with washing buffer (50 mM Tris, pH 7.5, 300 mM NaCl, 1% Protease inhibitor cocktail, 1 mM PMSF, 10% glycerol, and 1.8 % DDM). Co-Immunoprecipitated proteins were eluted with 2× Laemmli buffer at 80 °C for 5 min. Then loaded in SDS PAGE: Gel, 4-20 % (Eurogentec, Belgium, #ID-PA4201-010), and detected by Western blot analysis. A variety of antibodies was used: Polyclonal anti-AtTSPO antibody (Guillaumot et al., 2009a; Vanhee et al., 2011a; Hachez et al., 2014; Jurkiewicz et al., 2020), polyclonal anti-IRT1 purchased from Agrisera (#AS11 1780), anti-mCherry from ROCKLAND antibodies and assays (#600-401-P16), anti-GFP was from Abcam (#ab290), and *Arabidopsis* ATG8 described previously and used accordingly (Hachez et al., 2014).

5.4.4 BiFC experiment and cell imaging

BiFC assay was performed as described by (Jurkiewicz *et al.*, 2020). Full-length IRT1 was amplified from pJNC1 IRT1 and full length from LTI6B pB7RWG2 LTI6B. All TSPO mutants resulted from swapping between *A.thaliana* and *E. salsugenum,* and AtTSPO(C94R) was created by overlapping PCR mediated site-directed mutagenesis using primers listed in Supplemental data. Transient expression in tobacco (*Nicotiana tabacum*) was performed as described (Jurkiewicz *et al.*, 2020).

Confocal imaging using a Zeiss LSM 710 Confocal Scanner Inverted point-scanning laser confocal microscope with spectral detection and Airyscan super-resolution detector. In the confocal module, the image processing was performed as described (Guillaumot, Guillon, Déplanque, *et al.*, 2009; Vanhee, Zapotoczny, *et al.*, 2011; Hachez *et al.*, 2014; Jurkiewicz *et al.*, 2020). A 458-nm laser was used to excite GFP, and the amplified emitted light was recorded between 463 and 510 nm. YFP and the reconstituted mVenus fluorophores were simultaneously excited with a 514-nm argon multiline laser, and the amplified emitted light was recorded between 520 and 610 nm. mCherry / RFP fluorophores were excited with a 561-nm laser, and the amplified emitted light was recorded between 570 and 635 nm. 445 nm laser was used to excite mTurquoise2, and the amplified emitted light was recorded between 460 and 480 nm. MDC-incorporated structures were excited by a laser of 405 nm and detected at 400 to 580 nm (Wang *et al.*, 2015; Zhou *et al.*, 2014). For the Airy scan super-resolution module, mCherry fluorescence was detected through Zeiss #63 HE filters for mCherry-Texas Red/TRITC: Ch. A_BP 495-550 + LP 570_SBS SP 615_MBS 488/561/633_561 laser. The microscope images were processed using Zen_2 Blue edition software (Carl Zeiss, Oberkochen, Germany). Relative BiFC fluorescence was measured by the same software using automatic segmentation. The threshold section is set by the tolerance parameter to 1% and fixed for all images. The fluorescence area was automatically marked and overlaid to calculate the average relative fluorescence per total area with an arbitrary unit. The punctate structures per root cell were quantified using ImageJ2-Fiji plugin physion/puncta-analyzer v2.0 (https://github.com/physion/puncta-analyzer) (Beckman *et al.*, 2018).

Mander's overlap coefficient (MOC) was determined using ImageJ2-Fuji plugin JACoP (https://imagej.nih.gov/ij/plugins/track/jacop.html) (Wu and Zhao, 2019; Dubeaux *et al.*, 2018).

5.4.5 Statistical Analysis of the Data

Data were analyzed using a two-way analysis of variance (ANOVA) ($p = 0.05$, with Tukey's multiple comparisons test) using GraphPad Prism version 8 for macOS (GraphPad Software; San Diego, California, USA; www.graphpad.com). The number of replicates and statistical methods for each experiment is stated within figure legends.

5.4.6 Phylogenetic analysis and protein sequence analysis

TSPO homologs were identified from blast searches using *Arabidopsis* coding sequence as a query. Multiple sequence alignment and the phylogenic cladogram were performed using CLC Main Workbench 7. The analyses of amino acid substitutions were performed by the PROVEAN server (http://provean.jcvi.org) using the default cut-off score of −2.5.

5.4.7 Senescence analysis

To evaluate the progression of senescence between plant transgenic lines in the rosette leaves, we measured the color thread via an automated colorimetric assay (ACA). The color category definition and their percentage by color pixel-wise were analyzed by the ImageJ2-Fiji plugin Color_Inspector_3D (https://imagej.nih.gov/ij/plugins/color-inspector.html).

5.5 Supplemental figures

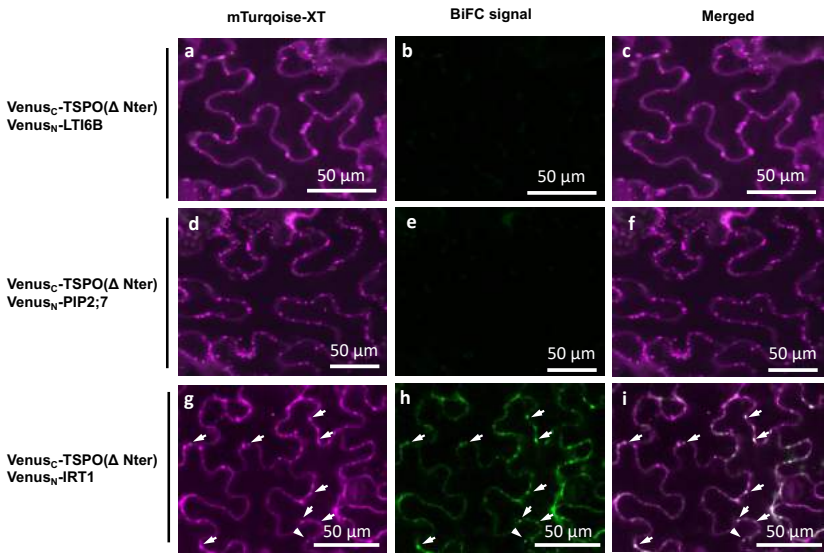

Figure. S4 AtTSPO polybasic N-terminal extension is not involved in the physical interaction with IRT1**. (a-i)** Representative confocal images of tobacco epidermal cells transiently expressing Venus$_c$-TSPO(ΔNter) + Venus$_N$-LTI6B **(a-c)**, Venus$_c$-TSPO(ΔNter) + Venus$_N$-PIP2;7 **(d-f)**, and Venus$_c$-TSPO(ΔNter) + Venus$_N$-IRT1 **(g-i)**. BiFC signal in the middle panels was shown in green. Left panels show XT-mtq2 signal (magenta). Right panels show merged signals. White arrows show colocalized BiFC with the Golgi marker.

(A)


3 cm
WT TSPO
KO TSPO
OE TSPO
OE TSPO(H91A)

(B)

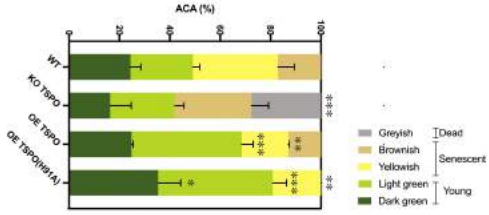
ACA (%)
0
20
40
60
80
100
WT
KO TSPO
OE TSPO
OE TSPO(H91A)
Greyish
Brownish
Yellowish
Light green
Dark green
Dead
Senescent
Young

(C)

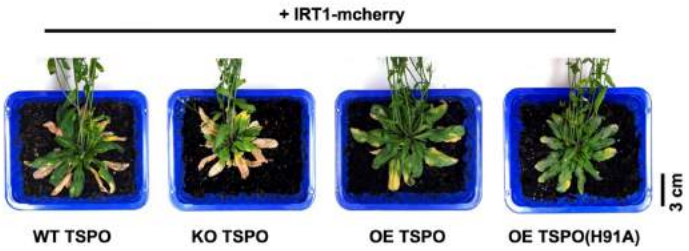
+ IRT1-mcherry
3 cm
WT TSPO
KO TSPO
OE TSPO
OE TSPO(H91A)

(D)

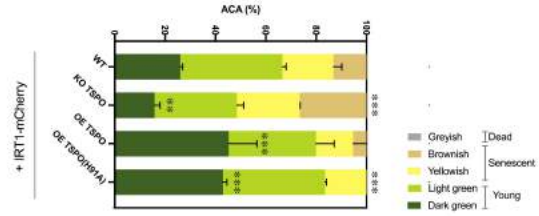
ACA (%)
0
20
40
60
80
100
+ IRT1-mCherry
WT
KO TSPO
OE TSPO
OE TSPO(H91A)
Greyish
Brownish
Yellowish
Light green
Dark green
Dead
Senescent
Young

(E)

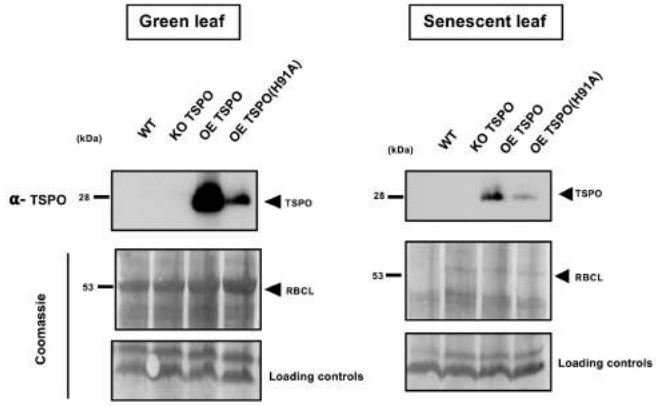
Green leaf
Senescent leaf
WT
KO TSPO
OE TSPO
OE TSPO(H91A)
(kDa)
α- TSPO
28
TSPO
53
RBCL
Coomassie
Loading controls

(F)

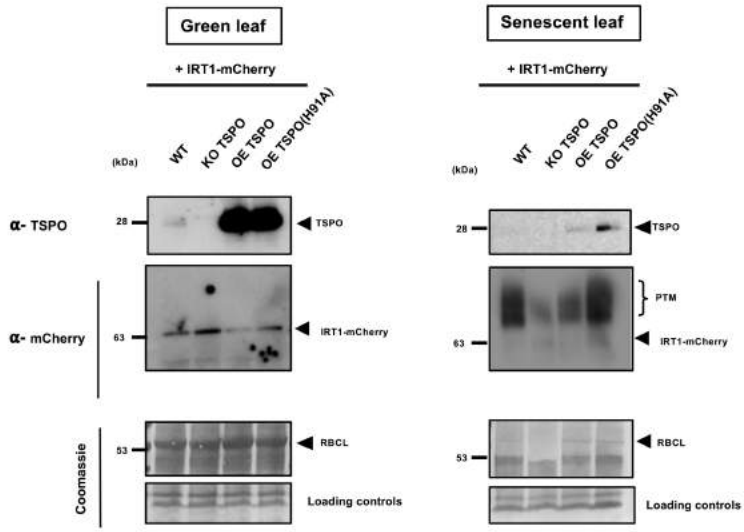
Green leaf
Senescent leaf
+ IRT1-mCherry
WT
KO TSPO
OE TSPO
OE TSPO(H91A)
(kDa)
α- TSPO
28
TSPO
α- mCherry
63
IRT1-mCherry
PTM
53
RBCL
Coomassie
Loading controls

Figure S5. Senescence triggers downregulation of AtTSPO and IRT1. **(A)** and **(C)** Natural senescence. Plants were grown for 75 days in a phytotron (average temperature 20°C, approx. 65% humidity, 16 h photoperiod, ≈120mmol.m^{-2}.s^{-1}). **(B)** and **(D)** Automatic color detection of rosette leaves by ACA. Five color categories were defined (dark green, light green, yellowish, brownish, and greyish (dry)). Data are mean ± SD, n=3. Tukey test was performed to calculate statistically significant differences in all values compared with WT backgrounds (*P≤0.05, **P≤0.01, ***P≤0.001). **(E)** and **(F)** Gel immuno-blotting analysis: The levels of IRT1-mCherry (≈63 kDa) and AtTSPO (≈21 kDa) were monitored by immunoblotting of total protein extract from respectively green and senescent leaves through anti-TSPO and anti-mCherry antibodies. Coomassie blue staining was used as a loading control to show each sample's Rubisco level.

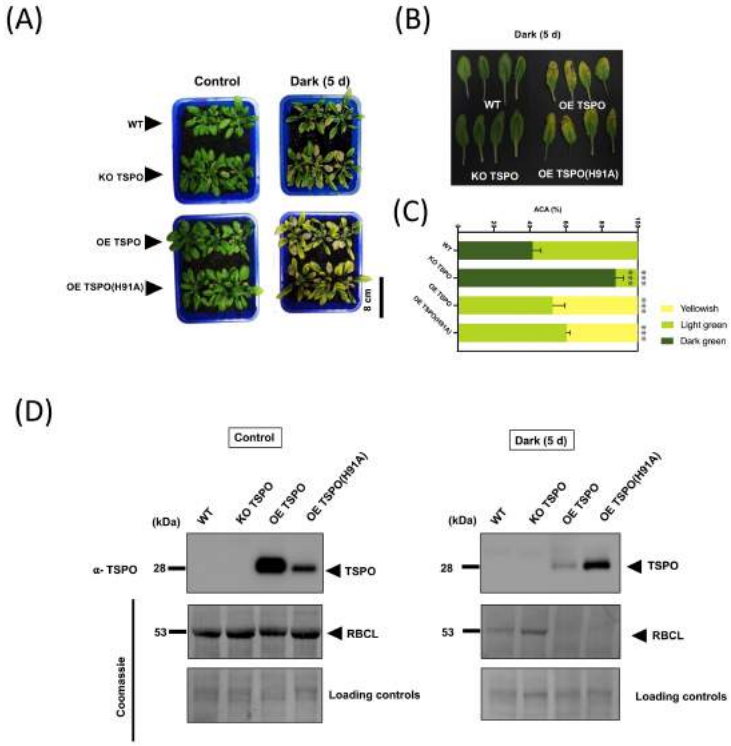

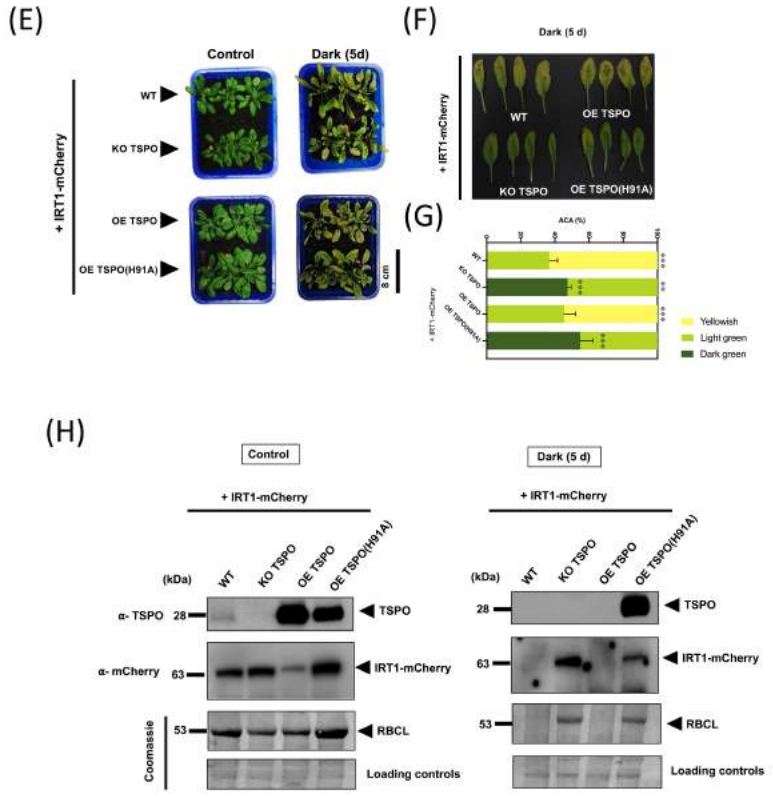

Figure S6. Dark inducing senescence triggers downregulation of IRT1-mCherry by AtTSPO. **(A)** and **(E)** Dark inducing senescence. Plants were grown for 20 days in a phytotron (average temperature 20°C, approx. 65% humidity, 16 h photoperiod, ≈120mmol.m^{-2}.s^{-1}). Then, they were transferred in a respectively transparent box and a dark box under the same previous growth condition for five days. **(B)** and **(F)** Detached leaves after five days in the dark. **(C)** and **(G)** Automatic color detection of rosette leaves by ACA. Five color categories were defined (dark green, light green, yellowish, brownish, and greyish (dry)). Data are mean ± SD, n=3. Tukey test was performed to calculate statistically significant differences in all values compared with WT backgrounds (*P≤0.05, **P≤0.01, ***P≤0.001). **(D)** and **(H)** Gel immuno-blotting analysis: The levels of IRT1-mCherry (≈63 kDa) and AtTSPO (≈21 kDa) were monitored by immunoblotting of total protein extract from respectively green and senescent leaves

through anti-TSPO and anti-mCherry antibodies. Coomassie blue staining was used as a loading control to show each sample's Rubisco level.

Primers used to generate genetic constructs for BiFC analyses

Primer name	Sequence
AatII-AtTSPO Fw	5-GGGGGGGACGTCATGGATTCTCAGGACATCAG-3
AtTSPO-AsisI RV	5-CCCCCCGCGATCGCTCACGCGACTGCAAGCTTTAC-3
AatII-2HA-EsTSPO Fw	5-GGGGGGGACGTCATGTACCCATACGATGTTCCAGATTACGCTTACCCATACGATGTTCCAGATTACGCTATGGACTCTCAGGACATCAG-3
EsTSPO-AsisI Rv	5-CCCCCCGCGATCGCTCACGCGATTGCAAGCTTTAC-3
ΩEs/AtTSPO Fw	5-GTGGATCCCACCTCTGTGGGTCCTACACGCCATACGTCTCGCTTCTAGTGGTCTGA-3
ΩEs/AtTSPO Rv	5-TCAGACCACTAGAAGCGAGACGTATGGCGTGTAGGACCCACAGAGGTGGGATCCAC-3
ΩAt/EsTSPO Fw	5-TGGATCCCACCTCTGTGGCTCCTACACACAACGTGTCTCGCGTCAAGTGGTCTTA-3
ΩAt/EsTSPO Rv	5-TAAGACCACTTGACGCGAGACACGTTGTGTGTAGGAGCCACAGAGGTGGGATCCA-3
Int.TSPO.C94R Rv	5-TCAGACCACTAGAAGCGAGACGCGTTGTGTGTAGGAGCCAC-3
Int.TSPO.C94R Fw	5-GTGGCTCCTACACACAACGCGTCTCGCTTCTAGTGGTCTGA-3
BamhI-ATG8 Fw	5-GGGGGGGGATCCATGAATAAAGGAAGCATCTTTA-3
ATG8-ASC1 Rv	5-CCCCCCGGCGCGCCTTAGATTGAAGAAGCACCGAA-3
AatII-ATG8 Fw	5-GGGGGGGACGTCATGAATAAAGGAAGCATCTTTA-3
ATG8-Asis1 Rv	5-CCCCCCGCGATCGCTTAGATTGAAGAAGCACCGAA-3
AscI-IRT1 Fw	5-GGGGGGGGCGCGCCATGGCTTCAAATTCAGCACTTCT-3
NcoI-AtIRT1 Fw	5-GGGGGGCCATGGATGGCTTCAAATTCAGCACTTCT-3
AtIRT1-XbaI Rv	5-GGGGGGTCTAGATTAAGCCCATTTGGCGATAATC-3
NcoI-2HA-LTI6B Fw	5-GGGGGGCCATGGTACCCATACGATGTTCCAGATTACGCTTACCCATACGATGTTCCAGATTACGCTATGAGTACAGCCACTTTCGTAG-3
LTI6B-XbaI Rv	5-GGGGGGTCTAGATCACTTGGTGATGATATAAAGAGC-3
NcoI- LTI6B Fw	5-GGGGGCCATGGATGAGTACAGCCACTTTCGTAG-3
SpeI.PIP2;7 Fw	5-GGGGGGACTAGTATGTCGAAAGAAGTGAGCGA-3
PIP2;7.XbaI Rv	5-GGGGGGTCTAGATTAATTGGTTGCGTTGCTTCGG-3
AatII-TSPO(H91) Fw	5-AAAAAGACGTCATGGATTCTCAGGACATCAGATA-3
TSPO(H91)-AsisI Rv	5-AAAAAGCGATCGCTCACGCGACTGCAAGCTTTACATT-3
AatII-TSTSPO Fw	5-AAAAAGACGTCATGGACTCTCAGGACATCAGGCA-3
EsTSPO-AsisI Rv	5-AAAAAGCGATCGCTCACGCGATTGCAAGCTTTACATT-3

Primers used for genetic screening

Primer name	Sequence
AtIRT1 Control1 Fw	5- CTTCTCATGAAAACAATCTTC -3
AtIRT1 Control1 Rv	5- TCCACCGCACCCGAGAAGAGC -3
AtIRT1 Control2 Fw	5-ATGGCTTCAAATTCAGCACTTCTCATGAAAACAATCTTCCTCGTACTC-3
AtIRT1 Control2 Rv	5-GCAGCAAAAGTTTTATTTATTTATATGAGATGCAAAAACATTACACGAT-3
35S Fw Control	5-CCTCCTCGGATTCCATTGCCC-3
mCherry Control Fw	5-ATGGTGAGCAAGGGCGAGGA-3
mCherry Control Rv	5-TCACTTGTACAGCTCGTCCATG-3
AtTSPO Control Fw	5-ATGGATTCTCAGGACATCAG-3
AtTSPO Control Rv	5-TCACGCGACTGCAAGCTTTAC-3
EsTSPO Control Rv	5-TCACGCGATTGCAAGCTTTAC-3
LTI6B Control Fw	5-ATGAGTACAGCCACTTTCGTAG-3
LTI6B Control Rv	5-TCACTTGGTGATGATATAAAGAGC-3

Figure S7. Primers used in the study

PART VI

General discussion, General conclusion, & Perspectives

6 Chapter VI: General discussion: Molecular and physiologic evidence of co-regulation between the stress-induced hemoprotein TSPO and the iron transporter IRT1 in *A. thaliana* under stress conditions

6.1 TSPO regulates the iron transporter IRT1 levels under stress conditions in A. thaliana

Under multi-stress conditions, such as salinity, osmotic stress, and dry, the regulatory protein TSPO is transiently induced in *Arabidopsis thalalina* cells. This protein also accumulates by abscisic acid stress phytohormone (ABA) treatment (Guillaumot *et al.,* 2009). These stress conditions trigger an increase in the hyperaccumulation of tetrapyrroles in plant plastids. The production of tetrapyrroles, especially by the heme branch, plays an essential role in crucial cell processes (Photosynthesis, respiration, electron transfer, and tolerance to oxidative stress). Heme is a cofactor of major importance in cell signaling. It is mainly related to the detoxification of reactive oxygen species (ROS) generated under stress, preventing ROS overaccumulation in the cell and leading to oxidative damage. (Nagahatenna *et al.,* 2015; Busch and Montgomery, 2015). Heme is a cyclic molecule that contains an iron atom in the center. Under oxidative stress, the over accumulated heme is mainly exported from the plastid to the cytosol. Primarily, free cytosolic heme is used as a specific electron donor during the reduction process of H_2O_2 to H_2O,

provided by hemoproteins such as catalases and peroxidases. (Anjum *et al.,* 2016). Part of the heme that remains free in the cytosol is considered very toxic through its ability to catalyze ROS production by reacting with oxygen (Kumar and Bandyopadhyay, 2005; Sassa, 2004). During oxidative stress, the TSPO protein is known to bind free toxic heme and lead to its degradation in the vacuole. Moreover, the mechanism of heme-binding requires the amino acid histidine at position 91 in TSPO. While any substitution at this residue severely impairs the ability of TSPO to bind heme. The TSPO-heme complex requires an active and selective autophagy pathway to be delivered to the lytic vacuole. Inside this mechanism, TSPO plays the crucial role of the autophagy-receptor through physical interaction with the protein ATG8, essential for the initiation of autophagosome formation **(Figure 36)**. To interact with ATG8, TSPO requires its AIM/LIR peptide sequence motif (Vanhee et *al.,* 2011). The heme biosynthesis mechanism is based on the quantity imported of Fe^{2+} into the chloroplasts. Iron level in the chloroplast depends primarily on the intracellular iron content. It is known that during iron deficiency, the level of heme in the cell is highly decreased. (Hirayama *et al.,* 2018; Santos *et al.,* 2019). In *A. thaliana*, a reduction strategy based on several proteins ensures the iron uptake process in the root cell epidermis from the rhizosphere. The ferric iron is chelated and reduced to ferrous iron accessible to be imported into the cell cytoplasm through the plasma membrane transporter protein, the main iron transporter IRT1. Therefore, any decrease or inhibition in IRT1 expression engenders severe consequences of iron deficiency in the cell. (Vert *et al.,* 2002; Henriques *et al.,* 2002; Barberon *et al.,* 2011; Shanmugam *et al.,* 2011).

IRT1 is essential for iron homeostasis in the cell. On the other hand, most of this transporter protein is shuttling between the plasma membrane and early endosomes. During iron limitation, IRT1 expression is enhanced. During this condition, IRT1 became toxic because of its capacity to transport divalent metals other than iron. IRT1 stabilization at the PM triggers toxic metal levels inside the cell. Thereby, any decrease in the IRT1 level at the PM indirectly influences the process of heme production in the plastids.

This work shows that the iron deficiency transiently induced TSPO in *A. thaliana* roots during the first 24 hours. Interestingly, iron deficiency leads to a decrease in the level of TSPO expressed in transgenic plants, which over-express the wild-type protein and the relatively stable H91A form. We found that TSPO level was also influenced by IRT1 expression under standard conditions or iron deficiency. It is known that in iron sufficiency, IRT1 is weakly detected due to the strict regulatory mechanism regulating this protein. Non required IRT1 is rapidly ubiquitinated and returned to endosomes, where it will be recycled and sent back to the plasma membrane, or most of the time, it will be sent to late endosomes to join the degradation pathway provided by the ESCRT complex machinery (Barberon *et al.,* 2011; Shin *et al.,* 2013; Ivanov and Vert, 2021; Dubeaux *et al.,* 2018). Interestingly, knockout TSPO leads to an increase in the levels of IRT1 detected in standard conditions. Moreover, the constitutive expression of the WT TSPO decreased the levels of IRT1 in the root cells. We have shown a downregulating effect of TSPO on the expression of IRT1. This effect is also variable under iron deficiency. The expression of TSPO leads to a reduction in IRT1 levels. Furthermore, the TSPO regulative effect on IRT1 expression is reversible. The constitutive

coexpression of IRT1-mCherry in TSPO transgenic plants triggers to decrease in the level of TSPO detected. It is known that TSPO is undetectable in the wild *A. thaliana* plant under standard conditions. In contrast, it is transiently expressed during oxidative stress. (Guillaumot *et al.,* 2009; Vanhee *et al.,* 2011; Jurkiewicz *et al.,* 2020). Interestingly, the overexpression of IRT1-mCherry in the WT plants leads to induce TSPO. Otherwise, by the Knockout of TSPO, the IRT1-mCherry degradation product (free mCherry) became undetectable, which indicates the regulatory effect of TSPO on the functional levels and the dynamic of IRT1 in the cell. In addition, the knockout of IRT1 or its knockdown (by PDR9 knockout) triggers TSPO induction.

Furthermore, TSPO is known for its direct involvement in heme degradation. TSPO induction promotes increasing the vacuolar iron pool through the heme degradation process. Vacuolar iron is reusable and exported to the cytoplasm via the metal vacuolar transporters NRAMP1 and NRAMP3. (Thomine *et al.,* 2003; Gollhofer *et al.,* 2014; Curie *et al.,* 2000; Wang *et al.,* 2000). The availability of a vacuolar iron pool in amount organs is essential for storage (sink) organs, such as during seed germination. This mechanism of heme iron recycling through TSPO leads to translocating more iron to seeds. It is known that IRT1 is mainly expressed at the root level and in flowers (Vert *et al.,* 2002). By controlling IRT1 levels in the cells of amount organs (root cells), TSPO also plays a preventive role against iron hyperaccumulation in seeds. It is known that TSPO accumulates in dry seeds of wild Arabidopsis plants. Then, TSPO begins to degrade during seed imbibition (Guillaumot *et al.,* 2009; Jurkiewicz *et al.,* 2020).

6.2 TSPO and the active autophagy pathway constitute a novel selective degradation mechanism for IRT1 in *A. thaliana* during oxidative stress

When expressed, it is known that the transmembrane protein TSPO is localized at Golgi stacks and TGN as well as the endoplasmic reticulum. (Guillaumot, Guillon, Déplanque, *et al.*, 2009; Hachez *et al.*, 2014; Jurkiewicz *et al.*, 2020). TSPO is known for its capacity for physical interaction with the aquaporin PIP2;7. TSPO and PIP2;7 interact at Golgi/TGN membranes as well as ER membranes. TSPO is involved in the degradation of this aquaporin via the selective autophagy pathway. This leads to the regulation of leaf transpiration during water stress. Moreover, it limits water loss related to the decrease of the functional level of the aquaporin at the PM (Hachez *et al.*, 2014; Jurkiewicz *et al.*, 2020). During cellular trafficking from the ER to the plasma membrane, IRT1 passes through the Golgi / TGN, where TSPO is mainly localized. This work showed that TSPO and IRT1 interact physically in vitro and in vivo. Interestingly, the confocal microscopy demonstrated that this interaction does not occur at the Golgi/TGN level. It was also shown that the substitution of histidine at position 91 by alanine in TSPO strongly affects but does not inhibit the interaction between TSPO and IRT1. This histidine is conserved in *Brassicaceae*. Moreover, the TSPO of the halophyte plant *Eutrema salsugeneum* (EsTSPO) cannot interact with IRT1. Interestingly, the phylogenetic analysis showed a natural cysteine substitution (at position 94 in *A. thaliana*) by arginine in all halophyte TSPOs. Furthermore, through swapping peptide fragments (containing this cysteine) between AtTSPO and EsTSPO, the ability to interact with

IRT1 was established in the mutated form of EsTSPO. On the other hand, the mutated form of AtTSPO has lost this function. A specific mutation was created in AtTSPO by substituting cysteine 94 with arginine for greater precision. This mutation abolished the ability of AtTSPO to interact with IRT1.

On the other hand, high-resolution Airyscan imaging showed a significant effect of TSPO on the dynamics and subcellular localization of the fluorescent tagged IRT1. Constitutive expression of TSPO leads to a decrease in the level of IRT1 at the plasma membrane. In addition, there is a higher increase in cytoplasmic vesicular structures. The knockout of TSPO leads to the decrease of these structures, which favors the localization of IRT1 in PM. The TSPO expression does not affect another transmembrane protein's subcellular distribution, mainly localizing at the PM (fluorescent tagged LTI6B constitutively expressed). Furthermore, to identify the origin of these vesicular structures, we showed that TSPO and IRT1 do not interact in Golgi/TGNs. In addition, the interaction TSPO-IRT1 does not occur in endosomes (where IRT1 is mainly retained under standard conditions) and not in the PM.

Moreover, it is known that TSPO is strongly induced by ABA treatment, salinity, and osmotic stress. (Guillaumot, Guillon, Déplanque, *et al.*, 2009). We showed, only when TSPO was expressed, that these treatments intensively increased the vesicular structures that led to IRT1 degradation. Moreover, TSPO and IRT1 interacted in MDC-marked structures. The MDC generally marks a wide range of acidic structures, mainly autophagosomes. (Contento *et al.*, n.d.; Olenieva *et al.*; Floyd *et al.*, 2015; Patel and Dinesh-Kumar, 2008;

Merkulova *et al.*, n.d.; Ping Wang *et al.*, 2019). Accordingly, the chemical inhibition of autophagy by using 3-MA decreases the level of vesicular structures containing the fluorescence-tagged IRT1 in the root cell. It is known that autophagy is induced through drug treatments with BTH (a salicylic acid analog) and AZD8055 which inhibits the TOR-kinase complex and leads to the accumulation of ABA in the cell. (Covarrubias *et al.*, 2021; Pu, Luo, Bassham, *et al.*, 2017; Brillada *et al.*, n.d.; Yoshimoto, 2010). These two chemical treatments increased the IRT1 localization in vesicular structures only in the presence of TSPO. Also, in the presence of TSPO, the level of vesicles containing fluorescence tagged IRT1 accumulated in the vacuole under treatment with ConcA. Based on these results. We showed, furthermore, that the TSPO-IRT1 complex localizes with the ATG8 protein. This protein is well known to be a marker of autophagy and is essential for phagophore initiation. (Kirisako *et al.*, 2000; Nakatogawa *et al.*, 2007; Xie *et al.*, 2008). The TSPO-IRT1 complex and ATG8 interact in vitro and in vivo. In addition, TSPO has been shown to act as a physical link between IRT1 and ATG8. The IRT1 engulfment process in the autophagosome, strictly depends on the selective interaction between TSPO and IRT1. This interaction leads to establishing an IRT1-TSPO-ATG8 heterocomplex initiating a functional autophagic pathway **(Figure 36)**.

(A)

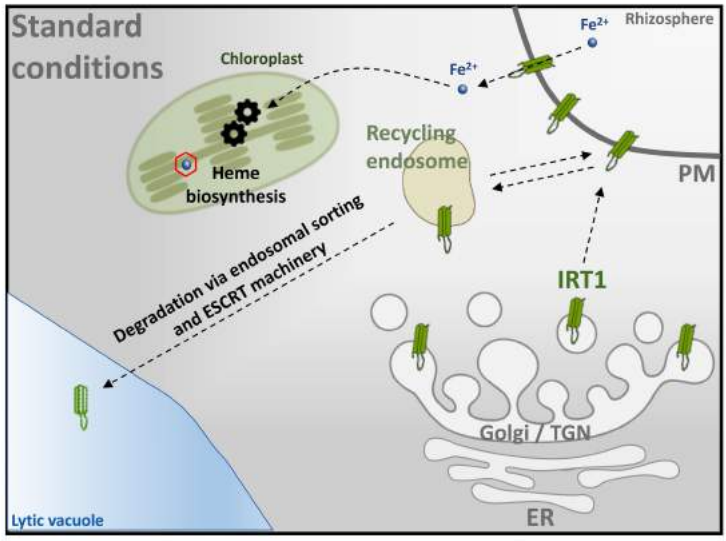
Standard conditions
Chloroplast
Heme biosynthesis
Fe2+
Rhizosphere
Recycling endosome
PM
Degradation via endosomal sorting and ESCRT machinery
IRT1
Golgi / TGN
ER
Lytic vacuole

(B)

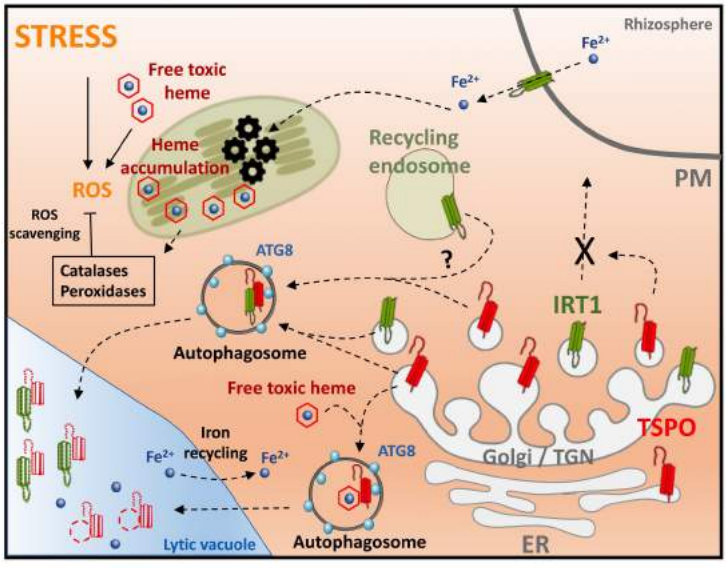
STRESS
Free toxic heme
Heme accumulation
ROS
ROS scavenging
Catalases Peroxidases
Fe2+
Rhizosphere
Recycling endosome
PM
ATG8
Autophagosome
?
X
IRT1
Free toxic heme
Iron recycling
Fe2+
Fe2+
ATG8
TSPO
Golgi / TGN
Lytic vacuole
Autophagosome
ER

Figure 36. Hypothetical model of TSPO regulative involvement in IRT1 downregulation and heme scavenging to mitigate oxidative stress**. (A)** Subcellular trafficking and degradation of IRT1 during standard conditions **(B)** The impact of TSPO in binding free heme, triggering its degradation via autophagy pathway under oxidative stress conditions, which promotes cellular iron recycling. Under the same conditions, induced TSPO leads to a decrease in the level of IRT1 en route to the plasma membrane. TSPO physically interacts with IRT1 and triggers its degradation via selective autophagy. This IRT1 degradation process limits the over-uptake of iron and metals in the cell under stress conditions.

7 Chapter VII: General conclusion

This study revealed the physiological and molecular evidence of the coregulation between the multi-stress regulator protein TSPO and the main iron transporter IRT1 under oxidative stress conditions to maintain iron homeostasis and prevent oxidative stress in the cell. This novel and non-classical pathway of IRT1 regulation through autophagy related to TSPO led the *A.thaliana* root cells to establish a rapid intervention mechanism to decrease the level of IRT1 en route to the plasma membrane **(Figure 36)**. This process leads to managing the iron uptake activity, limiting metal toxicity risks, and reducing the bioproduction of free and toxic cytosolic heme **(Figure 36)**.

8 Chapter VIII: Perspectives

In this study, we revealed the physiological and molecular involvement of TSPO in iron-uptake modulation under oxidative stress. More precisely, it downregulates the iron transporter (IRT1) levels in the cell by triggering the degradation of IRT1 en route to the plasma membrane via autophagy. The downregulation of IRT1 through TSPO establishes a rapid preventive mechanism to manage the cell's iron and metals uptake capacity.

Several aspects of the functioning in this regulative mechanism remain to be highlighted. More points need to be clarified about the coregulation of the two proteins:

1) The origin of IRT1 interacting with TSPO and then targeted to the engulfment in the autophagosome has not yet been identified.

2) Will the ubiquitinated form of recycled IRT1 from the PM in the EE be delivered back to the Golgi/TGN to face TSPO?

3) Under stress conditions, does the polyubiquitinated IRT1 exocytosed to LE/MVBs be a target for autophagic degradation?

4) Does the autophagic degradation pathway of the complex TSPO-IRT1 interfere with the classic IRT1 degradation pathway via ESCRT?

Further expectations about IRT1 post-translational modification: new bridges about IRT1 downregulation via autophagic pathway.

As a membrane protein, the mature IRT1, after being ER-transported, follows a traffic path to reach the PM's outer polar domain finally. The final IRT1 destination is strictly dependent on the cellular need for iron and the metal level. Under standard level on non-iron divalent metals, IRT1 is mainly monoubiquitinated and endocytosed via the clathrin-dependent mechanism in EE for further recycling to the PM or to follow the degradation pathway. During the recycling mechanism, IRT1 polar delivery from endosomes to the PM principally depends on a phosphatidylinositol-3-phosphate-binding protein (hereafter called FREE1/FYVE1). It has been shown that the interaction between FREE1 and IRT1 is crucial for IRT1 recycling and subsequently reaching the cell surface, as well as in IRT1 degradation via endosomal sorting complex for transport (ESCRT) (Barberon, Zelazny, Robert, Conéjéro, Curie, Jiří Friml, *et al.*, 2011; Dubeaux and Vert, 2017; Barberon *et al.*, 2014; Zelazny and Vert, 2015; Ivanov and Vert, 2021). Moreover, it has been shown that the mature *Malus xiaojinesis* IRT1 ER-export process depends on the COPII vesicular transport machinery. MxIRT1 exit the ER surface by interacting with several COPII proteins (Tan *et al.*, 2018; P., Zhang *et al.*, 2014). Furthermore, IRT1 also was found to interact with COPTII proteins probably through specific cytoplasmic diacidic motifs (D/E)x(D/E), which leads to its delivery from ER membranes to the Golgi apparatus (Martín-Barranco *et al.*, 2020; Chung *et al.*, 2016; Zelazny *et al.*, 2009). Interestingly, it has been shown that fluorescent tagged FREE1 was detected in autophagosomes near the ER. FREE1 interacts simultaneously with the small GTPase Secretion-associated Ras-related GTPase 1 (SAR1), crucial for COPII vesicles formation, and the autophagy-related protein ATG18A known to be a PI3P effector on the phagophore membrane.

Confocal microscopy imaging showed that SAR1 targeted lytic vacuole via FREE1-dependent autophagy. FREE1 controls the crosstalk between COPII vesicles delivery machinery from ER and the autophagy degradation pathway (Kim *et al.*, 2022; B., Li *et al.*, 2022). Putting it all together, we wonder if, under stress conditions, the mature ER-exported IRT1 via COPII vesicle delivery machinery is targeted to the FREE1-dependent autophagy pathway? Will IRT1 be the target of the autophagy-dependent pathway via the autophagosome formation process at ER-PM contact sites (EPS)? Considering the crosstalk between actin and endocytic machinery depends on the interaction between EH proteins (components of endocytic TPLATE complex (TPC)) to promote autophagy (Pengwei Wang *et al.*, 2019).

9 References

Alers, S., Löffler, A.S., Wesselborg, S. and Stork, B. (2012) Role of AMPK-mTOR-Ulk1/2 in the regulation of autophagy: cross talk, shortcuts, and feedbacks. *Mol. Cell. Biol.*, **32**, 2–11. Available at: https://journals.asm.org/journal/mcb [Accessed September 13, 2022].

Anjum, N.A., Sharma, P., Gill, S.S., et al. (2016) Catalase and ascorbate peroxidase—representative H2O2-detoxifying heme enzymes in plants. *Environ. Sci. Pollut. Res.*, **23**, 19002–19029. Available at: https://link.springer.com/article/10.1007/s11356-016-7309-6 [Accessed July 3, 2021].

Apitz, J., Nishimura, K., Schmied, J., Wolf, A., Hedtke, B., Wijk, K.J. van and Grimm, B. (2016) Posttranslational Control of ALA Synthesis Includes GluTR Degradation by Clp Protease and Stabilization by GluTR-Binding Protein. *Plant Physiol.*, **170**, 2040–2051. Available at: https://academic.oup.com/plphys/article/170/4/2040/6114152 [Accessed January 13, 2022].

Assunção, A.G.L., Persson, D.P., Husted, S., Schjørring, J.K., Alexander, R.D. and Aarts, M.G.M. (2013) Model of how plants sense zinc deficiency. *Metallomics*, **5**, 1110–1116. Available at: https://academic.oup.com/metallomics/article/5/9/1110/6015674 [Accessed September 17, 2022].

Astolfi, S., Celletti, S., Vigani, G., Mimmo, T. and Cesco, S. (2021) Interaction Between Sulfur and Iron in Plants. *Front. Plant Sci.*, **12**. Available at: /pmc/articles/PMC8329491/ [Accessed November 14, 2022].

Augustine, R.C. (2019) You Are What You Eat: An ATG1-Independent Path to Autophagy. *Plant Cell*, **31**, 2821–2822. Available at: https://academic.oup.com/plcell/article/31/12/2821/5985806 [Accessed September 13, 2022].

Avin-Wittenberg, T., Baluška, F., Bozhkov, P. V., et al. (2018) Autophagy-related approaches for improving nutrient use efficiency and crop yield protection. *J. Exp. Bot.*, **69**, 1335–1353. Available at: https://academic.oup.com/jxb/article/69/6/1335/4883495 [Accessed September 15, 2022].

Babst, M. (2005) A Protein's Final ESCRT. *Traffic*, **6**, 2–9. Available at: https://onlinelibrary.wiley.com/doi/full/10.1111/j.1600-0854.2004.00246.x [Accessed May 18, 2022].

Baisa, G.A., Mayers, J.R. and Bednarek, S.Y. (2013) Budding and braking news about clathrin-mediated endocytosis. *Curr. Opin. Plant Biol.*, **16**, 718–725.

Balk, J. and Schaedler, T.A. (2014) Iron cofactor assembly in plants. *Annu. Rev. Plant Biol.*, **65**, 125–53. Available at: http://www.ncbi.nlm.nih.gov/pubmed/24498975 [Accessed July 2, 2021].

Barberon, M. (2017) The endodermis as a checkpoint for nutrients. *New Phytol.*, **213**, 1604–1610.

Barberon, M., Dubeaux, G., Kolb, C., Isono, E., Zelazny, E. and Vert, G. (2014) Polarization of IRON-REGULATED TRANSPORTER 1 (IRT1) to the plant-soil interface plays crucial role in metal homeostasis. *Proc. Natl. Acad. Sci. U. S. A.*, **111**, 8293–8. Available at: http://www.ncbi.nlm.nih.gov/pubmed/24843126 [Accessed June 28, 2021].

Barberon, M., Zelazny, E., Robert, S., Conéjéro, G., Curie, C., Friml, Jìří and Vert, G. (2011) Monoubiquitin-dependent endocytosis of the IRON-REGULATED TRANSPORTER 1 (IRT1) transporter controls iron uptake in plants. *Proc. Natl. Acad. Sci.*, **108**, E450–E458. Available at: https://www.pnas.org/content/108/32/E450 [Accessed June 8, 2021].

Barberon, M., Zelazny, E., Robert, S., Conéjéro, G., Curie, C., Friml, Jirí and Vert, G. (2011) Monoubiquitin-dependent endocytosis of the transporter controls iron uptake in plants.

Proc. Natl. Acad. Sci. U. S. A., **108**, e450–e458.

Barros, J.A.S., Siqueira, J.A.B., Cavalcanti, J.H.F., Araújo, W.L. and Avin-Wittenberg, T. (2020) Multifaceted Roles of Plant Autophagy in Lipid and Energy Metabolism. *Trends Plant Sci.*, **25**, 1141–1153.

Bassham, D.C. (2007) Plant autophagy—more than a starvation response. *Curr. Opin. Plant Biol.*, **10**, 587–593.

Bastow, E.L., Garcia de la Torre, V.S., Maclean, A.E., Green, R.T., Merlot, S., Thomine, S. and Balk, J. (2018) Vacuolar iron stores gated by NRAMP3 and NRAMP4 are the primary source of iron in germinating seeds. *Plant Physiol.*, **177**, 1267–1276. Available at: www.plantphysiol.org/cgi/doi/10.1104/pp.18.00478 [Accessed July 1, 2021].

Batoko, H., Veljanovski, V. and Jurkiewicz, P. (2015) Enigmatic Translocator protein (TSPO) and cellular stress regulation. *Trends Biochem. Sci.*, **40**, 497–503. Available at: http://dx.doi.org/10.1016/j.tibs.2015.07.001.

Batoko, H., Zheng, H.Q., Hawes, C. and Moore, I. (2000) A Rab1 GTPase is required for transport between the endoplasmic reticulum and golgi apparatus and for normal Golgi movement in plants. *Plant Cell*, **12**, 2201–2217. Available at: www.plantcell.org [Accessed June 24, 2021].

Beckman, D., Donis-Cox, K., Ott, S., et al. (2018) Quantitative analysis of synaptic pathology and neuroinflammation: an initial study in a female rhesus monkey model of the “synaptic” phase of Alzheimer’s disease. *bioRxiv*, 251025. Available at: https://doi.org/10.1101/251025 [Accessed June 23, 2021].

Begara-Morales, J.C., Sánchez-Calvo, B., Chaki, M., et al. (2014) Dual regulation of cytosolic ascorbate peroxidase (APX) by tyrosine nitration and S-nitrosylation. *J. Exp. Bot.*, **65**, 527–538. Available at: https://academic.oup.com/jxb/article/65/2/527/486370 [Accessed January 24, 2022].

Belda-Palazón, B., Adamo, M., Valerio, C., et al. (2020) A dual

function of SnRK2 kinases in the regulation of SnRK1 and plant growth. *Nat. Plants 2020 611*, **6**, 1345–1353. Available at: https://www.nature.com/articles/s41477-020-00778-w [Accessed September 16, 2022].

Bessey, C.E. (1896) The Natural History of Plants.

Besson-Bard, A. and Wendehenne, D. (2009) NO contributes to cadmium toxicity in Arabidopsis thaliana by mediating an iron deprivation response. *Plant Signal. Behav.*, **4**, 252–254. Available at: https://www.tandfonline.com/action/journalInformation?journalCode=kpsb20 [Accessed June 8, 2021].

Blindauer, C.A. (2015) Advances in the molecular understanding of biological zinc transport. *Chem. Commun.*, **51**, 4544–4563. Available at: https://pubs.rsc.org/en/content/articlehtml/2015/cc/c4cc10174j [Accessed October 15, 2022].

Blum, A., Brumbarova, T., Bauer, P. and Ivanov, R. (2014) Hormone influence on the spatial regulation of IRT1 expression in iron-deficient *Arabidopsis thaliana* roots. *Plant Signal. Behav.*, **9**, e28787. Available at: http://www.tandfonline.com/doi/abs/10.4161/psb.28787.

Blum, M., Chang, H.Y., Chuguransky, S., et al. (2021) The InterPro protein families and domains database: 20 years on. *Nucleic Acids Res.*, **49**, D344–D354. Available at: https://academic.oup.com/nar/article/49/D1/D344/5958491 [Accessed October 6, 2022].

Boruc, J. and Damme, D. Van (2015) Endomembrane trafficking overarching cell plate formation. *Curr. Opin. Plant Biol.*, **28**, 92–98.

BRIAT, J. and LOBREAUX, S. (1997) Iron transport and storage in plants. *Trends Plant Sci.*, **2**, 187–193.

Briat, J.F., Rouached, H., Tissot, N., Gaymard, F. and Dubos, C. (2015) Integration of P, S, Fe, and Zn nutrition signals in Arabidopsis thaliana: Potential involvement of PHOSPHATE STARVATION RESPONSE 1 (PHR1). *Front. Plant Sci.*, **6**,

290.
Brillada, C., Teh, O.-K., Anicet Ditengou, F., et al. Exocyst subunit Exo70B2 is linked to immune signaling and autophagy. Available at: https://academic.oup.com/plcell/article/33/2/404/6017825.
Brown, J.C. and Jolley, V.D. (1989) Plant Metabolic Responses to Iron-Deficiency Stress. *Bioscience*, **39**, 546–551.
Brumbarova, T., Bauer, P. and Ivanov, R. (2015) Molecular mechanisms governing Arabidopsis iron uptake. *Trends Plant Sci.*, **20**, 124–133. Available at: http://dx.doi.org/10.1016/j.tplants.2014.11.004 [Accessed June 8, 2021].
Brumm, S., Singh, M.K., Nielsen, M.E., et al. (2020) Coordinated activation of ARF1 GTPases by ARF-GEF GNOM dimers is essential for vesicle trafficking in arabidopsis. *Plant Cell*, **32**, 2491–2507. Available at: www.plantcell.org/cgi/doi/10.1105/tpc.20.00240 [Accessed June 29, 2021].
Bu, F., Yang, M., Guo, X., et al. (2020) *Multiple Functions of ATG8 Family Proteins in Plant Autophagy*, Frontiers Media S.A. Available at: www.frontiersin.org [Accessed June 24, 2021].
Burkart, G.M. and Brandizzi, F. (2021) A Tour of TOR Complex Signaling in Plants. *Trends Biochem. Sci.*, **46**, 417–428.
Cai, Y., Zhuang, X., Gao, C., Wang, X. and Jiang, L. (2014) The arabidopsis endosomal sorting complex required for transport III regulates internal vesicle formation of the prevacuolar compartment and is required for plant development. *Plant Physiol.*, **165**, 1328–1343. Available at: www.plantphysiol.org/cgi/doi/10.1104/pp.114.238378 [Accessed June 30, 2021].
Callis, J. (2014) The ubiquitination machinery of the ubiquitin system. *Arab. B.*, **12**, e0174. Available at: https://pubmed.ncbi.nlm.nih.gov/25320573/ [Accessed August 21, 2022].
Cao, Y., He, Q., Qi, Z., Zhang, Y., Lu, L., Xue, J., Li, J. and Li, R.

(2020) Dynamics and endocytosis of Flot1 in Arabidopsis require CPI1 function. *Int. J. Mol. Sci.*, **21**, 1552. Available at: www.mdpi.com/journal/ijms [Accessed June 29, 2021].

Cheeseman, J.M. (2015) The evolution of halophytes, glycophytes and crops, and its implications for food security under saline conditions. *New Phytol.*, **206**, 557–570. Available at: https://onlinelibrary.wiley.com/doi/full/10.1111/nph.13217 [Accessed May 17, 2022].

Chen, L., Liao, B., Qi, H., et al. (2015) Autophagy contributes to regulation of the hypoxia response during submergence in Arabidopsisï¿¿thaliana. *Autophagy*, **11**, 2233–2246. Available at: https://www.tandfonline.com/action/journalInformation?journalCode=kaup20.

Chen, L., Su, Z.Z., Huang, L., Xia, F.N., Qi, H., Xie, L.J., Xiao, S. and Chen, Q.F. (2017) The AMP-activated protein kinase kin10 is involved in the regulation of autophagy in arabidopsis. *Front. Plant Sci.*, **8**, 1201.

Chen, Q., Shinozaki, D., Luo, J., et al. (2019) Autophagy and Nutrients Management in Plants. *Cells 2019, Vol. 8, Page 1426*, **8**, 1426. Available at: https://www.mdpi.com/2073-4409/8/11/1426/htm [Accessed September 19, 2022].

Chen, Q., Soulay, F., Saudemont, B., Elmayan, T., Marmagne, A. and Masclaux-Daubresse, C. (2019) Overexpression of ATG8 in Arabidopsis Stimulates Autophagic Activity and Increases Nitrogen Remobilization Efficiency and Grain Filling. *Plant Cell Physiol.*, **60**, 343–352. Available at: https://pubmed.ncbi.nlm.nih.gov/30407574/ [Accessed September 17, 2022].

Chen, X., Irani, N.G. and Friml, J. (2011) Clathrin-mediated endocytosis: The gateway into plant cells. *Curr. Opin. Plant Biol.*, **14**, 674–682.

Chen, Y.-Y.Y., Wang, Y., Shin, L.-J.J., et al. (2013) Iron is involved in the maintenance of circadian period length in Arabidopsis. *Plant Physiol.*, **161**, 1409–20. Available at:

http://www.plantphysiol.org.ezproxy.usherbrooke.ca/content/161/3/1409 [Accessed January 15, 2022].

Cheng, X. and Wang, A. (2017) The Potyvirus Silencing Suppressor Protein VPg Mediates Degradation of SGS3 via Ubiquitination and Autophagy Pathways. *J. Virol.*, **91**. Available at: https://doi.org/10.1128/JVI.01478-16. [Accessed September 5, 2022].

Chung, K.P., Zeng, Y. and Jiang, L. (2016) COPII Paralogs in Plants: Functional Redundancy or Diversity? *Trends Plant Sci.*, **21**, 758–769.

Chung, T., Phillips, A.R. and Vierstra, R.D. (2010) ATG8 lipidation and ATG8-mediated autophagy in Arabidopsis require ATG12 expressed from the differentially controlled ATG12A AND ATG12B loci. *Plant J.*, **62**, 483–493. Available at: https://onlinelibrary.wiley.com/doi/full/10.1111/j.1365-313X.2010.04166.x [Accessed June 26, 2021].

Chutia, R., Scharfenberg, S., Neumann, S., Abel, S. and Ziegler, J. (2021) Modulation of Phosphate Deficiency-Induced Metabolic Changes by Iron Availability in Arabidopsis thaliana. *Int. J. Mol. Sci. 2021, Vol. 22, Page 7609*, **22**, 7609. Available at: https://www.mdpi.com/1422-0067/22/14/7609/htm [Accessed September 18, 2022].

Clark, D., Durner, J., Navarre, D.A. and Klessig, D.F. (2007) Nitric Oxide Inhibition of Tobacco Catalase and Ascorbate Peroxidase. *http://dx.doi.org/10.1094/MPMI.2000.13.12.1380*, **13**, 1380–1384. Available at: https://apsjournals.apsnet.org/doi/abs/10.1094/MPMI.2000.13.12.1380 [Accessed January 24, 2022].

Clavel, M., Michaeli, S. and Genschik, P. (2017) Autophagy: A Double-Edged Sword to Fight Plant Viruses. *Trends Plant Sci.*, **22**, 646–648. Available at: http://www.cell.com/article/S136013851730119X/fulltext [Accessed September 5, 2022].

Clough, S.J. and Bent, A.F. (1998) Floral dip: A simplified method for Agrobacterium-mediated transformation of Arabidopsis

thaliana. *Plant J.*, **16**, 735–743. Available at: www.stanford.edu/cgi-bin/biosci_arabidopsis [Accessed June 8, 2021].

Cointry, V. and Vert, G. (2019) The bifunctional transporter-receptor IRT1 at the heart of metal sensing and signalling. *New Phytol.*, **223**, 1173–1178. Available at: www.newphytologist.com [Accessed June 24, 2021].

Colombo, C., Palumbo, G., Sellitto, V.M., Rizzardo, C., Tomasi, N., Pinton, R. and Cesco, S. (2012) Characteristics of Insoluble, High Molecular Weight Iron-Humic Substances used as Plant Iron Sources. *Soil Sci. Soc. Am. J.*, **76**, 1246–1256. Available at: https://onlinelibrary.wiley.com/doi/full/10.2136/sssaj2011.0393 [Accessed February 4, 2022].

Connolly, E.L., Campbell, N.H., Grotz, N., Prichard, C.L. and Guerinot, M. Lou (2003) Overexpression of the FRO2 Ferric Chelate Reductase Confers Tolerance to Growth on Low Iron and Uncovers Posttranscriptional Control. *Plant Physiol.*, **133**, 1102–1110. Available at: http://www.plantphysiol.org/content/133/3/1102.abstract.

Connolly, E.L., Fett, J.P. and Guerinot, M. Lou (2002) Expression of the IRT1 metal transporter is controlled by metals at the levels of transcript and protein accumulation. *Plant Cell*, **14**, 1347–1357. Available at: www.plantcell.org/cgi/doi/10.1105/tpc.001263. [Accessed June 8, 2021].

Conte, S.S., Chu, H.H., Chan-Rodriguez, D., Punshon, T., Vasques, K.A., Salt, D.E. and Walker, E.L. (2013) Arabidopsis thaliana yellow stripe1-like4 and yellow stripe1-like6 localize to internal cellular membranes and are involved in metal ion homeostasis. *Front. Plant Sci.*, **4**, 283.

Conte, S.S. and Walker, E.L. (2011) Transporters Contributing to Iron Trafficking in Plants. *Mol. Plant*, **4**, 464–476.

Contento, A.L., Xiong, Y. and Bassham, D.C. Visualization of autophagy in Arabidopsis using the fluorescent dye monodansylcadaverine and a GFP-AtATG8e fusion protein.

Corsi, L., Avallone, R., Geminiani, E., Cosenza, F., Venturini, I. and Baraldi, M. (2004) Peripheral benzodiazepine receptors in potatoes (Solanum tuberosum). *Biochem. Biophys. Res. Commun.*, **313**, 62–66.

Covarrubias, A.A., Todaka, D., Coello, P., et al. (2021) ABSCISIC ACID INSENSITIVE5 Interacts With RIBOSOMAL S6 KINASE2 to Mediate ABA Responses During Seedling Growth in Arabidopsis. *Front. Plant Sci.*, **11**, 2328. Available at: www.frontiersin.org [Accessed June 24, 2021].

Czarnecki, O., Hedtke, B., Melzer, M., Rothbart, M., Richter, A., Schröter, Y., Pfannschmidt, T. and Grimm, B. (2011) An Arabidopsis GluTR Binding Protein Mediates Spatial Separation of 5-Aminolevulinic Acid Synthesis in Chloroplasts. *Plant Cell*, **23**, 4476–4491. Available at: https://academic.oup.com/plcell/article/23/12/4476/6097648 [Accessed January 12, 2022].

Dahuja, A., Kumar, R.R., Sakhare, A., Watts, A., Singh, B., Goswami, S., Sachdev, A. and Praveen, S. (2021) Role of ATP-binding cassette transporters in maintaining plant homeostasis under abiotic and biotic stresses. *Physiol. Plant.*, **171**, 785–801.

Dalchau, N., Baek, S.J., Briggs, H.M., et al. (2011) The circadian oscillator gene GIGANTEA mediates a long-term response of the Arabidopsis thaliana circadian clock to sucrose. *Proc. Natl. Acad. Sci. U. S. A.*, **108**, 5104–5109. Available at: https://www.pnas.org/content/108/12/5104 [Accessed January 18, 2022].

Das, R. and Baker, D. (2008) Macromolecular Modeling with Rosetta. Available at: www.annualreviews.org [Accessed October 6, 2022].

Davletova, S., Schlauch, K., Coutu, J. and Mittler, R. (2005) The Zinc-Finger Protein Zat12 Plays a Central Role in Reactive Oxygen and Abiotic Stress Signaling in Arabidopsis . *Plant Physiol.*, **139**, 847–856. Available at: https://doi.org/10.1104/pp.105.068254.

Deribe, Y.L., Pawson, T. and Dikic, I. (2010) Post-translational modifications in signal integration. *Nat. Struct. Mol. Biol. 2010 176*, **17**, 666–672. Available at: https://www.nature.com/articles/nsmb.1842 [Accessed May 17, 2022].

Derrien, B., Baumberger, N., Schepetilnikov, M., Viotti, C., Cillia, J. De, Ziegler-Graff, V., Isono, E., Schumacher, K. and Genschik, P. (2012) Degradation of the antiviral component ARGONAUTE1 by the autophagy pathway. *Proc. Natl. Acad. Sci. U. S. A.*, **109**, 15942–15946. Available at: https://www.pnas.org/doi/abs/10.1073/pnas.1209487109 [Accessed September 5, 2022].

DeWitt, N.D., Hong, B., Sussman, M.R. and Harper, J.F. (1996) Targeting of Two Arabidopsis H+-ATPase Isoforms to the Plasma Membrane. *Plant Physiol.*, **112**, 833–844. Available at: https://academic.oup.com/plphys/article/112/2/833/6070565 [Accessed February 2, 2022].

Diaz, C., Saliba-Colombani, V., Loudet, O., Belluomo, P., Moreau, L., Daniel-Vedele, F., Morot-Gaudry, J.F. and Masclaux-Daubresse, C. (2006) Leaf Yellowing and Anthocyanin Accumulation are Two Genetically Independent Strategies in Response to Nitrogen Limitation in Arabidopsis thaliana. *Plant Cell Physiol.*, **47**, 74–83. Available at: https://academic.oup.com/pcp/article/47/1/74/1867545 [Accessed September 18, 2022].

Divol, F., Couch, D., Conejero, G., Roschzttardtz, H., Mari, S. and Curie, C. (2013) The Arabidopsis YELLOW STRIPE LIKE4 and 6 Transporters Control Iron Release from the Chloroplast. *Plant Cell*, **25**, 1040–1055.

Doblas, V.G., Geldner, N. and Barberon, M. (2017) The endodermis, a tightly controlled barrier for nutrients. *Curr. Opin. Plant Biol.*, **39**, 136–143.

Doherty, G.J. and McMahon, H.T. (2009) Mechanisms of Endocytosis. *http://dx.doi.org/10.1146/annurev.biochem.78.081307.110540*,

78, 857–902. Available at: https://www.annualreviews.org/doi/abs/10.1146/annurev.biochem.78.081307.110540 [Accessed May 18, 2022].

Domínguez, F. and Cejudo, F.J. (2021) Chloroplast dismantling in leaf senescence. *J. Exp. Bot.*, **72**, 5905–5918. Available at: https://academic.oup.com/jxb/article/72/16/5905/6271278 [Accessed November 15, 2022].

Drew, M.C. (1997) Oxygen deficiency and root metabolism: Injury and Acclimation under Hypoxia and Anoxia. *Annu. Rev. Plant Biol.*, **48**, 223–250. Available at: https://www.annualreviews.org/doi/abs/10.1146/annurev.arplant.48.1.223 [Accessed June 24, 2021].

Du, Y.Y., Wang, P.C., Chen, J. and Song, C.P. (2008) Comprehensive Functional Analysis of the Catalase Gene Family in Arabidopsis thaliana. *J. Integr. Plant Biol.*, **50**, 1318–1326. Available at: https://onlinelibrary.wiley.com/doi/full/10.1111/j.1744-7909.2008.00741.x [Accessed January 24, 2022].

Dubeaux, G., Neveu, J., Zelazny, E. and Vert, G. (2018) Metal Sensing by the IRT1 Transporter-Receptor Orchestrates Its Own Degradation and Plant Metal Nutrition. *Mol. Cell*, **69**, 953-964.e5.

Dubeaux, G. and Vert, G. (2017) Zooming into plant ubiquitin-mediated endocytosis. *Curr. Opin. Plant Biol.*, **40**, 56–62.

Dubeaux, G., Zelazny, E. and Vert, G. (2015) Getting to the root of plant iron uptake and cell-cell transport: Polarity matters! *http://www.tandfonline.com/action/authorSubmission?journalCode=kcib20&page=instructions*, **8**. Available at: https://www.tandfonline.com/doi/abs/10.1080/19420889.2015.1038441 [Accessed October 15, 2022].

Duc, C., Cellier, F., Lobréaux, S., Briat, J.F. and Gaymard, F. (2009) Regulation of Iron Homeostasis in Arabidopsis thaliana by the Clock Regulator Time for Coffee. *J. Biol. Chem.*, **284**, 36271–36281.

Durrett, T.P., Gassmann, W. and Rogers, E.E. (2007) The FRD3-

mediated efflux of citrate into the root vasculature is necessary for efficient iron translocation. *Plant Physiol.*, **144**, 197–205. Available at: www.plantphysiol.org/cgi/doi/10.1104/pp.107.097162 [Accessed June 8, 2021].

Duy, D., Stü, R., Wanner, G. and Philippar, K. (2011) The Chloroplast Permease PIC1 Regulates Plant Growth and Development by Directing Homeostasis and Transport of Iron 1[W]. Available at: www.plantphysiol.org/cgi/doi/10.1104/pp.110.170233.

Duy, D., Wanner, G., Meda, A.R., Wirén, N. Von, Soll, J. and Philippar, K. (2007) PIC1, an ancient permease in Arabidopsis chloroplasts, mediates iron transport. *Plant Cell*, **19**, 986–1006. Available at: https://academic.oup.com/plcell/article/19/3/986/6091923 [Accessed January 11, 2022].

Eide, D., Broderius, M., Fett, J. and Guerinot, M. Lou (1996) A novel iron-regulated metal transporter from plants identified by functional expression in yeast. *Proc. Natl. Acad. Sci. U. S. A.*, **93**, 5624–5628. Available at: https://www.pnas.org/content/93/11/5624 [Accessed June 8, 2021].

Eng, B.H., Guerinot, M.L., Eide, D. and Saier, M.H. (1998) Sequence Analyses and Phylogenetic Characterization of the ZIP Family of Metal Ion Transport Proteins. *J. Membr. Biol.*, **166**, 1–7. Available at: https://doi.org/10.1007/s002329900442 [Accessed June 28, 2021].

Eroglu, S., Giehl, R.F.H., Meier, B., et al. (2017) Metal Tolerance Protein 8 Mediates Manganese Homeostasis and Iron Reallocation during Seed Development and Germination. *Plant Physiol.*, **174**, 1633–1647. Available at: https://academic.oup.com/plphys/article/174/3/1633/6117411 [Accessed June 7, 2022].

Espinas, N.A., Kobayashi, K., Takahashi, S., Mochizuki, N. and Masuda, T. (2012) Evaluation of Unbound Free Heme in Plant

Cells by Differential Acetone Extraction. *Plant Cell Physiol.*, **53**, 1344–1354. Available at: https://academic.oup.com/pcp/article/53/7/1344/1906960 [Accessed January 25, 2022].

Fan, J., Lindemann, P., G.J. Feuilloley, M., Papadopoulos, V., Feuilloley, M.G.J. and Papadopoulos, V. (2012) Structural and Functional Evolution of the Translocator Protein (18 kDa). *Curr. Mol. Med.*, **12**. Available at: https://pubmed.ncbi.nlm.nih.gov/22364126/ [Accessed June 25, 2021].

Fan, L., Hao, H., Xue, Y., Zhang, L., Song, K., Ding, Z., Botella, M.A., Wang, H. and Lin, J. (2013) Dynamic analysis of Arabidopsis AP2 σ subunit reveals a key role in clathrin-mediated endocytosis and plant development. *Dev.*, **140**, 3826–3837.

Fan, S.K., Fang, X.Z., Guan, M.Y., Ye, Y.Q., Lin, X.Y., Du, S.T. and Jin, C.W. (2014) Exogenous abscisic acid application decreases cadmium accumulation in arabidopsis plants, which is associated with the inhibition of IRT1-mediated cadmium uptake. *Front. Plant Sci.*, **5**, 721. Available at: www.frontiersin.org [Accessed June 8, 2021].

Fan, T., Roling, L., Meiers, A., Brings, L., Ortega-Rodés, P., Hedtke, B. and Grimm, B. (2019) Complementation studies of the Arabidopsis fc1 mutant substantiate essential functions of ferrochelatase 1 during embryogenesis and salt stress. *Plant. Cell Environ.*, **42**, 618–632. Available at: https://onlinelibrary.wiley.com/doi/full/10.1111/pce.13448 [Accessed January 20, 2022].

Feild, T.S., Lee, D.W. and Holbrook, N.M. (2001) Why Leaves Turn Red in Autumn. The Role of Anthocyanins in Senescing Leaves of Red-Osier Dogwood. *Plant Physiol.*, **127**, 566–574. Available at: https://academic.oup.com/plphys/article/127/2/566/6103261 [Accessed September 18, 2022].

Felipe, W., Rodrigues, C., Breno, A., Lisboa, P., Lima, J.E., Klein

Ricachenevsky, F. and Del-Bem, L.-E. (2022) Ferrous iron uptake via IRT1/ZIP evolved at least twice in green plants. *bioRxiv*, 2022.07.21.501042. Available at: https://www.biorxiv.org/content/10.1101/2022.07.21.501042v1 [Accessed October 15, 2022].

Feugier, F.G. and Satake, A. (2013) Dynamical feedback between circadian clock and sucrose availability explains adaptive response of starch metabolism to various photoperiods. *Front. Plant Sci.*, **3**, 305.

Finkelstein, R.R., Gampala, S.S.L. and Rock, C.D. (2002) Abscisic acid signaling in seeds and seedlings. *Plant Cell*, **14**, S15–S45. Available at: www.plantcell.org/cgi/doi/10.1105/tpc.010441. [Accessed June 8, 2021].

Fleishman, S.J., Unger, V.M. and Ben-Tal, N. (2006) Transmembrane protein structures without X-rays. *Trends Biochem. Sci.*, **31**, 106–113.

Floyd, B.E., Morriss, S.C., Macintosh, G.C. and Bassham, D.C. (2015) Evidence for autophagy-dependent pathways of rRNA turnover in Arabidopsis. Available at: https://www.tandfonline.com/action/journalInformation?journalCode=kaup20.

Fourcroy, P., Sisó-Terraza, P., Sudre, D., et al. (2014) Involvement of the ABCG37 transporter in secretion of scopoletin and derivatives by Arabidopsis roots in response to iron deficiency. *New Phytol.*, **201**, 155–167. Available at: www.newphytologist.com [Accessed June 8, 2021].

Fourcroy, P., Tissot, N., Gaymard, F., Briat, J.-F.F. and Dubos, C. (2016) Facilitated Fe nutrition by phenolic compounds excreted by the Arabidopsis ABCG37/PDR9 transporter requires the IRT1/FRO2 high-affinity root Fe2+ transport system. *Mol. Plant*, **9**, 485–488. Available at: https://pubmed.ncbi.nlm.nih.gov/26415695/ [Accessed June 8, 2021].

Fourcroy, P., Vansuyt, G., Kushnir, S., Inzé, D. and Briat, J.F. (2004) Iron-Regulated Expression of a Cytosolic Ascorbate

Peroxidase Encoded by the APX1 Gene in Arabidopsis Seedlings. *Plant Physiol.*, **134**, 605–613. Available at: http://www.plantphysiol.org/cgi/doi/10.1104/pp.103.029876. [Accessed June 9, 2021].

Friso, G. and Wijk, K.J. Van (2015) Posttranslational Protein Modifications in Plant Metabolism. *Plant Physiol.*, **169**, 1469–1487. Available at: https://academic.oup.com/plphys/article/169/3/1469/6114070 [Accessed September 19, 2022].

Fujioka, Y., Noda, N.N., Fujii, K., Yoshimoto, K., Ohsumi, Y. and Inagaki, F. (2008) In vitro reconstitution of plant Atg8 and Atg12 conjugation systems essential for autophagy. *J. Biol. Chem.*, **283**, 1921–1928. Available at: http://www.jbc.org/article/S0021925820776246/fulltext [Accessed June 28, 2021].

Fujita, Y., Fujita, M., Satoh, R., et al. (2005) AREB1 is a transcription activator of novel ABRE-dependent ABA signaling that enhances drought stress tolerance in Arabidopsis. *Plant Cell*, **17**, 3470–3488. Available at: www.plantcell.org/cgi/doi/10.1105/tpc.105.035659. [Accessed June 8, 2021].

Fukao, Y., Ferjani, A., Tomioka, R., Nagasaki, N., Kurata, R., Nishimori, Y., Fujiwara, M. and Maeshima, M. (2011) iTRAQ Analysis Reveals Mechanisms of Growth Defects Due to Excess Zinc in Arabidopsis. *Plant Physiol.*, **155**, 1893–1907. Available at: https://academic.oup.com/plphys/article/155/4/1893/6108827 [Accessed September 18, 2022].

Gadeyne, A., Sánchez-Rodríguez, C., Vanneste, S., et al. (2014) The TPLATE adaptor complex drives clathrin-mediated endocytosis in plants. *Cell*, **156**, 691–704.

Gallie, D.R. and Chen, Z. (2019) Chloroplast-localized iron superoxide dismutases FSD2 and FSD3 are functionally distinct in Arabidopsis. *PLoS One*, **14**, e0220078. Available at: https://doi.org/10.1371/journal.pone.0220078 [Accessed June 8,

2021].
Gao, C., Luo, M., Zhao, Q., Yang, R., Cui, Y., Zeng, Y., Xia, J. and Jiang, L. (2014) A Unique plant ESCRT component, FREE1, regulates multivesicular body protein sorting and plant growth. *Curr. Biol.*, **24**, 2556–2563. Available at: http://dx.doi.org/10.1016/j.cub.2014.09.014 [Accessed June 21, 2021].
Gao, C., Zhuang, X., Shen, J. and Jiang, L. (2017) *Plant ESCRT Complexes: Moving Beyond Endosomal Sorting*, Elsevier Ltd. Available at: http://dx.doi.org/10.1016/j.tplants.2017.08.003 [Accessed June 30, 2021].
Geng, J. and Klionsky, D.J. (2008) *The Atg8 and Atg12 ubiquitin-like conjugation systems in macroautophagy. "Protein Modifications: Beyond the Usual Suspects" Review Series*, John Wiley & Sons, Ltd. Available at: https://www.embopress.org/doi/full/10.1038/embor.2008.163 [Accessed June 28, 2021].
Golubitsky, M. and Stewart, I. (2018) Homeostasis with Multiple Inputs. *https://doi.org/10.1137/17M115147X*, **17**, 1816–1832. Available at: https://epubs.siam.org/doi/abs/10.1137/17M115147X [Accessed May 17, 2022].
Gomes, L.C. and Dikic, I. (2014) Autophagy in antimicrobial immunity. *Mol. Cell*, **54**, 224–233. Available at: https://pubmed.ncbi.nlm.nih.gov/24766886/ [Accessed November 15, 2022].
Gómez-Sánchez, R., Rose, J., Guimarães, R., et al. (2018) Atg9 establishes Atg2-dependent contact sites between the endoplasmic reticulum and phagophores. *J. Cell Biol.*, **217**, 2743–2763. Available at: https://doi.org/10.1083/jcb.201710116 [Accessed September 13, 2022].
Gookin, T.E. and Assmann, S.M. (2014) Significant reduction of BiFC non-specific assembly facilitates in planta assessment of heterotrimeric G-protein interactors. *Plant J.*, **80**, 553–567. Available at:

https://onlinelibrary.wiley.com/doi/full/10.1111/tpj.12639 [Accessed June 24, 2021].

Gough, C. and Sadanandom, A. (2021) Understanding and Exploiting Post-Translational Modifications for Plant Disease Resistance. , **11**, 1122. Available at: https://www.mdpi.com/2218-273X/11/8/1122 [Accessed August 19, 2022].

Green, L.S. and Rogers, E.E. (2004) FRD3 Controls Iron Localization in Arabidopsis. *Plant Physiol.*, **136**, 2523–2531. Available at: https://academic.oup.com/plphys/article/136/1/2523/6112400 [Accessed February 3, 2022].

Grillo, S., Leone, A., Xu, Y., Tucci, M., Francione, R., Hasegawa, P.M., Monti, L. and Bressan, R.A. (1995) Control of osmotin gene expression by ABA and osmotic stress in vegetative tissues of wild-type and ABA-deficient mutants of tomato. *Physiol. Plant.*, **93**, 498–504. Available at: https://onlinelibrary.wiley.com/doi/full/10.1111/j.1399-3054.1995.tb06849.x [Accessed June 13, 2021].

Grossoehme, N.E., Akilesh, S., Guerinot, M. Lou and Wilcox, D.E. (2006) Metal-binding thermodynamics of the histidine-rich sequence from the metal-transport protein IRT1 of Arabidopsis thaliana. *Inorg. Chem.*, **45**, 8500–8508. Available at: https://pubs.acs.org/sharingguidelines [Accessed June 8, 2021].

Gruber, B.D., Giehl, R.F.H., Friedel, S. and Wirén, N. von (2013) Plasticity of the Arabidopsis root system under nutrient deficiencies. *Plant Physiol.*, **163**, 161–179. Available at: www.plantphysiol.org/cgi/doi/10.1104/pp.113.218453 [Accessed June 8, 2021].

Gu, S., Wang, X., Bai, J., Wei, T., Sun, M., Zhu, L., Wang, M., Zhao, Y. and Wei, W. (2021) The kinase CIPK11 functions as a positive regulator in cadmium stress response in Arabidopsis. *Gene*, **772**, 145372.

Guerinot, M. Lou (2000) The ZIP family of metal transporters. *Biochim. Biophys. Acta - Biomembr.*, **1465**, 190–198.

Guiamét, J.J., Tyystjärvi, E., Tyystjärvi, T., John, I., Kairavuo, M., Pichersky, E. and Noodén, L.D. (2002) Photoinhibition and loss of photosystem II reaction centre proteins during senescence of soybean leaves. Enhancement of photoinhibition by the 'stay-green' mutation cytG. *Physiol. Plant.*, **115**, 468–478. Available at: https://onlinelibrary.wiley.com/doi/full/10.1034/j.1399-3054.2002.1150317.x [Accessed September 17, 2022].

Guiboileau, A., Avila-Ospina, L., Yoshimoto, K., Soulay, F., Azzopardi, M., Marmagne, A., Lothier, J. and Masclaux-Daubresse, C. (2013) Physiological and metabolic consequences of autophagy deficiency for the management of nitrogen and protein resources in Arabidopsis leaves depending on nitrate availability. *New Phytol.*, **199**, 683–694. Available at: https://onlinelibrary.wiley.com/doi/full/10.1111/nph.12307 [Accessed September 17, 2022].

Guiboileau, A., Yoshimoto, K., Soulay, F., Bataillé, M.P., Avice, J.C. and Masclaux-Daubresse, C. (2012) Autophagy machinery controls nitrogen remobilization at the whole-plant level under both limiting and ample nitrate conditions in Arabidopsis. *New Phytol.*, **194**, 732–740. Available at: https://onlinelibrary.wiley.com/doi/full/10.1111/j.1469-8137.2012.04084.x [Accessed September 17, 2022].

Guillaumot, D., Guillon, S., Déplanque, T., Vanhee, C., Gumy, C., Masquelier, D., Morsomme, P. and Batoko, H. (2009) The Arabidopsis TSPO-related protein is a stress and abscisic acid-regulated, endoplasmic reticulum-Golgi-localized membrane protein. *Plant J.*, **60**, 242–256.

Guillaumot, D., Guillon, S., Planque, T. De, Vanhee, C., Gumy, C., Masquelier, D., Morsomme, P. and Batoko, H. (2009) The Arabidopsis TSPO-related protein is a stress and abscisic acid regulated, endoplasmic reticulum-Golgi-localized membrane protein. *Plant J.*, **60**, 242–256.

Ha, T., Do, T., Martinoia, E., Lee, Y. and Hwang, J.-U. (2021) 2021 update on ATP-binding cassette (ABC) transporters: how

they meet the needs of plants. *Plant Physiol.*, **187**, 1876–1892. Available at: https://academic.oup.com/plphys/article/187/4/1876/6270926 [Accessed January 11, 2022].

Hachez, C., Veljanovski, V., Reinhardt, H., Guillaumot, D., Vanhee, C., Chaumont, F. and Batoko, H. (2014) The Arabidopsis Abiotic Stress-Induced TSPO-Related Protein Reduces Cell-Surface Expression of the Aquaporin PIP2;7 through Protein-Protein Interactions and Autophagic Degradation . *Plant Cell Online*, **26**, 4974–4990. Available at: http://www.plantcell.org/lookup/doi/10.1105/tpc.114.134080.

Hafrén, A., Üstün, S., Hochmuth, A., Svenning, S., Johansen, T. and Hofius, D. (2018) Turnip Mosaic Virus Counteracts Selective Autophagy of the Viral Silencing Suppressor HCpro. *Plant Physiol.*, **176**, 649–662. Available at: https://academic.oup.com/plphys/article/176/1/649/6117265 [Accessed September 4, 2022].

Han, B., Yang, Z., Xie, Y., Nie, L., Cui, J. and Shen, W. (2014) Arabidopsis HY1 confers cadmium tolerance by decreasing nitric oxide production and improving iron homeostasis. *Mol. Plant*, **7**, 388–403.

Hanada, T., Satomi, Y., Takao, T. and Ohsumi, Y. (2009) The amino-terminal region of Atg3 is essential for association with phosphatidylethanolamine in Atg8 lipidation. *FEBS Lett.*, **583**, 1078–1083.

Hänsch, R. and Mendel, R.R. (2009) Physiological functions of mineral micronutrients (Cu, Zn, Mn, Fe, Ni, Mo, B, Cl). *Curr. Opin. Plant Biol.*, **12**, 259–266.

Hantzis, L.J., Kroh, G.E., Jahn, C.E., Cantrell, M., Peers, G., Pilon, M. and Raveta, K. (2018) A program for iron economy during deficiency targets specific Fe proteins. *Plant Physiol.*, **176**, 596–610. Available at: www.plantphysiol.org/cgi/doi/10.1104/pp.17.01497 [Accessed June 8, 2021].

Havé, M., Marmagne, A., Chardon, F. and Masclaux-Daubresse,

C. (2017) Nitrogen remobilization during leaf senescence: lessons from Arabidopsis to crops. *J. Exp. Bot.*, **68**, 2513–2529. Available at: https://academic.oup.com/jxb/article/68/10/2513/2627441 [Accessed September 17, 2022].

Haydon, M.J., Mielczarek, O., Frank, A., Román, Á. and Webb, A.A.R. (2017) Sucrose and Ethylene Signaling Interact to Modulate the Circadian Clock. *Plant Physiol.*, **175**, 947–958. Available at: https://academic.oup.com/plphys/article/175/2/947/6116852 [Accessed January 18, 2022].

He, X.L., Fan, S.K., Zhu, J., Guan, M.Y., Liu, X.X., Zhang, Y.S. and Jin, C.W. (2017) Iron supply prevents Cd uptake in Arabidopsis by inhibiting IRT1 expression and favoring competition between Fe and Cd uptake. *Plant Soil*, **416**, 453–462. Available at: https://link.springer.com/article/10.1007/s11104-017-3232-y [Accessed February 3, 2022].

Henne, W.M., Buchkovich, N.J. and Emr, S.D. (2011) The ESCRT Pathway. *Dev. Cell*, **21**, 77–91.

Henriques, R., Jásik, J., Klein, M., Martinoia, E., Feller, U., Schell, J., Pais, M.S. and Koncz, C. (2002) Knock-out of Arabidopsis metal transporter gene IRT1 results in iron deficiency accompanied by cell differentiation defects. *Plant Mol. Biol.*, **50**, 587–597. Available at: http://www.ncbi.nlm.nih.gov [Accessed June 8, 2021].

Hermans, C., Vuylsteke, M., Coppens, F., Craciun, A., Inzé, D. and Verbruggen, N. (2010) Early transcriptomic changes induced by magnesium deficiency in Arabidopsis thaliana reveal the alteration of circadian clock gene expression in roots and the triggering of abscisic acid-responsive genes. *New Phytol.*, **187**, 119–131. Available at: http://www.microarrays.be [Accessed June 8, 2021].

Hirayama, T., Lei, G.J., Yamaji, N., Nakagawa, N. and Ma, J.F. (2018) The Putative Peptide Gene FEP1 Regulates Iron

Deficiency Response in Arabidopsis. *Plant Cell Physiol.*, **59**, 1739–1752. Available at: www.pcp.oxfordjournals.org [Accessed June 8, 2021].

Hirsch, J., Marin, E., Floriani, M., Chiarenza, S., Richaud, P., Nussaume, L. and Thibaud, M.C. (2006) Phosphate deficiency promotes modification of iron distribution in Arabidopsis plants. *Biochimie*, **88**, 1767–1771.

Hoffmann, R.D., Olsen, L.I., Ezike, C. V., Pedersen, J.T., Manstretta, R., López-Marqués, R.L. and Palmgren, M. (2019) Roles of plasma membrane proton ATPases AHA2 and AHA7 in normal growth of roots and root hairs in Arabidopsis thaliana. *Physiol. Plant.*, **166**, 848–861. Available at: http://blast.ncbi.nlm.nih.gov/ [Accessed July 1, 2021].

Hong, S., Kim, S.A., Guerinot, M. Lou and Robertson McClung, C. (2013) Reciprocal Interaction of the Circadian Clock with the Iron Homeostasis Network in Arabidopsis. *Plant Physiol.*, **161**, 893–903. Available at: https://academic.oup.com/plphys/article/161/2/893/6110791 [Accessed January 15, 2022].

Hou, Z., Pang, X., Hedtke, B. and Grimm, B. (2021) In vivo functional analysis of the structural domains of FLUORESCENT (FLU). *Plant J.*, **107**, 360–376. Available at: https://onlinelibrary.wiley.com/doi/full/10.1111/tpj.15293 [Accessed January 13, 2022].

Hu, B., Deng, F., Chen, G., Chen, X., Gao, W., Long, L., Xia, J. and Chen, Z.H. (2020) Evolution of Abscisic Acid Signaling for Stress Responses to Toxic Metals and Metalloids. *Front. Plant Sci.*, **11**, 1. Available at: /pmc/articles/PMC7379394/ [Accessed June 8, 2021].

Hu, J., Guo, H., Li, J., Gan, Q., Wang, Y. and Xing, B. (2017) Comparative impacts of iron oxide nanoparticles and ferric ions on the growth of Citrus maxima. *Environ. Pollut.*, **221**, 199–208.

Hu, Z. and Liu, L. (2002) Quality assurance for the analytical data of micro elements in food. *Meas. Uncertain. Chem. Anal.*, 138–142. Available at: https://link.springer.com/chapter/10.1007/978-

3-662-05173-3_25 [Accessed February 4, 2022].
Hua, Z., Doroodian, P. and Vu, W. (2018) Contrasting duplication patterns reflect functional diversities of ubiquitin and ubiquitin-like protein modifiers in plants. *Plant J.*, **95**, 296–311. Available at: https://onlinelibrary.wiley.com/doi/full/10.1111/tpj.13951 [Accessed September 5, 2022].
Huang, X., Zheng, C., Liu, F., et al. (2019) Genetic Analyses of the Arabidopsis ATG1 Kinase Complex Reveal Both Kinase-Dependent and Independent Autophagic Routes during Fixed-Carbon Starvation. *Plant Cell*, **31**, 2973–2995. Available at: https://academic.oup.com/plcell/article/31/12/2973/5985896 [Accessed September 12, 2022].
Huffman, D.L. and Vincent O'halloran, T. (2001) Function, Structure, and Mechanism of Intracellular Copper Trafficking Proteins. *Artic. Annu. Rev. Biochem.* Available at: https://www.researchgate.net/publication/11944863 [Accessed October 14, 2022].
Hulsmans, S., Rodriguez, M., Coninck, B. De and Rolland, F. (2016) The SnRK1 Energy Sensor in Plant Biotic Interactions. *Trends Plant Sci.*, **21**, 648–661.
Humayan Kabir, A., Swaraz, A.M. and Stangoulis, J. (2014) Zinc-deficiency resistance and biofortification in plants. *J. Plant Nutr. Soil Sci.*, **177**, 311–319. Available at: https://onlinelibrary.wiley.com/doi/full/10.1002/jpln.201300326 [Accessed September 17, 2022].
Ishida, H., Yoshimoto, K., Izumi, M., Reisen, D., Yano, Y., Makino, A., Ohsumi, Y., Hanson, M.R. and Mae, T. (2008) Mobilization of Rubisco and Stroma-Localized Fluorescent Proteins of Chloroplasts to the Vacuole by an ATG Gene-Dependent Autophagic Process. *Plant Physiol.*, **148**, 142–155. Available at: https://academic.oup.com/plphys/article/148/1/142/6107379 [Accessed September 16, 2022].
Ishizaki, K., Larson, T.R., Schauer, N., Fernie, A.R., Graham, I.A. and Leaver, C.J. (2005) The Critical Role of Arabidopsis

Electron-Transfer Flavoprotein:Ubiquinone Oxidoreductase during Dark-Induced Starvation. *Plant Cell*, **17**, 2587. Available at: /pmc/articles/PMC1197437/ [Accessed September 17, 2022].

Ivanov, R., Brumbarova, T., Blum, A., Jantke, A.-M.M., Fink-Straube, C. and Bauer, P. (2014) SORTING NEXIN1 Is Required for Modulating the Trafficking and Stability of the Arabidopsis IRON-REGULATED TRANSPORTER1. *Plant Cell*, **26**, 1294–1307. Available at: www.plantcell.org/cgi/doi/10.1105/tpc.113.116244 [Accessed June 8, 2021].

Ivanov, R. and Vert, G. (2021) Endocytosis in plants: Peculiarities and roles in the regulated trafficking of plant metal transporters. *Biol. Cell*, **113**, 1–13. Available at: www.biolcell.net [Accessed June 8, 2021].

Izumi, M., Hidema, J., Makino, A. and Ishida, H. (2013) Autophagy Contributes to Nighttime Energy Availability for Growth in Arabidopsis. *Plant Physiol.*, **161**, 1682–1693. Available at: http://www.plantphysiol.org/cgi/doi/10.1104/pp.113.215632.

Izumi, M., Ishida, H., Nakamura, S. and Hidema, J. (2017) Entire Photodamaged Chloroplasts Are Transported to the Central Vacuole by Autophagy. *Plant Cell*, **29**, 377–394. Available at: https://pubmed.ncbi.nlm.nih.gov/28123106/ [Accessed September 3, 2022].

Izumi, M., Wada, S., Makino, A. and Ishida, H. (2010) The Autophagic Degradation of Chloroplasts via Rubisco-Containing Bodies Is Specifically Linked to Leaf Carbon Status But Not Nitrogen Status in Arabidopsis. *Plant Physiol.*, **154**, 1196–1209. Available at: https://academic.oup.com/plphys/article/154/3/1196/6111303 [Accessed September 17, 2022].

Jaillais, Y. and Gaude, T. (2007) Sorting out the sorting functions of endosomes in Arabidopsis. *Plant Signal. Behav.*, **2**, 556–558. Available at: https://www.tandfonline.com/action/journalInformation?journal

Code=kpsb20 [Accessed June 29, 2021].
Jain, A. and Connolly, E.L. (2013) Mitochondrial iron transport and homeostasis in plants. *Front. Plant Sci.*, **4**, 348. Available at: http://www.pubmedcentral.nih.gov/articlerender.fcgi?artid=3764374&tool=pmcentrez&rendertype=abstract [Accessed June 8, 2022].
Jeong, J., Cohu, C., Kerkeb, L., Pilon, M., Connolly, E.L. and Guerinot, M. Lou (2008) *Chloroplast Fe(III) chelate reductase activity is essential for seedling viability under iron limiting conditions*, Available at: www.pnas.org/cgi/content/full/.
Jeong, J. and Connolly, E.L. (2009) *Iron uptake mechanisms in plants: Functions of the FRO family of ferric reductases*, Elsevier.
Jeong, J., Merkovich, A., Clyne, M. and Connolly, E.L. (2017) Directing iron transport in dicots: regulation of iron acquisition and translocation. *Curr. Opin. Plant Biol.*, **39**, 106–113.
Ji, L.L. and Yeo, D. (2021) Oxidative stress: an evolving definition. *Fac. Rev.*, **10**. Available at: /pmc/articles/PMC7894272/ [Accessed May 17, 2022].
Jia, W., Wang, Y., Zhang, S. and Zhang, J. (2002) Salt-stress-induced ABA accumulation is more sensitively triggered in roots than in shoots. *J. Exp. Bot.*, **53**, 2201–2206. Available at: https://academic.oup.com/jxb/article/53/378/2201/426542 [Accessed June 13, 2021].
Johnson, A. and Vert, G. (2016) Unraveling K63 Polyubiquitination Networks by Sensor-Based Proteomics. *Plant Physiol.*, **171**, 1808–1820. Available at: https://academic.oup.com/plphys/article/171/3/1808/6115236 [Accessed September 24, 2022].
Jones, D.T. (2007) Improving the accuracy of transmembrane protein topology prediction using evolutionary information. *Bioinformatics*, **23**, 538–544. Available at: https://academic.oup.com/bioinformatics/article/23/5/538/239106 [Accessed May 17, 2022].
Jurkiewicz, P., Senicourt, L., Ayeb, H., Lequin, O., Lacapere, J.J.

and Batoko, H. (2020) A Plant-Specific N-terminal Extension Reveals Evolutionary Functional Divergence within Translocator Proteins. *iScience*, **23**, 100889.

Kanwar, P., Baby, D. and Bauer, P. (2021) *Interconnection of iron and osmotic stress signalling in plants: is FIT a regulatory hub to cross-connect abscisic acid responses?*, Available at: https://onlinelibrary.wiley.com/doi/full/10.1111/plb.13261 [Accessed June 8, 2021].

Kapoor, D., Bhardwaj, S., Gautam, S., Rattan, A., Bhardwaj, R. and Sharma, A. (2022) Brassinosteroids in plant nutrition and heavy metal tolerance. *Brassinosteroids Plant Dev. Biol. Stress Toler.*, 217–235.

Kathpalia, R. and Bhatla, S.C. (2018) Plant Mineral Nutrition. *Plant Physiol. Dev. Metab.*, 37–81. Available at: https://link.springer.com/chapter/10.1007/978-981-13-2023-1_2 [Accessed October 29, 2021].

Katsiarimpa, A., Kalinowska, K., Anzenberger, F., et al. (2013) The deubiquitinating enzyme AMSH1 and the ESCRT-III subunit VPS2.1 are required for autophagic degradation in Arabidopsis. *Plant Cell*, **25**, 2236–2252. Available at: www.plantcell.org/cgi/doi/10.1105/tpc.113.113399 [Accessed June 30, 2021].

Kaufmann, A., Beier, V., Franquelim, H.G. and Wollert, T. (2014) Molecular Mechanism of Autophagic Membrane-Scaffold Assembly and Disassembly. *Cell*, **156**, 469–481.

Kelekar, A. (2006) Autophagy. *Ann. N. Y. Acad. Sci.*, **1066**, 259–271. Available at: https://onlinelibrary.wiley.com/doi/full/10.1196/annals.1363.015 [Accessed May 18, 2022].

Kerkeb, L., Mukherjee, I., Chatterjee, I., Lahner, B., Salt, D.E. and Connolly, E.L. (2008) Iron-induced turnover of the Arabidopsis IRON-REGULATED TRANSPORTER1 metal transporter requires lysine residues. *Plant Physiol.*, **146**, 1964–1973. Available at: https://academic.oup.com/plphys/article/146/4/1964/6107306

[Accessed June 28, 2021].

Khan, I., Gratz, R., Denezhkin, P., et al. (2019) Calcium-promoted interaction between the C2-domain protein EHB1 and metal transporter IRT1 inhibits arabidopsis iron acquisition. *Plant Physiol.*, **180**, 1564–1581. Available at: www.plantphysiol.org/cgi/doi/10.1104/pp.19.00163 [Accessed June 8, 2021].

Khan, M.A., Castro-Guerrero, N.A., McInturf, S.A., et al. (2018) Changes in iron availability in Arabidopsis are rapidly sensed in the leaf vasculature and impaired sensing leads to opposite transcriptional programs in leaves and roots. *Plant. Cell Environ.*, **41**, 2263–2276. Available at: https://onlinelibrary.wiley.com/doi/full/10.1111/pce.13192 [Accessed February 3, 2022].

Kieu, N.P., Aznar, A., Segond, D., Rigault, M., Simond-Côte, E., Kunz, C., Soulie, M.C., Expert, D. and Dellagi, A. (2012) Iron deficiency affects plant defence responses and confers resistance to dickeya dadantii and botrytis cinerea. *Mol. Plant Pathol.*, **13**, 816–827.

Kikuchi, Y., Nakamura, S., Woodson, J.D., Ishida, H., Ling, Q., Hidema, J., Jarvis, R.P., Hagihara, S. and Izumi, M. (2020) Chloroplast Autophagy and Ubiquitination Combine to Manage Oxidative Damage and Starvation Responses. *Plant Physiol.*, **183**, 1531–1544. Available at: https://pubmed.ncbi.nlm.nih.gov/32554506/ [Accessed September 3, 2022].

Kim, J.-G., Back, K., Hyoung, ·, Lee, Y., Lee, H.-J., Phung, T.-H., Grimm, B. and Jung, S. (2014) Increased expression of Fe-chelatase leads to increased metabolic flux into heme and confers protection against photodynamically induced oxidative stress. *Plant Mol Biol*, **86**, 271–287.

Kim, J.H., Lee, H.N., Huang, X., Jung, H., Otegui, M.S., Li, F. and Chung, T. (2022) FYVE2, a phosphatidylinositol 3-phosphate effector, interacts with the COPII machinery to control autophagosome formation in Arabidopsis. *Plant Cell*, **34**, 351–

373. Available at: https://academic.oup.com/plcell/article/34/1/351/6414627 [Accessed May 16, 2022].

Kim, J.H., Lee, Y., Kim, E.J., Gu, S., Sohn, E.J., Seo, Y.S., An, H.J. and Chang, Y.S. (2014) Exposure of iron nanoparticles to Arabidopsis thaliana enhances root elongation by triggering cell wall loosening. *Environ. Sci. Technol.*, **48**, 3477–3485. Available at: https://pubs.acs.org/doi/full/10.1021/es4043462 [Accessed September 17, 2022].

Kim, L.J., Tsuyuki, K.M., Hu, F., et al. (2021) Ferroportin 3 is a dual-targeted mitochondrial/chloroplast iron exporter necessary for iron homeostasis in Arabidopsis. *Plant J.*, **107**, 215–236. Available at: https://onlinelibrary.wiley.com/doi/full/10.1111/tpj.15286 [Accessed January 12, 2022].

Kim, S.A. and Guerinot, M. Lou (2007) Mining iron: Iron uptake and transport in plants. *FEBS Lett.*, **581**, 2273–2280.

Kirisako, T., Ichimura, Y., Okada, H., et al. (2000) *The Reversible Modification Regulates the Membrane-Binding State of Apg8/Aut7 Essential for Autophagy and the Cytoplasm to Vacuole Targeting Pathway*, Available at: http://www.jcb.org/cgi/content/full/151/2/263.

Klatte, M., Schuler, M., Wirtz, M., Fink-Straube, C., Hell, R. and Bauer, P. (2009) The analysis of arabidopsis nicotianamine synthase mutants reveals functions for nicotianamine in seed iron loading and iron deficiency responses. *Plant Physiol.*, **150**, 257–271. Available at: www.plantphysiol.org/cgi/doi/10.1104/pp.109.136374 [Accessed June 8, 2021].

Kleffner, R., Flatten, J., Leaver-Fay, A., Baker, D., Siegel, J.B., Khatib, F. and Cooper, S. (2017) Foldit Standalone: a video game-derived protein structure manipulation interface using Rosetta. *Bioinformatics*, **33**, 2765–2767. Available at: https://academic.oup.com/bioinformatics/article/33/17/2765/3803439 [Accessed October 6, 2022].

Knight, H., Thomson, A.J.W. and McWatters, H.G. (2008) SENSITIVE TO FREEZING6 Integrates Cellular and Environmental Inputs to the Plant Circadian Clock. *Plant Physiol.*, **148**, 293–303. Available at: https://academic.oup.com/plphys/article/148/1/293/6107566 [Accessed January 20, 2022].

Koen, E., Besson-Bard, A., Duc, C., et al. (2013) Arabidopsis thaliana nicotianamine synthase 4 is required for proper response to iron deficiency and to cadmium exposure. *Plant Sci.*, **209**, 1–11.

Koen, E., Szymańska, K., Klinguer, A., Dobrowolska, G., Besson-Bard, A. and Wendehenne, D. (2012) Plant Signaling & Behavior Nitric oxide and glutathione impact the expression of iron uptake-and iron transport-related genes as well as the content of metals in A. thaliana plants grown under iron deficiency. *Plant Signal. Behav.*, **7**, 1246–1250. Available at: https://www.tandfonline.com/action/journalInformation?journalCode=kpsb20http://dx.doi.org/10.4161/psb.21548 [Accessed January 21, 2022].

Kolb, C., Nagel, M.K., Kalinowska, K., et al. (2015) FYVE1 is essential for vacuole biogenesis and intracellular trafficking in arabidopsis. *Plant Physiol.*, **167**, 1361–1373. Available at: www.plantphysiol.org/cgi/doi/10.1104/pp.114.253377 [Accessed June 30, 2021].

Kong, L., Rodrigues, B., Kim, J.H., He, P. and Shan, L. (2021) More than an on-and-off switch: Post-translational modifications of plant pattern recognition receptor complexes. *Curr. Opin. Plant Biol.*, **63**, 102051.

Korshunova, Y.O., Eide, D., Clark, W.G., Guerinot, M. Lou and Pakrasi, H.B. (1999) The IRT1 protein from Arabidopsis thaliana is a metal transporter with a broad substrate range. *Plant Mol. Biol.*, **40**, 37–44. Available at: http://www.springerlink.com/content/h300333075965762/%5Cnpapers3://publication/uuid/D803266B-435A-4376-97BB-8EC93CE9E32D [Accessed February 3, 2022].

Kotani, T., Kirisako, H., Koizumi, M., Ohsumi, Y. and Nakatogawa, H. (2018) The Atg2-Atg18 complex tethers pre-autophagosomal membranes to the endoplasmic reticulum for autophagosome formation. *Proc. Natl. Acad. Sci. U. S. A.*, **115**, 10363–10368. Available at: https://www.pnas.org/doi/abs/10.1073/pnas.1806727115 [Accessed September 13, 2022].

Koyama-Honda, I., Tsuboyama, K. and Mizushima, N. (2017) ATG conjugation-dependent degradation of the inner autophagosomal membrane is a key step for autophagosome maturation. *Autophagy*, **13**, 1252–1253. Available at: https://www.tandfonline.com/action/journalInformation?journalCode=kaup20 [Accessed June 28, 2021].

Krämer, U. (2005) MTP1 mops up excess zinc in Arabidopsis cells. *Trends Plant Sci.*, **10**, 313–315.

Kranner, I. and Colville, L. (2011) Metals and seeds: Biochemical and molecular implications and their significance for seed germination. *Environ. Exp. Bot.*, **72**, 93–105.

Kravale, D., Kreicberga, A. and Ositis, U. (2007) Forms of micro-elements and its role in cattle organism. *Z. katram Zemn. un lauku uznemejam*.

Krebs, M., Held, K., Binder, A., Hashimoto, K., Herder, G. Den, Parniske, M., Kudla, J. and Schumacher, K. (2012) FRET-based genetically encoded sensors allow high-resolution live cell imaging of Ca2+ dynamics. *Plant J.*, **69**, 181–192. Available at: https://onlinelibrary.wiley.com/doi/full/10.1111/j.1365-313X.2011.04780.x [Accessed June 24, 2021].

Kreps, J.A., Wu, Y., Chang, H.-S.S., Zhu, T., Wang, X. and Harper, J.F. (2002) Transcriptome changes for Arabidopsis in response to salt, osmotic, and cold stress. *Plant Physiol.*, **130**, 2129–2141. Available at: www.plantphysiol.org/cgi/doi/10.1104/pp.008532. [Accessed June 8, 2021].

Kroh, Gretchen Elizabeth and Pilon, M. (2020) Iron deficiency and the loss of chloroplast iron–sulfur cluster assembly trigger

distinct transcriptome changes in Arabidopsis rosettes. *Metallomics*, **12**, 1748–1764. Available at: https://academic.oup.com/metallomics/article/12/11/1748/6071929 [Accessed June 8, 2022].

Kroh, Gretchen E. and Pilon, M. (2020) Regulation of Iron Homeostasis and Use in Chloroplasts. *Int. J. Mol. Sci. 2020, Vol. 21, Page 3395*, **21**, 3395. Available at: https://www.mdpi.com/1422-0067/21/9/3395/htm [Accessed January 11, 2022].

Krüger, F. and Schumacher, K. (2018) Pumping up the volume − vacuole biogenesis in Arabidopsis thaliana. *Semin. Cell Dev. Biol.*, **80**, 106–112.

Kuma, A., Komatsu, M. and Mizushima, N. (2017) Autophagy-monitoring and autophagy-deficient mice. *Autophagy*, **13**, 1619–1628. Available at: https://www.tandfonline.com/action/journalInformation?journalCode=kaup20 [Accessed June 28, 2021].

Kumar, S. and Bandyopadhyay, U. (2005) Free heme toxicity and its detoxification systems in human. *Toxicol. Lett.*, **157**, 175–188.

Kurt, F. and Filiz, E. (2020) Subcellular iron transport genes in Arabidopsis thaliana: insights into iron homeostasis. *J. Biosci. Biotechnol.*, **9**, 1–10. Available at: https://editorial.uni-plovdiv.bg/index.php/JBB/article/view/295 [Accessed January 25, 2022].

Kushwaha, N.K., Hafrén, A. and Hofius, D. (2019) Autophagy–virus interplay in plants: from antiviral recognition to proviral manipulation. *Mol. Plant Pathol.*, **20**, 1211–1216. Available at: https://onlinelibrary.wiley.com/doi/full/10.1111/mpp.12852 [Accessed September 4, 2022].

Lam, S.K., Tse, Y.C., Robinson, D.G. and Jiang, L. (2007) Tracking down the elusive early endosome. *Trends Plant Sci.*, **12**, 497–505.

Lamark, T. and Johansen, T. (2021) Mechanisms of Selective Autophagy. *Annu. Rev. Cell Dev. Biol.*, **37**, 143–169. Available

at: https://pubmed.ncbi.nlm.nih.gov/34152791/ [Accessed September 4, 2022].

Landeweert, R., Hoffland, E., Finlay, R.D., Kuyper, T.W. and Breemen, N. Van (2001) Linking plants to rocks: ectomycorrhizal fungi mobilize nutrients from minerals. *Trends Ecol. Evol.*, **16**, 248–254.

LaRosa, P.C., Hasegawa, P.M., Rhodes, D., Clithero, J.M., Watad, A.-E.A. and Bressan, R.A. (1987) Abscisic Acid Stimulated Osmotic Adjustment and Its Involvement in Adaptation of Tobacco Cells to NaCl 1. *Plant Physiol.*, **85**, 174–181. Available at: https://doi.org/10.1104/pp.85.1.174 [Accessed June 24, 2021].

Laureano-Marín, A.M., Aroca, Á., Pérez-Pérez, M.E., Yruela, I., Jurado-Flores, A., Moreno, I., Crespo, J.L., Romero, L.C. and Gotor, C. (2020) Abscisic Acid-Triggered Persulfidation of the Cys Protease ATG4 Mediates Regulation of Autophagy by Sulfide. *Plant Cell*, **32**, 3902–3920. Available at: https://academic.oup.com/plcell/article/32/12/3902/6118616 [Accessed September 15, 2022].

Lee, H.J., Mochizuki, N., Masuda, T. and Buckhout, T.J. (2012) Disrupting the bimolecular binding of the haem-binding protein 5 (AtHBP5) to haem oxygenase 1 (HY1) leads to oxidative stress in Arabidopsis. *J. Exp. Bot.*, **63**, 5967–5978. Available at: https://academic.oup.com/jxb/article/63/16/5967/729956 [Accessed January 13, 2022].

Lee, H.N., Jung, H. and Chung, T. (2020) Subcellular Localization of PI3P in Arabidopsis. In *Methods in Molecular Biology*. Humana Press Inc., pp. 109–118. Available at: https://link.springer.com/protocol/10.1007/978-1-0716-0767-1_10 [Accessed June 29, 2021].

Lee, Y., Park, Y., Nam, H., Lee, J.W. and Yu, S.W. (2020) Translocator protein (TSPO): the new story of the old protein in neuroinflammation. *BMB Rep.*, **53**, 20. Available at: /pmc/articles/PMC6999824/ [Accessed January 29, 2022].

Leene, J. Van, Han, C., Gadeyne, A., et al. (2019) Capturing the

phosphorylation and protein interaction landscape of the plant TOR kinase. *Nat. Plants 2019 53*, **5**, 316–327. Available at: https://www.nature.com/articles/s41477-019-0378-z [Accessed September 13, 2022].

Lefèvre, F., Fourmeau, J., Pottier, M., Baijot, A., Cornet, T., Abadía, J., Álvarez-Fernández, A. and Boutry, M. (2018) The Nicotiana tabacum ABC transporter NtPDR3 secretes O-methylated coumarins in response to iron deficiency. *J. Exp. Bot.*, **69**, 4419–4431. Available at: https://pubs.acs.org/sharingguidelines [Accessed June 8, 2021].

Lei, G.J., Zhu, X.F., Wang, Z.W., Dong, F., Dong, N.Y. and Zheng, S.J. (2014) Abscisic acid alleviates iron deficiency by promoting root iron reutilization and transport from root to shoot in Arabidopsis. *Plant, Cell Environ.*, **37**, 852–863. Available at: http://www.dna.affrc [Accessed June 8, 2021].

Leitner, J., Petrášek, J., Tomanov, K., Retzer, K., Pařezová, M., Korbei, B., Bachmair, A., Zažímalová, E. and Luschnig, C. (2012) Lysine63-linked ubiquitylation of PIN2 auxin carrier protein governs hormonally controlled adaptation of Arabidopsis root growth. *Proc. Natl. Acad. Sci. U. S. A.*, **109**, 8322–8327. Available at: https://www.pnas.org/doi/abs/10.1073/pnas.1200824109 [Accessed September 24, 2022].

Leong, J.X., Langin, G., Suayib¨, S. and Suayib¨ustün, S.S. (2022) Selective autophagy: adding precision in plant immunity. *Essays Biochem.*, **66**, 189–206. Available at: /essaysbiochem/article/66/2/189/231368/Selective-autophagy-adding-precision-in-plant [Accessed September 5, 2022].

Leong, J.X., Raffeiner, M., Spinti, D., et al. (2022) A bacterial effector counteracts host autophagy by promoting degradation of an autophagy component. *EMBO J.*, **41**, e110352. Available at: https://onlinelibrary.wiley.com/doi/full/10.15252/embj.2021110352 [Accessed September 5, 2022].

Levine, S. (1985) A Definition of Stress? *Anim. Stress*, 51–69.

Li, B., Zeng, Y., Jiang, L. and Jiang, C.L. (2022) COPII vesicles in

plant autophagy and endomembrane trafficking. *FEBS Lett.* Available at: https://onlinelibrary.wiley.com/doi/full/10.1002/1873-3468.14362 [Accessed May 16, 2022].

Li, F., Chung, T. and Vierstra, R.D. (2014) AUTOPHAGY-RELATED11 Plays a Critical Role in General Autophagy- and Senescence-Induced Mitophagy in Arabidopsis. *Plant Cell*, **26**, 788–807. Available at: https://academic.oup.com/plcell/article/26/2/788/6097976 [Accessed September 11, 2022].

Li, H., Liao, Y., Zheng, X., Zhuang, X., Gao, C. and Zhou, J. (2022) Shedding Light on the Role of Phosphorylation in Plant Autophagy. *FEBS Lett.* Available at: https://onlinelibrary.wiley.com/doi/full/10.1002/1873-3468.14352 [Accessed September 10, 2022].

Li, H., Song, J.B., Zhao, W.T. and Yang, Z.M. (2013) AtHO1 is Involved in Iron Homeostasis in an NO-Dependent Manner. *Plant Cell Physiol.*, **54**, 1105–1117. Available at: https://academic.oup.com/pcp/article/54/7/1105/1847436 [Accessed January 21, 2022].

Li, Q., Shortreed, M.R., Wenger, C.D., Frey, B.L., Schaffer, L. V., Scalf, M. and Smith, L.M. (2017) Global Post-Translational Modification Discovery. *J. Proteome Res.*, **16**, 1383–1390. Available at: https://pubs.acs.org/doi/abs/10.1021/acs.jproteome.6b00034 [Accessed May 17, 2022].

Li, R., Liu, P., Wan, Y., et al. (2012) A membrane microdomain-associated protein, Arabidopsis Flot1, is involved in a clathrin-independent endocytic pathway and is required for seedling development. *Plant Cell*, **24**, 2105–2122. Available at: www.plantcell.org/cgi/doi/10.1105/tpc.112.095695 [Accessed June 29, 2021].

Li, T., Wu, R., Liu, Z., Wang, J., Guo, C., Zhou, Y., Bawa, G. and Sun, X. (2021) GUN4 Affects the Circadian Clock and Seedlings Adaptation to Changing Light Conditions. *Int. J. Mol.*

Sci. 2022, Vol. 23, Page 194, **23**, 194. Available at: https://www.mdpi.com/1422-0067/23/1/194/htm [Accessed January 18, 2022].

Li, W., Han, X. and Lan, P. (2022) Emerging roles of protein phosphorylation in plant iron homeostasis. *Trends Plant Sci.*, **27**, 908–921.

Li, Y., Pan, L., Zhu, Y., et al. (2019) How does zero valent iron activating peroxydisulfate improve the dewatering of anaerobically digested sludge? *Water Res.*, **163**, 114912.

Liao, C.Y. and Bassham, D.C. (2020) Combating stress: the interplay between hormone signaling and autophagy in plants. *J. Exp. Bot.*, **71**, 1723–1733. Available at: https://academic.oup.com/jxb/article/71/5/1723/5625842 [Accessed September 13, 2022].

Lima, M.D.R., Barros Junior, U. de O., Batista, B.L. and Lobato, A.K. da S. (2018) Brassinosteroids mitigate iron deficiency improving nutritional status and photochemical efficiency in Eucalyptus urophylla plants. *Trees - Struct. Funct.*, **32**, 1681–1694. Available at: https://link.springer.com/article/10.1007/s00468-018-1743-7 [Accessed November 14, 2022].

Lindemann, P., Koch, A., Degenhardt, B., Hause, G., Grimm, B. and Papadopoulos, V. (2004) A novel Arabidopsis thaliana protein is a functional peripheral-type benzodiazepine receptor. *Plant Cell Physiol.*, **45**, 723–733. Available at: https://academic.oup.com/pcp/article/45/6/723/1857399 [Accessed June 24, 2021].

Lindsay, W.L. (2008) Soil and plant relationships associated with iron deficiency with emphasis on nutrient interactions. *https://doi.org/10.1080/01904168409363215*, **7**, 489–500. Available at: https://www.tandfonline.com/doi/abs/10.1080/01904168409363215 [Accessed February 4, 2022].

Lindsey, B.E., Rivero, L., Calhoun, C.S., Grotewold, E. and Brkljacic, J. (2017) Standardized method for high-throughput

sterilization of Arabidopsis seeds. *J. Vis. Exp.*, **2017**, 56587. Available at: www.jove.comurl:https://www.jove.com/video/56587 [Accessed June 8, 2021].

Ling, Q., Huang, W., Baldwin, A. and Jarvis, P. (2012) Chloroplast biogenesis is regulated by direct action of the ubiquitin-proteasome system. *Science (80-.).*, **338**, 655–659. Available at: https://www.science.org/doi/10.1126/science.1225053 [Accessed September 3, 2022].

Liu, Y. and Bassham, D.C. (2012) Autophagy: Pathways for Self-Eating in Plant Cells Autophagosome: a double-membrane structure formed upon autophagy induction; it engulfs portions of cytoplasm and delivers them to the vacuole for degradation. Available at: www.annualreviews.org [Accessed June 28, 2021].

Liu, Y. and Bassham, D.C. (2010) TOR Is a Negative Regulator of Autophagy in Arabidopsis thaliana. *PLoS One*, **5**, e11883. Available at: https://journals.plos.org/plosone/article?id=10.1371/journal.pone.0011883 [Accessed September 13, 2022].

Lobreaux, S., Hardy, T. and Briat, J.F. (1993) Abscisic acid is involved in the iron-induced synthesis of maize ferritin. *EMBO J.*, **12**, 651–657. Available at: https://www.embopress.org/doi/full/10.1002/j.1460-2075.1993.tb05698.x [Accessed June 8, 2021].

Lockhart, J. (2017) Family Chores: TRAF Family Proteins Help Recycle Cellular Rubbish by Regulating Autophagy Dynamics. *Plant Cell*, **29**, 607–607. Available at: https://academic.oup.com/plcell/article/29/4/607/6100940 [Accessed September 2, 2022].

López-Millán, A.F., Grusak, M.A., Abadía, A. and Abadía, J. (2013) Iron deficiency in plants: An insight from proteomic approaches. *Front. Plant Sci.*, **4**, 254. Available at: www.frontiersin.org [Accessed June 8, 2021].

Lu, S., Zhuo, C., Wang, X. and Guo, Z. (2014) Nitrate reductase (NR)-dependent NO production mediates ABA- and H2O2-

induced antioxidant enzymes. *Plant Physiol. Biochem.*, **74**, 9–15.
Luk´, L., Luká˘, L., Pravda, L., et al. (2018) MOLEonline: a web-based tool for analyzing channels, tunnels and pores (2018 update). *Nucleic Acids Res.*, **46**, W368–W373. Available at: https://academic.oup.com/nar/article/46/W1/W368/4990029 [Accessed October 6, 2022].
Magen, S., Seybold, H., Laloum, D. and Avin-Wittenberg, T. (2022) Metabolism and autophagy in plants-a perfect match. *FEBS Lett.*, **596**. Available at: https://pubmed.ncbi.nlm.nih.gov/35470431/ [Accessed September 16, 2022].
Mahfouz, M.M., Kim, S., Delauney, A.J. and Verma, D.P.S. (2006) Arabidopsis TARGET of RAPAMYCIN interacts with RAPTOR, which regulates the activity of S6 kinase in response to osmotic stress signals. *Plant Cell*, **18**, 477–490. Available at: www.plantcell.org/cgi/doi/10.1105/tpc.105.035931. [Accessed June 24, 2021].
Mann, M. and Jensen, O.N. (2003) Proteomic analysis of post-translational modifications. *Nat. Biotechnol. 2003 213*, **21**, 255–261. Available at: https://www.nature.com/articles/nbt0303-255 [Accessed May 17, 2022].
Mariani, V., Biasini, M., Barbato, A. and Schwede, T. (2013) lDDT: a local superposition-free score for comparing protein structures and models using distance difference tests. *Bioinformatics*, **29**, 2722. Available at: /pmc/articles/PMC3799472/ [Accessed October 14, 2022].
Marion, J., Bars, R. Le, Besse, L., Batoko, H. and Satiat-Jeunemaitre, B. (2018) Multiscale and Multimodal Approaches to Study Autophagy in Model Plants. *Cells 2018, Vol. 7, Page 5*, **7**, 5. Available at: https://www.mdpi.com/2073-4409/7/1/5/htm [Accessed September 19, 2022].
Marschner, H. and Römheld, V. (1995) Strategies of plants for acquisition of iron. *Iron Nutr. Soils Plants*, 375–388. Available at: https://link.springer.com/chapter/10.1007/978-94-011-0503-3_52 [Accessed February 2, 2022].

Marschner, H., Romheld, V. and Kissel, M. (1986) Different strategies in higher plants in mobilization and uptake of iron. *J. Plant Nutr.*, **9**, 695–713.

Marsh, H. V., Evans, H.J. and Matrone, G. (1963) Investigations of the Role of Iron in Chlorophyll Metabolism. II. Effect of Iron Deficiency on Chlorophyll Synthesis. *Plant Physiol.*, **38**, 638–642. Available at: https://www.ncbi.nlm.nih.gov/pmc/articles/PMC549988/ [Accessed June 8, 2021].

Marshall, R.S., Li, F., Gemperline, D.C., Book, A.J. and Vierstra, R.D. (2015) Autophagic Degradation of the 26S Proteasome Is Mediated by the Dual ATG8/Ubiquitin Receptor RPN10 in Arabidopsis. *Mol. Cell*, **58**, 1053–1066.

Marshall, R.S. and Vierstra, R.D. (2018) Autophagy: The Master of Bulk and Selective Recycling. *https://doi.org/10.1146/annurev-arplant-042817-040606*, **69**, 173–208. Available at: https://www.annualreviews.org/doi/abs/10.1146/annurev-arplant-042817-040606 [Accessed September 8, 2022].

Marshall, R.S. and Vierstra, R.D. (2019) Dynamic regulation of the 26S proteasome: From synthesis to degradation. *Front. Mol. Biosci.*, **6**, 40.

Martín-Barranco, A., Spielmann, J., Dubeaux, G., Vert, G. and Zelazny, E. (2020) Dynamic Control of the High-Affinity Iron Uptake Complex in Root Epidermal Cells. *Plant Physiol.*, **184**, 1236–1250. Available at: https://academic.oup.com/plphys/article/184/3/1236/6118257 [Accessed January 6, 2022].

Martins, S., Dohmann, E.M.N., Cayrel, A., et al. (2015) Internalization and vacuolar targeting of the brassinosteroid hormone receptor BRI1 are regulated by ubiquitination. *Nat. Commun. 2015 61*, **6**, 1–11. Available at: https://www.nature.com/articles/ncomms7151 [Accessed September 24, 2022].

Masclaux-Daubresse, C., Chen, Q. and Havé, M. (2017) Regulation of nutrient recycling via autophagy. *Curr. Opin. Plant Biol.*, **39**,

8–17.
Masclaux-Daubresse, C., Clément, G., Anne, P., Routaboul, J.M., Guiboileau, A., Soulay, F., Shirasu, K. and Yoshimoto, K. (2014) Stitching together the Multiple Dimensions of Autophagy Using Metabolomics and Transcriptomics Reveals Impacts on Metabolism, Development, and Plant Responses to the Environment in Arabidopsis. *Plant Cell*, **26**, 1857–1877. Available at: https://academic.oup.com/plcell/article/26/5/1857/6099904 [Accessed September 17, 2022].
Masuda, T., Shimizu, T., Yasuda, R., Mukai, Y., Tanoue, R., Shimada, T., Imamura, S., Tanaka, K. and Watanabe, S. (2020) Proteomic analysis of haem-binding protein from Arabidopsis thaliana and Cyanidioschyzon merolae. Available at: http://dx.doi.org/10.1098/rstb.2019.0488 [Accessed January 18, 2022].
Mayland, H.F. and Wilkinson, S.R. (1996) Mineral Nutrition 1.
McMahon, H.T. and Boucrot, E. (2011) Molecular mechanism and physiological functions of clathrin-mediated endocytosis. *Nat. Rev. Mol. Cell Biol.*, **12**, 517–533. Available at: https://www.nature.com/articles/nrm3151 [Accessed June 29, 2021].
Meiser, J., Lingam, S. and Bauer, P. (2011) Posttranslational Regulation of the Iron Deficiency Basic Helix-Loop-Helix Transcription Factor FIT Is Affected by Iron and Nitric Oxide. *Plant Physiol.*, **157**, 2154–2166. Available at: www.plantphysiol.org/cgi/doi/10.1104/pp.111.183285 [Accessed June 29, 2021].
Mellman, I. (2003) ENDOCYTOSIS AND MOLECULAR SORTING. *http://dx.doi.org/10.1146/annurev.cellbio.12.1.575*, **12**, 575–625. Available at: https://www.annualreviews.org/doi/abs/10.1146/annurev.cellbio.12.1.575 [Accessed May 18, 2022].
Mendoza-Cózatl, D.G., Xie, Q., Akmakjian, G.Z., et al. (2014) OPT3 Is a Component of the Iron-Signaling Network between

Leaves and Roots and Misregulation of OPT3 Leads to an Over-Accumulation of Cadmium in Seeds. *Mol. Plant*, **7**, 1455–1469.

Merkulova, E.A., Guiboileau, A., Naya, L., Masclaux-Daubresse, C. and Yoshimoto, K. Assessment and Optimization of Autophagy Monitoring Methods in Arabidopsis Roots Indicate Direct Fusion of Autophagosomes with Vacuoles. Available at: www.pcp.oxfordjournals.org.

Mhamdi, A., Queval, G., Chaouch, S., Vanderauwera, S., Breusegem, F. Van and Noctor, G. (2010) Catalase function in plants: a focus on Arabidopsis mutants as stress-mimic models. *J. Exp. Bot.*, **61**, 4197–4220. Available at: https://academic.oup.com/jxb/article/61/15/4197/436494 [Accessed January 25, 2022].

Michaeli, S., Clavel, M., Lechner, E., et al. (2019) The viral F-box protein P0 induces an ER-derived autophagy degradation pathway for the clearance of membrane-bound AGO1. *Proc. Natl. Acad. Sci. U. S. A.*, **116**, 22872–22883. Available at: https://www.pnas.org/doi/abs/10.1073/pnas.1912222116 [Accessed September 5, 2022].

Michaeli, S., Galili, G., Genschik, P., Fernie, A.R. and Avin-wittenberg, T. (2016) Autophagy in Plants – What ' s New on the Menu ? *Trends Plant Sci.*, **21**, 134–144. Available at: http://dx.doi.org/10.1016/j.tplants.2015.10.008.

Miyake, C. and Asada, K. (1996) *Inactivation Mechanism of Ascorbate Peroxidase at Low Concentrations of Ascorbate; Hydrogen Peroxide Decomposes Compound I of Ascorbate Peroxidase*, Oxford Academic. Available at: https://academic.oup.com/pcp/article/37/4/423/1850497 [Accessed January 24, 2022].

Mizushima, N. (2007) Autophagy: process and function. *Genes Dev.*, **21**, 2861–2873. Available at: http://genesdev.cshlp.org/content/21/22/2861.full [Accessed May 18, 2022].

Modell, H., Cliff, W., Michael, J., McFarland, J., Wenderoth, M.P. and Wright, A. (2015) A physiologist's view of

homeostasis. *Adv. Physiol. Educ.*, **39**, 259–266. Available at: https://journals.physiology.org/doi/full/10.1152/advan.00107.2015 [Accessed May 17, 2022].

Moon, J., Parry, G. and Estelle, M. (2004) The Ubiquitin-Proteasome Pathway and Plant Development. *Plant Cell*, **16**, 3181–3195. Available at: https://academic.oup.com/plcell/article/16/12/3181/6010268 [Accessed August 27, 2022].

Mori, S. (1998) Iron transport in graminaceous plants. *Met. Ions Biol. Syst.*, **35**, 215–238.

Mori, S. (1994) Mechanisms of iron acquisition by graminaceous (strategy II) plants. *Biochem. Met. Micronutr. Rhizosph.*, 225–249.

Morrissey, J., Baxter, I.R., Lee, J., Li, L., Lahner, B., Grotz, N., Kaplan, J., Salt, D.E. and Guerinot, M. Lou (2009) The Ferroportin Metal Efflux Proteins Function in Iron and Cobalt Homeostasis in Arabidopsis. *Plant Cell*, **21**, 3326–3338. Available at: https://academic.oup.com/plcell/article/21/10/3326/6096245 [Accessed February 3, 2022].

Morrissey, J. and Guerinot, M. Lou (2009) Iron uptake and transport in plants: The good, the bad, and the ionome. *Chem. Rev.*, **109**, 4553–4567. Available at: https://pubs.acs.org/sharingguidelines [Accessed June 8, 2021].

Mosesso, N., Bläske, T., Nagel, M.K., Laumann, M. and Isono, E. (2019) Preparation of clathrin-coated vesicles from arabidopsis thaliana seedlings. *Front. Plant Sci.*, **9**, 1972. Available at: www.frontiersin.org [Accessed June 29, 2021].

Müdsam, C., Wollschläger, P., Sauer, N. and Schneider, S. (2018) Sorting of Arabidopsis NRAMP3 and NRAMP4 depends on adaptor protein complex AP4 and a dileucine-based motif. *Traffic*, **19**, 503–521. Available at: https://onlinelibrary.wiley.com/doi/full/10.1111/tra.12567 [Accessed January 25, 2022].

Mugume, Y., Kazibwe, Z. and Bassham, D.C. (2020) Target of

Rapamycin in Control of Autophagy: Puppet Master and Signal Integrator. *Int. J. Mol. Sci. 2020, Vol. 21, Page 8259*, **21**, 8259. Available at: https://www.mdpi.com/1422-0067/21/21/8259/htm [Accessed September 12, 2022].

Mukherjee, I., Campbell, N.H., Ash, J.S. and Connolly, E.L. (2006) Expression profiling of the Arabidopsis ferric chelate reductase (FRO) gene family reveals differential regulation by iron and copper. *Planta*, **223**, 1178–1190. Available at: https://link.springer.com/article/10.1007/s00425-005-0165-0 [Accessed February 2, 2022].

Müller, J., Toev, T., Heisters, M., Teller, J., Moore, K.L., Hause, G., Dinesh, D.C., Bürstenbinder, K. and Abel, S. (2015) Iron-Dependent Callose Deposition Adjusts Root Meristem Maintenance to Phosphate Availability. *Dev. Cell*, **33**, 216–230.

Nagahatenna, D.S.K., Langridge, P. and Whitford, R. (2015) Tetrapyrrole-based drought stress signalling. *Plant Biotechnol. J.*, **13**, 447–459. Available at: https://onlinelibrary.wiley.com/doi/full/10.1111/pbi.12356 [Accessed July 3, 2021].

Nagai, S., Koide, M., Takahashi, S., Kikuta, A., Aono, M., Sasaki-Sekimoto, Y., Ohta, H., Takamiya, K.I. and Masuda, T. (2007) Induction of Isoforms of Tetrapyrrole Biosynthetic Enzymes, AtHEMA2 and AtFC1, under Stress Conditions and Their Physiological Functions in Arabidopsis. *Plant Physiol.*, **144**, 1039–1051. Available at: https://academic.oup.com/plphys/article/144/2/1039/6106819 [Accessed January 20, 2022].

Nakamura, S. and Izumi, M. (2018) Regulation of Chlorophagy during Photoinhibition and Senescence: Lessons from Mitophagy. *Plant Cell Physiol.*, **59**, 1135–1143. Available at: https://pubmed.ncbi.nlm.nih.gov/29767769/ [Accessed September 17, 2022].

Nakatogawa, H., Ichimura, Y. and Ohsumi, Y. (2007) Atg8, a Ubiquitin-like Protein Required for Autophagosome Formation, Mediates Membrane Tethering and Hemifusion. *Cell*, **130**, 165–

178. Available at: https://pubmed.ncbi.nlm.nih.gov/17632063/ [Accessed June 19, 2021].

Naumann, C., Müller, J., Sakhonwasee, S., Wieghaus, A., Hause, G., Heisters, M., Bürstenbinder, K. and Abel, S. (2019) The Local Phosphate Deficiency Response Activates Endoplasmic Reticulum Stress-Dependent Autophagy. *Plant Physiol.*, **179**, 460–476. Available at: https://academic.oup.com/plphys/article/179/2/460/6116355 [Accessed September 18, 2022].

Nenova, V.R. (2008) Growth and photosynthesis of pea plants under different iron supply.

Noack, L.C. and Jaillais, Y. (2017) Precision targeting by phosphoinositides: how PIs direct endomembrane trafficking in plants. *Curr. Opin. Plant Biol.*, **40**, 22–33.

Noctor, G., Hager, J. and Li, S. (2011) Biosynthesis of NAD and Its Manipulation in Plants☆. *Adv. Bot. Res.*, **58**, 153–201.

Noda, N.N. and Inagaki, F. (2015) Mechanisms of Autophagy. , **44**, 101–122. Available at: https://www.annualreviews.org/doi/abs/10.1146/annurev-biophys-060414-034248 [Accessed June 19, 2021].

Noda, N.N., Ohsumi, Y. and Inagaki, F. (2010) *Atg8-family interacting motif crucial for selective autophagy*, No longer published by Elsevier.

Nolan, T.M., Brennan, B., Yang, M., et al. (2017) Selective Autophagy of BES1 Mediated by DSK2 Balances Plant Growth and Survival. *Dev. Cell*, **41**, 33-46.e7. Available at: http://www.cell.com/article/S1534580717301661/fulltext [Accessed September 3, 2022].

Nott, A., Jung, H.-S., Koussevitzky, S. and Chory, J. (2006) Plastid-to-Nucleus Retrograde Signaling. Available at: www.annualreviews.org.

Nouet, C., Motte, P. and Hanikenne, M. (2011) Chloroplastic and mitochondrial metal homeostasis. *Trends Plant Sci.*, **16**, 395–404. Available at: http://dx.doi.org/10.1016/j.tplants.2011.03.005 [Accessed

September 17, 2022].
Oborník, M. (2021) Enigmatic Evolutionary History of Porphobilinogen Deaminase in Eukaryotic Phototrophs. Available at: https://doi.org/10.3390/biology10050386.
Olenieva, V., Lytvyn, D., Yemets, A., Bergounioux, C. and Blume, Y. Tubulin acetylation accompanies autophagy development induced by different abiotic stimuli in Arabidopsis thaliana. , **43**, 1056–1064. Available at: http://rsb.info.nih.gov/ij/ [Accessed September 18, 2022].
Ono, Y., Wada, S., Izumi, M., Makino, A. and Ishida, H. (2013) Evidence for contribution of autophagy to Rubisco degradation during leaf senescence in Arabidopsis thaliana. *Plant. Cell Environ.*, **36**, 1147–1159. Available at: https://onlinelibrary.wiley.com/doi/full/10.1111/pce.12049 [Accessed September 17, 2022].
Overmyer, K., Brosché, M. and Kangasjärvi, J. (2003) Reactive oxygen species and hormonal control of cell death. *Trends Plant Sci.*, **8**, 335–342.
Paciorek, T., Zazímalová, E., Ruthardt, N., et al. (2005) Auxin inhibits endocytosis and promotes its own efflux from cells. *Nature*, **435**, 1251–1256.
Page, M.T., Garcia-Becerra, T., Smith, A.G. and Terry, M.J. (2020) Overexpression of chloroplast-targeted ferrochelatase 1 results in a genomes uncoupled chloroplast-to-nucleus retrograde signalling phenotype. *Philos. Trans. R. Soc. B Biol. Sci.*, **375**.
Pan, W., You, Y., Shentu, J.L., Weng, Y.N., Wang, S.T., Xu, Q.R., Liu, H.J. and Du, S.T. (2020) Abscisic acid (ABA)-importing transporter 1 (AIT1) contributes to the inhibition of Cd accumulation via exogenous ABA application in Arabidopsis. *J. Hazard. Mater.*, **391**, 122189.
Pandey, R. (2015) Mineral nutrition of plants. *Plant Biol. Biotechnol. Plant Divers. Organ. Funct. Improv.*, **1**, 499–538. Available at: https://link.springer.com/chapter/10.1007/978-81-322-2286-6_20 [Accessed June 8, 2022].
Papenbrock, J. and Grimm, B. (2001) Regulatory network of

tetrapyrrole biosynthesis – studies of intracellular signalling involved in metabolic and developmental control of plastids. *Planta 2001 2135*, **213**, 667–681. Available at: https://link.springer.com/article/10.1007/s004250100593 [Accessed January 13, 2022].

Park, H.J., Park, H.C., Lee, S.Y., Bohnert, H.J. and Yun, D.J. (2011) Ubiquitin and Ubiquitin-like Modifiers in Plants. *J. Plant Biol.*, **54**, 275–285. Available at: https://link.springer.com/article/10.1007/s12374-011-9168-5 [Accessed September 5, 2022].

Park, S.-H., Jeong, J.S., Zhou, Y., Binte Mustafa, N.F. and Chua, N.-H. (2022) Deubiquitination of BES1 by UBP12/UBP13 promotes brassinosteroid signaling and plant growth. *Plant Commun.*, 100348.

Patel, S. and Dinesh-Kumar, S.P. (2008) Arabidopsis ATG6 is required to limit the pathogen-associated cell death response. *Autophagy*, **4**, 20. Available at: https://www.tandfonline.com/action/journalInformation?journalCode=kaup20.

Pellegrini-Calace, M., Maiwald, T. and Thornton, J.M. (2009) PoreWalker: A Novel Tool for the Identification and Characterization of Channels in Transmembrane Proteins from Their Three-Dimensional Structure. *PLOS Comput. Biol.*, **5**, e1000440. Available at: https://journals.plos.org/ploscompbiol/article?id=10.1371/journal.pcbi.1000440 [Accessed May 17, 2022].

PETIT, J.-M., BRIAT, J.-F. and LOBRÉAUX, S. (2001) Structure and differential expression of the four members of the Arabidopsis thaliana ferritin gene family. *Biochem. J.*, **359**, 575–582. Available at: /biochemj/article/359/3/575/39208/Structure-and-differential-expression-of-the-four [Accessed January 12, 2022].

Pettersen, E.F., Goddard, T.D., Huang, C.C., Couch, G.S., Greenblatt, D.M., Meng, E.C. and Ferrin, T.E. (2004) UCSF Chimera—A visualization system for exploratory research and

analysis. *J. Comput. Chem.*, **25**, 1605–1612. Available at: https://onlinelibrary.wiley.com/doi/full/10.1002/jcc.20084 [Accessed October 6, 2022].

Phillips, A.R., Suttangkakul, A. and Vierstra, R.D. (2008) The ATG12-Conjugating Enzyme ATG10 Is Essential for Autophagic Vesicle Formation in Arabidopsis thaliana. *Genetics*, **178**, 1339. Available at: /pmc/articles/PMC2278079/ [Accessed September 17, 2022].

Potocki, S., Valensin, D., Camponeschi, F. and Kozlowski, H. (2013) The extracellular loop of IRT1 ZIP protein - The chosen one for zinc? *J. Inorg. Biochem.*, **127**, 246–252. Available at: http://dx.doi.org/10.1016/j.jinorgbio.2013.05.003 [Accessed June 28, 2021].

Pottier, M., Dumont, J., Masclaux-Daubresse, C. and Thomine, S. (2019) Autophagy is essential for optimal translocation of iron to seeds in Arabidopsis. *J. Exp. Bot.*, **70**, 845–858. Available at: https://academic.oup.com/jxb/article/70/3/859/5160064 [Accessed June 8, 2021].

Pottier, M., Masclaux-Daubresse, C., Yoshimoto, K. and Thomine, S. (2014) Autophagy as a possible mechanism for micronutrient remobilization from leaves to seeds. *Front. Plant Sci.*, **5**, 11. Available at: www.frontiersin.org [Accessed June 9, 2021].

Pu, Y., Luo, X. and Bassham, D.C. (2017) Tor-dependent and -independent pathways regulate autophagy in arabidopsis thaliana. *Front. Plant Sci.*, **8**, 1204.

Pu, Y., Luo, X., Bassham, D.C., Liu, Y., Xiao, S., Jiang, L., Bassham, D.C., Pu, Y. and Luo, X. (2017) No Title. *Front. Plant Sci.*, **8**, 1204. Available at: www.frontiersin.org [Accessed June 24, 2021].

Pu, Y., Soto-Burgos, J. and Bassham, D.C. (2017) Regulation of autophagy through SnRK1 and TOR signaling pathways. *https://doi.org/10.1080/15592324.2017.1395128*, **12**, e1395128. Available at: https://www.tandfonline.com/doi/abs/10.1080/15592324.2017.1

395128 [Accessed September 13, 2022].
Qi, H., Lei, X., Wang, Y., et al. (2022) 14-3-3 proteins contribute to autophagy by modulating SINAT-mediated degradation of ATG13. *Plant Cell*. Available at: https://academic.oup.com/plcell/advance-article/doi/10.1093/plcell/koac273/6687134 [Accessed September 13, 2022].
Qi, H., Li, J., Xia, F.N., Chen, J.Y., Lei, X., Han, M.Q., Xie, L.J., Zhou, Q.M. and Xiao, S. (2020) Arabidopsis SINAT Proteins Control Autophagy by Mediating Ubiquitylation and Degradation of ATG13. *Plant Cell*, **32**, 263–284. Available at: https://academic.oup.com/plcell/article/32/1/263/6099258 [Accessed September 2, 2022].
Qi, H., Xia, F.N. and Xiao, S. (2021) Autophagy in plants: Physiological roles and post-translational regulation. *J. Integr. Plant Biol.*, **63**, 161–179. Available at: https://onlinelibrary.wiley.com/doi/full/10.1111/jipb.12941 [Accessed September 8, 2022].
Qi, H., Xia, F.N., Xie, L.J., et al. (2017) TRAF Family Proteins Regulate Autophagy Dynamics by Modulating AUTOPHAGY PROTEIN6 Stability in Arabidopsis. *Plant Cell*, **29**, 890–911. Available at: https://academic.oup.com/plcell/article/29/4/890/6100962 [Accessed September 3, 2022].
Quintana, J., Bernal, M., Scholle, M., Holländer-Czytko, H., Nguyen, N.T., Piotrowski, M., Mendoza-Cózatl, D.G., Haydon, M.J. and Krämer, U. Root-to-shoot iron partitioning in Arabidopsis requires IRON-REGULATED TRANSPORTER1 (IRT1) protein but not its iron(II) transport function. *Plant J.*, **109**, 992–1013. Available at: https://onlinelibrary.wiley.com/doi/full/10.1111/tpj.15611 [Accessed February 3, 2022].
Rabinowitz, J.D. and White, E. (2010) Autophagy and metabolism. *Science (80-.).*, **330**, 1344–1348. Available at: https://www.science.org/doi/full/10.1126/science.1193497

[Accessed May 18, 2022].

Rasheed, S., Bashir, K., Kim, J.M., Ando, M., Tanaka, M. and Seki, M. (2018) The modulation of acetic acid pathway genes in Arabidopsis improves survival under drought stress. *Sci. Reports 2018 81*, **8**, 1–15. Available at: https://www.nature.com/articles/s41598-018-26103-2 [Accessed June 3, 2022].

Ravet, K., Touraine, B., Boucherez, J., Briat, J.F., Gaymard, F. and Cellier, F. (2009) Ferritins control interaction between iron homeostasis and oxidative stress in Arabidopsis. *Plant J.*, **57**, 400–412. Available at: https://onlinelibrary.wiley.com/doi/full/10.1111/j.1365-313X.2008.03698.x [Accessed June 8, 2021].

Reynolds, G.D., Wang, C., Pan, J. and Bednarek, S.Y. (2018) Inroads into internalization: Five years of endocytic exploration. *Plant Physiol.*, **176**, 208–218. Available at: www.plantphysiol.org/cgi/doi/10.1104/pp.17.01117 [Accessed June 29, 2021].

Reyt, G., Boudouf, S., Boucherez, J., Gaymard, F. and Briat, J.F. (2015) Iron- and Ferritin-Dependent Reactive Oxygen Species Distribution: Impact on Arabidopsis Root System Architecture. *Mol. Plant*, **8**, 439–453.

Richards, S.L., Wilkins, K.A., Swarbreck, S.M., Anderson, A.A., Habib, N., Smith, A.G., McAinsh, M. and Davies, J.M. (2015) The hydroxyl radical in plants: from seed to seed. *J. Exp. Bot.*, **66**, 37–46. Available at: https://academic.oup.com/jxb/article/66/1/37/2893394 [Accessed September 17, 2022].

Richter, A.S., Banse, C. and Grimm, B. (2019) The GluTR-binding protein is the heme-binding factor for feedback control of glutamyl-tRNA reductase. *Elife*, **8**.

Robe, K., Conejero, G., Gao, F., et al. (2021) Coumarin accumulation and trafficking in Arabidopsis thaliana: a complex and dynamic process. *New Phytol.*, **229**, 2062–2079. Available at: www.newphytologist.com [Accessed July 1, 2021].

Robe, K., Izquierdo, E., Vignols, F., Rouached, H. and Dubos, C. (2021) The Coumarins: Secondary Metabolites Playing a Primary Role in Plant Nutrition and Health. *Trends Plant Sci.*, **26**, 248–259.

Robinson, N.J., Procter, C.M., Connolly, E.L. and Guerinot, M. Lou (1999) A ferric-chelate reductase for iron uptake from soils. , **397**, 694–697. Available at: www.nature.com [Accessed June 8, 2021].

Rodrigues, A., Adamo, M., Crozet, P., et al. (2013) ABI1 and PP2CA phosphatases are negative regulators of Snf1-related protein kinase1 signaling in Arabidopsis. *Plant Cell*, **25**, 3871–3884. Available at: https://pubmed.ncbi.nlm.nih.gov/24179127/ [Accessed September 16, 2022].

Rodríguez-Celma, J., Connorton, J.M., Kruse, I., et al. (2019) Arabidopsis BRUTUS-LIKE E3 ligases negatively regulate iron uptake by targeting transcription factor FIT for recycling. *Proc. Natl. Acad. Sci. U. S. A.*, **116**, 17584–17591. Available at: http://www.ncbi.nlm.nih.gov/pubmed/31413196 [Accessed June 29, 2021].

Rogers, E.E., Eide, D.J. and Guerinot, M. Lou (2000a) Altered selectivity in an Arabidopsis metal transporter. *Proc. Natl. Acad. Sci.*, **97**, 12356–12360. Available at: https://www.pnas.org/content/97/22/12356 [Accessed February 3, 2022].

Rogers, E.E., Eide, D.J. and Guerinot, M. Lou (2000b) Altered selectivity in an Arabidopsis metal transporter. *Proc. Natl. Acad. Sci. U. S. A.*, **97**, 12356–12360. Available at: www.pnas.orgcgidoi10.1073pnas.210214197 [Accessed June 28, 2021].

Rogers, E.E. and Guerinot, M. Lou (2002) FRD3, a Member of the Multidrug and Toxin Efflux Family, Controls Iron Deficiency Responses in Arabidopsis. *Plant Cell*, **14**, 1787–1799. Available at: https://academic.oup.com/plcell/article/14/8/1787/6009790 [Accessed September 17, 2022].

Rojo, E., Gillmor, C.S., Kovaleva, V., Somerville, C.R. and

Raikhel, N. V. (2001) VACUOLELESS1 Is an Essential Gene Required for Vacuole Formation and Morphogenesis in Arabidopsis. *Dev. Cell*, **1**, 303–310.

Romero-Barrios, N. and Vert, G. (2018) Proteasome-independent functions of lysine-63 polyubiquitination in plants. *New Phytol.*, **217**, 995–1011. Available at: https://onlinelibrary.wiley.com/doi/full/10.1111/nph.14915 [Accessed September 25, 2022].

Ronen, E. (2022) Micro-elements in agriculture. *Pract. Hydroponics Greenhouses*. Available at: https://search.informit.org/doi/10.3316/informit.818252429782665.

Roschzttardtz, H., Conéjéro, G., Curie, C., Mari, S., Ve Conéjéro, G., Curie, C. and Mari, S. (2009) Identification of the endodermal vacuole as the iron storage compartment in the Arabidopsis embryo. *Plant Physiol.*, **151**, 1329–38. Available at: www.plantphysiol.org/cgi/doi/10.1104/pp.109.144444 [Accessed October 19, 2022].

Roschzttardtz, H., Séguéla-Arnaud, M., Briat, J.-F.F., Vert, G. and Curie, C. (2011) The FRD3 Citrate Effluxer Promotes Iron Nutrition between Symplastically Disconnected Tissues throughout Arabidopsis Development. *Plant Cell*, **23**, 2725–2737. Available at: https://academic.oup.com/plcell/article/23/7/2725/6097215 [Accessed February 3, 2022].

Rubinsztein, D.C., Mariño, G. and Kroemer, G. (2011) Autophagy and aging. *Cell*, **146**, 682–695.

Rubio, V., Bustos, R., Irigoyen, M.L., Cardona-López, X., Rojas-Triana, M. and Paz-Ares, J. (2009) Plant hormones and nutrient signaling. *Plant Mol. Biol.*, **69**, 361–373. Available at: https://link.springer.com/article/10.1007/s11103-008-9380-y [Accessed September 16, 2022].

Saint-Jore-Dupas, C., Gomord, V. and Paris, N. (2004) Protein localization in the plant Golgi apparatus and the trans-Golgi network. *Cell. Mol. Life Sci.*, **61**, 159–171. Available at:

www.univ-rouen.fr/UMR6037, [Accessed June 29, 2021].
Salomé, P.A., Oliva, M., Weigel, D. and Krämer, U. (2013) Circadian clock adjustment to plant iron status depends on chloroplast and phytochrome function. *EMBO J.*, **32**, 511–523. Available at: https://pubmed.ncbi.nlm.nih.gov/23241948 [Accessed January 15, 2022].
Santana-Codina, N. and Mancias, J.D. (2018) The Role of NCOA4-Mediated Ferritinophagy in Health and Disease. *Pharmaceuticals (Basel).*, **11**. Available at: https://pubmed.ncbi.nlm.nih.gov/30360520/ [Accessed September 17, 2022].
Santi, S. and Schmidt, W. (2009) Dissecting iron deficiency-induced proton extrusion in Arabidopsis roots. *New Phytol.*, **183**, 1072–1084. Available at: https://onlinelibrary.wiley.com/doi/full/10.1111/j.1469-8137.2009.02908.x [Accessed June 8, 2021].
Santos, C.S., Ozgur, R., Uzilday, B., Turkan, I., Roriz, M., Rangel, A.O.S.S., Carvalho, S.M.P. and Vasconcelos, M.W. (2019) Understanding the role of the antioxidant system and the tetrapyrrole cycle in iron deficiency chlorosis. *Plants*, **8**, 348. Available at: www.mdpi.com/journal/plants [Accessed June 8, 2021].
Santos, L.R. dos, Paula, L. de S., Pereira, Y.C., Silva, B.R.S. da, Batista, B.L., Alsahli, A.A. and Lobato, A.K. da S. (2020) Brassinosteroids-Mediated Amelioration of Iron Deficiency in Soybean Plants: Beneficial Effects on the Nutritional Status, Photosynthetic Pigments and Chlorophyll Fluorescence. *J. Plant Growth Regul. 2020 405*, **40**, 1803–1823. Available at: https://link.springer.com/article/10.1007/s00344-020-10232-y [Accessed November 14, 2022].
Satbhai, S.B., Setzer, C., Freynschlag, F., Slovak, R., Kerdaffrec, E. and Busch, W. (2017) Natural allelic variation of FRO2 modulates Arabidopsis root growth under iron deficiency. *Nat. Commun.*, **8**, 1–10. Available at: www.nature.com/naturecommunications [Accessed June 8,

2021].
Saxena, I. and Shekhawat, G.S. (2013) Nitric oxide (NO) in alleviation of heavy metal induced phytotoxicity and its role in protein nitration. *Nitric Oxide*, **32**, 13–20.
Schagerlöf, U., Wilson, G., Hebert, H., Al-Karadaghi, S. and Hägerhäll, C. (2006) Transmembrane topology of FRO2, a ferric chelate reductase from Arabidopsis thaliana. , **62**, 215–221. Available at: http://dx.doi.org/10.1007/s11103-006-9015-0 [Accessed July 1, 2021].
Scheepers, M., Spielmann, J., Boulanger, M., Carnol, M., Bosman, B., Pauw, E. De, Goormaghtigh, E., Motte, P. and Hanikenne, M. (2020) Intertwined metal homeostasis, oxidative and biotic stress responses in the Arabidopsis frd3 mutant. *Plant J.*, **102**, 34–52. Available at: https://onlinelibrary.wiley.com/doi/full/10.1111/tpj.14610 [Accessed February 3, 2022].
Schmidt, O. and Teis, D. (2012) The ESCRT machinery. *Curr. Biol.*, **22**, R116–R120.
Schmidt, S.B., Eisenhut, M. and Schneider, A. (2020) Chloroplast Transition Metal Regulation for Efficient Photosynthesis. *Trends Plant Sci.*, **25**, 817–828. Available at: https://doi.org/10.1016/j.tplants.2020.03.003 [Accessed July 1, 2021].
Schmidt, W. (2003) Iron solutions: Acquisition strategies and signaling pathways in plants. *Trends Plant Sci.*, **8**, 188–193.
Schuler, M., Rellán-Álvarez, R., Fink-Straube, C., Abadía, J. and Bauera, P. (2012) Nicotianamine functions in the phloem-based transport of iron to sink organs, in pollen development and pollen tube growth in Arabidopsis. *Plant Cell*, **24**, 2380–2400. Available at: www.plantcell.org/cgi/doi/10.1105/tpc.112.099077 [Accessed June 8, 2021].
Séguéla, M., Briat, J.F., Vert, G. and Curie, C. (2008) Cytokinins negatively regulate the root iron uptake machinery in Arabidopsis through a growth-dependent pathway. *Plant J.*, **55**, 289–300.

Selote, D., Samira, R., Matthiadis, A., Gillikin, J.W. and Long, T.A. (2014) Iron-Binding E3 Ligase Mediates Iron Response in Plants by Targeting Basic Helix-Loop-Helix Transcription Factors. *Plant Physiol.*, **167**, 273–286. Available at: https://academic.oup.com/plphys/article/167/1/273/6113576 [Accessed October 6, 2022].

Sertsuvalkul, N., DeMell, A. and Dinesh-Kumar, S.P. (2022) The complex roles of autophagy in plant immunity. *FEBS Lett.*, **596**, 2163–2171. Available at: https://onlinelibrary.wiley.com/doi/full/10.1002/1873-3468.14356 [Accessed September 13, 2022].

Shanmugabalaji, V., Grimm, B. and Kessler, F. (2020) Characterization of a Plastoglobule-Localized SOUL4 Heme-Binding Protein in Arabidopsis thaliana. *Front. Plant Sci.*, **11**, 2. Available at: www.frontiersin.org [Accessed July 2, 2021].

Shanmugam, V., Lo, J.C., Wu, C.L., Wang, S.L., Lai, C.C., Connolly, E.L., Huang, J.L. and Yeh, K.C. (2011) Differential expression and regulation of iron-regulated metal transporters in Arabidopsis halleri and Arabidopsis thaliana - the role in zinc tolerance. *New Phytol.*, **190**, 125–137. Available at: www.newphytologist.com [Accessed June 8, 2021].

Sharma, S.S., Dietz, K.-J. and Mimura, T. (2016) Vacuolar compartmentalization as indispensable component of heavy metal detoxification in plants. *Plant. Cell Environ.*, n/a-n/a. Available at: http://doi.wiley.com/10.1111/pce.12706.

Shatil-Cohen, A., Attia, Z. and Moshelion, M. (2011) Bundle-sheath cell regulation of xylem-mesophyll water transport via aquaporins under drought stress: A target of xylem-borne ABA? *Plant J.*, **67**, 72–80. Available at: https://onlinelibrary.wiley.com/doi/full/10.1111/j.1365-313X.2011.04576.x [Accessed June 8, 2021].

Shi, L., Wu, Y. and Sheen, J. (2018) TOR signaling in plants: conservation and innovation. *Development*, **145**. Available at: https://journals.biologists.com/dev/article/145/13/dev160887/19289/TOR-signaling-in-plants-conservation-and [Accessed

September 13, 2022].
Shibuya, K., Niki, T. and Ichimura, K. (2013) Pollination induces autophagy in petunia petals via ethylene. *J. Exp. Bot.*, **64**, 1111–1120. Available at: https://academic.oup.com/jxb/article/64/4/1111/436528 [Accessed September 17, 2022].
Shimizu, T., Kacprzak, S.M., Mochizuki, N., et al. (2019) The retrograde signaling protein GUN1 regulates tetrapyrrole biosynthesis. *Proc. Natl. Acad. Sci. U. S. A.*, **116**, 24900–24906. Available at: www.pnas.org/cgi/doi/10.1073/pnas.1911251116 [Accessed January 18, 2022].
Shimoni-Shor, E., Hassidim, M., Yuval-Naeh, N. and Keren, N. (2010) Disruption of Nap14, a plastid-localized non-intrinsic ABC protein in Arabidopsis thaliana results in the over-accumulation of transition metals and in aberrant chloroplast structures. *Plant. Cell Environ.*, **33**, 1029–1038. Available at: https://onlinelibrary.wiley.com/doi/full/10.1111/j.1365-3040.2010.02124.x [Accessed January 11, 2022].
Shin, L.J.L.-J., Lo, J.C.J.-C., Chen, G.H.G.-H., Callis, J., Fu, H. and Yeh, K.C.K.-C.K.C. (2013) IRT1 DEGRADATION FACTOR1, a RING E3 Ubiquitin Ligase, Regulates the Degradation of IRON-REGULATED TRANSPORTER1 in Arabidopsis. *Plant Cell*, **25**, 3039–3051. Available at: www.plantcell.org/cgi/doi/10.1105/tpc.113.115212 [Accessed June 8, 2021].
Shinozaki, D., Merkulova, E.A., Naya, L., Horie, T., Kanno, Y., Seo, M., Ohsumi, Y., Masclaux-Daubresse, C. and Yoshimoto, K. (2020) Autophagy Increases Zinc Bioavailability to Avoid Light-Mediated Reactive Oxygen Species Production under Zinc Deficiency. *Plant Physiol.*, **182**, 1284–1296. Available at: https://academic.oup.com/plphys/article/182/3/1284/6116152 [Accessed September 17, 2022].
Shinozaki, D., Tanoi, K. and Yoshimoto, K. (2021) Optimal Distribution of Iron to Sink Organs via Autophagy Is Important

for Tolerance to Excess Zinc in Arabidopsis. *Plant Cell Physiol.*, **62**, 515–527. Available at: https://academic.oup.com/pcp/article/62/3/515/6126429 [Accessed May 4, 2022].

Shinozaki, D. and Yoshimoto, K. (2021) Autophagy balances the zinc–iron seesaw caused by Zn-stress. *Trends Plant Sci.*, **26**, 882–884.

Shinozawa, A., Otake, R., Takezawa, D., et al. (2019) SnRK2 protein kinases represent an ancient system in plants for adaptation to a terrestrial environment. *Commun. Biol.*, **2**, 30. Available at: https://doi.org/10.1038/s42003-019-0281-1 [Accessed June 16, 2021].

Shpilka, T., Weidberg, H., Pietrokovski, S. and Elazar, Z. (2011) Atg8: An autophagy-related ubiquitin-like protein family. *Genome Biol.*, **12**, 1–11. Available at: http://genomebiology.com/2011/12/7/226 [Accessed June 28, 2021].

Siddiqi, K.S. and Husen, A. (2021) Significance of brassinosteroids and their derivatives in the development and protection of plants under abiotic stress. *Biol. 2021 7610*, **76**, 2837–2857. Available at: https://link.springer.com/article/10.1007/s11756-021-00853-3 [Accessed November 14, 2022].

Signorelli, S., Tarkowski, Ł.P., Ende, W. Van den and Bassham, D.C. (2019) *Linking Autophagy to Abiotic and Biotic Stress Responses*,.

Sinclair, S.A. and Krämer, U. (2012) The zinc homeostasis network of land plants. *Biochim. Biophys. Acta - Mol. Cell Res.*, **1823**, 1553–1567.

Singh, N. and Bhatla, S.C. (2016) Nitric oxide and iron modulate heme oxygenase activity as a long distance signaling response to salt stress in sunflower seedling cotyledons. *Nitric Oxide*, **53**, 54–64.

Sirko, A. and Masclaux-daubresse, C. (2021) Advances in Plant Autophagy. *Cells 2021, Vol. 10, Page 194*, **10**, 194. Available at: https://www.mdpi.com/2073-4409/10/1/194/htm [Accessed

September 3, 2022].

Sirko, A., Wawrzy´nska, A., Wawrzy´nska, W., Brzywczy, J. and Sié, M. (2021) Molecular Sciences Control of ABA Signaling and Crosstalk with Other Hormones by the Selective Degradation of Pathway Components. *Int. J. Mol. Sci*, **22**, 4638. Available at: https://doi.org/10.3390/ijms22094638.

Sivitz, A., Grinvalds, C., Barberon, M., Curie, C. and Vert, G. (2011) Proteasome-mediated turnover of the transcriptional activator FIT is required for plant iron-deficiency responses. *Plant J.*, **66**, 1044–1052.

Smalle, J. and Vierstra, R.D. (2004) THE UBIQUITIN 26S PROTEASOME PROTEOLYTIC PATHWAY. *http://dx.doi.org/10.1146/annurev.arplant.55.031903.141801*, **55**, 555–590. Available at: https://www.annualreviews.org/doi/abs/10.1146/annurev.arplant.55.031903.141801 [Accessed August 27, 2022].

Son, O., Kim, S., Kim, D., Hur, Y.S., Kim, J. and Cheon, C.I. (2018) Involvement of TOR signaling motif in the regulation of plant autophagy. *Biochem. Biophys. Res. Commun.*, **501**, 643–647.

Song, C., Yan, Y., Rosado, A., Zhang, Z. and Castellarin, S.D. (2019) ABA alleviates uptake and accumulation of zinc in grapevine (Vitis vinifera l.) by inducing expression of ZIP and detoxification-related genes. *Front. Plant Sci.*, **10**, 872. Available at: www.frontiersin.org [Accessed June 8, 2021].

Song, J., Feng, S.J., Chen, J., Zhao, W.T. and Yang, Z.M. (2017) A cadmium stress-responsive gene AtFC1 confers plant tolerance to cadmium toxicity. *BMC Plant Biol.*, **17**, 1–15. Available at: https://link.springer.com/articles/10.1186/s12870-017-1141-0 [Accessed January 20, 2022].

Soto-Burgos, J. and Bassham, D.C. (2017) SnRK1 activates autophagy via the TOR signaling pathway in Arabidopsis thaliana. Available at: https://doi.org/10.1371/journal.pone.0182591 [Accessed June 13, 2021].

Spallek, T., Beck, M., Khaled, S. Ben, Salomon, S., Bourdais, G., Schellmann, S. and Robatzek, S. (2013) ESCRT-I Mediates FLS2 Endosomal Sorting and Plant Immunity. *PLoS Genet.*, **9**, 1004035. Available at: www.plosgenetics.org [Accessed June 29, 2021].

Spiller, S. and Terry, N. (1980) Limiting Factors in PhotosynthesisII. IRON STRESS DIMINISHES PHOTOCHEMICAL CAPACITY BY REDUCING THE NUMBER OF PHOTOSYNTHETIC UNITS. *Plant Physiol.*, **65**, 121–125. Available at: https://academic.oup.com/plphys/article/65/1/121/6076058 [Accessed February 4, 2022].

Spiller, S.C., Kaufman, L.S., Thompson, W.F. and Briggs, W.R. (1987) Specific mRNA and rRNA Levels in Greening Pea Leaves during Recovery from Iron Stress. *Plant Physiol.*, **84**, 409–414. Available at: https://academic.oup.com/plphys/article/84/2/409/6082452 [Accessed February 4, 2022].

Spitzer, C., Schellmann, S., Sabovljevic, A., et al. (2006) The Arabidopsis elch mutant reveals functions of an ESCRT components in cytokinesis. *Development*, **133**, 4679–4689.

Stacey, M.G., Patel, A., McClain, W.E., Mathieu, M., Remley, M., Rogers, E.E., Gassmann, W., Blevins, D.G. and Stacey, G. (2008) The Arabidopsis AtOPT3 Protein Functions in Metal Homeostasis and Movement of Iron to Developing Seeds. *Plant Physiol.*, **146**, 589. Available at: /pmc/articles/PMC2245856/ [Accessed September 17, 2022].

Stein, A., Ruggiano, A., Carvalho, P. and Rapoport, T.A. (2014) Key steps in ERAD of luminal ER proteins reconstituted with purified components. *Cell*, **158**, 1375–1388.

Su, T., Yang, M., Wang, P., Zhao, Y. and Ma, C. (2020) Interplay between the Ubiquitin Proteasome System and Ubiquitin-Mediated Autophagy in Plants. *Cells 2020, Vol. 9, Page 2219*, **9**, 2219. Available at: https://www.mdpi.com/2073-4409/9/10/2219/htm [Accessed August 30, 2022].

Sun, S., Feng, L., Chung, K.P., et al. (2022) Mechanistic insights into an atypical interaction between ATG8 and SH3P2 in Arabidopsis thaliana. *Autophagy*, **18**, 1350–1366. Available at: https://www.tandfonline.com/doi/abs/10.1080/15548627.2021.1976965 [Accessed September 9, 2022].

Suttangkakul, A., Li, F., Chung, T. and Vierstra, R.D. (2011) The ATG1/ATG13 protein kinase complex is both a regulator and a target of autophagic recycling in Arabidopsis. *Plant Cell*, **23**, 3761–3779. Available at: https://pubmed.ncbi.nlm.nih.gov/21984698/ [Accessed September 11, 2022].

Svitáková, L. (2018) *Univerzita Karlova Přírodovědecká fakulta*, Univerzita Karlova, Přírodovědecká fakulta. Available at: https://dspace.cuni.cz/handle/20.500.11956/101297 [Accessed June 29, 2021].

Sylvestre-Gonon, E., Schwartz, M., Girardet, J.M., Hecker, A. and Rouhier, N. (2020) Is there a role for tau glutathione transferases in tetrapyrrole metabolism and retrograde signalling in plants? *Philos. Trans. R. Soc. B*, **375**. Available at: https://royalsocietypublishing.org/doi/abs/10.1098/rstb.2019.0404 [Accessed January 13, 2022].

T J Flowers, P F Troke, and and Yeo, A.R. (2003) The Mechanism of Salt Tolerance in Halophytes. *http://dx.doi.org/10.1146/annurev.pp.28.060177.000513*, **28**, 89–121. Available at: https://www.annualreviews.org/doi/abs/10.1146/annurev.pp.28.060177.000513 [Accessed May 17, 2022].

Takahashi, H., Kopriva, S., Giordano, M., Saito, K. and Hell, R. (2011) Sulfur Assimilation in Photosynthetic Organisms: Molecular Functions and Regulations of Transporters and Assimilatory Enzymes. *http://dx.doi.org/10.1146/annurev-arplant-042110-103921*, **62**, 157–184. Available at: https://www.annualreviews.org/doi/abs/10.1146/annurev-arplant-042110-103921 [Accessed June 8, 2022].

Takemoto, J.Y., Chang, C.W.T., Chen, D. and Hinton, G. (2019)

Heme-Derived Bilins. *Isr. J. Chem.*, **59**, 378–386. Available at: https://onlinelibrary.wiley.com/doi/full/10.1002/ijch.201800167 [Accessed September 18, 2022].

Taketani, S., Kakimoto, K., Ueta, H., Masaki, R. and Furukawa, T. (2003) Involvement of ABC7 in the biosynthesis of heme in erythroid cells: interaction of ABC7 with ferrochelatase. *Blood*, **101**, 3274–3280.

Tan, K., Sather, A., Robertson, J.L., Moy, S., Roux, B. and Joachimiak, A. (2009) Structure and electrostatic property of cytoplasmic domain of ZntB transporter. *Protein Sci.*, **18**, 2043–2052. Available at: https://onlinelibrary.wiley.com/doi/full/10.1002/pro.215 [Accessed October 14, 2022].

Tan, S., Zhang, P., Xiao, W., et al. (2018) TMD1 domain and CRAC motif determine the association and disassociation of MxIRT1 with detergent-resistant membranes. *Traffic*, **19**, 122–137. Available at: https://onlinelibrary.wiley.com/doi/full/10.1111/tra.12540 [Accessed May 16, 2022].

Tan, X., Thapa, N., Liao, Y., Choi, S. and Anderson, R.A. (2016) PtdIns(4,5)P2 signaling regulates ATG14 and autophagy. *Proc. Natl. Acad. Sci. U. S. A.*, **113**, 10896–10901. Available at: www.pnas.org/cgi/doi/10.1073/pnas.1523145113 [Accessed June 28, 2021].

Tanaka, R., Kobayashi, K. and Masuda, T. (2011) Tetrapyrrole Metabolism in Arabidopsis thaliana. , 145.

Tanaka, R. and Tanaka, A. (2007) Tetrapyrrole Biosynthesis in Higher Plants. *Annu. Rev. Plant Biol.*, **58**, 321–346. Available at: http://www.annualreviews.org/doi/10.1146/annurev.arplant.57.032905.105448 [Accessed June 26, 2021].

Tang, J. and Bassham, D.C. (2021) Autophagy during drought: function, regulation, and potential application. *Plant J.*

Tarantino, D., Petit, J.M., Lobreaux, S., Briat, J.F., Soave, C. and Murgia, I. (2003) Differential involvement of the IDRS cis-element in the developmental and environmental regulation of

the AtFer1 ferritin gene from Arabidopsis. *Planta*, **217**, 709–716. Available at: https://link.springer.com/article/10.1007/s00425-003-1038-z [Accessed September 17, 2022].

Tarnowski, L., Collados Rodriguez, M., Brzywczy, J., Cysewski, D., Wawrzynska, A. and Sirko, A. (2020) Overexpression of the Selective Autophagy Cargo Receptor NBR1 Modifies Plant Response to Sulfur Deficit. *Cells 2020, Vol. 9, Page 669*, **9**, 669. Available at: https://www.mdpi.com/2073-4409/9/3/669/htm [Accessed September 3, 2022].

Tarnowski, L., Rodriguez, M.C., Brzywczy, J., Piecho-Kabacik, M., Krčkova, Z., Martinec, J., Wawrzynska, A. and Sirko, A. (2020) A selective autophagy cargo receptor NBR1 modulates abscisic acid signalling in Arabidopsis thaliana. *Sci. Reports 2020 101*, **10**, 1–15. Available at: https://www.nature.com/articles/s41598-020-64765-z [Accessed September 3, 2022].

Terry, M.J. and Kendrick, R.E. (1999) Feedback inhibition of chlorophyll synthesis in the phytochrome chromophore-deficient aurea and yellow-green-2 mutants of tomato. *Plant Physiol.*, **119**, 143–152. Available at: https://pubmed.ncbi.nlm.nih.gov/9880355/ [Accessed January 14, 2022].

Thimm, O., Essigmann, B., Kloska, S., Altmann, T. and Buckhout, T.J. (2001) Response of Arabidopsis to iron deficiency stress as revealed by microarray analysis. *Plant Physiol.*, **127**, 1030–1043. Available at: www.plantphysiol.org/cgi/doi/10.1104/pp.010191. [Accessed June 24, 2021].

Thompson, A.R., Doelling, J.H., Suttangkakul, A. and Vierstra, R.D. (2005) Autophagic nutrient recycling in Arabidopsis directed by the ATG8 and ATG12 conjugation pathways. , **138**, 2097–2110. Available at: https://pubmed.ncbi.nlm.nih.gov/16040659/ [Accessed June 26, 2021].

Ticconi, C.A., Lucero, R.D., Sakhonwasee, S., Adamson, A.W., Creff, A., Nussaume, L., Desnos, T. and Abel, S. (2009) ER-resident proteins PDR2 and LPR1 mediate the developmental response of root meristems to phosphate availability. *Proc. Natl. Acad. Sci. U. S. A.*, **106**, 14174–14179. Available at: https://www.pnas.org/doi/abs/10.1073/pnas.0901778106 [Accessed September 18, 2022].

Tsuboyama, K., Koyama-Honda, I., Sakamaki, Y., Koike, M., Morishita, H. and Mizushima, N. (2016) The ATG conjugation systems are important for degradation of the inner autophagosomal membrane. *Science (80-.).*, **354**, 1036–1041. Available at: www.sciencemag.org/content/354/6315/1031/suppl/DC1 [Accessed June 28, 2021].

Tuteja, N. (2007) Abscisic Acid and Abiotic Stress Signaling. *Plant Signal. Behav.*, **2**, 135–138. Available at: https://doi.org/10.4161/psb.2.3.4156.

Uemura, T., Ueda, T., Ohniwa, R.L., Nakano, A., Takeyasu, K. and Sato, M.H. (2004) Systematic Analysis of SNARE Molecules in *Arabidopsis*: Dissection of the post-Golgi Network in Plant Cells. *Cell Struct. Funct.*, **29**, 49–65.

Uno, Y., Furihata, T., Abe, H., Yoshida, R., Shinozaki, K. and Yamaguchi-Shinozaki, K. (2000) Arabidopsis basic leucine zipper transcription factors involved in an abscisic acid-dependent signal transduction pathway under drought and high-salinity conditions. *Proc. Natl. Acad. Sci. U. S. A.*, **97**, 11632–7. Available at: http://www.ncbi.nlm.nih.gov/pubmed/11005831 [Accessed June 8, 2021].

Uren, N.C. (2008) Forms, reactions and availability of iron in soils. *https://doi.org/10.1080/01904168409363183*, **7**, 165–176. Available at: https://www.tandfonline.com/doi/abs/10.1080/01904168409363183 [Accessed February 4, 2022].

Vanhee, C. and Batoko, H. (2011a) Arabidopsis TSPO and porphyrins metabolism. *Plant Signal. Behav.*, **6**, 1383–1385.

Available at: http://www.tandfonline.com/doi/abs/10.4161/psb.6.9.16477.

Vanhee, C. and Batoko, H. (2011b) Autophagy involvement in responses to abscisic acid by plant cells. *https://doi.org/10.4161/auto.7.6.15307*, **7**, 655–656. Available at: https://www.tandfonline.com/action/journalInformation?journalCode=kaup20 [Accessed October 13, 2022].

Vanhee, C., Guillon, S., Masquelier, D.D.D., Degand, H., Deleu, M., Morsomme, P. and Batoko, H. (2011) A TSPO-related protein localizes to the early secretory pathway in Arabidopsis, but is targeted to mitochondria when expressed in yeast. *J. Exp. Bot.*, **62**, 497–508. Available at: https://academic.oup.com/jxb/article/62/2/497/587768 [Accessed June 8, 2021].

Vanhee, C., Zapotoczny, G., Masquelier, D., Ghislain, M. and Batoko, H. (2011) The Arabidopsis multistress regulator TSPO is a heme binding membrane protein and a potential scavenger of porphyrins via an autophagy-dependent degradation mechanism. *Plant Cell*, **23**, 785–805. Available at: http://www.plantcell.org/lookup/doi/10.1105/tpc.110.081570.

Varadi, M., Anyango, S., Deshpande, M., et al. (2022) AlphaFold Protein Structure Database: massively expanding the structural coverage of protein-sequence space with high-accuracy models. *Nucleic Acids Res.*, **50**, D439–D444. Available at: https://academic.oup.com/nar/article/50/D1/D439/6430488 [Accessed October 6, 2022].

Varotto, C., Maiwald, D., Pesaresi, P., Jahns, P., Salamini, F. and Leister, D. (2002) The metal ion transporter IRT1 is necessary for iron homeostasis and efficient photosynthesis in Arabidopsis thaliana. *Plant J.*, **31**, 589–599. Available at: https://onlinelibrary.wiley.com/doi/full/10.1046/j.1365-313X.2002.01381.x [Accessed June 8, 2021].

Vatansever, R., Filiz, E. and Ozyigit, I.I. (2015) Genome-wide analysis of iron-regulated transporter 1 (IRT1) genes in plants.

Hortic. Environ. Biotechnol., **56**, 516–523. Available at: https://link.springer.com/article/10.1007/s13580-015-0014-4 [Accessed June 28, 2021].

Veljanovski, V., Batoko, H., Bassham, D.C. and Vitale, A. (2014) Selective autophagy of non-ubiquitylated targets in plants: looking for cognate receptor/adaptor proteins. Available at: www.frontiersin.org.

Verbon, E.H., Trapet, P.L., Stringlis, I.A., Kruijs, S., Bakker, P.A.H.M. and Pieterse, C.M.J. (2017) Iron and Immunity. Available at: https://doi.org/10.1146/annurev-phyto-080516-.

Vert, G.G., Grotz, N., Dédaldéchamp, F., et al. (2002) IRT1, an Arabidopsis transporter essential for iron uptake from the soil and for plant growth. *Plant Cell*, **14**, 1223–1233. Available at: http://www.ncbi.nlm.nih.gov/pubmed/12084823%5Cnhttp://www.pubmedcentral.nih.gov/articlerender.fcgi?artid=PMC150776 [Accessed June 8, 2021].

Vierstra, R.D. (2012) The Expanding Universe of Ubiquitin and Ubiquitin-Like Modifiers. *Plant Physiol.*, **160**, 2–14. Available at: https://academic.oup.com/plphys/article/160/1/2/6109727 [Accessed September 5, 2022].

Vigani, G., Solti, Á., Thomine, S. and Philippar, K. (2019a) Essential and Detrimental - An Update on Intracellular Iron Trafficking and Homeostasis. *Plant Cell Physiol.*, **60**, 1420–1439. Available at: https://academic.oup.com/pcp [Accessed July 1, 2021].

Vigani, G., Solti, Á., Thomine, S. and Philippar, K. (2019b) Essential and Detrimental — an Update on Intracellular Iron Trafficking and Homeostasis. *Plant Cell Physiol.*, **60**, 1420–1439. Available at: https://academic.oup.com/pcp/article/60/7/1420/5489919 [Accessed January 11, 2022].

Vijay-kumar, S., Bugg, C.E. and Cook, W.J. (1987) Structure of ubiquitin refined at 1.8Åresolution. *J. Mol. Biol.*, **194**, 531–544.

Voigt, C., Oster, U., Börnke, F., et al. (2010) In-depth analysis of the distinctive effects of norflurazon implies that tetrapyrrole

biosynthesis, organellar gene expression and ABA cooperate in the GUN-type of plastid signalling. *Physiol. Plant.*, **138**, 503–519. Available at: https://onlinelibrary.wiley.com/doi/full/10.1111/j.1399-3054.2009.01343.x [Accessed July 2, 2021].

Voith von Voithenberg, L., Park, J., Stübe, R., Lux, C., Lee, Y. and Philippar, K. (2019) A Novel Prokaryote-Type ECF/ABC Transporter Module in Chloroplast Metal Homeostasis. *Front. Plant Sci.*, **10**, 1264.

Vu, L.D., Gevaert, K. and Smet, I. De (2018) *Protein Language: Post-Translational Modifications Talking to Each Other*,.

Walczak, M. and Martens, S. (2013) Dissecting the role of the Atg12–Atg5-Atg16 complex during autophagosome formation. *https://doi.org/10.4161/auto.22931*, **9**, 424–425. Available at: https://www.tandfonline.com/doi/abs/10.4161/auto.22931 [Accessed September 8, 2022].

Walsh, G. (2010) Post-translational modifications of protein biopharmaceuticals. *Drug Discov. Today*, **15**, 773–780.

Wang, F.Q., Yang, J., Dai, C., Wu, M.Z., Zhang, Y.H. and Shen, W.B. (2016) Characterization of the Arabidopsis thaliana heme oxygenase 1 promoter in response to salinity, iron deficiency, and mercury exposure. *Biol. Plant. 2017 611*, **61**, 35–47. Available at: https://link.springer.com/article/10.1007/s10535-016-0646-y [Accessed January 31, 2022].

Wang, H.J., Hsu, Y.W., Guo, C.L., Jane, W.N., Wang, H., Jiang, L. and Jauh, G.Y. (2017) VPS36-dependent multivesicular bodies are critical for plasmamembrane protein turnover and vacuolar biogenesis. *Plant Physiol.*, **173**, 566–581. Available at: www.plantphysiol.org/cgi/doi/10.1104/pp.16.01356 [Accessed June 30, 2021].

Wang, J., Guo, Q., Li, X., Wang, X. and Liu, L. (2020) The Arabidopsis locus AT3G03890 encodes a dimeric β-barrel protein implicated in heme degradation. *Biochem. J.*, **477**, 4785–4796. Available at: /biochemj/article/477/24/4785/227151/The-Arabidopsis-locus-AT3G03890-encodes-a-dimeric [Accessed

July 2, 2021].
Wang, Ping, Nolan, T.M., Yin, Y. and Bassham, D.C. (2019) Identification of transcription factors that regulate ATG8 expression and autophagy in Arabidopsis. Available at: https://www.tandfonline.com/action/journalInformation?journalCode=kaup20.
Wang, Pengwei, Pleskot, R., Zang, J., et al. (2019) Plant AtEH/Pan1 proteins drive autophagosome formation at ER-PM contact sites with actin and endocytic machinery. *Nat. Commun. 2019 101*, **10**, 1–16. Available at: https://www.nature.com/articles/s41467-019-12782-6 [Accessed May 16, 2022].
Wang, P., Zhao, Y., Li, Z., et al. (2018) Reciprocal Regulation of the TOR Kinase and ABA Receptor Balances Plant Growth and Stress Response. , **69**, 100-112.e6. Available at: https://pubmed.ncbi.nlm.nih.gov/29290610/ [Accessed June 16, 2021].
Wang, Q. and Hou, S. (2022) The emerging roles of ATG1/ATG13 kinase complex in plants. *J. Plant Physiol.*, **271**, 153653.
Wang, Y., Cai, S., Yin, L., Shi, K., Xia, X., Zhou, Y., Yu, J. and Zhou, J. (2015) Tomato HsfA1a plays a critical role in plant drought tolerance by activating ATG genes and inducing autophagy) Tomato HsfA1a plays a critical role in plant drought tolerance by activating ATG genes and inducing autophagy Tomato HsfA1a plays a critical role in plant drought tolerance by activating ATG genes and inducing autophagy. *Autophagy*, **11**, 2033–2047. Available at: https://www.tandfonline.com/action/journalInformation?journalCode=kaup20 [Accessed June 23, 2021].
Waters, B.M., Chu, H.H., DiDonato, R.J., Roberts, L.A., Eisley, R.B., Lahner, B., Salt, D.E. and Walker, E.L. (2006) Mutations in Arabidopsis Yellow Stripe-Like1 and Yellow Stripe-Like3 Reveal Their Roles in Metal Ion Homeostasis and Loading of Metal Ions in Seeds. *Plant Physiol.*, **141**, 1446–1458. Available at:

https://academic.oup.com/plphys/article/141/4/1446/6103555 [Accessed September 17, 2022].
Wawrzyńska, A. and Sirko, A. (2020) The Role of Selective Protein Degradation in the Regulation of Iron and Sulfur Homeostasis in Plants. *Int. J. Mol. Sci. 2020, Vol. 21, Page 2771*, **21**, 2771. Available at: https://www.mdpi.com/1422-0067/21/8/2771/htm [Accessed September 17, 2022].
Weber, K.A., Achenbach, L.A. and Coates, J.D. (2006) Microorganisms pumping iron: Anaerobic microbial iron oxidation and reduction. *Nat. Rev. Microbiol.*, **4**, 752–764. Available at: https://www.nature.com/articles/nrmicro1490 [Accessed June 8, 2021].
Wei, J. and Theil, E.C. (2000) Identification and characterization of the iron regulatory element in the ferritin gene of a plant (soybean). *J. Biol. Chem.*, **275**, 17488–17493. Available at: https://pubmed.ncbi.nlm.nih.gov/10748212/ [Accessed June 28, 2021].
Willems, P., Horne, A., Parys, T. Van, Goormachtig, S., Smet, I. De, Botzki, A., Breusegem, F. Van and Gevaert, K. (2019) The Plant PTM Viewer, a central resource for exploring plant protein modifications. *Plant J.*, **99**, 752–762. Available at: https://onlinelibrary.wiley.com/doi/full/10.1111/tpj.14345 [Accessed September 13, 2022].
Winder, T.L. and Nishio, J.N. (1995) Early Iron Deficiency Stress Response in Leaves of Sugar Beet. *Plant Physiol.*, **108**, 1487–1494. Available at: https://academic.oup.com/plphys/article/108/4/1487/6069769 [Accessed June 24, 2021].
Winter, D., Vinegar, B., Nahal, H., Ammar, R., Wilson, G. V. and Provart, N.J. (2007) An "electronic fluorescent pictograph" Browser for exploring and analyzing large-scale biological data sets. *PLoS One*, **2**, 718. Available at: www.bar.utoronto.ca/, [Accessed June 8, 2021].
Wintz, H., Fox, T., Wu, Y.Y., Feng, V., Chen, W., Chang, H.S., Zhu, T. and Vulpe, C. (2003) Expression Profiles of

Arabidopsis thaliana in Mineral Deficiencies Reveal Novel Transporters Involved in Metal Homeostasis. *J. Biol. Chem.*, **278**, 47644–47653. Available at: http://www.jbc.org/article/S002192582075790X/fulltext [Accessed September 17, 2022].

Withers, J. and Dong, X. (2017) Post-translational regulation of plant immunity. *Curr. Opin. Plant Biol.*, **38**, 124–132.

Wiuf, A., Steffen, J.H., Becares, E.R., et al. (2022) The two-domain elevator-type mechanism of zinc-transporting ZIP proteins. *Sci. Adv.*, **8**, 4331. Available at: https://www.science.org/doi/10.1126/sciadv.abn4331 [Accessed October 14, 2022].

Woodson, J.D., Joens, M.S., Sinson, A.B., Gilkerson, J., Salomé, P.A., Weigel, D., Fitzpatrick, J.A. and Chory, J. (2015) Ubiquitin facilitates a quality-control pathway that removes damaged chloroplasts. *Science (80-.).*, **350**, 450–454. Available at: https://www.science.org/doi/10.1126/science.aac7444 [Accessed September 3, 2022].

Woodson, J.D., Perez-Ruiz, J.M. and Chory, J. (2011) Heme synthesis by plastid ferrochelatase i regulates nuclear gene expression in plants. *Curr. Biol.*, **21**, 897–903.

Wu, H. and Zhao, J. (2019) Disruption of the Golgi apparatus mediates zinc deficiency-induced impairment of cognitive function in mice. *Metallomics*, **11**, 1984–1987. Available at: https://academic.oup.com/metallomics/article/11/12/1984/5961761 [Accessed June 24, 2021].

Wun, C.L., Quan, Y. and Zhuang, X. (2020) Recent Advances in Membrane Shaping for Plant Autophagosome Biogenesis. *Front. Plant Sci.*, **11**, 565.

Xia, F.N., Zeng, B., Liu, H.S., et al. (2020) SINAT E3 Ubiquitin Ligases Mediate FREE1 and VPS23A Degradation to Modulate Abscisic Acid Signaling. *Plant Cell*, **32**, 3290–3310. Available at: https://academic.oup.com/plcell/article/32/10/3290/6099462 [Accessed September 3, 2022].

Xiao, Z., Yang, C., Liu, C., et al. (2020) SINAT E3 ligases regulate

the stability of the ESCRT component FREE1 in response to iron deficiency in plants. *J. Integr. Plant Biol.*, **62**, 1399–1417. Available at: https://onlinelibrary.wiley.com/doi/full/10.1111/jipb.13005 [Accessed November 15, 2022].

Xie, Y., Mao, Y., Duan, X., Zhou, H., Lai, D., Zhang, Y. and Shen, W. (2016) Arabidopsis HY1-Modulated Stomatal Movement: An Integrative Hub Is Functionally Associated with ABI4 in Dehydration-Induced ABA Responsiveness. *Plant Physiol.*, **170**, 1699–1713. Available at: https://academic.oup.com/plphys/article/170/3/1699/6114349 [Accessed January 31, 2022].

Xie, Z., Nair, U. and Klionsky, D.J. (2008) Atg8 Controls Phagophore Expansion during Autophagosome Formation. *Mol. Biol. Cell*, **19**, 3290–3298. Available at: http://www.molbiolcell.org/cgi/doi/10.1091/mbc.E07-12-1292.

Xing, Y., Jia, W. and Zhang, J. (2007) AtMEK1 mediates stress-induced gene expression of CAT1 catalase by triggering H2O2 production in Arabidopsis. *J. Exp. Bot.*, **58**, 2969–2981. Available at: https://academic.oup.com/jxb/article/58/11/2969/611869 [Accessed January 24, 2022].

Xing, Y., Jia, W. and Zhang, J. (2008) AtMKK1 mediates ABA-induced CAT1 expression and H2O2 production via AtMPK6-coupled signaling in Arabidopsis. *Plant J.*, **54**, 440–451. Available at: https://onlinelibrary.wiley.com/doi/full/10.1111/j.1365-313X.2008.03433.x [Accessed January 24, 2022].

Xiong, L. and Zhu, J.K. (2003) Regulation of abscisic acid biosynthesis. *Plant Physiol.*, **133**, 29–36. Available at: http://www.plantphysiol.org/cgi/doi/10.1104/pp.103.025395. [Accessed June 8, 2021].

Xu, G., Jiang, Z., Wang, H. and Lin, R. (2018) The central circadian clock proteins CCA1 and LHY regulate iron homeostasis in Arabidopsis. Available at: www.jipb.net.

Yamada, T., Ichimura, K., Kanekatsu, M. and Doorn, W.G. Van (2009) Homologs of Genes Associated with Programmed Cell Death in Animal Cells are Differentially Expressed During Senescence of Ipomoea nil Petals. *Plant Cell Physiol.*, **50**, 610–625. Available at: https://academic.oup.com/pcp/article/50/3/610/1845518 [Accessed September 17, 2022].

Yan, N., Doelling, J.H., Falbel, T.G., Durski, A.M. and Vierstra, R.D. (2000) The Ubiquitin-Specific Protease Family from Arabidopsis.AtUBP1 and 2 Are Required for the Resistance to the Amino Acid Analog Canavanine. *Plant Physiol.*, **124**, 1828–1843. Available at: https://academic.oup.com/plphys/article/124/4/1828/6109892 [Accessed August 25, 2022].

Yasuda, M., Ishikawa, A., Jikumaru, Y., et al. (2008) Antagonistic Interaction between Systemic Acquired Resistance and the Abscisic Acid–Mediated Abiotic Stress Response in Arabidopsis . *Plant Cell*, **20**, 1678–1692. Available at: https://doi.org/10.1105/tpc.107.054296.

Yi, Y. and Guerinot, M. Lou (1996) Genetic evidence that induction of root Fe(III) chelate reductase activity is necessary for iron uptake under iron deficiency†. *Plant J.*, **10**, 835–844. Available at: https://onlinelibrary.wiley.com/doi/full/10.1046/j.1365-313X.1996.10050835.x [Accessed February 3, 2022].

Yoshida, T., Christmann, A., Yamaguchi-Shinozaki, K., Grill, E. and Fernie, A.R. (2019) Revisiting the Basal Role of ABA – Roles Outside of Stress. *Trends Plant Sci.*, **24**, 625–635.

Yoshimoto, K. (2010) Plant autophagy puts the brakes on cell death by controlling salicylic acid signaling. *Autophagy*, **6**, 192–193. Available at: https://www.tandfonline.com/action/journalInformation?journalCode=kaup20.

Yoshimoto, K. and Ohsumi, Y. (2018) Unveiling the Molecular Mechanisms of Plant Autophagy—From Autophagosomes to Vacuoles in Plants. *Plant Cell Physiol.*, **59**, 1337–1344.

Available at: https://academic.oup.com/pcp/article/59/7/1337/5034900 [Accessed January 25, 2022].

Yoshitake, Y., Nakamura, S., Shinozaki, D., Izumi, M., Yoshimoto, K., Ohta, H. and Shimojima, M. (2021) RCB-mediated chlorophagy caused by oversupply of nitrogen suppresses phosphate-starvation stress in plants. *Plant Physiol.*, **185**, 318–330. Available at: https://pubmed.ncbi.nlm.nih.gov/33721901/ [Accessed September 18, 2022].

Yoshitake, Y., Shinozaki, D. and Yoshimoto, K. (2022) Autophagy triggered by iron-mediated ER stress is an important stress response to the early phase of Pi starvation in plants. *Plant J.*, **110**, 1370–1381. Available at: https://pubmed.ncbi.nlm.nih.gov/35306710/ [Accessed September 18, 2022].

Yperman, K., Wang, J., Eeckhout, D., et al. (2021) Molecular architecture of the endocytic TPLATE complex. *Sci. Adv.*, **7**, 7999–8025. Available at: http://advances.sciencemag.org/ [Accessed June 29, 2021].

Yu, F. and Xie, Q. (2017) *Non-26S Proteasome Endomembrane Trafficking Pathways in ABA Signaling*, Elsevier Ltd. Available at: http://dx.doi.org/10.1016/j.tplants.2017.08.009 [Accessed June 16, 2021].

Yuan, S., Lin, R. and Larkin, R.M. (2016) Tetrapyrrole Signaling in Plants. Available at: www.frontiersin.org.

Yuan, W., Zhang, D., Song, T., et al. (2017) Arabidopsis plasma membrane H+-ATPase genes AHA2 and AHA7 have distinct and overlapping roles in the modulation of root tip H+ efflux in response to low-phosphorus stress. *J. Exp. Bot.*, **68**, 1731–1741. Available at: https://academic.oup.com/jxb/article/68/7/1731/3091861 [Accessed February 2, 2022].

Yuan, Y., Wu, H., Wang, N., Li, J., Zhao, W., Du, J., Wang, D. and Ling, H.-Q.Q. (2008) FIT interacts with AtbHLH38 and

AtbHLH39 in regulating iron uptake gene expression for iron homeostasis in Arabidopsis. *Cell Res.*, **18**, 385–97. Available at: www.cell-research.com [Accessed June 8, 2021].

Zargar, S.M., Kurata, R., Inaba, S., Oikawa, A., Fukui, R., Ogata, Y., Agrawal, G.K., Rakwal, R. and Fukao, Y. (2015) Quantitative proteomics of Arabidopsis shoot microsomal proteins reveals a cross-talk between excess zinc and iron deficiency. *Proteomics*, **15**, 1196–1201. Available at: https://onlinelibrary.wiley.com/doi/full/10.1002/pmic.201400467 [Accessed September 18, 2022].

Zelazny, E., Miecielica, U., Borst, J.W., Hemminga, M.A. and Chaumont, F. (2009) An N-terminal diacidic motif is required for the trafficking of maize aquaporins ZmPIP2;4 and ZmPIP2;5 to the plasma membrane. *Plant J.*, **57**, 346–355.

Zelazny, E. and Vert, G. (2015) Regulation of Iron Uptake by IRT1: Endocytosis Pulls the Trigger. *Mol. Plant*, **8**, 977–979. Available at: https://doi.org/10.1016/j.molp.2015.03.006 [Accessed June 24, 2021].

Zelicourt, A. de, Colcombet, J. and Hirt, H. (2016) The Role of MAPK Modules and ABA during Abiotic Stress Signaling. *Trends Plant Sci.*, **21**, 677–685.

Zeng, Y., Li, B., Lin, Y. and Jiang, L. (2019) The interplay between endomembranes and autophagy in plants. *Curr. Opin. Plant Biol.*, **52**, 14–22. Available at: https://doi.org/10.1016/j.pbi.2019.05.009 [Accessed January 25, 2022].

Zhai, Z., Gayomba, S.R., Jung, H. Il, et al. (2014) OPT3 Is a Phloem-Specific Iron Transporter That Is Essential for Systemic Iron Signaling and Redistribution of Iron and Cadmium in Arabidopsis. *Plant Cell*, **26**, 2249–2264. Available at: https://academic.oup.com/plcell/article/26/5/2249/6099969 [Accessed February 3, 2022].

Zhang, B., Shao, L., Wang, J., Zhang, Y., Guo, X., Peng, Y., Cao, Y. and Lai, Z. Phosphorylation of ATG18a by BAK1 suppresses autophagy and attenuates plant resistance against

necrotrophic pathogens. *Autophagy*, **17**, 2093–2110. Available at: https://www.tandfonline.com/doi/abs/10.1080/15548627.2020.1810426 [Accessed September 13, 2022].

Zhang, C., Hao, Z., Ning, Y. and Wang, G.L. (2019) SINA E3 Ubiquitin Ligases: Versatile Moderators of Plant Growth and Stress Response. *Mol. Plant*, **12**, 610–612.

Zhang, M., Zhang, F., Fang, Y., Chen, X., Chen, Y., Zhang, W., Dai, H.E., Lin, R. and Liu, L. (2015) The Non-canonical Tetratricopeptide Repeat (TPR) Domain of Fluorescent (FLU) Mediates Complex Formation with Glutamyl-tRNA Reductase *. *J. Biol. Chem.*, **290**, 17559–17565. Available at: http://www.jbc.org/article/S0021925820353564/fulltext [Accessed January 13, 2022].

Zhang, P., Tan, S., Berry, J.O., et al. (2014) An uncleaved signal peptide directs the malus xiaojinensis iron transporter protein Mx IRT1 into the ER for the PM secretory pathway. *Int. J. Mol. Sci.*, **15**, 20413–20433. Available at: https://www.mdpi.com/1422-0067/15/11/20413/htm [Accessed May 16, 2022].

Zhang, P., Wang, R., Ju, Q., Li, W., Tran, L.S.P. and Xu, J. (2019) The R2R3-MYB Transcription Factor MYB49 Regulates Cadmium Accumulation. *Plant Physiol.*, **180**, 529–542. Available at: https://academic.oup.com/plphys/article/180/1/529/6117750 [Accessed January 29, 2022].

Zhang, T., Xiao, Z., Liu, C., Yang, C., Li, J., Li, H., Gao, C. and Shen, W. (2021) Autophagy Mediates the Degradation of Plant ESCRT Component FREE1 in Response to Iron Deficiency. *Int. J. Mol. Sci. 2021, Vol. 22, Page 8779*, **22**, 8779. Available at: https://www.mdpi.com/1422-0067/22/16/8779/htm [Accessed November 15, 2022].

Zhang, W. and Chen, W. (2020) Role of salicylic acid in alleviating photochemical damage and autophagic cell death induction of cadmium stress in Arabidopsis thaliana. *Photochem. Photobiol.*

Sci. 2011 106, **10**, 947–955. Available at: https://link.springer.com/article/10.1039/c0pp00305k [Accessed September 17, 2022].

Zhang, X., Zhang, D., Sun, W. and Wang, T. (2019) The Adaptive Mechanism of Plants to Iron Deficiency via Iron Uptake, Transport, and Homeostasis. *Int. J. Mol. Sci. 2019, Vol. 20, Page 2424*, **20**, 2424. Available at: https://www.mdpi.com/1422-0067/20/10/2424/htm [Accessed February 2, 2022].

Zhang, Y. and Chen, Z. (2020) Broad and Complex Roles of NBR1-Mediated Selective Autophagy in Plant Stress Responses. *Cells 2020, Vol. 9, Page 2562*, **9**, 2562. Available at: https://www.mdpi.com/2073-4409/9/12/2562/htm [Accessed September 3, 2022].

Zhang, Y., Wu, H., Wang, N., Fan, H., Chen, C., Cui, Y., Liu, H. and Ling, H.Q. (2014) Mediator subunit 16 functions in the regulation of iron uptake gene expression in Arabidopsis. *New Phytol.*, **203**, 770–783. Available at: https://onlinelibrary.wiley.com/doi/full/10.1111/nph.12860 [Accessed January 20, 2022].

Zhao, A., Fang, Y., Chen, X., Zhao, S., Dong, W., Lin, Y., Gong, W. and Liu, L. (2014) Crystal structure of Arabidopsis glutamyl-tRNA reductase in complex with its stimulator protein. *Proc. Natl. Acad. Sci. U. S. A.*, **111**, 6630–6635. Available at: https://www.pnas.org/content/111/18/6630 [Accessed January 12, 2022].

Zhao, Q., Gao, C., Lee, P.S., et al. (2015) Fast-Suppressor Screening for New Components in Protein Trafficking, Organelle Biogenesis and Silencing Pathway in Arabidopsis thaliana Using DEX-Inducible FREE1-RNAi Plants. *J. Genet. Genomics*, **42**, 319–330.

Zhao, W.T., Feng, S.J., Li, H., Faust, F., Kleine, T., Li, L.N. and Yang, Z.M. (2017) Salt stress-induced FERROCHELATASE 1 improves resistance to salt stress by limiting sodium accumulation in Arabidopsis thaliana. , **7**, 1–16. Available at: www.nature.com/scientificreports/ [Accessed July 2, 2021].

Zhou, J., Wang, J., Cheng, Y., Chi, Y.J., Fan, B., Yu, J.Q. and Chen, Z. (2013) NBR1-Mediated Selective Autophagy Targets Insoluble Ubiquitinated Protein Aggregates in Plant Stress Responses. *PLoS Genet.*, **9**, 1003196. Available at: /pmc/articles/PMC3547818/ [Accessed September 3, 2022].

Zhou, J., Wang, J., Yu, J.Q. and Chen, Z. (2014) Role and regulation of autophagy in heat stress responses of tomato plants. *Front. Plant Sci.*, **5**. Available at: /pmc/articles/PMC4012191/ [Accessed June 23, 2021].

Zhuang, X., Chung, K.P., Luo, M. and Jiang, L. (2018) Autophagosome Biogenesis and the Endoplasmic Reticulum: A Plant Perspective. *Trends Plant Sci.*, **23**, 677–692.

Zhuang, X. and Jiang, L. (2014) Autophagosome biogenesis in plants Roles of SH3P2. Available at: https://www.tandfonline.com/action/journalInformation?journalCode=kaup20 [Accessed September 9, 2022].

Zhuang, X., Wang, H., Lam, S.K., Gao, C., Wang, X., Cai, Y. and Jiang, L. (2013) A BAR-Domain Protein SH3P2, Which Binds to Phosphatidylinositol 3-Phosphate and ATG8, Regulates Autophagosome Formation in Arabidopsis. *Plant Cell*, **25**, 4596–4615. Available at: https://academic.oup.com/plcell/article/25/11/4596/6096753 [Accessed September 9, 2022].

Zimmermann, P., Hirsch-Hoffmann, M., Hennig, L. and Gruissem, W. (2004) GENEVESTIGATOR. Arabidopsis microarray database and analysis toolbox. *Plant Physiol.*, **136**, 2621–2632. Available at: www.plantphysiol.org/cgi/doi/10.1104/pp.104.046367. [Accessed June 8, 2021].